High-resolution modelling with bi-dimensional shallow water equations based codes : high-resolution topographic data use for flood hazard assessment over urban and industrial environments

Morgan Abily

UNIVERSITE NICE-SOPHIA ANTIPOLIS

ECOLE DOCTORALE STIC

SCIENCES ET TECHNOLOGIES DE L'INFORMATION ET DE LA COMMUNICATION

T H E S E

pour l'obtention du grade de

Docteur en Sciences

de l'Université Nice-Sophia Antipolis

Mention: Automatique, Traitement du Signal et des Images

présentée et soutenue par

Morgan ABILY

High-resolution modelling with bi-dimensional shallow water equations based codes – High-resolution topographic data use for flood hazard assessment over urban and industrial environments –

Thèse dirigée par *Philippe* GOURBESVILLE,

co-encadrée par *Claire-Marie* DULUC & *Olivie*r DELESTRE

soutenue le 11 décembre 2015

Jury:

M. Shie-Yui Liong, Professeur - National University of Singapore	Rapporteur
M. Nigel Wright, Professeur - De Montfort University Leicester	Rapporteur
Mme. Nicole Goutal, Directeur de recherches - Lab. d'Hydraulique de Saint Venant, EDF R&D	Examinateur
Mme. Claire-Marie Duluc, Ingénieur/chercheur et chef de Bureau - IRSN	Examinateur
M. Olivier Delestre, Maître de conférence - Université Nice Sophia Antipolis	Examinateur
Mme. Nathalie Bertrand, Ingénieur/chercheur - IRSN	Invitée
M. Philippe Audra, Professeur - Université Nice Sophia Antipolis	Président du jury
M. Philippe Gourbesville, Professeur - Université Nice Sophia Antipolis	Directeur de thèse

ACKNOWLEDGMENT

Among many reasons I have to express my thank to them, I would like here to thank Philippe Gourbesville and Claire-Marie Duluc for pushing me to work on this thesis project. They gave me the chance to review the work I have accomplished during my first years of practice as a research engineer at IRSN and Polytech. It is an invaluable luxury.

I would like to express my thanks to the jury of this thesis and particularly to the reviewers for their commitment and valuable feedbacks.

I am grateful to the two colleagues with whom I work with since our CEMRACS 2013 collaboration: Olivier Delestre and Nathalie Bertrand. This thesis project started after the CEMRACS summer school and was an extra workload for them as well.

Part of the material used in this theses have been kindly provided by Nice Côte d'Azur Metropolis for research purpose.

This work was granted access to (i) the HPC and visualization resources of "Centre de Calcul Interactif" hosted by "Université Nice Sophia Antipolis" and (ii) the high performance computation resources of Aix-Marseille Université financed by the project Equip@Meso (ANR-10-EQPX-29-01) of the program "Investissements d'Avenir" supervised by the Agence Nationale pour la Recherche.

Technical support for codes adaptation on high performance computation centers has been provided by Fabrice Lebas, Yann Richet, Hélène Coullon, Christian Laguerre and Minh-Hoang Le.

I also take this opportunity to thank the colleagues from BEHRIG and I-CiTy laboratory I had the pleasure of spending time with these past years. I would like to thanks as well the numerous scientists (from experienced ones to interns) with whom I had the chance to be in touch, exchange and collaborate regarding this work. Lastly, I am thankful to my family and friends. Dany, Didier, Maité, Eugénie, Bernard, Cynthia, Shéba, Tibo, Sébastien, Steph, Alex(s) and Mag, the love and friendship I receive from you is the best daily support one can dream of.

NOTE TO THE READER

This PhD work started in November 2013, results from the research framework built from the collaborative activities initiated in 2011 between the Institute for Radioprotection and Nuclear Safety (IRSN, Institut de Radioprotection et de Sûreté Nucléaire) and the water department of the Engineering school Polytech Nice Sophia. Two main topics were defined for the research work conducted during this collaboration.

Need for runoff modelling with highly detailed information at industrial site scale. The IRSN wanted to test a specific approach for runoff hazard concern that has been specifically enhanced in the guide for protection of basic nuclear installation against flooding elaborated by the IRSN for the French Nuclear Safety Authority (ASN, 2013). In the guide, a specific runoff Reference Flood Situation (RFS) states that a nuclear installation has to be able to cope with a one hour long rainfall event of one over hundred years return period. IRSN wanted to test feasibility of standard 2D Shallow Water Equations (SWEs) based numerical tools for the runoff RFS. Spreading of High-Resolution (HR) topographic information techniques goes in this direction of a HR dataset (*e.g.* Light Detection and Ranging or imagery based) easily available for a specific study purpose. Consequently, hydraulic numerical modelling community increasingly uses Digital Elevation Models (DEM) generated from airborne technologies for urban flooding modelling. For a purpose like local runoff flood risk modelling over an industrial site which is a complex environment, added value of High-Resolution (HR) topographic data use that describes in detail the physical properties of the environment was interesting to test. Moreover, Runoff flow paths influencing above-ground features are not equally represented in DEM generated based on LiDAR and photogrammetric data. Lastly, feasibility of HR data in standard 2D numerical modelling tools might be challenging. Possibilities and challenges of these surface features inclusion in highly detailed 2D runoff models for runoff flood hazard assessment deserve a specific consideration and were therefore the key stone which motivated us to work on this thesis.

Need to check uncertainties of the High-Resolution overland flow models - Even though HR classified datasets have high horizontal and vertical accuracy levels (in a range of few centimeters), this data set is assorted of errors and uncertainties. Moreover, in order to optimize models creation and numerical computation, hydraulic modellers make choices regarding procedure for this type of dataset use. These sources of uncertainties might produce variability in hydraulic flood models outputs. Addressing models output variability related to model input parameters uncertainty is an active topic that is one of the main concern for practitioners and decision makers involved in the assessment and development

of flood mitigation strategies. IRSN and Polytech Nice Sophia wish to strengthen the assessment of confidence level in these deterministic hydraulic models outputs.

SUMMARY

High-resolution (infra-metric) topographic data, including LiDAR data and photogrammetric based classified data, are becoming commonly available at large range of spatial extent, such as municipality or industrial site scale. This category of dataset is promising for High-Resolution (HR) Digital Elevation Model (DEM) generation, allowing inclusion of fine above-ground structures (walls, sidewalks, road gutters, *etc.*), which might influence overland flow hydrodynamic in urban environment. DEMs are one key input data in Hydroinformatics for practitioner willing to perform free surface hydraulic modelling using standard 2D Shallow Water Equations (SWEs) based numerical codes (*e.g.* modeller wishing to assess flood hazard). Nonetheless, several categories of technical and numerical challenges arise from this type of data use with standard 2D SWEs numerical codes.

Objective of this thesis is to tackle possibilities, advantages and limits of High-Resolution (HR) topographic data use within standard categories of 2D hydraulic numerical modelling tools for flood hazard assessment purpose.

Review of concepts regarding 2D SWEs based numerical modelling and HR topographic data are presented. Methods to encompass HR surface elevation data in standard modelling tools are tested and evaluated. Two types of phenomena generating flooding issues are tested for High-Resolution modelling: *(i)* intense runoff and *(ii)* river flood event using in both cases LiDAR and photo-interpreted datasets. Three scales of spatial extent are tested, from a small industrial site scale to a city district scale (Nice low Var valley, France). In this thesis, test studies are performed using a wide range of categories of standard numerical modelling tools based on 2D SWE, from commercial (Mike 21, Mike 21 FM) to open source (TELEMAC 2D, FullSWOF_2D) codes. Comparison is performed with 2D SWEs simplified approaches (diffusive wave approximation using Mike SHE code) and with Navier-Stokes volume of fluid resolution approach (Open FOAM code). Tools and methods for assessing uncertainties aspects with 2D SWEs based models are developed and tested to perform a Global Sensitivity Analysis (GSA) related to HR topographic data use.

Chapter 1 of this thesis introduces state of the art of HR topographic data gathering techniques considering their possibility for a HR description of industrial and urban environment. Moreover, chapter 1 summarizes the background of the theoretical framework of SWEs, in order to raise questions up regarding validity of the approach of 2D SWEs based modelling over complex environments. As the framework of this type of application is different from the one for which SWEs have originally been designed for, the expected limits that might be encountered for HR topographic data use in standards codes are enhanced.

Indeed, if from a practical point of view, codes relying on approximation of SWEs are already commonly used for urban environment overland flow modelling, theoretical questions arise and remain open regarding several conceptual and mathematical aspects. Mainly, due to high gradient occurrences, boundary conditions and initial condition are seldom properly known.

In **chapter 2**, three case study are used to give a proof of concept of HR topographic data use feasibility, *(i)* to produce a HR DEM for intense flood simulations in complex environment, and *(ii)* to integrate this HR DEM information in standard 2D SWEs based codes. Feasibility, performances and relevance of the HR modelling are evaluated with a selection of different codes approximating the 2D SWEs based on various spatial discretization strategies (structured and non-structured) and with different numerical approaches (finite differences, finite elements, finite volumes). A comparison is conducted over computed maximal water depth and water deep evolution. The results confirmed the feasibility of these tools use for the studied specific purpose of HR modelling. Tested categories of 2D SWEs based codes, show in a large extent similar results in water depth calculation under important optimization procedure. Actually, major requirements were involved to get comparable results with a reasonable balance/ratio between mesh generation procedure - computational time - numerical parameters optimization (*e.g.* for wet/dry treatment).

The inclusion of detailed/thin features in DEM and in hydraulic models lead to considerable differences in local overland flow depth calculations compared to HR models that do not describe the industrial or urban environment with such level of detail. Moreover, added value of fine features inclusion in DEM is clearly observed disregarding resolution used for their inclusion (either 0.3 m or 1 m). Indeed, tests to include fine features (extruding their elevation information on DEM), through an over sizing their horizontal extent to 1 m, lead to good results with respect to their inclusion at a finer resolution.

LiDAR and photo-interpreted HR datasets are tested to compare their ease of use for HR DEM devoted to hydraulic purpose elaboration. Results point out differences, notably regarding ways and possibilities to integrate HR topographic dataset in 2D SWEs based codes. Moreover, due to meshing algorithm properties, the over constraints created by the density of vectors (in case of a HR urban environment) lead to errors and difficulties for non-structured mesh generation. For these reasons, the use of a structured mesh representing the HR DEM is found to be a more efficient compromise.

Chapter 3 consists on a focus on uncertainties related to model inputs, and more specifically on uncertainties related to one type of inputs: HR topographic data use and inclusion in 2D SWEs based codes. The aim is:

(i) to be a proof of concept of spatial Global Sensitivity Analysis (GSA) applicability to 2D flood modelling studies using developed method and tools and implementing them on High Performance Computing (HPC) structures;

(ii) to quantify uncertainties related to HR topographic data use, spatially discriminating relative weight of uncertainties related to HR dataset internal errors with respect to modeller choices for HR dataset integration in models.

The Uncertainty Analysis (UA) leads to conclusive results on: output variability quantification, nonlinear behavior of the model, and on spatial heterogeneity. The considered uncertain parameters related to the HR topographic data accuracy and to the inclusion in hydraulic models, influence the variability of calculated overland flow maximal water depth is found to be considerable. This stresses out the point that even though hydraulic parameters are assumed to be fully known in our simulations, the uncertainty related to HR topographic data use cannot be omitted and needs to be assessed and understood.

Sensitivity indices (Sobol) are calculated at given points of interest, enhancing the relative weight of each uncertain parameter on variability of calculated overland flow. Sobol index maps production is achieved. The spatial distribution of Si illustrates the spatial variability and the major influence of the modeller choices, when using the HR topographic data in 2D hydraulic models with respect to the influence of HR dataset accuracy.

TABLE OF CONTENTS

INTRODUCTION

Over urban and industrialized areas, flood events might result in severe human, economic and environmental consequences (Dawson *et al*., 2008). For flood hazard assessment, numerical models help decision makers to mitigate the risk. Numerical modelling tools are based on conceptualization of complex natural phenomena, using physical and mathematical hypothesis. In hydraulics, for flood hazard assessment, numerical models aim at describing free surface behavior (mainly elevation and discharge) according to an engineering description, to provide decision makers information regarding flood hazard estimations. Considering that the modeller knows in detail what is the chain of concepts, leading from hypothesis to results, good practice is to provide numerical model results with description of performance and limits of these simulations. The aim is to provide to the stakeholders, what are the deviations between what has been modelled and the reality (Cunge, 2003; Cunge, 2012). In the context of flood events modelling over an urban environment, bi-dimensional Shallow Water Equations (2D SWEs) based modelling tools are commonly used in studies even though the framework for such application goes straight from some of the 2D SWEs system underlying assumptions (see chapter 1).

Indeed, for practical flood modelling applications over urban and industrialized areas, standard deterministic free surface hydraulic modelling approaches most commonly rely either on *(i)* 2D SWEs system, *(ii)* simplified version of 2D SWEs system (*e.g.* diffusive wave approximation (Moussa and Bocquillon, 2000; Fewtreel, 2011)) or *(iii)* multiple porosity shallow water approaches (Sanders *et al*., 2008; Guinot, 2012). Compare to *(i)*, approach *(ii)* is a simplification of the mathematical description of the flow whereas approach *(iii)* is based on a simplification of the geometry description that includes a term in the calculation to represent sub-grid topographic variations. These approaches are different in terms of conceptual description of flow behavior and of computational cost. They require dissimilar quantity and type of input data. At cities or at large suburbs scales, these methods give overall similar results (Guinot, 2012). However, at smaller scales (street, compound or building scales) for High-Resolution (HR) description of overland flow properties reached during a flood event, codes based on 2D SWEs system using fine description of the environment are required. Indeed, above-ground surface features (buildings, walls, sidewalks, *etc.*) that influence overland flow path are densely present. Furthermore, these structures have a high level of diversity, ranging from a few meters (buildings, sidewalks, roundabouts, crossroads, *etc.*) to a few centimeters width (walls, road gutters, *etc.*). It creates a complex environment highly influencing the overland flow properties.

Detailed information about flooding hazard are required in mega-cities flood resilience context (Djordjevic *et al*., 2011), and for nuclear plant flood risk safety assessment (ASN, 2013). The use of High-Resolution (HR) numerical modelling should provide valuable insight for flood hazard assessment (Gourbesville, 2004, 2009). Obviously, to perform HR models of complex environments, an accurate description of the topography is compulsory. To describe in detail overland flow, the level of detail of the Digital Elevation Model (DEM) should include above-ground features influencing flow paths.

Urban reconstruction relying on airborne topographic data gathering technologies, such as imagery and Light Detection and Ranging (LiDAR) scans, are intensively used by geomatics communities (Musialski *et al*., 2013). Indeed, modern aerial transportation vectors, such as Unmanned Aerial Vehicles (UVA), make HR LiDAR or imagery based datasets affordable in terms of acquisition time and financial cost (Remondino *et al*., 2011; Nex and Remondino, 2014; Leitã *et al*., 2015). During the last decade, topographic datasets created based on LiDAR and photogrammetry technologies have become widely used by other communities such as urban planners (for 3D reconstruction approach) and consulting companies for various applied study purposes including flood risk studies. These technologies allow to produce DEMs with a high accuracy level (Mastin *et al*., 2009; Lafarge *et al*., 2010; Lafarge and Mallet, 2011). Among HR topographic data, photogrammetry technology allows to process to an object based classification to produce a 3D classified topographic dataset (Andres, 2012).

Therefore, to understand or to predict surface flow properties during an extreme flood event, models based on 2D Shallow Water Equations (SWEs) using HR description of the urban environment are often used in practical engineering applications (Mandlburger *et al*., 2008; Aktaruzzaman and Schmidt, 2009; Erpicum *et al*., 2010; Tsubaki and Fujita, 2010; Fewtrell *et al*., 2011). In that case, the main role of hydraulic models is to accurately describe overland flow's maximal water depth reached at some specific points or area of interest. If most of modern 2D SWEs codes integrate strategies to perform computation using parallelization strategies of codes to take advantage of High Performance-Computing (HPC) power for computational swiftness (Sørensen *et al*., 2010; Moulinec *et al*., 2011; Cordier *et al*., 2013), several aspects requires to be addressed for a pertinent and optimized HR modelling. HR topographic information is considered as "*Big Data*", requiring development of method for their efficient implementation in hydraulic free surface numerical modelling tools. The operational possibilities and issues to integrate the HR topographic data in the numerical hydraulic models have to be assessed.

The objectives of the research presented in this thesis are to address feasibility, added value and limits of HR topographic data use with standard hydraulic numerical codes. The main concerns are to assess the validity of such an approach and the requirements related to specificities of the HR topographic data for HR hydraulic modelling. Moreover, information will be provided for practical aspects and ease of use for standard applications.

Through the following objectives:

- the first target (T1) is to develop method and to provide a list of good practices for HR urban flooding event modelling;
- the second target (T2) focuses on quantifying and ranking uncertainties related to HR topographic data use in 2D SWEs based models developing operational tools and method to carry out an uncertainty analysis.

Framework for T1

From an operational point of view, SWEs based codes are broadly used over urban environment, even though theoretical questions regarding several conceptual and mathematical aspects remain open. In fact, such framework is far from the one for what SWEs were originally been designed for, and it stresses out the fact that limits might be expected and encountered. Therefore, relevance, feasibility, added values and challenges of HR flood modelling in complex environment should be tested.

This target, tackles the problematic of high density topographic information inclusion in standard 2D modelling tools and a second subtask is the assessment of possibilities and impacts of fine features inclusion.

Different sets of HR topographic data gathered from *(i)* a LiDAR and *(ii)* a photogrammetric campaign are tested. The standard 2D numerical modelling tools used in our studies are based on 2D SWEs resolution. This category of modelling tools has various numerical strategies to solve 2D SWEs and discretize the spatial information in different ways. The aim is not to benchmark performance of different codes, this has already done by Hunter (2008). Here, the main interest has been keen on assessing possibilities and limits of strategies for spatial discretization used by modelling tools, investigating on HR DSM use with regular grid meshing and non-structured meshing approaches.

Framework for T2

Dealing with uncertainties in hydraulic models is an advancing concern for both practitioners (Iooss, 2011) and new guidance (ASN, 2013). Identification, classification and quantification

of the impact of sources of uncertainties on a given model output are a set of analysis steps which will enable to analyze uncertainties behavior in a given modelling problem, to elaborate methods to reduce uncertainties on a model output and to communicate on relevant uncertainties. Sources of uncertainties in hydraulic models come from *(i)* hypothesis in mathematical description of the natural phenomena, *(ii)* from input parameters of the model, *(iii)* from numerical aspects when solving the model. Input parameters are of prime interest for applied practitioners willing to decrease uncertainties in the results (Iooss, 2011; Iooss and Lemaître, 2015). Input parameters of hydraulic models have hydrological, hydraulic, topographic and numerical nature.

Although HR classified datasets are of high horizontal and vertical accuracy (in a range of few centimeters), produced HR DEMs are assorted with the same types of errors as coarser DEMs. Errors are due to limitations in measurement techniques and to operational restrictions. These errors can be categorized (Fisher and Tate, 2006; Wechsler, 2007) as follow:

(i) systematic, due to bias in measurement and processing;

(ii) nuggets (or blunder), which are local abnormal values resulting from equipment or user failure, or to occurrence of abnormal phenomena in the gathering process (*e.g.* birds passing between the ground and the measurement device);

(iii) random variations, due to measurement/operation inherent limits.

Moreover, amount of data that compose a HR classified topographic dataset is massive. Consequently, to handle HR dataset and to avoid prohibitive computational time, hydraulic modeller has to make choices to integrate this type of data in the hydraulic model. However, this may decrease HR DEM quality and can introduce uncertainty (Tsubaki and Kawahara, 2013; Abily *et al*., 2015c, 2016a, 2016b). As summarized in Dottori (2013), Tsubaki and Kawahara (2013), and Sanders (2007), HR flood models effects of uncertainties related to HR topographic data use on simulated flow is not yet quantitatively understood.

Consequently, our objective here is to define, quantify and rank the uncertainties related to the use of HR topographic data in HR flood modelling over densely urbanized areas. The aims are *(i)* to apply an Uncertainty Analysis (UA) and spatial Global Sensitivity Analysis (GSA) approaches in a 2D HR flood model having spatial inputs and outputs, and *(ii)* to producing sensitivity maps.

The first chapter of the thesis presents the state of the art of HR topographic data gathering techniques considered as relevant with applications aiming at a HR description of industrial and urban environment (**part 1**). The focus is on technique suitable to balance spatial extent

and resolution requirement to include fine overland flow influencing structures (walls, sidewalks, road gutters, *etc.*) in HR datasets. The concepts and the state of the art of standard spatial discretization procedure for inclusion of topographic data in 2D numerical flood models are presented. The second part of this chapter (**part 2**) reviews the background of the theoretical framework of SWEs, in order to raise questions up regarding validity of the approach of 2D SWEs based modelling over complex environments. The limits and challenges regarding conceptual, mathematical and numerical aspects that should be expected with HR topographic data use in standards codes are presented.

The second chapter tackles the target 1 (T1). A methodology and the good practices for HR urban flooding event modelling are presented in parts 3 and 4. Three case study are considered for our purpose at different scales: *(i)* over a small (60,000 m²) fictitious industrial site using a created 0.1 m resolution DSM, *(ii)* over a real site in Nice city (France) using a LiDAR and a 3D photo-interpreted dataset at a larger scale (600,000 m²) and *(iii)* over the low Var valley in Nice using 3D photo-interpreted dataset at a large scale (17.8 km²). Moreover, different types of flood scenarios were tested: *(i)* and *(ii)* are simulations of intense rainfall events and *(iii)* is a river flood event. The first part of this chapter (**part 3**) focuses on the validity, the relevance and the limits of HR flood modelling in complex environment. The idea is to check numerical solving of 2D SWEs over complex topographies having high topographic gradient and leading to overland flow with challenging properties for numerical codes. Therefore, the challenging case study *(i)* of HR flood risk modelling due to local intense runoff is over an accurately described industrial site is used. Several standard numerical 2D SWEs based codes relying on different numerical methods and spatial discretization strategies are tested. In the second part of this chapter (**part 4**), the problematic of high density topographic information inclusion in standard 2D modelling tools and the assessment of possibilities and impact of fine features inclusion at different scales for different types of 2D SWEs based codes are presented. Study relies on case study *(ii)* and *(iii)*.

The third chapter is devoted to target two (T2): a spatial Global Sensitivity Analysis (GSA) method for 2D HR flood modelling focusing on the spatial ranking of uncertain parameters related to the use of HR topographic data is introduced. The case study *(iii)* is used here. The objective is to study uncertainties related to two categories of uncertain parameters (measurement errors and uncertainties related to operator choices) with regards to the use of HR classified topographic data in a 2D urban flood model. The fact that spatial inputs and outputs are involved in our uncertainty analysis study is an important concern for the methodology application. A spatial GSA is implemented to produce sensitivity maps based on Sobol index computation. The first part of the chapter (**part 5**) introduces the test case

context for the uncertainty analysis, enhances description of used HR topographic dataset, and gives general overview of uncertainty analysis methods and concepts. Lastly implemented methodology for the spatial GSA and developed tools are described. The second part of the chapter (**part 6**) presents results, first at points of interest, then at spatial levels. Eventually, outcomes and limits of our approach are then discussed (**part 7**).

CHAPTER I - THEORETICAL BACKGROUND

The specificity of densely urbanized or industrialized environments relies in the fact that size of above-ground features influencing overland flow path, ranges from macro elements (*e.g.* buildings) to fine ones (*e.g.* walls, sidewalks, road curbs, roundabouts, *etc.*). If one aim is to use free surface hydraulic numerical model to assess in detail the flood risks in these environments (*e.g.* due to intense rainfall events or to river overbanking), influence of these features has to be considered.

A Digital Elevation Model (DEM) can be the spatial discretization of the continuous variation of the elevation of the ground; DEM is then called a Digital Terrain Model (DTM). A DEM can also represent the elevation of the ground plus the elevation of the above-ground features on it; DEM is then called a Digital Surface Model (DSM). High-Resolution Digital Elevation Models (HR DEMs) allow the detailed representation of surface features.

In a DEM, resolution of a topographic dataset gives a single elevation value (*z*) for a given cell area, whatever are in the reality the changes of *z* properties within this area. The *z* value can be either: an averaged value of the several elevations information gathered within a cell area; or a given point value applied for the whole area of the cell. Consequently, in a DEM, the physical properties of *z* are reduced to the resolution of the cell size.

This resolution aspect has to be kept in mind as being a limiting factor in terms of accuracy of the topographic representation. Indeed, even if a topographic data gathering technology is able to provide at a given point an accurate measurement of *z,* once the z value is averaged to the resolution of the DEM cells, the use of the original level of accuracy of the technique to characterize the accuracy of the DEM does not make sense anymore. This is particularly the case if in the reality the characteristic of *z* varies significantly within the cell area. Similarly, when an inaccurate set of *z* measurement is used, interpolated and then discretized to a higher resolution than the accuracy level of the technique to create a DEM, it would not make any sense either.

Accordingly, this work considers that the concept of High-Resolution (HR) of the topographic dataset depends on the scale and abruptness of change in physical properties of the elevation with respect to the spatial resolution of the cell. Indeed, if the topography of the system that is intended to be represented has an important spatial extent, and if the spatial variations of the topography are not important with respect to the resolution, a few meters discretization can be considered as HR. For instance, Bates (2003) modelled a flood plain

overland flow, over a river reach of 12 km, using a DEM having a 4 m resolution. Bates (2003) work was considered as based on HR topographic data. Erpicum (2010) uses topographic data over urban area and considered that data information with a resolution between 4 m and 1 m is of HR for such type of environment. In the case of an urban or industrial environment, a topographic dataset is considered to be of HR when it allows to include in the topographic information elevation of infra-metric elements (Le Bris *et al*., 2013). To achieve a horizontal topographical resolution fine enough to represent overland flow influencing structures in urban type environment, the interval of gathered points *z* data should be in the range of 0.1 m to 0.4 m for a HR DEM generation including fine features (Ole, 2004; Tsubaki, 2013).

For our concern, we will present in this chapter, topographic data gathering technologies - *(i)* Light Detection And Ranging (LiDAR) and *(ii)* photogrammetry – these techniques allow to represent infra-metric information. A focus is given on features classification carried out by photo-interpretation process, that allows to have high accuracy and highly detailed topographic information (Mastin *et al*., 2009; Andres, 2010; Larfarge *et al*., 2010; Lafarge and Mallet, 2011). Photo-interpreted HR datasets allow to generate HR DEMs including classes of impervious above-ground features (see chapter 2 and Abily *et al*., 2014a, 2015b). Produced HR DEMs can have a vertical and horizontal accuracy up to 0.1 m (Fewtrell *et al*., 2011). HR DEMs generated on photo-interpreted datasets based can include above-ground features elevation information depending on modeller selection among classes.

As presented in the introduction of this thesis, hydraulic numerical modelling community increasingly starts to use HR DSM information from airborne technologies to model urban flood scenarios (Tsubaki and Fujita, 2010) to understand or to predict surface flow properties during an extreme flood event. Objective of numerical approaches used in the SWEs codes is to approximate the solution (when existing) of equations as faithfully as possible by a method where the unknowns are the values of hydraulic variables (water depth and velocities or discharges) in a finite number of points (nodes) of the studied domain, and in a finite number of instances during the considered period of time (spatial and temporal discretization). In the 2D SWEs based codes, the topographic information is discretized (either using the DEM or performing a second discretization based on the DEM) to be included in the computation through the use of computational grid (or mesh).

The first part **(part 1)** of this theoretical chapter introduces in a first section the specificities of topographic data gathering techniques estimated to be suitable with the HR DEM production for our urban flood modelling purpose. The second section emphasizes the principles and

the common practices to include DEM information in a 2D hydraulic code, the computational grid generation.

The second part **(part 2)** of this chapter recalls and summarizes in its first section the basics behind 2D free surface modelling using numerical codes approximating the 2D SWEs solutions and then gives an overview of standard numerical methods to approximate the solution of the SWEs system.

PART. 1. HIGH-RESOLUTION TOPOGRAPHIC DATA IN URBAN ENVIRONMENT

Generally, for topographic information gathering campaign, the technologies -LiDAR or photogrammetry- are settled on a vector of transportation that can be terrestrial (*e.g.* cars) or aerial: Unmanned Aerial Vehicle (UAV, *e.g.* drones), specific flight (plane or helicopter) or satellite. For our range of applications vectors compatible with required balance between resolution and spatial extent are UAV and specific flight campaign. Terrestrial vector allows to produce HR and high accuracy dataset (Hervieu and Soheilian, 2013), but are discarded here due to the prohibitive size of the spatial extent to cover for an application over an urban area. Nevertheless, it has to be noticed that over a smaller extent (industrial site or district scale) such type of vector can be suitable. For instance, Fewtrell (2011) uses a HR topographic dataset gathered using a terrestrial vector for a modelling of an urban flooding over a district. Remote sensing from satellite can provide information for application at large scale (Weng, 2012), but is here discarded as the resolution and the vertical accuracy for an urban environment will not be sufficient for the scope of our study compare to resolution and accuracy that can be reached when using specific flights (Sanders, 2007). Indeed, specific flight for topographic data gathering campaign over urban environment using planes or drones allow to offer the best balance in terms of possibility to get a resolution/accuracy and spatial extent compatible for HR modelling (Küng *et al*., 2011).

1.1 LIDAR

LiDAR is a scanner system that uses a laser to pulse a beam that will be reflected by objects on its way and that will be received by a sensor embedded on the scanner system. This procedure enables to provide information of distance between the reached targets and the sensor by multiplying the speed of light by the time it takes for the light to transmit from and return back to the sensor (Priestnall *et al*., 2000; Weitkamp, 2005). The nature of LiDAR data offers the potential for extracting surface information for many ranges of applications (Priestnall *et al*., 2000).

When a LiDAR is mounted on board of a flying vector, the gathering system is composed of combined technologies (Figure 1.1) that allow to accurately georeference the LiDAR system (Habib *et al*., 2005; Gervaix, 2010). The material making up the system is generally:

- an accurate GPS system, allowing to locate the aircraft with a centimetric precision;
- an Inertial Measurement Unit (IMU) , to take consider the aeronef movements during the flight;

- the LiDAR scanner, that emits and receives back the beam, measuring the distance, the time and the angle of the scanning;
- a computer to store the data.

This equipment can be mounted on board an aeronef such as a plane or a helicopter but, mainly due to IMU important weight, LiDAR system can be mounted only on an UAV (such as drones) powerful enough to carry the weight of the whole system, discarding the ultra-light UAV (see Leitão *et al*., 2015).

The LiDAR system provides row information under the form of a geo-referenced point cloud. The LiDAR pulses can lead to single, multiple or waveform returns. In all these cases, the level of energy returned to the captor is different and can possibly be analyzed in case of multi-return or waveform return signals. Then, the first return will describe the first objects encountered by the beam (*e.g.* vegetation), whereas the last one will represent reflection from the ground surface. A classification of the points is then necessary and can be carried out through the use of specific software to discriminate elevation information of above-ground structures from the ground elevation information. LiDAR ground filtering algorithms within these software make different assumptions about ground characteristics to discriminate ground, non-ground features and above-ground objects (*e.g.* bridges, short walls, mixed areas, *etc.*). Abdullah (2012) gives illustration and application of a LiDAR filtering procedure for bridges and elevated roads removal in urban areas. Nevertheless, Meng (2010) underlined that complex conditions such as dense, various size and shape of above-ground features environments, lead to errors in the differentiation. These complex conditions are likely to occur in case of an urban environment.

In an aerial campaign, the point cloud density will depend on the following parameters in the methodology for the aerial LiDAR topographic data gathering campaign: *(i)* Laser pulse rate (Hz), *(ii)* flight height/speed ratio, and (3) scan angle. With recently developed LiDAR sensors, precision range can reach 2 to 3 cm (Lemmens, 2007).

The accuracy of LiDAR points highly depends on the accuracy of GPS and IMU systems. Airborne GPS is able to yield results having an accuracy up to 5 cm horizontally and 10 cm vertically, while IMU can generate altitude with accuracy within a couple of centimeters (Fisher and Tate, 2006; Liu, 2008).

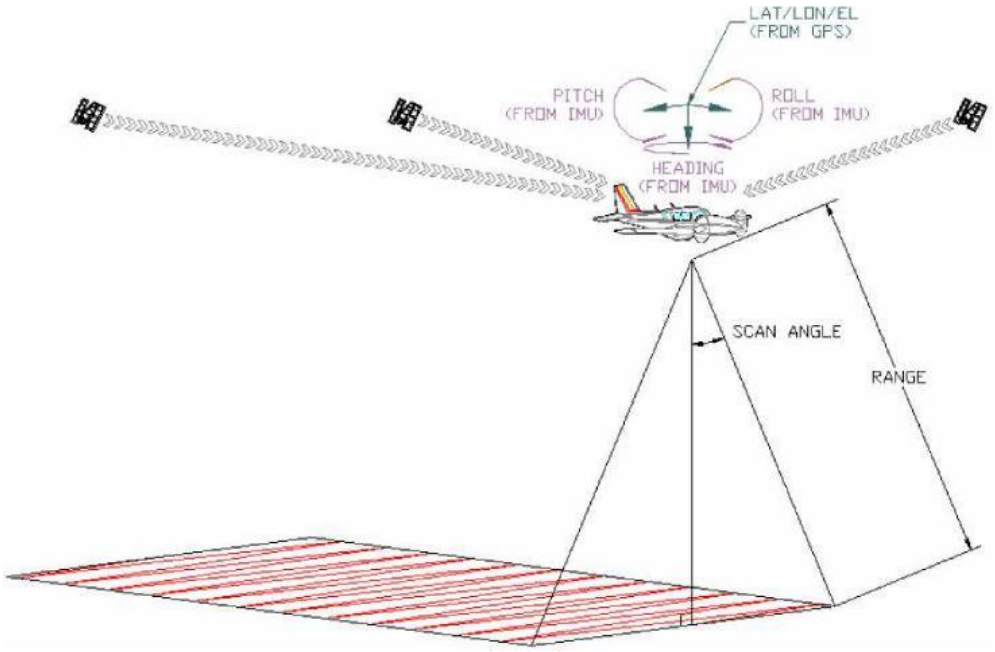

Figure 1.1. *Schematization of a LiDAR system mounted on a plane (from Gervaix 2010).*

1.2 PHOTOGRAMMETRY AND PHOTO-INTERPRETED DATASETS

1.1.2 Photogrammetry

Aerial photogrammetry technology allows to measure 3D coordinates of a space and its objects (features) using 2D pictures taken from different positions. The overlapping between pictures allows to calculate 3D properties of space and features based on stereoscopy principle (Baltsavias, 1999; Eagles, 2004; Liu, 2008) as conceptualized in figure 1.2. To measure accurately ground and features elevation, a step of aerotriangulation calculation is compulsory, requiring information on picture properties regarding their position, orientation and bonding (or tie) points. The orientation on how the camera lens was pointed varies in time depending on the lens rotation due to plane or UAV roll, pitch and yaw that lead to lens rotation angles (respectively called omega, phi and kappa). The use of ground control points allows to geo-reference the dataset.

A low flight elevation, a high number of aerial pictures with different points of view and high levels of overlapping, allow to increase the accuracy and the reliability of the 3D coordinates measurement (Küng *et al*., 2011). Indeed, sensitivity tests on parameters photogrammetric influencing dataset quality: *(i)* flight altitude, *(ii)* image overlapping, *(iii)* camera pitch and *(iv)* weather conditions, confirmed the major influence of flight altitude on dataset quality (Leitão *et al*., 2015).

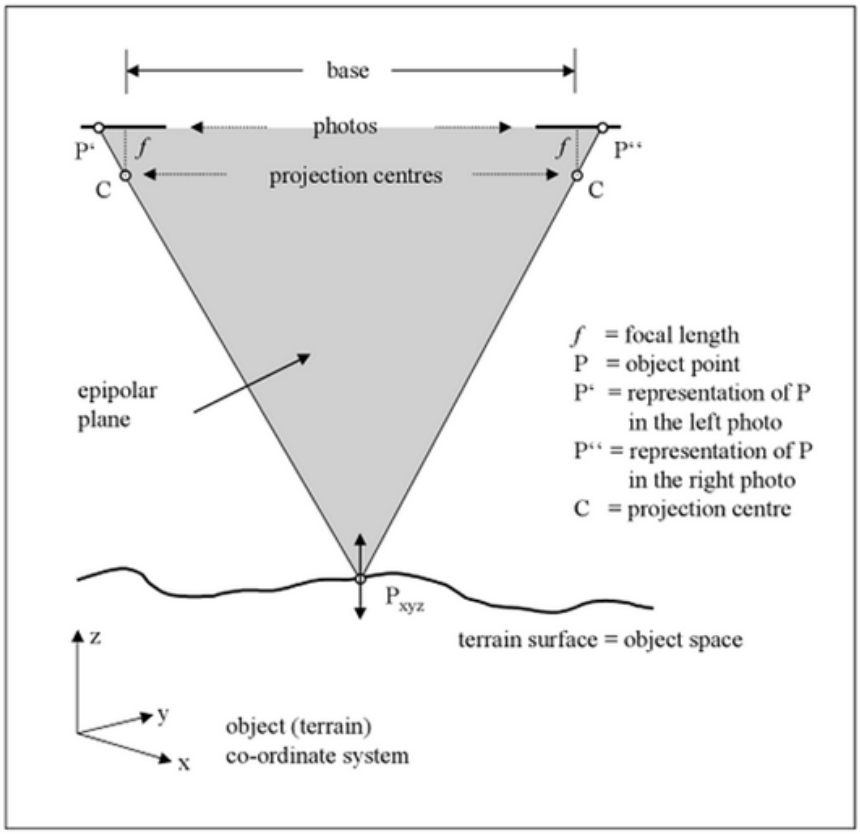

Figure 1.2. *Stereoscopy principle in photogrammetry to get ground or object x, y, and z properties (from Linder, 2006).*

In photogrammetry, the spatial resolution is the size of a pixel at the ground level. It has to be distinguished to the spectral resolution which is related to the number of spectral bands and gathered simultaneously (see Egels and Kasser, 2004). At a given spatial resolution, an object having a size three times bigger than the pixel size can be identified and interpreted.

1.1.3 Object based classification: photo-interpretation

For 3D classified dataset creation, a photo-interpretation step is necessary. Photo-interpretation allows creation of vectorial information based on photogrammetric dataset (Egels and Kasser, 2004; Linder, 2006). A photo-interpreted dataset is composed of classes of points, polylines and polygons digitalized based on photogrammetric data. Figure 1.3 illustrates the visualization of a sub-part of a photo-interpreted dataset composed of 50 classed of polylines and polygones. Important aspects in the photo-interpretation process are the classes' definition, the photo-interpretation techniques and the dataset quality used for the photo-interpretation. These aspects will impact the design of the output classified dataset (Lu and Weng, 2007).

Figure 1.3. *Visualization of elevation information of a photo-interpreted dataset gathered over an urban area (Nice, France). Details of this specific dataset are given in chapter 2.*

The step of classes' definition has to be elaborated prior to the photo-interpretation step. The number, the nature and criteria for the definition of classes will depend on the objectives of the photo-interpretation campaign.

Photo-interpretation techniques can be made *(i)* automatically by algorithm use, *(ii)* manually by a human operator on a Digital Photogrammetric Workstation (DPW) or *(iii)* by a combination of the two methods. The level of accuracy is higher when the photo-interpretation is done by a human operator on a DPW, but more resources are needed as the process becomes highly time consuming (Zou *et al*., 2004; Lafarge, 2010). Eventually, the 3D classification of features based on photo-interpretation allows to get 3D High-Resolution topographic data over territory that offers large and adaptable perspectives for its exploitation for different purposes (Andres, 2012).

Usually, when a photo-interpreted classified dataset is provided to a user, the data is assorted with a global mean error value and with a percentage of photo-interpretation accuracy. The mean error value encompasses errors, due to material accuracy limits, to biases and to nuggets (or blunder) that compose error within the row photogrammetric data. Furthermore, a percentage of accuracy representing errors in photo-interpretation is generally provided. This percentage of accuracy represents errors in photo-interpretation

which results from feature misinterpretation addition or omission. This percentage of accuracy results from the photo-interpreted dataset comparison with field ground measurements of elevation over sub-domains of the photo-interpretation campaign (Figure 1.4). This process of control is time consuming as often based on manual operation and control, resource requiring (to gathered field measurement) and subject to operator interpretation (Andres, 2012).

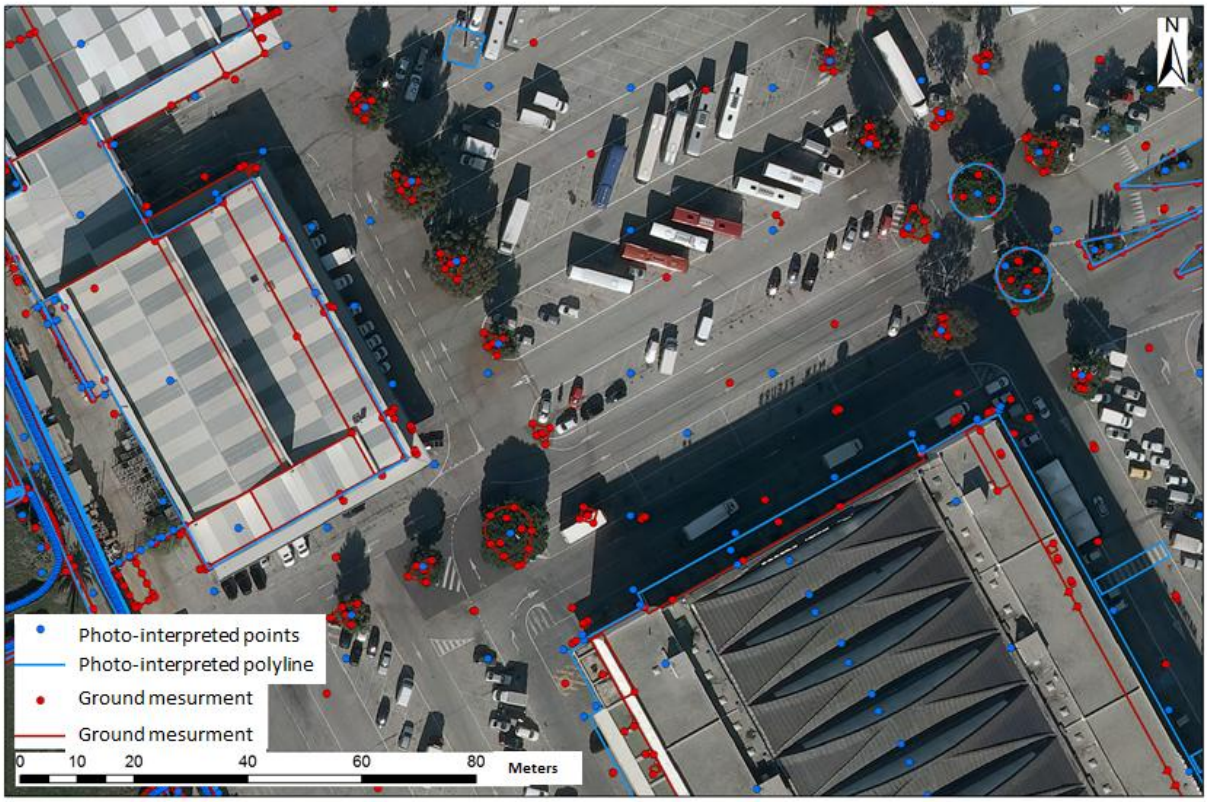

Figure 1.4. *Illustration of field and photo-interpreted measurement comparison that are performed to control the level of accuracy of the photo-interpretation process.*

A typical workflow to illustrate the process to achieve the photo-interpretation is given in figure 1.5. With this figure, idea is not to go into details into the description of this workflow, that can vary depending on the campaigns. Nevertheless, it is interesting for a non-specialist in geomatics to understand that three loops are interconnected in this process. First, the data gathering/measurement. Impact of camera properties is the main issue here. Second, loop is the treatment of geo-referencing/calibration part. Last part of the process is the photo-interpretation part itself.

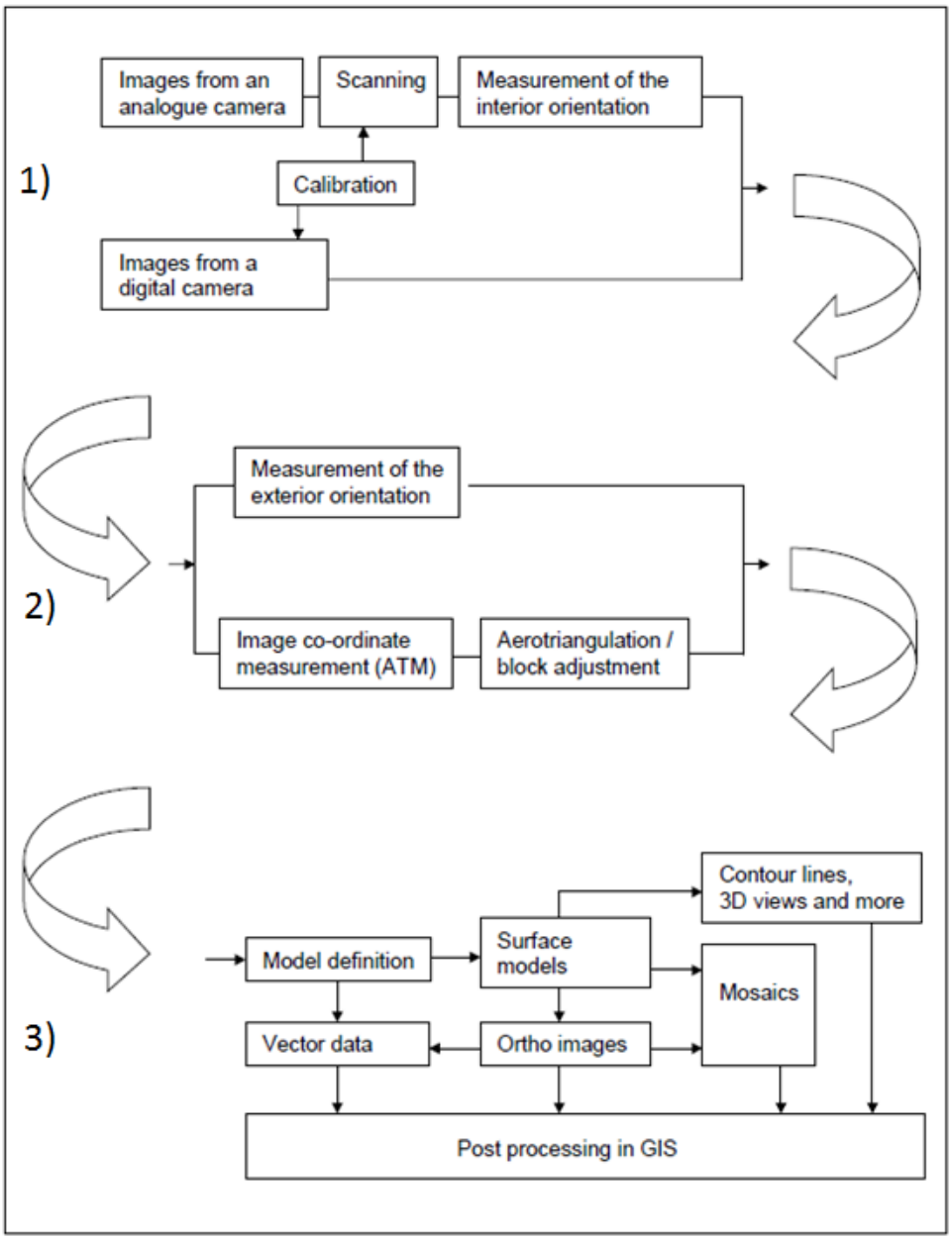

Figure 1.5. *Illustration of workflow process to produce a photo-interpreted dataset as described in Linder (2006).*

It has to be mentioned that both type LiDAR and Photogrammetric topographic data gathering techniques, when mounted on aerial vectors, are not well suited to gathered underwater bathymetry. New possibilities of post-treatment of these techniques to gather river bathymetry are developing (see Feurer *et al*., 2008). Nevertheless, beside for really low flow condition, issues are still likely to occur due to LiDAR inability to penetrate water masses (Podhoroanyi and Fedorcak, 2015) and due to visibility through water that will make photogrammetry use not relevant.

1.3 FOCUS ON SPATIAL DISCRETIZATION

In computing codes, the physical domain (Ω) can have 1, 2 or 3 dimensions in space. The discretization of Ω in 1D, 2D or 3D is respectively associated to variables x, y and *z* and called a *mesh* or a *computational grid*. The computational grid then represents the *continuum* where the governing partial differential equations are replaced by constructed discretized forms/solved by numerical methods (see part 2). For numerical resolution of the 2D SWEs system, the continuous variable topography information/elevation (*z*) is necessary for the computation, and therefore spatially discretized according to a 1D, 2D or 3D meshing process.

A mesh that arises from the discretization of *z* within Ω is composed of referenced points (computational points or nodes) and of cells (or elements) that link the points together. A mesh is characterized by its dimension - 1D to 3D -, and the geometry of its cells that can be flat elements (triangles, rectangles or polygons) or elements in volume (pyramids, tetrahedron, cubes, *etc.*), respectively for 2D or for 3D. As recalled in Weatherill (1992), the mesh has to represent accurately the geometrical boundaries, and “gap” in the computational domain cannot occur.

Main classification criteria of types of meshes are following:

- If elements have identical/regular size to discretize the Ω, the mesh is said to be structured, whereas if the mesh is composed of elements having different sizes (but always with the same geometry) they are qualified as non-structured (Figure 1.6). In a structured mesh, all interior nodes -not located on a boundary of Ω- have an equal number of adjacent elements. Hybrid meshing exists, Ω being then discretized mixing structured and non-structured sub-domains.
- If properties (size/shape) of elements constituting a mesh evolve with time, the mesh is referenced as Adaptive Mesh Refinment (AMR) while a mesh that has constant properties in time is referred as non-adaptive.

Parameters of a computational grid such as area or volume of the cells (resolution) and number of elements are inherent properties of the mesh. The smaller are the areas or volumes of the elements, the more the discretization gets close to the continuous variable (*z*), but the more the total number of elements increases. By increasing the number of cells in the mesh, the computational coast increases, not only because of the increased number of computational points in space, but also due to the temporal discretization that decreases – if

dt is adaptive in the numerical scheme - to fit with a numerical stability criterion (CFL criterion, see part 2, section 2.2.1).

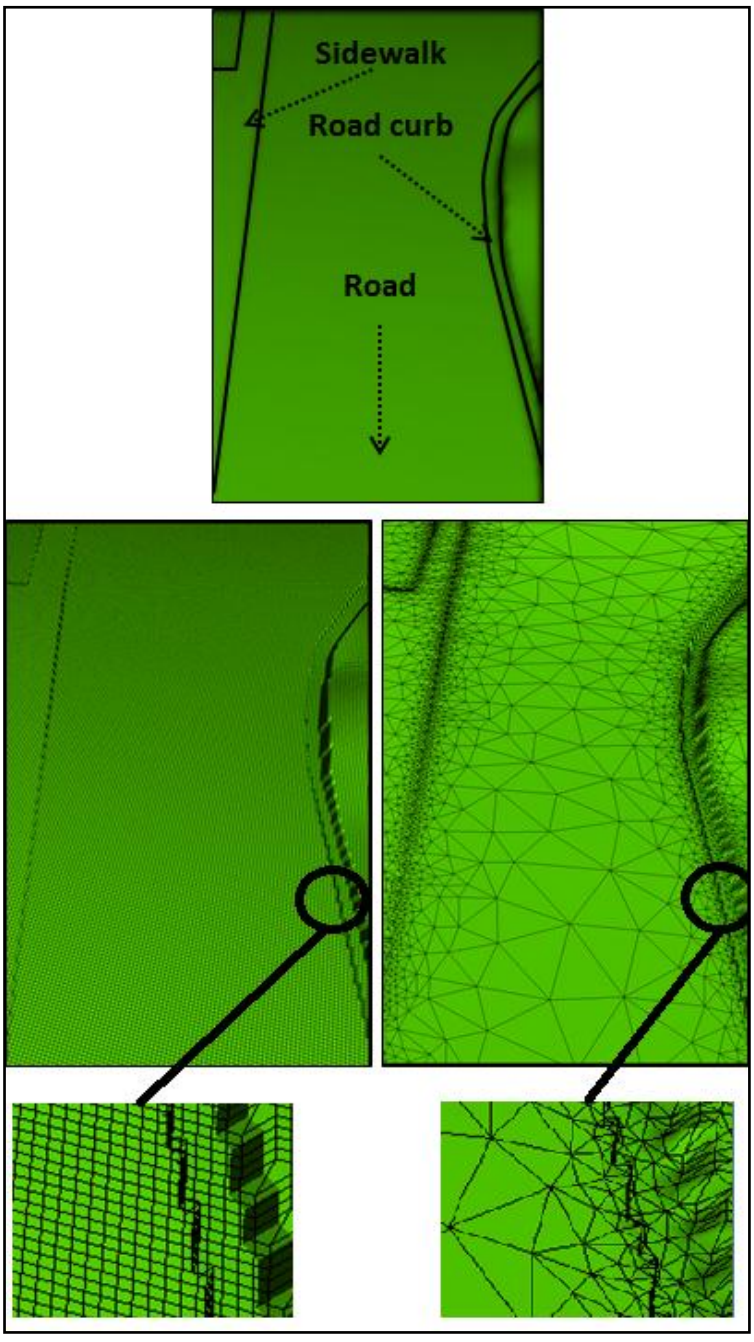

Figure 1.6. *Illustration of structured (left) and non-structured (right) meshing.*

In 2D free surface modelling, the different types of mesh -structured, non-structured and adaptive- are used in industrial codes.

Structured computational grids, such as the commonly used Cartesian structured mesh, have the main advantages that they are often easy to use. Indeed, the DEM representing the domain can be almost straight forwardly used as a computational grid (assuming that the

DEM representing the domain is considered as already suited for the hydraulic modelling application). For practical application degradation or resampling of a HR DEM can occur due to limitations in computation resources or in data handling.

Two main disadvantages arise from the use of structured mesh. First the regular size of elements implies that the highest mesh resolution one can expect from the discretization procedure is the same over Ω. Hence, in areas where the physical properties of the phenomena wished to be modelled, or where the variable (elevation) does not vary, there will be an unnecessary over-discretization of Ω. Consequently it will involve a high computational cost along with the storage of potentially unnecessary information. Second, disadvantage of a structured Cartesian mesh is that if the flow or any singularity is orientated, in the worst case, plus or minus 45° compared to the x or y direction, the computation will artificially go through a stepwise *zig-zag* processing (Ma *et al*., 2015). As a result, the number of cells, and therefore the length over which the water will flow, is artificially increased by this process.

Non-structured computational grid relies on a set of computational points that constitute the set of cells that all have the same shape (most commonly triangles in 2D), but that have variable sizes (and therefore variable areas). Most common practice is to generate first a plane mesh according to x and y directions. This process requires to give vector spatial information such as polygons, lines or points over the domain where the modeller wants the mesh to be refined. Then *z* values from the DEM are then applied to the mesh. Another approach, offers the possibility to direcly give criterions such as *z* gradient from the DEM for mesh generation and refinement.

The flexibility regarding mesh cell size, compared to structured meshes, allows to decrease the number of computational points where there is no need for accurate discretization of the variable (*e.g.* areas where elevation is constant) or where averaging assumptions are estimated to be fair. Automatic methods for non-structured mesh generation are reviewed in Löhner (1997) and Owens (1998). As generalized in Löhner (1997), an automatic non-structured grid generator requires:

- description of the bounding surface and of the domain to be gridded;
- description of elements to be generated (nature, size, shape, orientation, growing ratio criterion);
- grid generation techniques.

Most commonly used grid generation techniques in 2D hydraulic non-structured mesh generation rely on, advancing front method (George and Seveno 1994), Delaunay and

constrained Delaunay triangulation methods (Weatherill, 1992), or hybrid techniques. These techniques will not be reviewed here but it is interesting to mention that a limit of these meshing algorithms is that they are not well suited for over-constrained domain mesh generation. These meshing techniques are implemented in commercial and commonly used codes mesh generator (Mike 21 mesh generator DHI (2007b)) and BlueKenue for TELEMAC CHC (2010), see conclusion of this chapter).

Adaptive Mesh Refinement (AMR) is a discretization that evolves with space and time. The aim of this type of approach is *(i)* to reduce computational time by optimizing number of computational points to numerical constraints related to flow properties (*e.g.* CFL) and *(ii)* to improve accuracy of the solution. Two main types of approaches are used in 2D SWEs based flood modelling.

- Block-structured adaptive mesh refinement. This type of approach is a nesting of multiple levels of evolving patches of structured sub-grids that are pre-generated. Coarse grid or finer nested sub-grids are used depending on flow dynamic properties as these properties can impact numerical aspects in the solution computation. The patchwork of grids is user-chosen pre-specified refinement ratios. A modern and well-described method of AMR applied over the well documented Malpasset dam break case can be found in Georges (2011).
- The other approach is a sequence of grid operations that re-generate the non-structured mesh during the computation, again depending on flow dynamic properties. Main steps in mesh regeneration are: *(i)* node movement, *(ii)* edge splitting, *(iii)* edge collapsing, and *(iv)* node movement (Tam, 2000).

1.4 FEEBACK FOR HR TOPOGRAPHIC DATA USE IN 2D URBAN FLOOD MODELLING

This first part of chapter 1 introduced the concept of HR topographic datasets and the spatial discretization processes that will influence both possibilities and accuracy of HR topographic data inclusion within flood models. As a reminder, goals of the research presented in this thesis is to develop amethod and good practices for High-Resolution (HR) topographic data use (T1) and to focus on uncertainties related to HR topographic use and inclusion in 2D flood models (T2).

Within T1 framework it is set that for the spatial extent of our applications of interest, namely urban and industrial sites HR 2D overland flow modelling, LiDAR or photogrammetry technologies settled on an aerial vector are the best suited to gathered HR topographic datasets. As enhanced in this part, qualitative difference between LiDAR and

Photogrammetric based HR datasets rely in the interpretation/classification possibilities that are more important in photogrammetry. Photo-interpreted dataset offers a broader range of possibilities for HR DEM design, in accordance with descriptions of the above-ground structure that will influence overland flow. Indeed classification of above-ground features being more extensive in photo-interpreted datasets, it will allow hydraulic modeller to design its HR DEM having a control on which elevation information should be included in it. This is especially relevant for complex environment such as urban and industrial sites, where an important diversity of above-ground elements exists. These techniques are sometimes used in a combinatory way to gather HR datasets in urban areas (Zhou *et al.*, 2004; Abdullah *et al*., 2012). LiDAR and photo-interpreted datasets will be tested in our study in chapter 2. Moreover, HR topographic datasets errors have been briefly introduced in this chapter and within T2 framework, will be detailed in chapter 3 in order to compare impact of errors in HR topographic dataset and modeller choices in HR topographic data integration effects on flood modelling results.

Structured and non-structured approaches are selected as other discretization strategies (AMR) are not commonly used in practical applications. Structured and non-structured meshing processes will be tested to assess if they offer the same possibilities for HR topographic data integration within the 2D hydraulic codes (chapter 2). Idea is to compare performance of these two discretization strategies in terms of accuracy of HR urban flood models building. Moreover, ease of use and computational efficiency will be regarded as well.

Preconceived idea is that photo-interpreted dataset might be efficient for non-structured mesh generation as the data is vectorialized and should offer interesting possibilities for non-structured mesh generation. Another idea arising from the theoretical background would be the assumed advantage of non-structured grid compared to structured ones. Case study studies in chapter 2 will illustrate that these preconceived assumptions are not confirmed.

PART. 2. NUMERICAL MODELLING OF FREE SURFACE FLOW: APPROXIMATING SOLUTION OF SWES

2.1 *FROM HYPOTHESIS IN THE PHYSICAL DESCRIPTION OF THE PHENOMENA TO MATHEMATICAL FORMULATION*

2.1.1 From flow observation to de Saint-Venant hypothesis and mathematical formulation

- **Observation of channel flow to de Saint-Venant hypothesis**

In nature, examples of free surface water flow complexity are observable and numerous (*e.g.* flood event, runoff over urban area, *etc.*). In parallel there are needs for humans to use water resources and to protect themselves from flood hazard resulting from natural intense events. Engineering interest in knowing water stage and discharge along a given canal reach has conducted Barré de Saint-Venant to formulate a simplification framework from observation of flow behavior which lead to an idealistic situation or concept where flow behavior can be described and understood for practical perspectives (de Saint-Venant, 1871).

As reminded in Cunge (2012), basics behind the simplified idealistic situation is to switch from local detailed scale to a more macroscopic (several hundred meters) one. Then, at such a scale the only forces which are considered are gravity, inertial and resistance forces. Therefore, simplification introduced by de Saint-Venant are that *(i)* the water surface is the same over one cross section, *(ii)* it can be considered that flow has one privileged direction and that the flow velocity is the same over one vertical, *(iii)* hydrostatic pressure hypothesis and *(iv)* energy losses can be represented using empirical formula (Chézy like formulas). Originally, validity of this simplified framework is for a flow along an inclined channel of constant slope and cross sections.

- **Shallow Water Equations**

Laws of mechanics can be summed up as three principles: *(i)* mass conservation, *(ii)* variation of momentum and *(iii)* total energy conservation. Applying above mentioned hypothesis to mechanics laws, lead to the Shallow Water Equations system (SWEs) eq. (1). Writing equations system in one dimension over a control volume included between two rectangular cross sections separated by the distance *dx* for a given time interval *dt*; we have:

$$\begin{cases} \partial_t h + \partial_x(hu) = 0, \\ \partial_t(hu) + \partial_x\left(hu^2 + \frac{gh^2}{2}\right) = 0 \end{cases}, \quad t > 0, x \in \mathbb{R}, \qquad (1)$$

where: g is the acceleration of gravity constant, h(*t, x*) the water depth and u(*t, x*) the mean flow velocity. The system of equations of Partial Differential Equations (PDEs) expressed in eq. (1) does not consider any source terms (no friction included here and no variation of topography) and is therefore called a homogeneous writing of the system. Adding source terms eq. (2), the SWEs is called non-homogeneous system and writes as follow in 2D:

$$\begin{cases} \partial_t h + \partial_x(hu) + \partial_y(hv) = 0, \\ \partial_t(hu) + \partial_x\left(hu^2 + \frac{gh^2}{2}\right) + \partial_y(huv) = gh\left(S_{0x} - S_{fx}\right), \\ \partial_t(hv) + \partial_y\left(hv^2 + \frac{gh^2}{2}\right) + \partial_x(huv) = gh\left(S_{0y} - S_{fy}\right), \end{cases} \qquad (2)$$

$I \qquad II \quad III \qquad IV \qquad V$

where, the unknowns are the velocities vector components u(*x, y, t*), v(*x, y, t*) [m/s] and the water height h(*x, y, t*). The subscript x (respectively *y*) stands for the x-direction (respectively *y*-direction). $-S_{0x} = \partial_x z(x,y)$ and $-S_{0y} = \partial_y z(x,y)$ are the ground slopes and S_{fx} and S_{fy} are the friction terms. Component *I* of the momentum equations is the time evolution, *II* is the convection term, *III* is the hydrostatic pressure, *IV* is the transversal component (in 2D only) and the source term *V* includes the slope and the energy loses related to resistance (friction) against channel boundaries.

Analytical solutions of this system of equations exist only for a few theoretical cases where initial and boundary conditions are known (*e.g.* SWASHES library compiling a couple of 1D and 2D theoretical cases, see (Delestre *et al*., 2013)) or in case of backwater curve occurrences. Nevertheless for cases of flood event which are of prime interest for practitioners, no general analytical solution exists. Indeed, the perfect knowledge of information of initial and boundary conditions can only be assumed or approached in applied natural cases. Therefore, from a mathematical point of view, the exact solution of this system cannot be obtained in such a context. Consequently, the exact solution can only be approximated with a numerical method.

As it will be explained in section 1.2, the numerical resolution of SWEs system can be computationally resource demanding. Simplified versions of the SWEs system exist and are made from simplifying hypothesis regarding terms in the momentum equation of the SWEs system. Most commonly used approximate models are the kinematic waves, where the momentum equation (from eq. (2)) is reduced to the expression of the term V, and the

diffusive wave approximation, where the momentum equation then is reduced to termes III+V. Underlying simplification assumptions are restricting the applicability domain of the arising models, but these simplified models are suited for specific problems (Moussa and Bocquillon, 2000):

- kinematic wave, is suited to represent flow transfer in condition where changes in steep slope condition, but fails in case of flat or inverse slope conditions. The Kinematic wave approach is often used in hydrology for water transfer conceptualization modelling *e.g.* in HEC-HMS code (USACE-HEC, 2000).
- Diffusive wave approximation is commonly used for computation when inertial terms effects are negligible with respect to gravitational, friction and pressure terms in case of supercritical flow for instance. Hydrological applications at a catchment scale can be based on this approach that can be coupled with a full resolution of the SWEs in the river bed *e.g.* in Mike SHE code (Abbott *et al*., 1986; DHI, 2007).

- **Properties of the SWEs system and concept of friction for energy dissipation**

Conservation and hyperbolicity are two of the main properties of the SWEs system as explained below. The SWEs system can be written in one dimension under vectorial conservative form in an Euclidian space as follow:

$$\partial_t U + \partial_x F(U) = S(U,t,x),$$

with (3)

$$U = \begin{pmatrix} h \\ hu \end{pmatrix}, F = \begin{pmatrix} hu \\ hu^2 + g\frac{h^2}{2} \end{pmatrix} \text{and } S(U,t,x) = \begin{pmatrix} R - I \\ gh(S_0 - S_f) \end{pmatrix},$$

where U is the vector of conservative variables, F(U) the flux, S(U, t, x) the vector of source terms, R is rainfall source term and I is infiltration source term. This system writes also under the form:

$$\partial_t U + F'(U)\partial_x U = S(U,t,x), \qquad (4)$$

with F'(U) being the Jacobian matrix of F(U):

$$F'(U) = \begin{pmatrix} 0 & 1 \\ -u^2+gh & 2u \end{pmatrix}.$$

Showing that when the water depth is not null, F'(U), is diagonizable according to eigenvalues: $\lambda_1 = u - \sqrt{gh}$ and $\lambda_2 = u + \sqrt{gh}$. These eigenvalues are the propagation velocities of surface waves. In a surface flow, the surface waves will propagate differently depending on the ratio between gravitational and inertial force (Froude number). The Froude number is defined as follow:

$$Fr = \frac{u}{\sqrt{gh}} \qquad (5)$$

where u is the velocity ($m.s^{-1}$), g the acceleration of the gravity constant and h the water depth. Figure 2.1.1 illustrates

- If Fr>1, gravitational force drives the flow properties. Flow regime is qualified as supercritical (or torrential). In this type of flow, surface waves (λ_1 and λ_2) follow the flow direction. We have an upstream control.
- If Fr<1, the mass of the flow drives the flow properties. Flow regime is qualified as subcritical (or fluvial). In this situation, λ_1 and λ_2 move in both upstream and downstream directions. We have a downstream control.
- If Fr=1, flow regime is qualified as critical. A flow cannot be critical over a domain. It can be sub-critical and then it becomes supercritical through a critical point. In that case the flow is said to be transcritical. It often happens over a weir or through a Venturi. After a transcritical flow, we might also have energy dissipation through a hydraulic jump (Figure 2.1). Through a hydraulic jump, flow becomes subcritical.

Figure 2.1.1. Illustrates the flow regime changes where, as previously mentioned, eigenvalues sign changes depending on the type of flow: subcritical, critical or supercritical.

Key points regarding the physical meaning of the celerity, or wave propagation speed, is summarized by Guinot (2012) as follow: "*The celerity is the speed at which the variations in U propagate. A perturbation appearing in the profile of U at a given time propagates at speed of λ. The celerity can be viewed as the speed at which "information", or "signals" created by variations in U, propagates in space*". For someone moving at speed *λ*, *U* is invariant (Riemann invariant), herby reducing the PDEs to ordinary differential equations that are curves along which the perturbation propagates (characteristic curves).

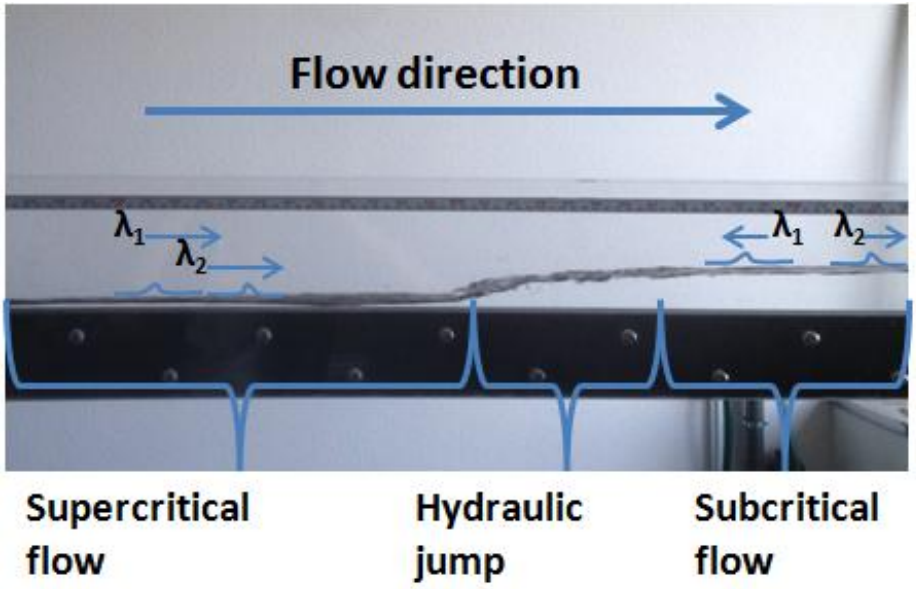

Figure 2.1. *Representation of possible eigenvalues/surface waves direction of propagation depending on the flow regime.*

2.1.2 Validity and limits of these hypothesis

- **Initial and Boundary conditions**

From a mathematical point of view the solution of the SWEs can be approximated over a calculation domain of finite length only if the problem is well-posed. Well-posed problem requires that the solution exists, is unique and that the initial condition that is a "function of the solution" over the domain at time *t=0* is known. Moreover one boundary condition has to be specified for each characteristic that enters the domain at the boundaries during the whole time of calculation (Cunge, 2012; Guinot, 2012). The number of characteristics entering the domain is function of the sign of the eigenvalues that depends on the flow regime. If the flow is supercritical (we have an upstream control), both eigenvalues are imposed upstream. If the flow is subcritical one is imposed upstream and the other one downstream.

Beside for simple cases (*e.g.* canal or backwater curve influence), in real practical cases with the objective to assess flood event extent in 2D, these conditions are seldom fully achieved, due to incomplete knowledge of these initial and boundary conditions.

Transcritical flow occurrences lead to a division of the solution domain in two subdomains separated by a stationary discontinuity. Indeed, as summarized in Sart (2010), transcritical condition leads to sign change in the slowest eigenvalue leading to a so called shock speed. As mentioned in previous section, hyperbolic properties of 2D SWEs allow discontinuous

solutions such as hydraulic jump (Hervouet, 2007), but then a Riemann problem occurs (Guinot, 2012).

- **Parametrisation of energy losses**

In the SWEs system, S_f represents energy losses which are assumed to represent energy dissipation (turbulence). Originally S_f is considered using Chézy empiric formula (eq. 6) or its derivates such as Manning formula (eq. 7). Therefore what has been conceptualized in the SWEs system is energy losses related to resistance (friction) against channel boundary.

$$u = k\sqrt{SR} \quad , \qquad (6)$$

$$u = \frac{1}{n} R^{2/3} \sqrt{S} \, , \qquad (7)$$

$$R = A/P \, , \qquad (8)$$

where u is the flow mean velocity, k is the Chézy coefficient, n is the Manning coefficient, R is the hydraulic radius, A is the wetted area, P is the wetted perimeter and S the slope. It has to be emphasized here that this empirical formulation of energy losses introducing one parameter in the SWEs system has been found to be empirically valid for steady-state flow over experimental channel.

As a partial conclusion, it is impossible to exactly solve the SWEs but only in the best case to approximate solution of the system if, the system is well posed, to guaranty from a mathematical point of view condition of existence of the solution. In fact, in practical cases the boundary and initial conditions are not well known, furthermore important topographic gradient occurs, and wet/dry of cells in 2D overland flow simulations are frequent. These aspects might lead to issues at least in the conservation aspects.

2.2 NUMERICAL METHODS TO APPROACH SOLUTION OF THE SWES SYSTEM

Numerical approaches to solve the set of PDE constituting the SWEs system are numerous (see reviews in Toro *et al*.,1994; Bouchut, 2004; Hervouet, 2007; YU-E, 2007; Novak *et al*., 2010; Guinot, 2012). Aim of this section is modestly to introduce concepts of most commonly used numerical approaches in standard codes. In the context of this thesis this will help reader not familiar with these concepts to understand them and their limitations.

2.2.1 Introduction to concepts for a numerical method

To approach the SWEs (eq. (1) and (2)) system solution, it is required to use numerical methods which allow to reach an approximate numerical solution (Cunge, 2012). Objectives of numerical method step is to approximate the set of PDE as faithfully as possible by a system of equations, where the unknowns are the values of hydraulic variables in a finite number of points (nodes) of the studied domain, and in a finite number of instants during the considered period of time (spatial and temporal discretization). It has to be reminded that numerical models, whichever would be the numerical approach that will be used, can only, in the best case, approximate solution of the original equation. This is related to the discretization and to the incomplete knowledge of the spatio-temporal variation of boundary conditions as mentioned in previous section (2.1).

Then, available methods are: central/semi-implicit, forward/explicit and backward/implicit in space and/or in time.

- With central methods (res. semi-implicit methods), solution at a point x_i (resp. at a time t^n) is calculated from points x_{i+1} and x_{i-1}, to find solution in x_i, (resp. from times t^{n+1} et t^{n-1} to find solution at t^n).
- With forward methods (resp. explicit method), solution at x_i (resp. at t^n) is calculated from solution at points x_{i-1} (resp. t^{n-1}). The numerical solution is then calculated going "forward" in space and/or time.
- With backward methods (resp. implicit methods), solution at x_i (resp. at t^n) is calculated from solution at points x_{i+1} (resp. at t^{n+1}) that are still not known. The numerical solution is then calculated going "backward" in space and/or time.

Properties of a numerical scheme

A numerical scheme is defined as a combination between a choice in the equations, a choice in the discretization strategy and a choice of a numerical method. The application of a numerical scheme should lead to the treatment of the Partial Differential system of Equations (PDEs). In order to ensure the efficiency of a numerical scheme as illustrated in figure 2.2, following properties have to be verified (Lax and Richtmyer, 1956):

- **Conservation:** a numerical scheme has to conserve physical quantities such as mass and momentum.
- **Consistency:** a finite differences scheme or operation is consistent if the scheme reduces to the original differential or partial differential equations as the increment in the independent variables vanish ($dx \rightarrow 0$ and $dt \rightarrow 0$). The difference between the discretized equation and the original equation is called truncation error.

- **Stability:** a stable numerical scheme prevents unlimited growth of numerical errors during computation. This property commonly implies important restrictions on the CFL condition, as the stability of the scheme often depends on it (CFL restriction is then a necessary condition but not sufficient to insure existence of stability). There are different ways to study the stability of a numerical method: *e.g.* a Von Neumann/Fourier stability analysis which is based on a Fourier decomposition of the the numerical error. The stability can also be studied considering the positivity preservation of some variables (such as water height, a pollutant concentration, *etc.*). A checking of the TVB (Total Variation Bounded) can also be performed to control that the overall amount of oscillation remains bounded. Most of the stability criteria are equivalent and conduct to the CFL condition.
- **Convergence:** the discrete solution U approaches the exact solution U (x, t) of the differential equation at every point and time of the space when *dx* ➔ 0 and *dt* ➔ 0. The equivalence theorem of Lax (Lax and Richtmyer, 1956) states that for a correctly posed initial value problem and a consistent discretization, stability is a necessary and sufficient condition for convergence.

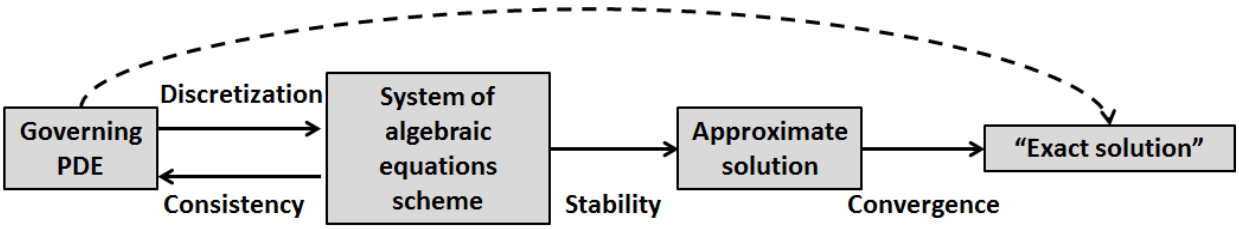

Figure 2.2. *Schematic view of necessary properties of a numerical scheme.*

The numerical method can introduce mathematical terms not originally present in the equations, which are terms introducing numerical diffusion and/or dispersion. Numerical diffusion and dispersion phenomena will respectively smooth and create spurious oscillations in the numerical solution (as shown in figure 2.3).

As explained for the convergence, a numerical result can be improved by increasing the number of cells and thus by decreasing the space step along with the time step. However, it is not always feasible due to lack of data, to important CPU cost, *etc.* Thus, the convergence can be increased and the truncation error decreased by increasing the order of the numerical method.

$$\epsilon = f(\Delta t^{\alpha}, \Delta x^{\beta}), \qquad (8)$$

where ϵ is the truncation error and then the scheme is said to be of order α in time and of order β in time. There are different ways to increase the order of a scheme which will depend on the type of scheme used (finite differences, finite elements or finite volumes).

As previously mentioned, without the source term (homogeneous system), the SWEs system, can be written as a system of two transport equations where the transport velocities are the eigenvalues $\lambda_1 = u - c$ and $\lambda_2 = u + c$ (where u is the velocity of the fluid, and $c = \sqrt{gh}$ the wave velocity). Depending on the flow regime, the surface waves can go either upstream and downstream (subcritical or fluvial flow) or both can go downstream (supercritical or torrential flow). Therefore, all the information in case of a torrential flow go downstream whereas, in a fluvial flow, information goes both upstream and downstream. Numerical schemes can be built in order to detect the direction (sign) of the characteristics to be purposely decentered (backward or forward) depending on where the information is coming from. This category of numerical scheme is called upwinded.

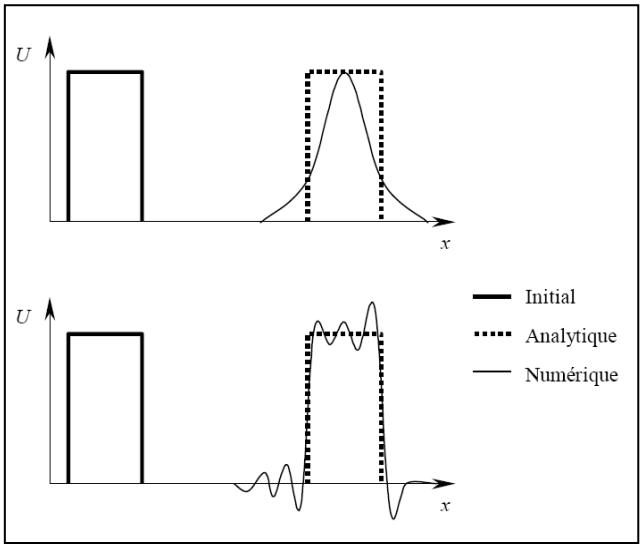

Figure 2.3. *Effects of numerical diffusion (up) and numerical dispersion (down) over profile under convection (from Guinot, 2005).*

2.2.2 Standard numerical methods

Various numerical methods exist to approximate the solutions of the SWEs. The most commonly used methods, namely finite differences, finite volumes and finite elements methods, are introduced in this section.

Finite differences

Finite differences method is a numerical technique built to approximate solutions of PDE. A finite space of grid functions is defined and equations of the continuous function are

converted to algebraic equations (using Taylor series development or the definition of the derivative). It results in a discretized form of the SWEs system. A relationship equation or system (numerical scheme) linking the values of the unknowns at the considered discrete points (close enough) is solved using computers algorithm. This numerical method has been historically the first numerical method to be used in hydraulics due to its stability (under conditions, see below), its robustness and simplicity. Moreover in terms of practical implementation, finite differences schemes allow swift computation due to the simplicity of matrix manipulations that are often diagonalizable (*e.g.* Abbott-Ionescu or Preissmann schemes). Drawback of finite differences method is, as it will be explained later, that linearized approaches have difficulties to treat discontinuities in the solution domain that occur in case of transcritical flow followed by hydraulic jump, due to the inherent hyperbolic nature of the SWEs system.

Designed finite differences schemes have to produce a well-posed problem. Depending on the scheme, it would require different number of points for computation and different numbers of discretized equations have to be provided along with the correct number of boundary conditions to close the problem. Illustration can be given with the space centered, time implicit Preissman scheme developed in the 60's for hydraulic applications (Cunge and Wegner, 1964; Cunge, 1966; Cunge *et al*, 1980). Under fully explicit writing, the values of the two unknowns flow variables of the SWEs (*e.g.* h and u under non-conservative form) at time t+1 can be calculated depending on their values at time t at points x-1 and x+1. Nevertheless this means that stability of such explicit approach mainly depends on CFL limitation, requiring:

$$dt < \frac{dx}{\sqrt{gh}+|u|} \qquad (9)$$

Interest of Preissmann scheme relies on a time implicitation coefficient: θ. This coefficient can range between 0 and 1. Preissmann scheme writes as following:

$$\frac{\partial_f}{\partial_t} = \Phi\left(\frac{f_{i+1}^{n+1} - f_{i+1}^{n}}{\partial_t}\right) + (1-\Phi)\left(\frac{f_{i}^{n+1} - f_{i}^{n}}{\partial_t}\right),$$

$$\frac{\partial_f}{\partial_x} = \theta\left(\frac{f_{i+1}^{n+1} - f_{i}^{n+1}}{\partial_x}\right) + (1-\theta)\left(\frac{f_{i+1}^{n} - f_{i}^{n}}{\partial_x}\right), \qquad (10)$$

$$f(x,t) = (1-\theta)[(1-\Phi)f_{i+1}^{n+1} + \Phi f_{i}^{n+1}] + \theta[(1-\Phi)f_{i+1}^{n} + \Phi f_{i}^{n})]$$

θ is here the time implicitation level of the scheme and Φ the spatial weighting fixed to 0.5 in this scheme. θ = 0 bring the scheme back to an explicit formulation. $0<\theta<0.5$ is unstable if CFL value is greater or equal to 1. For $0.5<\theta<1$, the scheme is unconditionally stable. Consequently the time step *dt* can be chosen freely. As Φ is fixed to 0.5, the two unknown flow variables derivatives are computed at the same computational grid points. Consequently, as observable in figure 2.4, f(x,t) is always calculated using four nodes. The schemes of Preissmann type have advantages over other schemes (*e.g.* Abbot-Ionescu scheme), because they allow grids with variable *dx* and compute both the discharge and the water level at the same point (Chau, 1990). Bi-diagonalizable matrices are therefore produced allowing easy algorithmic treatment instead of for instance tri-diagonalizable matrices for Abbot-Ionescu scheme (see Abbott, 1963; Abbott *et al*., 1973).

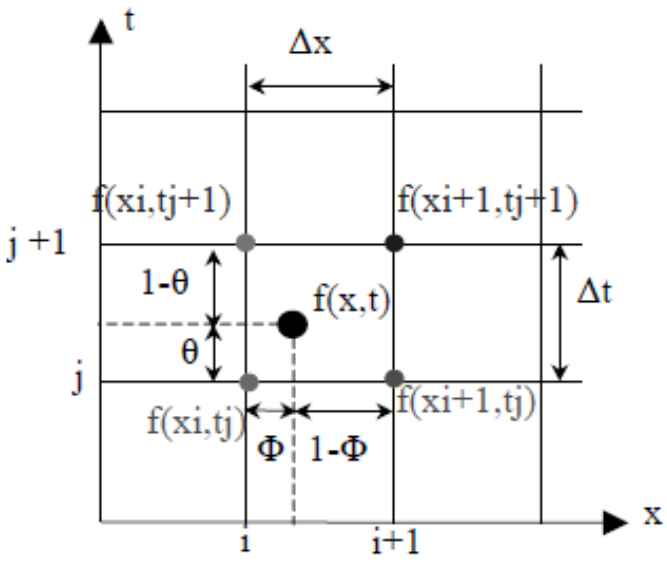

Figure 2.4. *Preissmann discretization scheme (from Ouarit, 2004).*

One of the widely spread numerical method relying on finite differences applied to 2D free surface hydraulic codes is the Alternating-Direction Implicit (ADI) using a structured grid for discretization. For instance Mike 21 code (see section 2.3 of this chapter and (DHI 2007a) for code description) is based on the resolution of 2D SWEs. ADI method proceeds in two stages, treating only one operator implicitly at each stage. First a half-step is taken implicitly in one direction (*e.g.* x direction) and explicitly in the other direction (y direction). Then a half-step is taken implicitly in the y direction and explicitly in the x direction. Idea is to obtain a method less sensitive compare to an explicit method to CFL criteria and compare to a fully implicit method in 2D (such as the Cranck-Nicholson scheme), ADI method produces tri-diagonal matrix of solution to compute at each step which are computationally not costly to handle and therefore allows swift and efficient computation.

It has to be enhanced that general drawback of some finite differences method is that their linearization lead to issues to handle transcritic flow occurrence due to appearing ill-posed problem see Meschel and Holly (1997). Adaptation of scheme to handle transcritical flow occurrence exists (Meschel and Holly, 1997; Sart *et al*., 2010). In 2D, ADI scheme has a drawback related to time splitting technique: in case of divergent flow, it will create mass and oscillation in the solution if no specific numerical treatment is added (Guinot, 2000).

Finite volumes

Finite volumes methods are particularly suited to SWEs system properties conservative and hyperbolic properties as explained below. In finite volumes, spatial discretization can use either structured mesh *e.g.* in FullSWOF_2D code or non-structured mesh *e.g.* in TELEMAC-2D or Mike 21 FM codes (these codes are introduced in the 2.3 section of this chapter).

Finite volume methods are indeed conservative as the integral/balance are calculated over volumes/cells, consequently constructing a conservative method (Bouchut , 2004), eq.11.

$$\int_{t^n}^{t^{n+1}} \int_{x_{i-1/2}}^{x_{i+1/2}} (\partial_t U + \partial_x F(U)) dx dt = 0 \qquad (11)$$

where U is the vector of conservative variables, F(U) the flux. Development of this double integral depends on the finite volume methods. We can get the following explicit scheme in time:

$$\frac{(U_i^{n+1} - U_i^n)}{dt} + \frac{(F_{i+1/2}^n - F_{i-1/2}^n)}{dx} = 0 \qquad (12)$$

The hyperbolic property of the SWEs (see section 2.2) is handled in the finite volume method using the rewriting of the system under the form of a Jacobian matrix. This matrix can admit two eigenvalues (λ_1 and λ_2). As previously mentioned, depending on the flow regime, the eigenvalues will propagate in different ways. As a reminder, both eigenvalues propagate downstream in case of a supercritical flow whereas one eigenvalue propagates downstream and the other one upstream, in case of subcritical flow regime. Therefore, for a numerical flux, the information has to be considered depending on where it is coming from. For the boundary conditions of the system, scheme imposes one of the conservative variables following the inflow characteristic (generally a discharge upstream and a water level downstream) and the other variable is calculated thanks to the other characteristic coming from the inside of the domain (Bristeau and Coussin, 2001). Following the same principle at the interface of each cell, an average is calculated between each sides of the cells interface. Many Riemann solvers or numerical fluxes exist like the Godunov solver,

which requires heavy workload for its implementation or approximating Rieman solvers like Rusanov, Roe, HLL. These approximating solvers upwind the fluxes depending on where the information comes from. Moreover, most of these solvers check the Rankine-Hugoniot relation and are therefore able to treat discontinuities in the solution (*e.g.* hydraulic jump).

Transcritical flow, wet/dry transitions and steady states are difficult to handle for Finite volume numerical fluxes. Explanations and methods adaptations to these numerical challenges are explained below.

For transcritical flows, when Fr=1, (when a sub critical flow becomes supercritical through a critical point) one of the eigenvalue is null and a stationary wave occurs. Some of the Riemann solvers can provide a solution (non-entropic solution) with a non-physical discontinuity. Roe solvers have this default; methods exist to correct this default.

Wet/dry transitions lead to the situation where at one side of the interface the water depth is positive and on the other water depth is null. It is well known that with a centered finite difference scheme the positivity of the solution cannot be guaranteed. This might occur as well with the finite volume numerical fluxes. It has been proven (see Bouchut, 2004) that HLL solvers and Rusanov are positivity preserving. Another commonly used treatment is to fix a low threshold value to fill up the dry cell to allow the computation to ensure the positivity at wet/dry transition (*e.g.* this solution is used with Mike 21, Mike 21 FM codes; see section 2.3 of this chapter). Drawback of such treatment is the possible mass creation in the system.

Stationary/permanent regime states lead to numerical difficulties for the numerical fluxes computation. For instance if a hydrostatic equilibrium is reached (u=0 and h+z =constant), there is an equilibrium between the flux of the pressure term and the sources term that include the topography (*z*). This represents an issue for preserving steady states at rest that can create spurious oscillation. Indeed, as identified in Bermudez and Vazquez (1994), due the upwind treatment of the hydrostatic fluxes term that is not applied to the topography fluxes term that is still centered. Solution of a so called *well-balanced* method (Greenberg and Leroux 1997) is to upwind the computation of the topography fluxes the same way as hydrostatic pressure fluxes are upwinded. Nevertheless, this will affect the positivity preservation property of the scheme and a technique has to be implemented to ensure positivity preservation of the scheme. Hydrostatic reconstruction can solve this issue (Audusse *et al.*, 2004; Audusse and Bristeau, 2005). Codes such as TELEMAC-2D or FullSWOF_2D method are based on well-balanced scheme properties including a rewriting of the SWEs using a hydrostatic reconstruction leading to an oscillation free and permanently positivity solution (Audusse *et al*., 2004; Delestre, 2010).

Finite elements

A finite elements method relies on the analysis of the PDEs systems. Each system of PDEs has its own specificities and cases can be really different. Like for the finite differences and finite volumes method, the finite elements method is based on the discretization of the computational domain in points (or nodes) that forms the computational grid cells. The FE method uses a series of basis functions in each cell to approximate the solution of the discretized PDE. Main steps of the finite elements method are:

1. discretization that can be non-structured;
2. definition of de basis function (polynomial approximation functions) that will be used at every cell to approximate the solution to create a stiffness matrix, but with the constraint to reach the “exact” solution (minimizing the error) at the boundaries of the cell (nodes) and that will have a value equal to zero for all the other cells of the domain;
3. look for an approximate solution of the whole system through the use of coefficients to move from basis function element equation to approximate functions;
4. consider the boundary conditions;
5. computation of matrices and vectors to get the gradients; solving the system.

Advantages of finite elements methods are that they allow non-structured discretization use and swift computation. Drawback of numerous finite methods, is that being linear, they are not suited to treat accurately occurrences of discontinuities in the solution. Finite elements methods dealing with this type of issues exist: for instance, methods relying on a Stream Upwind Petrov Galerkin (SUPG) scheme, upwinding the basic functions in order to account for the flow direction in the discretization of the advection terms as described in Bates (1999). SUPG can be interpreted as an artificial diffusion stabilizing a centered scheme. In 2 dimensions, by the effect of scalar product this diffusion applies only in the direction of the current.

Moreover, the SUPG method uses linear functions, but they can be discontinuous, allowing to treat discontinuities (due for instance to flow regime change) and keep at the same time their conservative properties (Hervouet, 2007). SUPG like method is one of the possible finite elements method that can be used in TELEMAC-2D (see section 2.3).

2.3 TESTED COMMERCIAL NUMERICAL CODES FOR HR TOPOGRAPHIC DATA USE

The aim is to test different spatial discretization standard strategies - structured and non-structured - and several numerical methods for HR topographic data use in 2D HR flood modelling. The standard codes used in the thesis are briefly described here.

Mike 21 code is developed and commercialized by the Danish Hydraulic Institute (DHI). Mike 21 is based on the resolution of 2D SWEs.. The mass conservation equation and the set of two Cartesian coordinate momentum equations are solved using finite differences approximation on a structured grid (DHI, 2007a). This category of numerical method, when satisfying smoothly varying flow conditions, has the ability to handle previously mentioned numerical discontinuities (Lax and Wendroff, 1960; Liang *et al*., 2006). Mike 21 code uses an alternate direction implicit (ADI) method to resolve SWEs (DHI 2007a). Usually, ADI methods are not considered to perform well in the case of transcritical flow occurrence (Meselhe and Holly 1997; Madsen *et al*., 2005; Liang *et al*., 2006). Nevertheless, modifications have been implemented in the Mike 21 ADI scheme by DHI, as presented by McCowan (2001), switching from central to upwind treatment of the convective terms of momentum equations in the case of change from infra to supercritical flow. This method adds a selective numerical dissipation in the case of supercritical flow, thereby reducing spurious numerical oscillation, and therefore increasing the calculation stability, but locally reducing its accuracy.

Mike 21 FM is developed and commercialized by the Danish Hydraulic Institute (DHI). Mike 21 FM is based on 2D SWEs resolved on a non-structured mesh with a Godunov' spatially centered finite volume scheme. An approximate Riemann problem solver (Roe) is used to calculate fluxes at each cell interface. This category of scheme can numerically handle treatment of discontinuities. The numerical scheme is space upwinded combined with a TVD-MUSCL slope limiter (to increase the order of the scheme in space) and time centered using explicit Euler (first order) or Runge-Kutta (second order) methods (DHI 2007b) are solver options available and tested with the software.

TELEMAC-2D is developed by EDF & TELEMAC-MASCARET consortium and can use either finite volumes or finite elements methods to approximate solutions of the SWEs system. In both cases, non-structured grids are used for the spatial discretization. Finite volumes method has been built with a "well-balanced" scheme including a rewriting of the SWEs using a hydrostatic reconstruction leading to an oscillation free and permanently positivity of the solution as described in Audusse (2004) and in Hervouet (2007). Tested TELEMAC-2D finite elements method relies on a fractional step method (Marchuk, 1975; Hervouet, 2007), where advection terms are solved initially, separately from propagation,

diffusion and source terms, which are solved together in a second step. Several finite element scheme can then be used. Stream Upwind Petrov Galerkin (SUPG) numerical scheme, decentring the basic functions in order to account for the flow direction in the discretization of the advection terms. This type of schemes has been shown to result in significant savings in both computational time and core storage (Bates *et al*, 1997). Other Finite elements schemes implemented in TELEMAC-2D were not tested here. A specific treatment has been added in case of finite elements method use to ensure positivity of the solution.

FullSWOF_2D. for Full Shallow Water equation for Overland Flow in 2 dimensions, is a code developed as free software based on 2D SWEs (Delestre *et al*., 2012, 2014). In FullSWOF_2D, the 2D SWEs are solved using a well-balanced finite volume scheme based on the hydrostatic reconstruction (see Audusse *et al*., 2004; Delestre,*et al*., 2010). The finite volume scheme is applied on a structured spatial discretization using regular Cartesian meshing. For the temporal discretization, based on the CFL criterion, a variable time step is used. The hydrostatic reconstruction (which is a well-balanced numerical strategy) allows to ensure that the numerical treatment of the system preserves water depth positivity and does not create numerical oscillation in case of a steady state, where pressures (in the flux) are balanced with the source term (the topography). Different solvers can be used HLL, Rusanov, Kinetic (Bouchut, 2004), VFRoe-ncv combined with first order or second order (MUSCL or ENO) space reconstruction.

Computational aspects

Fine meshes in case of HR modelling imply high computational costs. One solution to overcome this problem consists in parallelizing computation codes. Parallelization is a coding method which allows several calculations to be carried out simultaneously. This is based on the principle that large computations can often be divided into smaller ones and then solved in parallel. Parallel architectures have become dominant for all computers since the beginning of the 2000s.

Mike 21 code solves ADI method using sequential CPU solution algorithm (Thomas algorithm). Development is in progress at DHI and in latest version of the code to include GPU-accelerated solvers for Mike 21 (Aackermann *et al*., 2013). Mike 21 FM uses shared memory (open MP) and distributed memory (Message Passing Interface: MPI) architecture. These parallelisation methods rely on METIS domain decomposition algorithm (Karyps and Kumar, 1998; Sørensen *et al*., 2010) where computational domain is divided in sub-domains and where each CPU will compute solution for a given sub-domain. The exchange between sub-domains is computed using "*halo-cells*" (Sørensen *et al*., 2010). TELEMAC-2D is

parallelized using MPI. PARTEL is the utility used to proceed to mesh partitioning. PARTEL relies on METIS utility (Audouin *et al*., 2011). For FullSWOF_2D, two parallelization methods exist (Cordier *et al*., 2013). The first one is based on master-slave architecture using MPI library (Brugeas, 1996; Em Karniadakis and Kirby II, 2003) and the second one uses the implicit skelett parallelism library SkelGIS (Skeletons for Geographical Information Systems see Cordier *et al*., 2013; Coullon *et al*., 2013; and Coullon and Limet, 2013). Only the MPI version is used in this thesis work.

Mike 21 and Mike 21 FM cannot be implemented under Linux system and it seems therefore less flexible than TELEMAC-2D and FullSWOF_2D to implement them under High Performance Computing environments that are often used under Linux operating system.

CHAPTER I CONCLUSIONS: FORESEEN CHALLENGES RELATED TO HR TOPOGRAPHIC DATA USE WITH 2D SWES BASED NUMERICAL MODELLING CODES

High-resolution topographic datasets: perspectives and challenges

For the spatial extent of our applications, which are urban and industrial sites 2D HR overland flow modelling, principles of LiDAR and photogrammetry technologies were presented. Under the compromised framework between spatial extent and HR, the different combinations between aerial vectors (*e.g.* drones, specific plane or helicopter flights) and LiDAR or photogrammetry can lead to similar level of accuracy that can reach a few centimeters. All these combinations are therefore excellent information to produce datasets including fine concrete features influencing overland flow in case of flooding.

Qualitative difference between LiDAR and Photogrammetric based HR datasets rely in the interpretation/classification possibilities. Photo-interpreted dataset offers a broader range of possibilities for HR DEM design, in accordance with comprehensive descriptions of the above-ground structures that will influence overland flow. Indeed classification of above-ground features being more extensive in photo-interpreted datasets, it will allow hydraulic modeller to design its HR DEM having a control on which elevation information should be included in it. This is especially relevant for complex environment such as urban and industrial sites, where an important diversity of above-ground elements exists and where not all above ground elements have to be included in the model. Indeed a part of above ground elements are included in the HR dataset (*e.g.* elevated roads, fences, bridges, *etc.*) and will artificially block overland flow if included in the model. Nevertheless to get a satisfying level of quality in the photo-interpretation procedure, it requires to perform the photo-interpretation through manual operators process, this makes the photo-interpretation time consuming and costly. Difference arises as well regarding cost that will mainly vary as a function of the spatial extent to cover, which will impact the choice of the aerial vector and the duration of the campaign.

Issue that is likely to arise for hydraulic modeller is that to design HR DEMs, HR datasets manipulation, to remove flow blocking structures or to add overland flow influencing structures for instance, might be challenging on standard computers. Moreover, it raises question up for ease of use of HR DEM for structured and non-structured grid generation to include properly the detailed elevation information within codes. In case of structured grid, the number of computational points might be extremely important. Moreover in case of non-

structured mesh generation, standard algorithms might not be suitable to highly constrained environments such as dense urban or industrial environments. These aspects are studied in chapter 2.

Validity and feasibility of the approach

SWEs are originally valid for a given conceptual framework. The background of the theoretical framework of SWEs system was summarized in the second part of this chapter in order to raise questions up regarding validity of the approach of 2D SWEs based overland flow modelling over complex environments.

From a practical/operational point of view, SWEs based codes are already broadly used over urban environment, even though theoretical questions regarding several conceptual and mathematical aspects remain open. Indeed such application framework is far from the one for which SWEs have originally been designed for, and it stresses out the fact that limits might be expected and encountered. The HR description of an industrial or urban environment will make sharp topography gradient arise in the computation grid where overland flow occurs and has to be computed. Moreover, boundary conditions and initial conditions are seldom properly known, notwithstanding the fact that the empirical formulation of energy losses coefficient might not be valid anymore in such a context. Not all the numerical methods are able to properly handle these high gradient occurrences, wet/dry transition and the discontinuities related to flow regim changes.

By reducing even more the spatial discretization level (computational grid resolution) over complex environments that have steep slope, trend is to try to reach back the gradually varying slope that was the original framework for SWEs. To a certain extent it is the case but, *(i)* sharp gradients still occurs due to fine above ground features inclusion and *(ii)* reducing too much the discretization would drastically increase simulation computational time.

With HR topographic datasets, spatial discretization process (meshing generation process), it is predictable that it will often leads to operational choices from the modeller to reach an optimal balance between dataset ease of use, accuracy and time consumption aspects.

CHAPTER II – CASE STUDY OF HIGH-RESOLUTION TOPOGRAPHIC DATA USE WITH 2D SWES BASED NUMERICAL MODELLING TOOLS

Part of this chapter has been published as:

Abily, M., Duluc, C.-M., Faes, J. B., & Gourbesville, P. (2013). *Performance assessment of modelling tools for high resolution runoff simulation over an industrial site*. Journal of Hydroinformatics, 15(4), 1296-1311.

Abily, M., Gourbesville, Andres, L., & Duluc, C.-M. (2013). *Photogrammetric and LiDAR data for high resolution runoff modelling over industrial and urban sites*. In Zhaoyin, W., Lee, J. H.-W., Jizhang, G., and Shuyou, C., editors, Proceedings of the 35th IAHR World Congress, September 8-13, 2013, Chengdu, China. Tsinghua University Press, Beijing.

Abily, M., Duluc, C.-M., & Gourbesville, P. (2014). *Use of Standard 2D Numerical Modeling Tools to Simulate Surface Runoff Over an Industrial Site: Feasibility and Comparative Performance Survey Over a Test Case*. In Advances in Hydroinformatics,19-33. Springer Singapore.

Abily, M., Delestre, O., Amosse, L., Bertrand, N., Laguerre, C., Duluc, C.-M & Gourbesville, P. (2014). *Use of 3D classified topographic data with FullSWOF for High Resolution simulations of river flood event over a dense urban area*. 3rd IAHR Europe Congress, Book of Proceedings, 2014, Porto, Portugal.

Abily, M., Scarceriaux, C., & Duluc, C.-M. (2015*). Ruissellement de surface en milieu urbain: stratégies d'intégration de données topographiques haute résolution en modélisation hydraulique 2D.* Techniques Sciences Méthodes, (5), 31-46.

The optimal integration of high definition or High-Resolution (HR) Digital Elevation Model (DEM) is challenging in terms of feasibility of data integration within standard codes solving Shallow Water Equations (SWEs) system in 2D. As explained in chapter 1:

- HR description of an urban environment will make sharp topography gradient arise in the computation grid (mesh) where overland flow occurs with flow regime changes and frequent wet/dry transitions. This goes beyond the framework for which SWEs hypotheses were conceptualized. Moreover, from a numerical point of view, not all the numerical methods are able to properly handle these high gradient occurrences.
- Above-ground features influencing overland flow paths comprehensively integrated the same way in DSM generated based either on LiDAR or on photo-interpreted datasets.
- With HR topographic datasets, spatial discretization (meshing generation process), often leads to operational choices from the modeller to reach an optimal balance between dataset ease of use, accuracy and time consumption aspects. Moreover in case of non-structured mesh generation, standard algorithms might not be suitable to highly constrained environments such as dense urban or industrial environments.

Consequently, possibilities and challenges of fine surface features inclusion in highly detailed 2D overland flow models for flood hazard assessment deserves a specific consideration. As a reminder, one of the objectives of this thesis (target one: T1) is to tackle the problem of HR topographic information inclusion in standard 2D modelling tools, as well as to assess specifically possibilities and impacts of fine features inclusion in detailed flood models. This category of modelling tool has various numerical strategies to approximate 2D SWEs solution and they discretize the spatial information in different ways (see chapter 1, section 2.3).

This chapter presents tests performed using dissimilar sets of DSM, created based on different HR topographic datasets. Several standard 2D numerical modelling tools solving 2D SWEs are used. The created overland flow models are built using HR topographic data gathered from *(i)* a LiDAR and *(ii)* a photogrammetric campaign. For our interest focus is placed on assessing possibilities and limits of strategies for spatial discretization used by modelling tools, exploring HR DSM use with regular grid meshing and non-structured meshing approaches. Different types of urban flooding scenarios - local intense rainfall and river flood event – leading to different types of challenges (regarding numerical stability of HR topographic data integration) are carried out at different scales. Three case study are included in this chapter that is divided in two parts.

The first part of this chapter **(part 3)** aims to test the feasibility of HR topographic data use with approaches based on scenarios purposely going beyond hypothesis of the 2D SWEs domain of validity. This part is based on a study that has been directly conducted for IRSN to test the feasibility and relevance of local intense rainfall event flood risk numerical modelling using standard 2D SWEs based codes. The case study is small fictitious industrial site (60,000 m²) with a 0.1 m resolution DSM. This level of resolution is compatible with what could be expected for a DSM that would have been specifically gathered at the spatial extent scale of such type of site - *e.g.* using UAV flight. Different scenarios of local intense rainfall events are simulated. Interest is notably that runoff over industrial site might have flow regime changes, large flooding/drying areas, as well as small water height properties. This makes the use of standard codes relying on 2D SWEs particularly challenging. Indeed, numerical treatment of these properties might not be specifically supported by the codes. Accordingly, an assessment standard 2D SWEs based numerical tools use for such a purpose should to be studied in detailed to evaluate feasibility, performance and relevance of their use.

The second part of the chapter **(part 4)** aims to confirm the feasibility and to asses possibilities and impact of fine features inclusion in detailed 2D flood modelling. In the first place, intense rainfall events scenarios are simulated over a larger scale (600,000 m²) real industrial site in Nice city (France). In this test case, the used DSMs are built using a LiDAR and a 3D photo-interpreted dataset. Eventually in this part, using the 3D photo-interpreted topographic dataset at a large scale (17.8 km²), a river flood event is simulated at HR for a flood scenario over the low Var valley in Nice .

PART. 3. HIGH-RESOLUTION RUNOFF SIMULATION AT AN INDUSTRIAL SITE SCALE

A guide for nuclear power plant protection against flooding risk (ASN, 2013) has been elaborated by the Institute for Radioprotection and Nuclear Safety (IRSN) for the French safety authority (ASN). The guide defines a set of Reference Flood Situations (RFS) to consider for safety assessment of facilities having nuclear activities (Duluc *et al*., 2014). This guide notably includes a RFS defining a framework for intense pluvial generated runoff risk assessment. This RFS recommends that a plant has to be able to cope with a one hour long rainfall event with a hundred year return period, meanwhile sewer system network is considered as locally non available. Through this RFS, the aim is to consider two possible aspects in safety failure, which might occur during an intense rainfall event scenario: *(i)* a clogging of sewer network access, and *(ii)* a possibility of rainfall events occurrence exceeding the return period for which the sewer system were designed.

Different approaches for the runoff RFS application are possible:

- A spreading of the cumulated rainfall volume over the industrial site might be an approach to be considered for flat sites, to identify pounding areas. It should be noticed that this quantitative approach does not take hydrodynamic aspects into consideration.
- Another approach could be, using fine topographical data, to identify main drainage path and pounding areas. This method is rather qualitative and does not integrate quantitative aspects.
- Numerical modelling of runoff as a free surface flow is a practice often used at larger scale for flood risks assessment and might be applied for runoff over High-Resolution topography studies.

Nowadays techniques for HR topographic dataset are becoming commonly used and gaining ground of standard numerical modelling tools use for surface runoff component modelling at HR is observed (Ciliberti *et al*., 2008; Gomez *et al*, 2011; Gourvbesville, 2014). Actually, techniques such as Light Detection And Ranging (LiDAR) (Mandlburger *et al*., 2008; Aktaruzzaman and Schmidt., 2009; Erpicum *et al*., 2010; Fewtrell *et al*., 2011) and photogrammetry (Remondino *et al*., 2011; Leitão *et al*., 2015) can be mounted on Unmanned Aerial Vehicle (UAV) to produce Digital Elevation Models (DEMs) with a resolution consistent enough to finely represent surface drainage influencing structures, *e.g.* walls, sidewalks, curbs, etc. (see chapter 1, Part 2). Nevertheless, water runoff over an industrial site might

have rapid changes in flow regime and high gradient properties, representing numerical challenges for standards modelling tools. Moreover, if HR topographic data integration within hydraulic models might be interesting to represent small scale structures that affect surface flow patterns, issues might be encountered for these data uses with standard numerical modelling tools. Taking these aspects into consideration, the research presented in section of the chapter II investigates on relevance and feasibility of standard 2D numerical modelling tools use within the recommended runoff RFS context. The use of these tools for a purpose different from the ones for which they were designed for raises questions up about relevance of such an approach.

The objective of the test case based study presented in this part is to point out feasibility, relevance and limits of standard 2D numerical modelling tools use for HR runoff modelling in a context where the runoff dynamic and the overland flow maximal water depth have to be evaluated with a high accuracy. At a broader picture scale, objectives of this part are both, to tackle the feasibility of HR topographic information inclusion in standard 2D modelling tools, and to point out what should be regarded in methodology for HR models optimization and for reliability assessment.

For our purpose, standard industrial codes solving 2D SWEs using either structured grid (Mike 21) or non-structured grid (Mike 21 FM) are used (see chapter 1, section 1.3). Moreover, for comparison purpose, an OpenFOAM (distributed by OpenCFD *Ltd*) based on tri-dimensional Finite Volume Method (3D FVM), using pre- and post-processing tools developed by Néodyme Company is tested as well.

The comparison is based on water level calculation which is our parameter of interest. Parameter of interest and a selection of indicators of computation reliability (mass balance, CFL number, velocities and characteristic time) are compared to point out performances and limits of each modelling tool. This comparison is done over a selection of points of interest and over the industrial site domain.

- Section 3.1 introduces and presents the test case and its setup.
  The different types of numerical modelling approaches, the test case configuration and the strategies used for its spatial discretization, the runoff scenarios and lastly the performance assessment methodology are described in this section.
- Section 3.2 presents results, performance comparison and limits of tested numerical modelling tools.
- Section 3.3 discusses and raises up a feedback on validity, limits and relevance of standard numerical modelling tool performance for HR runoff modelling in the RFS

context. Discretization possibilities and high topographic gradient occurrences are discussed along with numerical issues related runoff modelling and with computational reliability. Lastly in this section, a comparison is opened with other tests that have been conducted with other codes relying either on 2D SWEs (TELEMAC-2D, FullSWOF_2D) or on diffusive wave approximation (Mike SHE).

3.1 TEST CASE SETUP

3.1.1 Presentation of mathematical and numerical approaches

The objective of the analysis is to assess possibilities and performances of standard commercial and open source modelling tools use for runoff scenarios computation over the High-Resolution test case. A detailed industrial topography (introduced in section 3.1.2) results in representation of flow obstacles that may leads to rapid changes of flow conditions (*e.g.* flow regime change, hydraulic jumps, flooding/drying, flood waves etc.). As 2D SWEs are hyperbolic partial differential equations, mathematical discontinuities represented by these rapid flow changes can be treated by these equations under certain conditions (Audusse *et al.*, 2004; Liang *et al*., 2006). Moreover, a fully 3D model can compute solutions for these flow specificities, but it usually requires high computational cost. The three modelling softwares tested for our study are: Mike 21, Mike 21 FM and NEODYME's 3D FVM.

Mike 21 and Mike 21 FM are based on the resolution of 2D SWEs. These codes were presented chapter 1, section 2.2 with all other codes approximating the 2D SWEs. Let us recall here that Mike 21 uses a finite difference method on a regular grid (DHI, 2007a). Mike 21 code uses an Alternate Direction Implicit (ADI) method to resolve SWEs equations (DHI 2007a). Mike 21 FM is based approximate the 2D SWEs on a non-structured mesh with a Godunov' spatially centred finite volume scheme. An approximate Riemann problem solver (Roe) is used to calculate convective fluxes at each cell interface. Time integration is performed thanks to a first order Euler method (DHI 2007b).

Neodyme's 3D FVM (Versteeg, 2007) is based on the Navier-Stokes equations (NSE) solved under their integral form. This method requires the discretization of the computational domain into elementary volumes (cells). Numerical resolution of the NSE in each cell is carried out by using the OpenFOAM suite (Hervoje, 1996). OpenFOAM is an open source computational fluid dynamic code containing C++ libraries designed to solve systems of partial differential equations encountered in fluid dynamic field (among others). From this OpenFOAM code library, the solver 'interFoam' was used for this study (Henrik, 2002). This solver is based on the volume of fluid (VOF) method (Gopala and Wachem, 2008) which requires the resolution of equations of conservation for the two considered phases (air and water). The fluids physical properties are thus calculated from the volume fraction of each fluid in each cell. Near the water surface, the air-water interface is not marked by a sharp discontinuity. Thus, the modelling of the liquid surface is enhanced by an artificial interface compression term. This solver use is proved to be very efficient in simulating free surface flow, for cases where the fraction of liquid in the domain is not negligible. In the present case,

a very narrow layer of water covers the ground of a large environment. That is not a standard case, and the solver used has not been tested on this type of environment. Therefore it leads to different type of limits in this method use. Physical difficulties are those encountered to find the optimum turbulence model and an adjustment of the roughness parameters (used to take care of sub-grid scale details) to fit experimental results. Such kinds of aspects were not explicitly treated here and standard values of the parameters have been set to carry the run test. Geometrical construction and meshing difficulties occur as well. Indeed, this method provides a field whose resolution depends on the 3D ground surface mesh resolution, but is able to capture any small height of water. Pre- and post-processing tools have been developed by Néodyme company R&D team to overcome these second types of issues.

3.1.2 Site configuration and spatial discretization

A fictitious industrial site is considered for this case study. The created test case is a 60,000 m² which includes representation of surface drainage influencing structures such as: roads with slopes orientating runoff to water collecting structures, side-walks, road curbs, gutters and door steps (see figure 3.1). To match within the RFS framework of the ASN guide, access to buried sewer network is considered as non-available. Indeed as introduced in this part, idea of the RFS is to be conservative by considering the sewers system as inefficient. To achieve a horizontal topographical resolution fine enough to represent surface drainage influencing structures in urban type environment, the interval of spot elevation data should be in the range of 0.1 m to 0.4 m for DEM generation (Ole *et al*., 2004). Created DEM is a 0.1 m per 0.1 m horizontal resolution grid. This grid resolution fits with required horizontal precision to represent above mentioned structures and is compatible with level of accuracy of standard geomatic technologies (Mandlburger *et al*., 2008; Aktaruzzaman and Schmidt, 2009; Erpicum *et al*., 2010; Fewtrell *et al*., 2011; Remondino *et al*., 2011; Leitã *et al*., 2015).

The modeled domain boundaries were closed to consider only local rainfall. For water evacuation and storage, a reservoir was located downstream of the domain of interest. This reservoir is located far enough downstream not to influence backward flow condition in the area of interest. An important aspect was to use a spatial discretization fine enough to keep on representing runoff influencing structures as included in the High-Resolution DEM. Consequently, for most of tested tools, temporal discretization had to be fine as well, mainly due to numerical methods inherent to Courant-Friedrichs-Lewy (CFL) number restrictions.

The selected modelling tools use different numerical schemes and notably different spatial discretization approaches that are illustrated in figure 3.2. For models using structured mesh,

the 0.1 m per 0.1 m resolution DEM grid was directly used as a staggered grid when possible (Mike 21). With Mike 21 FM, non-structured mesh was generated to discretize the domain with an important refinement in order to finely represent flow influencing infrastructures.

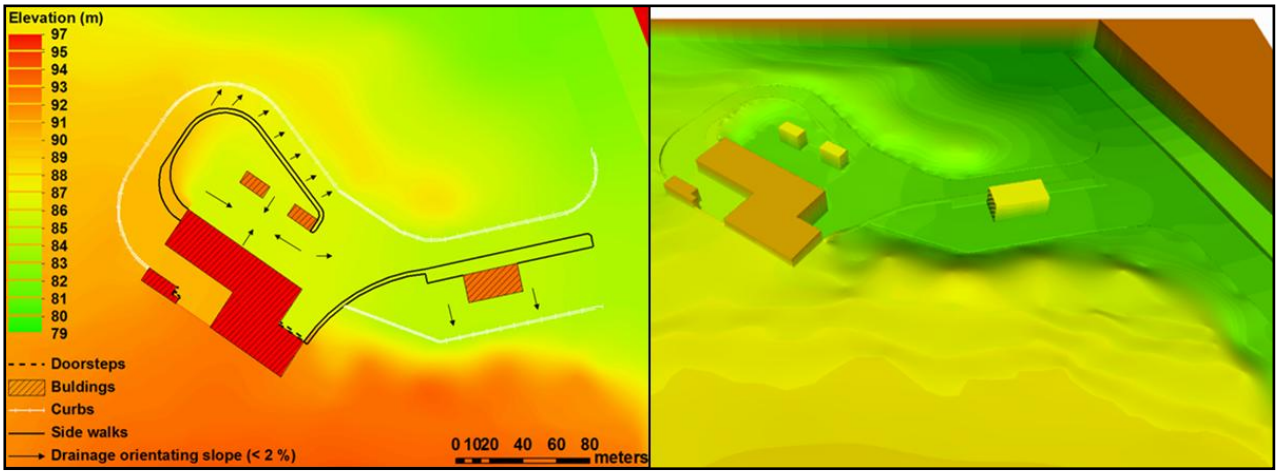

Figure 3.1. *Represented surface drainage influencing infrastructures on the test case (left) and 3D view of created 0.1 m horizontal resolution DEM (right).*

In the 3D FVM case, the chosen meshing method mainly consists in extruding surfaces meshed with quadrilaterals by use of the Q-Morph algorithm (Owen and Saigal, 2000). Powerful meshing tools have been developed by the Néodyme's R&D team and incorporated into the gmsh meshing software (Geuzaine and Remacle, 2009)], allowing the discretization of complex environments consisting of a topographical terrain and urban structures. An adaptive distribution of layers links the natural ground surfaces and urban structures to a horizontal flat surface, later assimilated to the atmosphere. Urban structures represent discontinuities in the topography that cannot be extruded. The points located near these strong gradients zones are first extracted from the original raster, and then collapsed along geometrical curves fitting the actual geometry. Finally, these lines are used to draw local 3D structured volume meshes with gmsh. These volumes are grouped into two categories: "*channels*" (hollow), and "*side mounts*" (elevations). Remaining areas consist in a continuous topography. This process is summed-up in figure 3.3. Finally, the goal is to build a surface covering the entire domain (including channels and mounts) sufficiently continuous to be extruded. In order to avoid prohibitive number of cells in the final mesh, the resolution is progressively degraded far from the discontinuities.

Two approaches for building representations were used. In Mike 21, buildings are represented as elevation data (Building Block method: "BB"). In Mike 21 FM, buildings are excluded from mesh using their footprints as break lines. In that case, a normal no-slip wall boundary condition was applied to account for the blockage effects of buildings (Building

Hole method: “BH”). For urban flooding simulations, these approaches equally fulfill requirements for building representation to predict flood extent (Schubert *et al*. 2008). Rain over building roof is included in models calculation through source points representing gutters discharges (Figure 3.4). Gutters discharges are assumed to be constant during rainfall events. Each gutter discharge is established simply by calculating contributing cumulated roof rainfall volume and dividing it by length of rainfall event. Calculated gutter discharges are ranging from 0.0015 $m^3.s^{-1}$ to 0.01 $m^3.s^{-1}$.

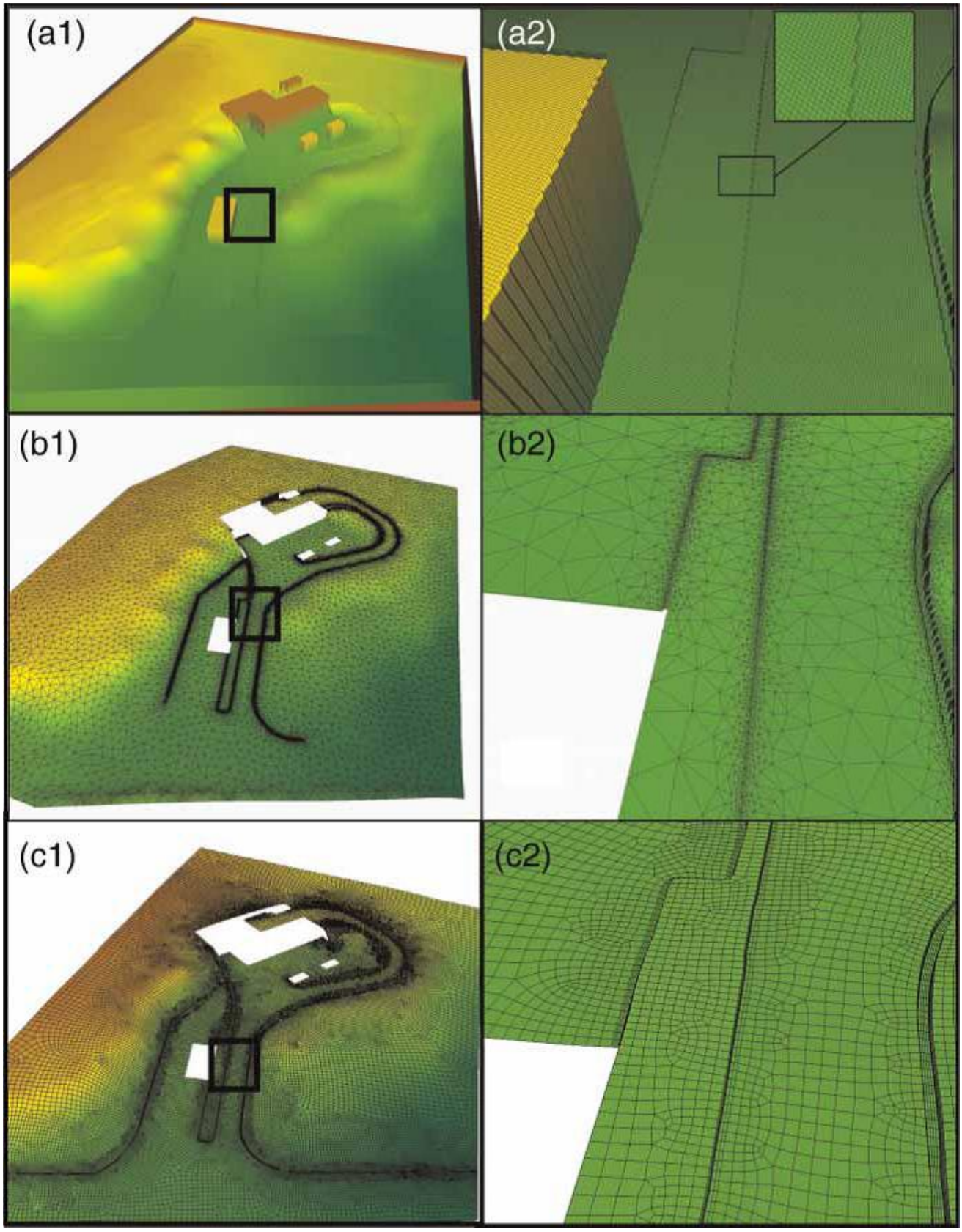

Figure 3.2. *Meshes used in the modelling tools (where a1, a2 are Mike 21 grid views; b1, b2 are Mike 21 FM mesh views; c1, c2 are Néodyme 3D FVM mesh views).*

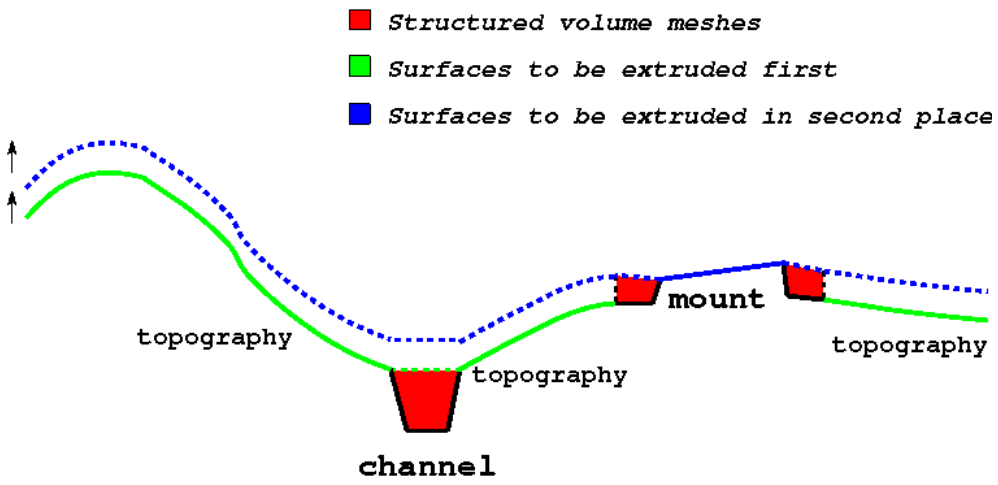

Figure 3.3. *Illustration of the method used to construct the final volume mesh for FVM used by Néodyme.*

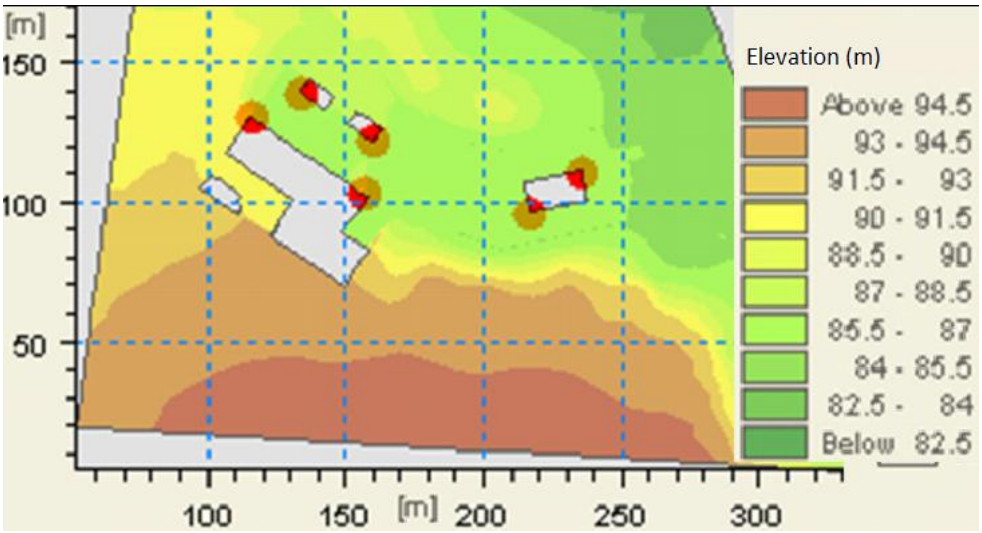

Figure 3.4. *Location of source points (red dots) where gutter discharges are introduced in the models (visualization from Mike 21 FM GUI).*

3.1.3 Runoff scenarios and models parameterization

Three runoff scenarios, suitable with the ASN guide RFS framework for local intense rainfall event, were tested (Figure 3.5). These scenarios introduce the same total quantity of water in the model and consider the infiltration process as negligible. This penalizing aspects regarding infiltration is justified by the will of the RFS approach to be conservative regarding the uncertainty of the saturation level natural of soil due to anterior rainfall events combined with the high level of urbanization of sites.

Scenarios S1 and S2 were both one hour long rainfall events cumulating 100 mm. It should be noted that a 100 $mm.h^{-1}$ intensity fits with the will to match with the RFS: this type of intensity is somehow within the magnitude of a one over a hundred year return period event

(considering the upper bound of the 95% confidence interval) in France. S1 has a constant 100 $mm.h^{-1}$ rainfall intensity. S2 is a rainfall event starting from 0 $mm.h^{-1}$ (at t=0) linearly rising up to a maximum of 200 $mm.h^{-1}$ in 30 min, then linearly decreasing back to 0 $mm.h^{-1}$ at 60 min. S2 event consequently has a triangular shape rainfall intensity variation as illustrated on figure 3.5.

Scenario S3 is a uniform 0.1 m height water surface initially covering the entire domain up. Even though S1/S2 and S3 lead to different hydrodynamic conditions, their inclusion in the tested method can give complementary insight: *(i)* to help for the hydrodynamic understanding and to point out sensitive configuration on a site, *(ii)* to highlight different categories of difficulties encountered by modelling tools.

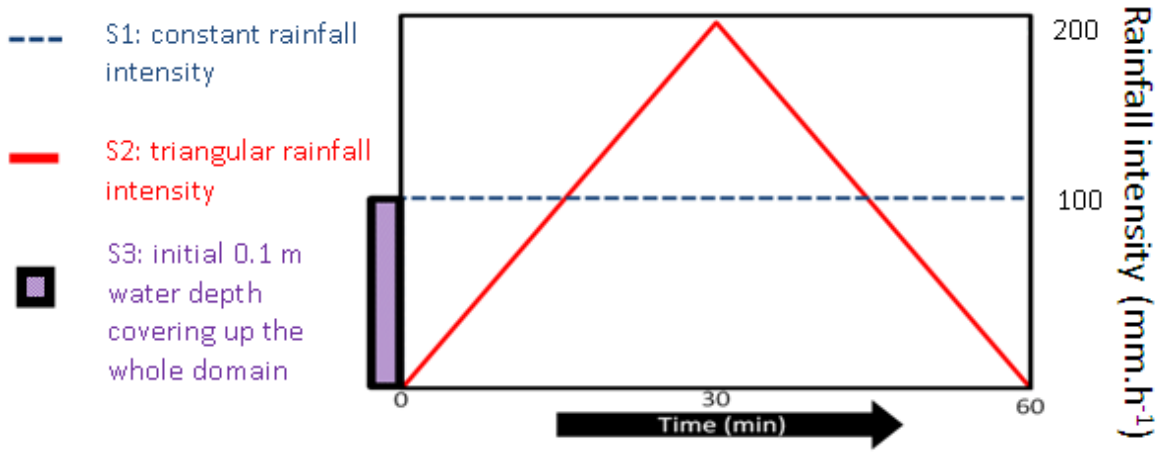

Figure 3.5. *Diagram representation of the 3 types of scenarios.*

For the models parameterization, choices to make simplest and comparable approaches boundary and initial conditions as well as for energy losses coefficient were selected as describe here after:

- ***Initial and boundary conditions***

General purpose for boundary conditions was to set them closed and far enough from interest area so that they do not interfere with flow in this area. Over the domain, initial condition for water depth (h_{init}) and velocities were null for scenario S1 and S2, whereas for S3, h_{init} was equal to 0.1 m and velocities were null. In both, Mike 21 and Mike 21 FM software, a cell is either considered as a part of the solution domain (wet) or as a boundary (dry) (DHI 2003, 2007a, 2007b). A threshold value (h_{dry}) represents the boundary value under which water can be accumulated, but 2D SWEs are not resolved. 2D SWEs are fully resolved when a cell water depth is above a user defined threshold value (h_{wet}). Between h_{dry}

and h_{wet}, only a part of the 2D SWEs are resolved (the mass conservation equation and the diffusive wave approximation of the momentum equation). For the study purpose, we are interested in the full resolution of 2D SWEs and therefore a minimization of these thresholds in models setup has been performed. Thus, only water levels above h_{wet} are analyzed.

- ***Energy losses coefficients***

For energy losses due to roughness and to eddy viscosity, chosen approach was to integrate them using standard practice and coefficient values commonly used in urban flooding modelling practice (Chow, 1959), notwithstanding that it would require a more important effort to assess if such kind of integration is still valid for our purpose. Strickler roughness coefficients of 60 $m^{1/3}.s^{-1}$ and 27 $m^{1/3}.s^{-1}$ were applied respectively to constructed and non-constructed areas. These values are standards when respectively considering concrete and grass covered areas. Smagorinsky eddy viscosity approach was used to represent energy losses due to horizontal turbulence (DHI, 2007a, 2007b). For Néodyme 3D FVM, the Reynolds Average Stress (RAS) approach is used for turbulence modelling, and the k-omega-SST turbulence model (Menter, 1993) has been chosen for the present case. The small-size details under grid cells size are taken into account effectively through the 'equivalent sand-grain roughness height' (Nikuradse, 1933), whose acceptable values are taken to be 1 cm and 3 cm for urban and natural surfaces respectively.

3.1.4 Performance assessment methodology

The parameter of interest was the maximal water depth (h_{max}) calculated by models for each category of tested scenarios. Some indicators for computation reliability check were analyzed and compared as well. Note that, even though models were conservative, errors in mass might be numerically inroduced. In general, mass errors might happen due to initial flooding cycle, to flooding and drying treatment, to a high gradient in topography, to a large time step use (MacCowan *et al*., 2001) or to a time splitting in a numerical scheme when divergent flow occurs (*e.g.* in ADI scheme see Guinot, 2000). Such causes, leading to spurious numerical oscillation, may yield negative water depth in models. Some numerical methods are implemented resetting negative values to small positive ones creating mass (volume). Therefore, it is commonly recommended to perform models mass balance checks (DHI, 2003). In addition, maximum courant number (CFL_{max}) reached in simulations were checked to look for potential numerical instabilities in models as well as for calculation accuracy purpose. Maximal velocities (U_{max}) as well as hydrograph characteristics time results were observed to check their coherence with physics of modelled phenomena. Velocity field evolutions were analyzed to detect any artificial polarization.

- ***Framework for models comparison***

Optimized setup for each of the codes and the scenarios were defined. To get stable and comparable models, several setup tests were carried out. The purpose was to model scenarios using optimal parameters and to get balanced computations and runs considering: objectives, codes possibilities and computer performances. Standards used to judged the setup as optimal were: a fine discretization use, a minimization of complete SWEs resolution threshold, a non-prohibitive computational time. The computational resource was here a desktop computer (Intel Core2 Duo Processor E8400) for Mike 21 and Mike 21 FM models runs. A set of 10 processors (Two Intel Xeon X5680) of a Linux workstation was used to perform the 3D finite volume calculation. Possibilities to reach a balanced model setup for our specific applications were compared.

- ***Optimization of models setup***

Depending on possibilities and limitations of the models for optimization, differences in parameterization were generated. Table 3.1 summarizes the models reached optimal setup considered for the comparison. With Mike 21, all categories of scenarios could be computed. Nevertheless, at a 0.1 m resolution the DEM use as structured mesh did not lead to stable runs. This resolution use would have probably been possible through a time step reduction (to match with the CFL condition restriction), but this software release does not allow a time step smaller than 0.01 s. It limits computational stability for such a fine spatial discretization use. Therefore the 0.1 m resolution grid has been resampled to a 0.3 m resolution grid which was used as structured mesh. Selected h_{wet} value is 0.008 m as for higher values, tests showed important spurious oscillations leading to a poor results quality. Here, computation time on a dual core computer was about 72 hours for S1 and S2 scenarios and 24 hours for S3 scenario runs.

Mike 21 FM could not perform the S2 scenario run. The use of higher order schemes option did not lead to stable runs. It was also not possible to have stable runs with a h_{wet} value smaller than 0.02 m for S1 and 0.025 m for S2. Computation time was about 140 hours for S1 and S2 scenarios. Moreover in case of high topographical gradient, calculation stability could not be maintained in models. Therefore, Building Hole (BH) treatment of a high wall was applied to remove it from the computational domain and allow stable runs.

Néodyme's 3D FVM could not model S1 and S2 category of scenario, as options to implement such kind of approach was still under development. For S3 category of scenario, vertical structures such as walls generate high gradient in flow and had to be removed from

simulated domain for computation stability's sake. Computation time was about 530 hours here.

Table 3.1. Summary of models setup.

Modelling software	Main parameters	Scenarios		
		S1	S2	S3
Mike 21	Numerical scheme	Finite differences (ADI)		Finite differences (ADI)
	Grid resolution	0.3 m * 0.3 m (based on 0.1 m resolution grid)		0.3 m * 0.3 m (Interpolated based on 0.1 m resolution grid)
	Number of cells	718,200		718,200
	dt (fixed)	0.01 s		0.01 s
	Boundary conditions	Closed		Closed
	Initial condition	0 m		0.1 m
	Wetting/drying threshold	0.008 m		0.008 m
	Flow evacuation	Sink		Reservoir
	Building representation	Building Block (elevation data)		Building Block (elevation data)
	Source point	Gutter		No
Mike 21 FM	Numerical scheme	Finite volume (Roe solver and Euler explicit)		Not stable
	Flexible Mesh	based on 0.1 m resolution grid		
	Number of elements	87,700		
	Elements area information	Minimal: $1*10^{-5}$ m^2 Maximal: 7.99 m^2 Average: 0.5 m^2		
	dt (varying)	0.1 to 10^{-12} s		
	Boundary conditions	Closed		
	Initial condition	0 m		
	Wetting/drying threshold	0.02 m	0.025 m	
	Flow evacuation	Sink		
	Building representation	Building Hole		
	Source point	Gutter		
Néodyme 3D FVM	Numerical scheme	Not possible to implement yet		Finite Volume (mixed explicit schemes)
	Mesh			Non-uniform hex-dominant
	Number of cells			697,262
	dt (varying)			10^{-3} to 10^{-2} s
	Boundary conditions			Closed everywhere but top-side opened to the atmospheric condition
	initial condition			0.1 m
	Wetting/drying threshold			0 m
	flow evacuation			Reservoir
	Building representation			By extrusion and partially structured mesh
	Source point			No

3.2 RESULTS

This section presents results for the variables of interest (h_{max} and water depth evolution) and on the computation reliability indicators. It should be noted that S1/ S2 categories of scenario and S3 do not have comparable hydrodynamics and their results comparison *stricto sensus* is not the purpose of this study. Nevertheless, they can give separately an insight on modelling tools limits and flexibility. The results comparison under the light of: *(i)* the approach specificity, *(ii)* the different numerical schemes properties and *(iii)* the optimization possibilities will be more specifically discussed in the next section.

3.2.1 Rainfall events scenarios (S1 and S2)

- ***Maximal water depth (h_{max})***

A general overview of h_{max} values calculated for rainfall scenarios (S1 and S2) with Mike 21 and Mike 21 FM is represented in figure 3.6. Within constructed zone of the study domain, all models and scenarios estimate the same four flooded areas (A to D) with a calculated h_{max} value ranging from 0.05 m to 0.15 m. The identified flooded areas have the following topographical configurations:

  - **Area A** is a depression, not connected to any surface drainage structures but by the crest line of the depression, leading to a unique surface overlandflow path;
  - **Area B** is a corner between a building and a sidewalk;
  - **Area C** is an almost plan shrank roadway, lined on one side by a sidewalk and on the other side by a flooded curb;
  - **Area D** is a parking zone with a slight slope (about 2 %).

h_{max} values and spatial extent of flooded areas - A to D – in accordance with their topographical and drainage paths configurations. For a given scenario, Mike 21 and Mike 21 FM models, computed h_{max} values had close values and flooded area had similar spatial extent.

Scenario S1 and S2 results show that h_{max} values in flooded areas were up to 0.06 m higher for scenario S1 than for scenario S2, representing a maximal difference in h_{max} value amongst scenarios up to 30% in these areas. S1 and S2 flooded areas spatial extents, with h_{max} values greater than 0.05 m, were compared. S2 lead to a 15% (with Mike 21) and to a 24 % (with Mike 21 FM) larger spatial extent of flooded areas compared to S1 (Figure 3.2.1.1).

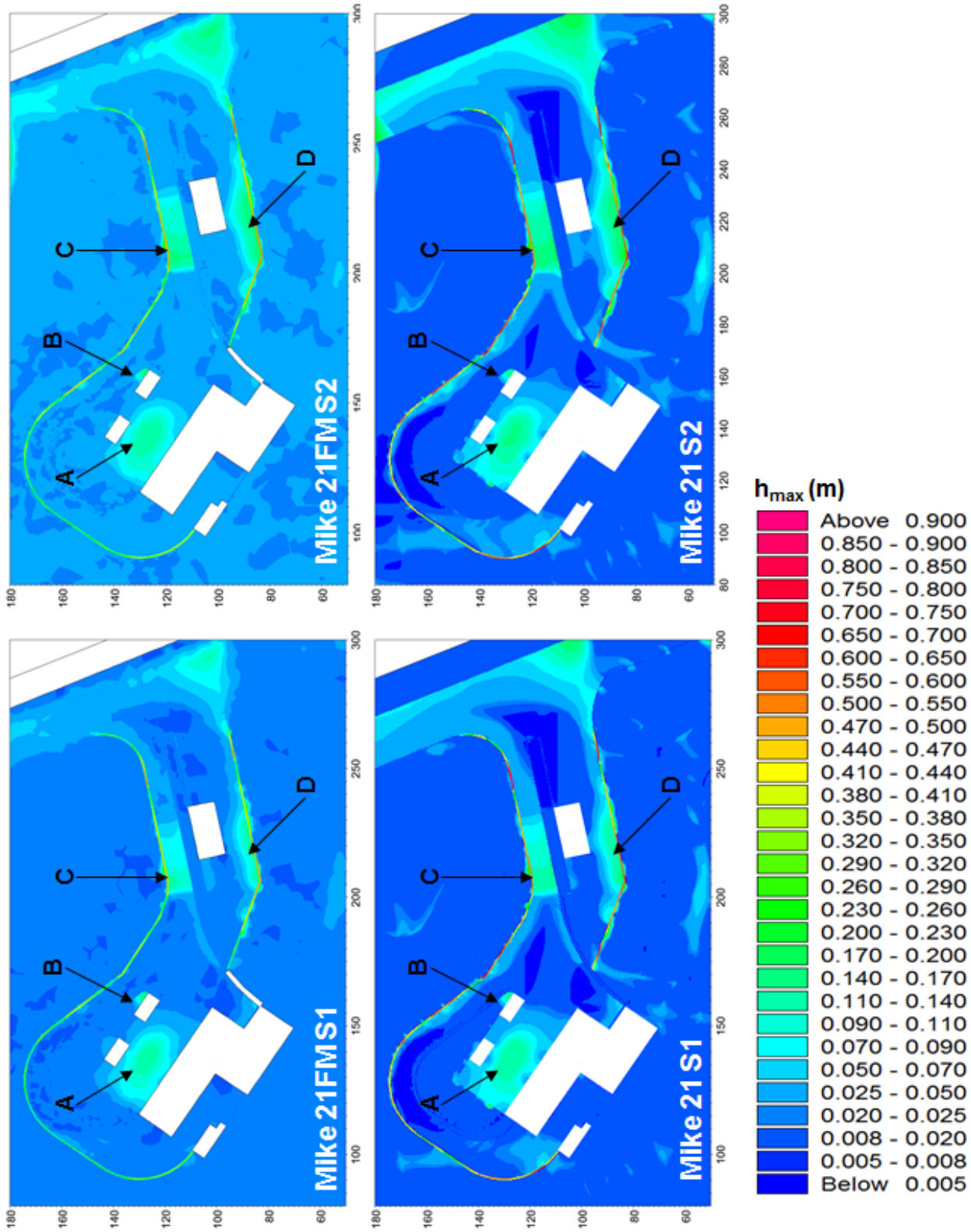

Figure 3.6. *Comparison of maximal water depth (h_{max}) values reached in cells for S1 and S2 scenarios simulations with Mike 21 and Mike 21 FM.*

A more detailed comparison was carried out for 18 points of interest over the industrial site (Figure 3.7). General trend shows for a given scenario higher h_{max} value calculated by Mike 21 compare to Mike 21 FM. This comparison shows an average difference between the Mike 21 and the Mike 21 FM models results of 0.01 m for S1 and 0.012 m for S2. Computed h_{max} values for 10 of these points of interest are presented in figure 3.7. Points 1 is located at the lowest point in the middle of flooded area A. Points 3 and 4 are located at two buildings entrance locations in flooded area A (Figure 3.6). Points 6 and 7 are respectively located above and below a 0.15 m high doorstep that was not flooded and with no upstream contributing area. Therefore, h_{max} values at point 6 are equal to models respective parameterized h_{wet} values. Same remark applies to point 10 located on a non-flooded sidewalk. Points 11 and 12 were located on a flooded road (in area C), observed h_{max} values for point 12 were equal to the close by sidewalk relative elevation, which was nonetheless not flooded. Point 18 was located on flooded area D.

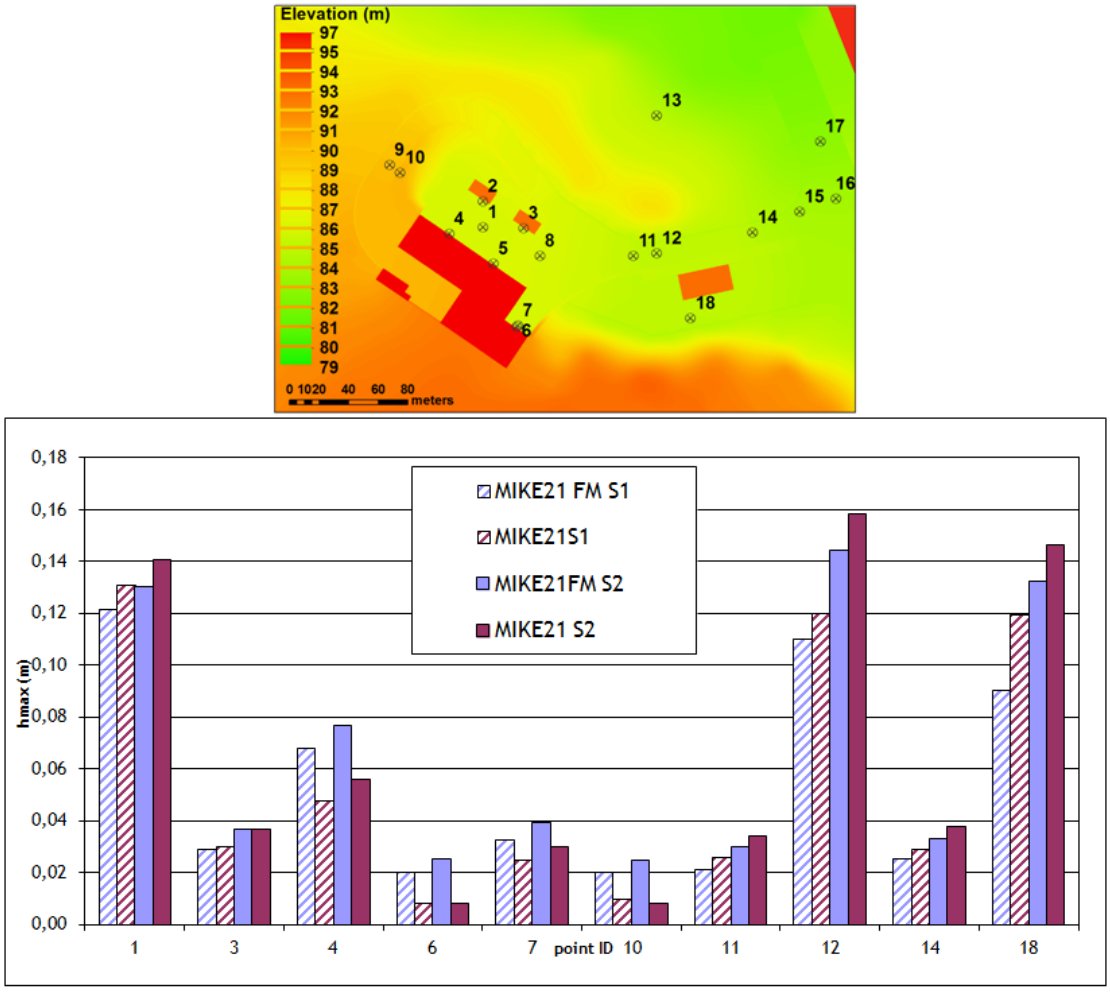

Figure 3.7. *Detail of h_{max} values at ten specific points of interest (down) and points location (up).*

Mesh resolution difference can be important, and as the h_{max} value is averaged over a cell area this might lead to differences. For instance at point 18, Mike 21 regular mesh cell area is 0.09 m², whereas Mike 21 FM cell size at this location is about 2 m². Overall discussion about differences is given in section 3.3.

- ***Water depth evolution***

Globally, for a given scenario, Mike 21 shows an agreement with Mike 21 FM in calculation of water depth evolution on the area of interest. Figure 3.8 illustrates the water depth evolution comparison at point 18, where differences in h_{max} calculations were important.

For scenarios S1 and S2, differences in rainfall intensity evolution results in differences in water depth evolutions. Moreover, differences in water depth evolution in the first minutes of the simulations are spotlighted in figure 3.2.1.3. These differences are related to models differences in h_{wet} parameter value. Indeed, 2D SWEs are not fully resolved over the whole domain until accumulated rainfall value exceeds h_{wet}. Below h_{wet} value, water in a cell is either considered as not moving (if below h_{dry} value) or only mass flux momentum SWEs are resolved (if between h_{dry} and h_{wet} values). As h_{wet} value was optimized to 0.008 m and to 0.02 m for S1, and to 0.008 m and 0.025 m for S2, the times for accumulated rainfall to exceed h_{wet} are respectively 5 min, 12.5 min and 12 min and 21.75 min.

Global water depth evolution is shown to respond quickly to rainfall events temporal variations. For instance, h_{max} at point 18 was observed about 3 min after the peak in S2 rainfall intensity which occurs at 30 min. This quick basin response is mainly due to modest spatial extent of the modelled area.

Even though, water depth values and evolutions of the Mike 21 models are comparable to the Mike 21 FM models results, they present slight spurious oscillations. In both models, numerical discretization cannot handle properly compatibility between numerical flux and source term. Nevertheless, the flexible time step used by Mike 21 FM tends to reduce magnitude of these oscillations.

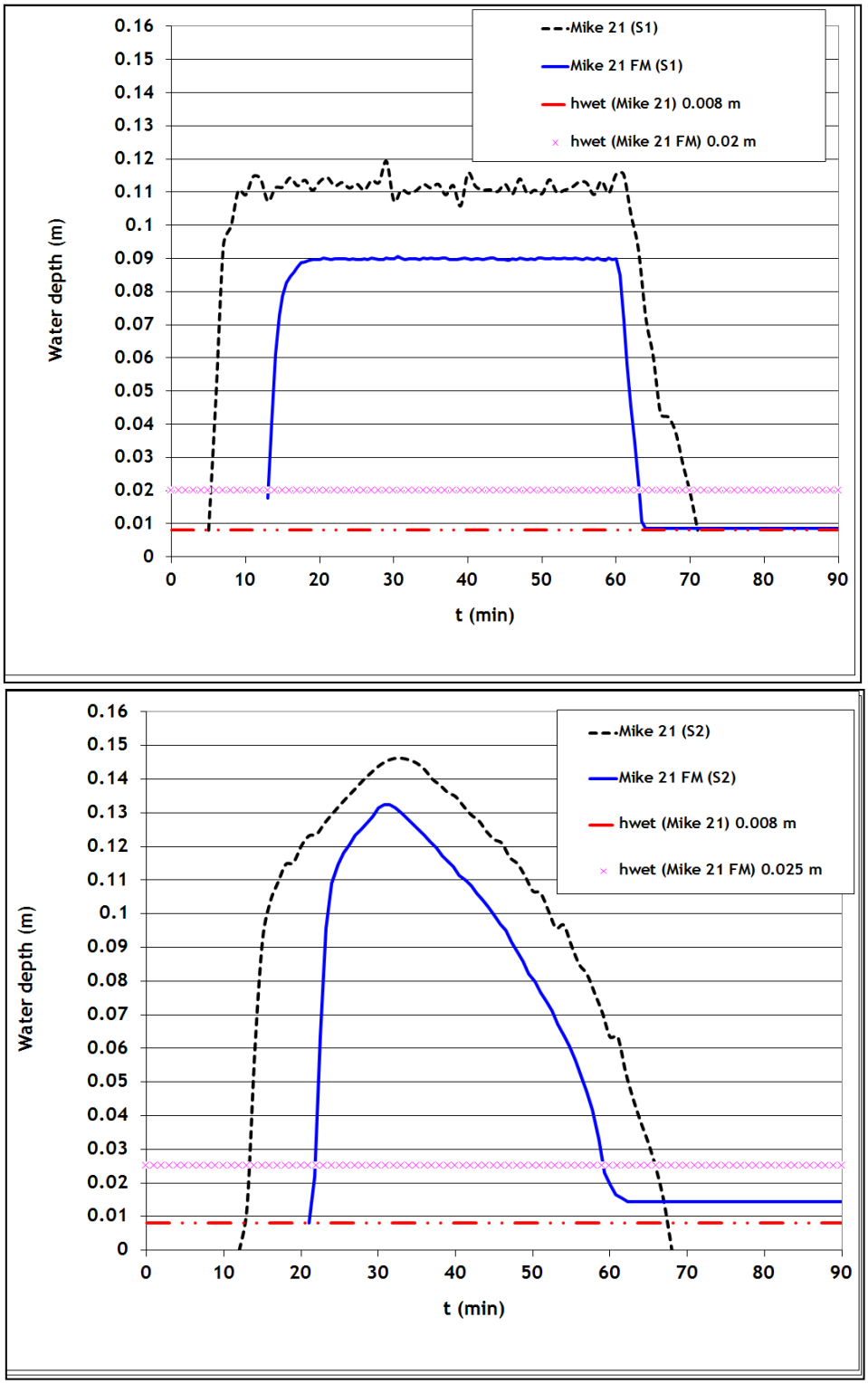

Figure 3.8. *Water depth evolution at point 18 with Mike 21 and Mike 21 FM, for scenarios S1 (up) and S2 (down).*

3.2.2 Initial 0.1 m water depth scenario (S3)

This section is devoted to the comparison of the results obtained with Mike 21 and those obtained with OpenFOAM, for scenario S3. Illustration of the S3 dynamic simulated with Mike 21 is given in the figure 3.9. Comparison between maximum water depth (h_{max}) simulated by Mike 21 and OpenFoam is presented in figure 3.10, which shows h_{max} reached at each point of the computational domain during the entire simulation.

A global agreement for maximal water depth values and repartition with the two models can be observed. Differences occur locally notably at the foot of the most right hand side building (Figure 3.10) and in more downstream areas. These differences are up to 0.1 m and mainly reflect difference in dynamic due to heterogeneities between models in topography representations, velocities calculations and numerical schematizations, as discussed below.

Dynamical aspects can be more finely compared on limnigraphs (Figure 3.11), and especially in the area of congestion located downhill on the right of the site, where point 14 lies. High hydro-dynamical flow effects and maximal water depth phenomena occurs during the first thirty seconds of the simulations. From t=0 s to t=20 s, three peaks occur successively, corresponding to directs arrivals of water flowing respectively from the close by side walk, the bank and the road. Arrivals times and magnitudes of these peaks differ between models. The maximal water depth peak starts at t=25 s and corresponds to the arrival of water from upstream area. The slope observed around 25 s on the limnigraph is shifted and appears sooner in the OpenFOAM simulation, and then the water height diminishes faster than in the Mike 21 simulation. In the Mike 21 simulation, the computational domain is drained after 30 min and only few puddles remain after this time. The OpenFOAM simulation ran for 30 min as well, but the domain was emptied earlier.

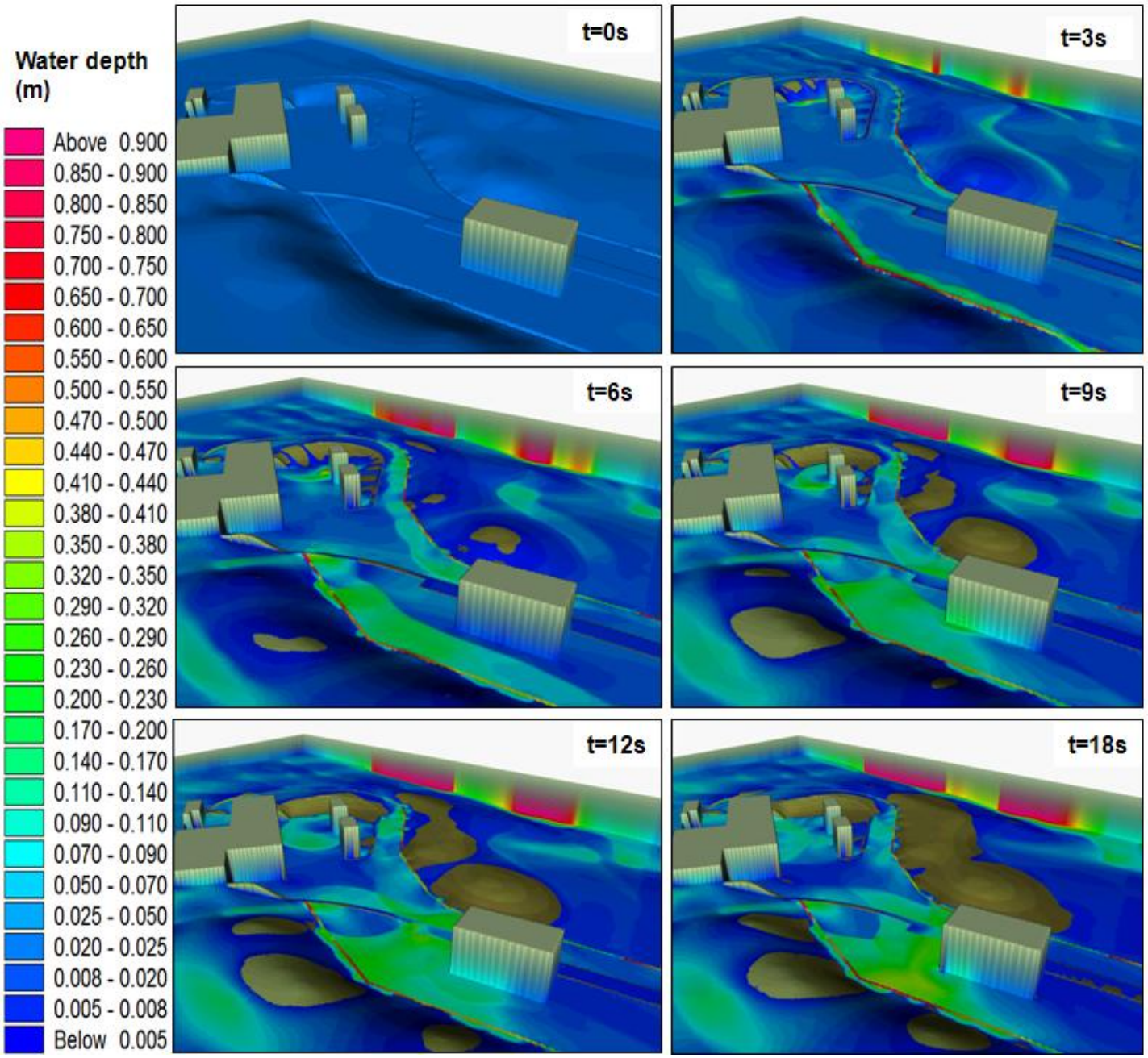

Figure 3.9. *Illustration of the first few seconds of S3 (0.1 m initial water depth) simulation run with Mike 21.*

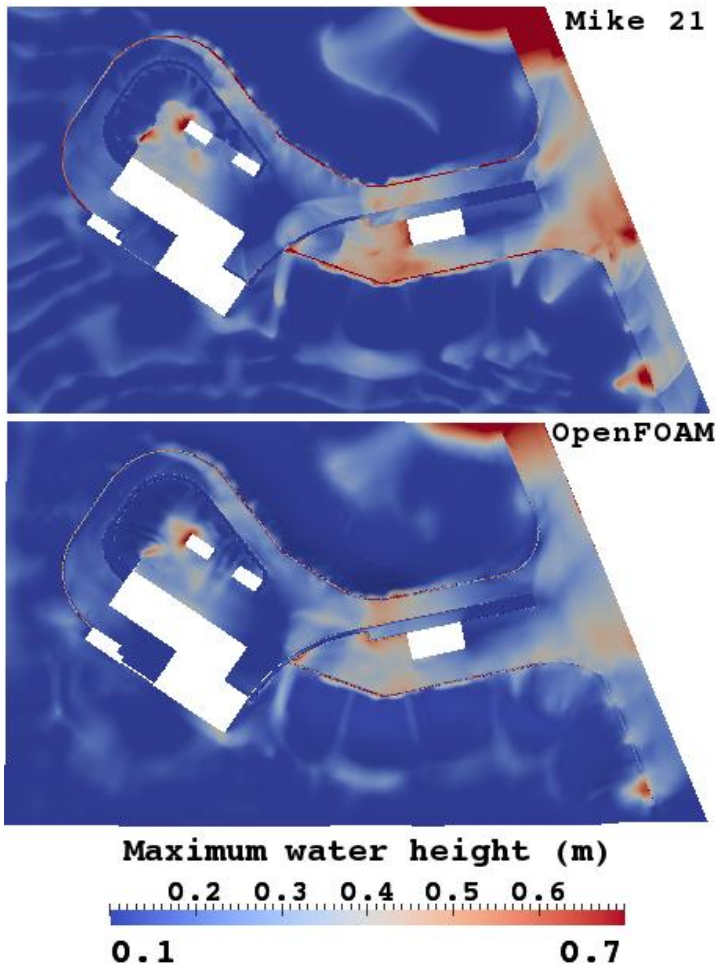

***Figure 3.10**. Maximal water depth (h_{max}) reached over the domain for S3 scenario simulations with Mike 21 (up) and with OpenFOAM (down).*

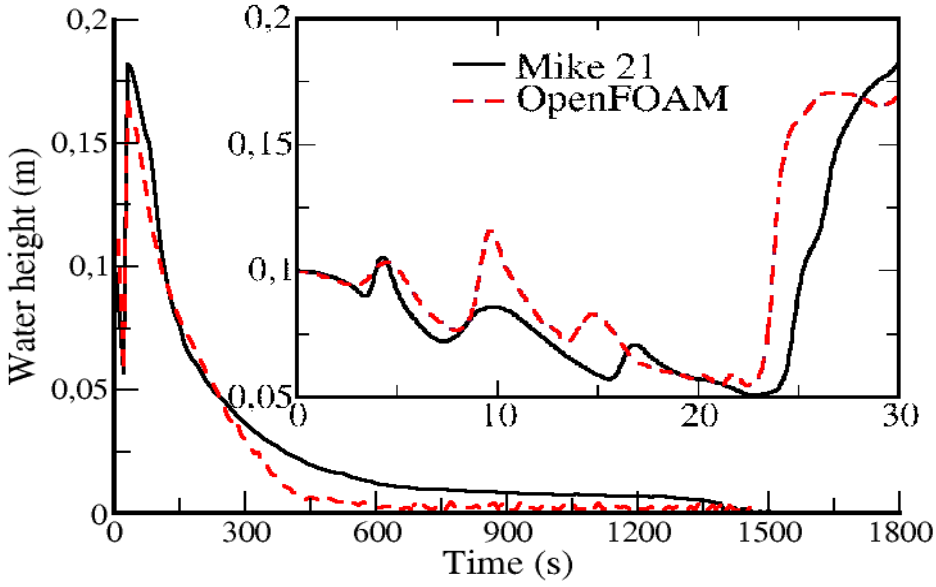

***Figure 3.11.** Limnigraph at point 14.*

Identified differences between the two models have three main origins as explained below:

First, the meshing method can alter the topography. The meshing tool developed by NEODYME projects a quadrilateral mesh onto the topography, and then unwraps the skew cells (Bidmon and Thomas, 2005). This unwrapping procedure locally affects the original topography. This results at global scale in smoothing of the topography, and thus reducing small topographical irregularities. Beside geometrical aspects, grid cell size resolution is finer at the ground level with Mike 21 compared to Néodyme model, as number of cells is 718,200 in Mike 21 regular grid, whereas number of cells is 697,262 (with 14 layers in the vertical dimenstion) Néodyme 3D FVM. Up to a certain point, larger cell size might speed up mass transfer computation and therefore influence results. That explains why the downhill accumulation of water is less pronounced in the OpenFOAM simulation, and why the domain is sooner emptied.

Next, the roughness definition leads to differences in the velocity field. Indeed, roughness parameters were separately evaluated in each model, and their conformity is not guarantee (this would need a study in itself, and is not the subject of the present research). Indeed, the higher is the water velocity flowing downward the bank, the faster is the fluid flow when impacting curbs and sidewalks, thus the more important might be the water quantity passing above them. Moreover, these structures overflow phenomena can be more accurately represented in Néodyme 3D FVM model as vertical velocity flow components occurring in such situation are considered in this model.

Finally, with Mike 21, the mesh is a regular grid directly taken from the raster. It leads to horizontal stairs shaped representation of urban structures. This limitation is inherent to regular mesh resolution and can have slowing down effects on the flow (see chapter 1). For instance, this is enhanced in the curbs, which are emptied later in Mike 21 than in OpenFOAM.

Despite the above-mentioned differences, a good general behavior agreement is observed, and is reinforced by the calculation of non-trivial quantities as surface flow rates. Discharge flowing through the section 1 was plotted (Figure 3.12). This figure enhances differences in discharges evolution and magnitude which are due to previously explained remarks.

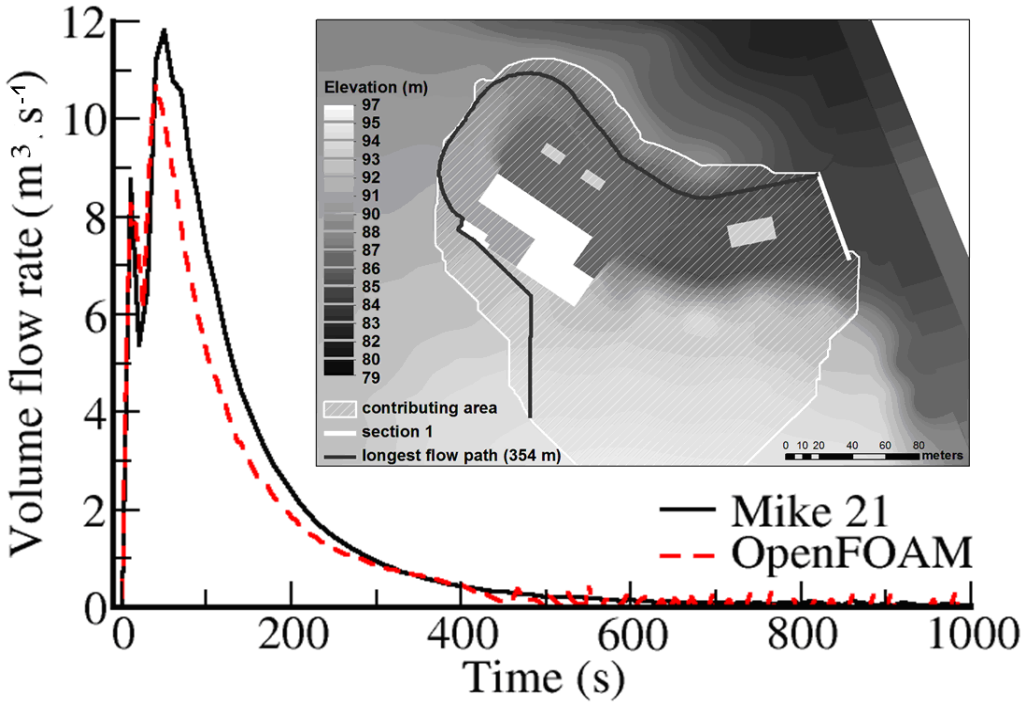

Figure 3.12. *Hydrograph at section 1 along with associated upstream contributing area and longest flow path.*

3.2.3 Indicators of computation reliability

- ***Mass balance***

To detect and quantify potential errors in mass, a control of water injected, present and flowed out of the model during the simulation was performed. This mass balance check for scenarios S1 and S2 with Mike 21 FM does not point out any mass defaults. With Mike 21 mass balance reveals up to a 4% excess in mass at the end of rainfall events (t=60min for S1 and S2) reaching 6% after 90 min. For S3 scenario, the mass error calculation reveals a 2 % mass excess with Mike 21. Indeed, it is well known and documented that in case of steep gradient and small water depth along with spurious oscillations occurrences, calculation can yield negative water depth (DHI, 2003). This being the case, Mike 21 automatically resets the water depth to a small positive value, therefore creates mass. In our cases, mass creation appears to be reasonable with Mike 21 and negligible with Mike 21 FM.

Though the OpenFOAM VOF method should be conservative, a 2 % mass loss is observed after 30 min of simulation. A fraction of water in cells situated near the atmosphere boundary can be a direct contribution to loss of mass. This phenomenon can be particularly important in the coarse regions of the mesh. Indirect contributions come from numerical diffusions and cumulative errors inherent to the used iterative method (Löhner, 2008).

- ***Maximal Courant number (CFL_{max})***

For both S1/ S2 and S3 scenarios, Mike 21 CFL_{max} values in x and y directions are below 0.2 (Figure 3.13), excepted for few cells in curbs where CFL_{max} values can reach 0.3.

With Mike 21 FM, CFL_{max} can be fixed as an input parameter controlling time step used in calculation. Fixed CFL_{max} conditions are not exceeded during the various simulations. Nevertheless, in curbs and road gutters, where cells size are low and flow velocities higher than for the rest of the domain, time steps have decreased up to 1^{-10} s to keep calculation under imposed CFL condition. It resulted in a drastic computational time increase. The solver used by Néodyme 3D FVM also relies on an adaptable time step, and for a CFL_{max} fixed at 0.5, no instabilities occurred (the time step does not decrease below 10^{-3} s). These differences in time step accommodations with both Mike 21 FM and OpenFOAM are directly related to differences in spatial discretization resolution.

- ***Maximal velocities (U_{max}) and Lag-time (Tl_{ag})***

An overview of computed maximal velocities (U_{max}) was performed. For S1 and S2, in road curbs and sloppy areas, computed U_{max} values can be as high as 3 $m.s^{-1}$. Globally for a given scenario, in area of interest, computed U_{max} values are comparable between the models.

For S3 scenarios, the range of U_{max} values is higher. This is due to high h_{init} value (0.1 m) especially over high topographical gradient areas, and to higher range of h_{max} values reached in computation. Magnitudes of U_{max} are slightly higher with Néodyme's 3D FVM compared to Mike 21 model due to differences in roughness energy losses computed in models. No mesh induced artificial polarization was detected through evolution of velocity vectors scan for any of created models.

A check of characteristic times was performed at the section 1 located downstream of our area of interest (Figure 3.12). Lag time (T_{lag}) is defined as the time separating a rainfall event centre of mass to the hydrograph peak. In case of the triangle rainfall event (S2), a 2 min T_{lag} is observed with both Mike 21 and Mike 21 FM. The concentration time (Tc) is calculated using Trisept (1969), Caquot (1949) and Kripich (1945) empirical formulas and converted to T_{lag} using the Soil Conservation Service (SCS) relationship: T_{lag} =0.6Tc. These T_{lag} values are in a range from 1 min 36 s (Kripich) to 2 min 36 s (Caquot). Empirically estimated T_{lag} and T_{lag} estimated using hydrographs extracted from simulations have the same order of magnitude. Moreover, as observed in figure 3.12, longest flow path is 354 m long which means that during the Tlag , the average flow velocity along is below 3 $m.s^{-1}$. This longest flow path goes through curbs in a great extent and during the Tlag the runoff quantity is at its

maxima. Therefore it sounds coherent to get values corroborating with the computed U_{max}. These flow velocities are in agreement with magnitude of flow velocities that can be observed for such phenomena in curbs and streets (Ciliberti *et al*., 2008).

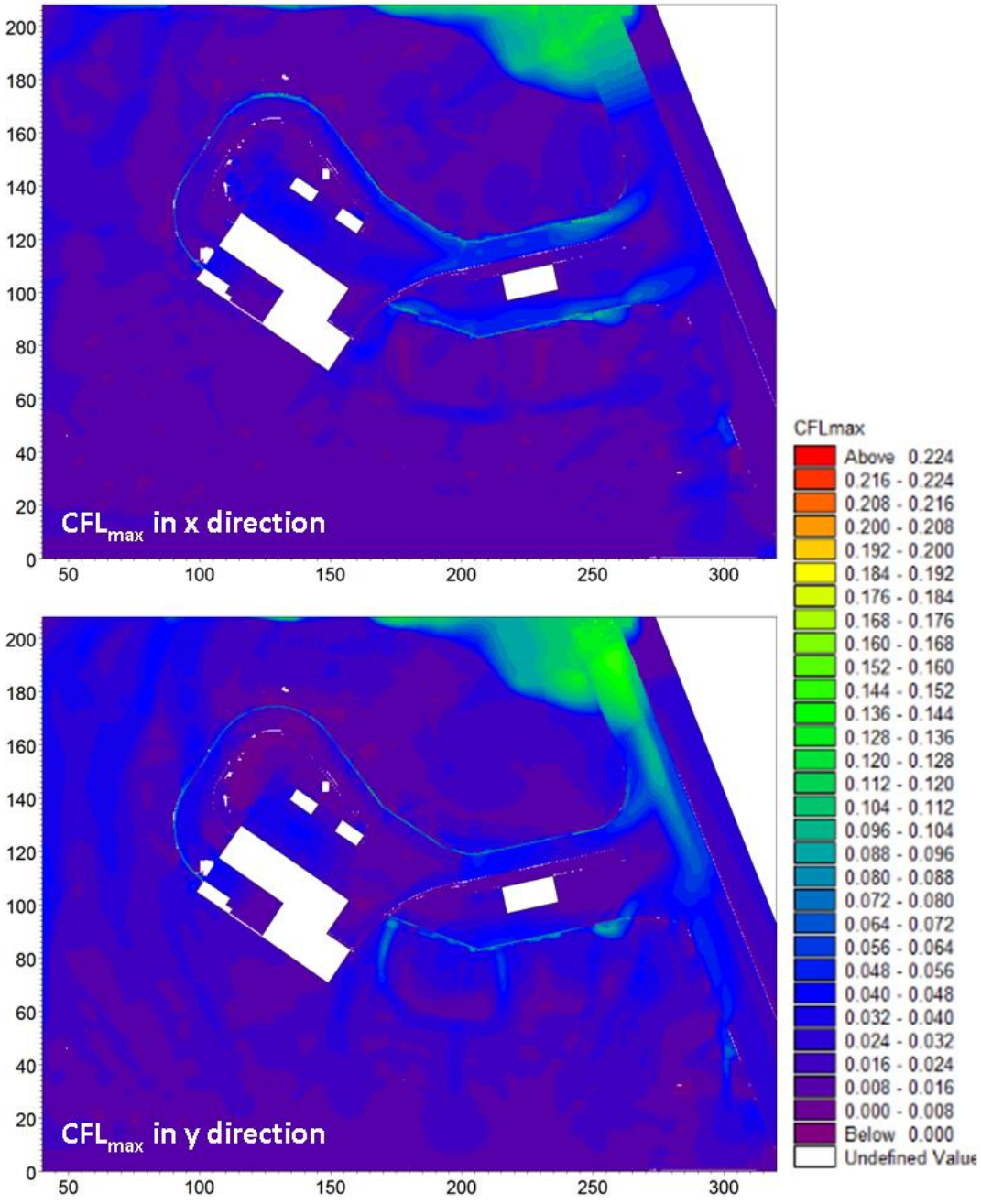

***Figure 3.13**. CFL$_{max}$ reached during S2 simulation with Mike 21 in both, y (up) and x (down) directions.*

3.3 DISCUSSION AND PERSPECTIVES

The comparisons of results and the scopes on indicators of computation reliability performed in this study give an insight on standard modelling tools possibilities and limits to simulate runoff over industrial site with HR topographical data use. Validations of models, through field

measurement would have been a reliable approach for the confirmation of the results and findings but could not be performed for this study. Moreover, some parameters and effects treated by 2D SWEs deserve to be more fundamentally studied (eddy and roughness coefficient notably) to see if the treatment of their influence in models is still valid in this application context and scale. Nevertheless implemented approach allows to point out some critical aspects inherent of tested categories of modelling tools to reach balanced computations, at least in terms of accuracy, stability and computation cost.

3.3.1 Discretization and high topographic gradients

Mike 21 was not the most convenient modelling tool for an adapted spatial discretization of a domain with detailed small-scale infrastructures. It should be noted that compared to non-structured mesh, it does not offer mesh refinement possibilities around structures in discretization. Mike 21 software time step lowest limit is 0.01 s. This time step restriction in software limits the stable use of a regular spatial discretization finer than a 0.30 m resolution with a reasonable CFL number for our type of application. In this case, smaller spatial and temporal discretization would have increased the simulation computational cost, but the gain would not have been relevant, as computed water depths are already comparable to models using a finer discretization (Mike 21 FM model for instance). Nevertheless this limit in discretization possibility might lead to restriction in Mike 21's use for runoff modelling over more complex industrial sites with structures requiring a finer discretization if the overland flow locally has high velocity properties (due to CFL restriction).

Mike 21 FM is more adapted for fine discretization of industrial environment but its numerical scheme cannot handle high gradient with the same flexibility as Mike 21 does. In fact, high gradient may yield to instabilities leading to computation failure. To overcome this difficulty, "*Building Hole*" (BH) representations of high topographical gradient structures (buildings, walls, *etc.*) can be used. This treatment leads to an exclusion of the structure from the computational domain. Such an approach can be partially automatically treated by Mike 21 FM mesh generator, but still requires time consuming manual operations. Moreover, limits of BH approach use to overcome high gradient generated instabilities were encountered. For instance, scenario S3 could not stably run with Mike 21 FM. In this case high gradient leading to numerical instabilities were gradients located along curbs. Curbs are infrastructures that cannot be treated through a BH approach. A mesh refinement optimization could have partially improved this high gradient issue for S3 scenario as well as reduced the computational cost for S1 and S2 scenarios, but is a time consuming task, especially with actual Mike Mesh generator.

Néodyme 3D FVM approach allows a fine spatial and temporal discretization. However, it still requires an important work for mesh construction as well as an important computational cost. The use of an automated hexahedral meshing tool (*e.g.* Owens and Saigal, 2000) would be the solution to overcome problems arising when extruding quadrilateral surface meshes, because it would facilitate the environment drawing/meshing, and it would provide better cell shape allowing time steps ten times bigger (or more), thus considerably reducing computational duration. In that work, high gradient zones of the topography were filled manually with local structured volume meshes. This method requires computer-aided design work, whereas the use of an automated non-structured hexahedral mesh generator would only necessitate the draw of the surfaces (part of the work that could be automated too). Work is in progress in this direction at Néodyme R&D team.

3.3.2 Flow regime changes treatment

Unsteady flow regime changes are numerically treated in a stable manner by Mike 21 ADI scheme in the test case under important CFL number restriction (< 0.2). It confirms Madsen's conclusion (2005) that states that the treatment implemented in Mike 21 to handle trans-critical flow can correctly deal with unsteady flow regimes changes only for a CFL number below 0.2. Such restriction leads to a high computational cost, due to low time step used for CFL condition respect. Moreover, for our scenarios simulations over the test case, such a low CFL restriction is found to be compulsory to have stable runs with small spurious oscillations as higher time step configurations were tested and led to numerical instabilities. For both Mike 21 FM and Néodyme models, flow regime changes can be handled in a stable manner by numerical schemes involving a high computational cost as well.

3.3.3 Threshold for complete 2D SWEs resolution

Wetting/drying of cells represents a dynamic change of flow domain boundary condition problem, which occurs in the case of runoff modelling. In both, Mike 21 and Mike 21 FM modelling tools, technique for this problem treatment consists in modification of equations numerical treatment in very shallow regions. With our test case, Mike 21 numerical method allows a lower h_{wet} value compare to Mike 21 FM for complete SWEs resolution. For both modelling tools, this threshold value, which represents the limit for the starts of complete SWEs resolution, can be low enough for presented practical application purpose. However, when cells switch from dry to wet (*e.g.* all over the domain when amount of cumulated rainfall exceeds h_{wet} value) or vice versa, numerical oscillations are generated. Thus, instabilities might occur especially with low threshold values. On the other hand, increasing these

threshold values leads to more important spurious oscillations (with Mike 21) and to a greater restriction in approach reliability.

3.3.4 Computation reliability

Few indicators were checked to spotlight possible troubles in computation and results. Used indicators did not point out major default in computation and even if it was not possible to validate results with measures, values sound in accordance with physics of modelled runoff phenomena as well as among models. However, in tested modelling tools, the applied numerical schemes are not “well-balanced” scheme (see chapter 1, section 2.2.2) and they do not handle compatibility between numerical flux and source terms (Audusse, 2004; Delestre, 2010). It results in numerically created spurious oscillations. This represents an issue for preserving steady states at rest and to properly handle flooding and drying. Thus, spurious oscillations, mass creation and instabilities might occur with standard numerical tools use for such application. Checking these computation reliability markers, and keeping them under an acceptable level, is compulsory and requires modeller expertise. It conditions this approach of High-Resolution runoff modelling relevance itself, and impacts numerical uncertainty significance.

3.4 COMPLEMENTARY TESTS AND CONCLUDING REMARKS

3.4.1 Complementary tests

Complementary tests have been performed using *(i)* Mike SHE code that solves the diffusive wave approximation of the shallow water equations (see chapter 1, section 2.1.1), and *(ii)* TELEMAC-2D code that solves the 2D SWE. Justifications for these tests and their outcome are summarized below.

The modelling tool using 2D SWEs diffusive wave approximation (Mike SHE) was included in the comparison to check if the underlying assumptions of inertial terms neglecting sound acceptable for HR runoff modelling purpose and to see if this category of tool can be used to give a first quick h_{max} estimation. The structures computational mesh used here is the same as the one used for Mike 21 (0.3 m resolution grid). Even though roughly matching with the results we get with other complete 2D SWEs based models, some areas around buildings that are found to be flooded with other models are not with Mike SHE. Moreover runoff hydrodynamic over flat areas and pounded areas is inaccurately treated. An illustration of water depth evolution for S1 and S2 with Mike SHE compared to codes solving 2D SWES (Mike 21 and Mike 21FM) at a given point is illustrated in figure 3.14. This is due to the fact that only gravitational forces are considered for flow motion within Mike SHE (DHI, 2007c).

Therefore, codes relying on diffusive wave approximation (such as Mike SHE) will not be considered as relevant for our HR modelling objectives, even for a swift rough computation.

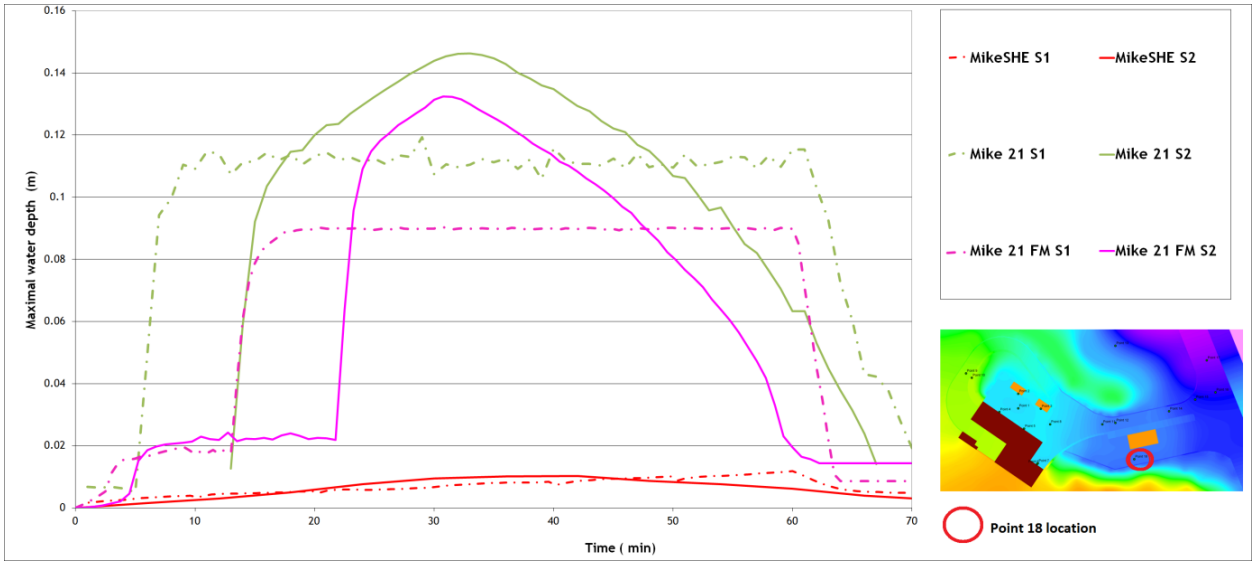

Figure 3.14. *Water depth evolution computed with MikeSHE at a point 18 for S1 and S2 compared with codes fully solving 2D SWEs system.*

TELEMAC-2D (version *v6p1*) is based on resolution of the 2D SWEs system with the possibility to choose either finite elements or finite volumes method over non-structured grids. This code is widely used to simulate free-surface flows in two dimensions of horizontal space for various hydrodynamic modelling applications (dam-break, river flood etc.). TELEMAC-2D finite elements method relies on a Stream Upwind Petroy Galerkin (SUPG) numerical scheme, decentering the basic functions in order to account for the flow direction in the discretization of the advection terms. Telemac-2D finite volumes method has well-balanced scheme properties including a rewriting of the SWEs using a hydrostatic reconstruction leading to an oscillation free and permanently positivity solution (Audusse *et al*., 2014). Figure 3.15 illustrates the non-structured mesh used for TELEMAC model. This mesh was generated using BlueKenue (CHC, 2010) which is a pre/post-treatment tool, allowing to perform the meshing process. For our test, this non-structured meshing tool has been found to be efficient in terms of data manipulation as it allows to import points, polygons and polylines from GIS native format and offers several strategies for meshing refinement processing.

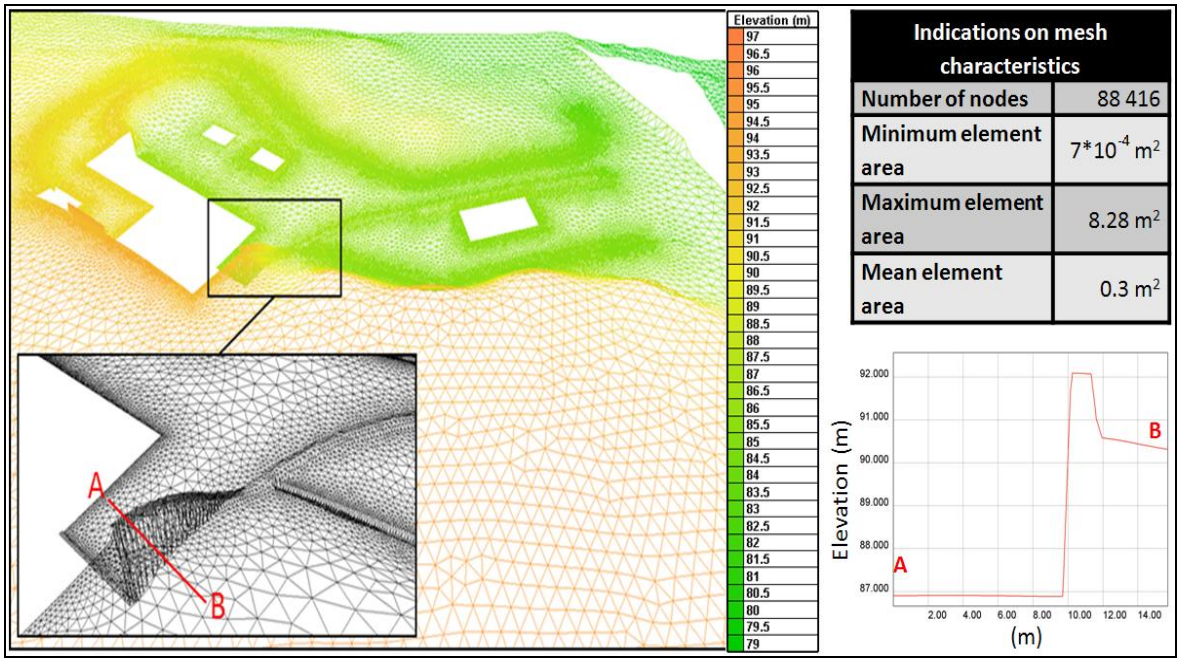

Figure 3.15. *Illustration of the unstructured mesh created for TELEMAC model with details on refinement around structures.*

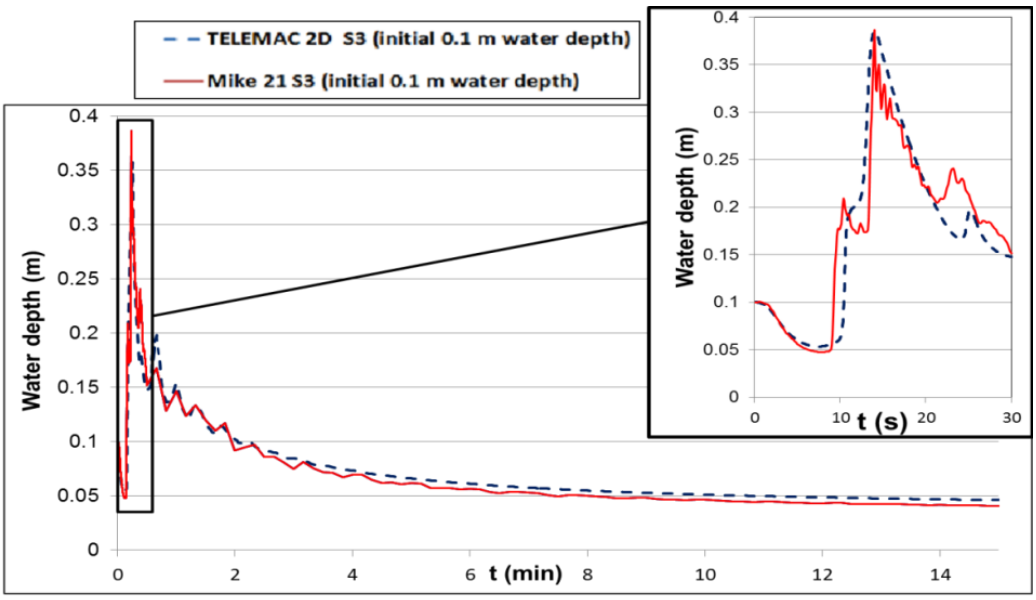

Figure 3.16. *Water depth evolution computed at point 18 for S3 with TELEMAC-2D (using the Finite volume method) and Mike 21.*

In TELEMAC-2D (v6p1), introduction of rainfall as a source term is not an available option and would require programming effort. Therefore, it was not possible to run S1 and S2 scenarios with TELEMAC-2D. This option of rainfall introduction as source term will be included in next TELEMAC-2D version (v6p2). The TELEMAC results for S3 were compared

to results obtained with Mike 21 and Mike 21 FM for h_{max} estimations (e.g. figure 3.16). Overall results were comparable (Abily *et al*., 2014a).

3.4.2 Concluding remarks

High topographic gradient with respect to the water height occurs, especially when it comes to HR modelling of runoff scenarios. This makes the validity of the resolution of the momentum equation questionable in these specific cases. Reduction of the spatial discretization might reduce these effects (Delestre *et al*., 2012). Nevertheless due to fine features inclusions, these steep gradient occur anyway. Moreover HR flood modelling requires from a numerical point of view an attentive control from practitioners. For instance, especially if numerical scheme uses a threshold value for positivity preservation: masse balance check, spurious oscillation, velocity control *etc*. This is due to the fact that such resource requiring simulations enhance the difficulties that might be encountered by numerical codes. As seen in chapter 1, numerical methods and solvers are not always suited for treatment of numerical difficulties related to wetting/drying and to flow regime changes.

Tested 2D SWEs based codes show in a large extent similar results in water depth calculation under important optimization procedure. Major requirements are involved to get comparable results with a reasonable balance/ratio between mesh generation procedure - computational time - numerical parameters optimization (*e.g.* for wet/dry treatment). If results are found to be comparable between the different codes solving SWEs, advantage of finite volume well balanced scheme for steady state, equilibrium and wet/dry transition is enhanced, drawback being elevated computational cost compare to other numerical methods (*e.g.* Mike 21 ADI). Moreover to ensure that no important errors occurs, controls have to be carefully effectuated (*e.g.* on mass balance, velocities, *etc.*).

Table 3.2 summarizes the possible scenarios simulated with the different codes and the possibilities and limits that the HR runoff modelling over industrial site encountered with the different codes.

Table 3.2. Modelling tools main possibilities and limits encountered over our test case for High-Resolution runoff modelling.

	Use with 3 scenarios	High-Resolution data use and discretization	Stability and high gradient induced limitations	Wet/dry treatment and oscillation occurrences
Mike SHE	Possible with S1, S2, S3	2D SWEs simplification lead to differences with other models results, over our test case this category of model use is not considered as properly performing for our specific purpose		
Mike 21	Possible with S1, S2, S3	software *dt* lower limit induce a CFL dependent limit for fine grid use	stable through diffusion introduction under important CFL restrictions	threshold value can be low enough for our purpose, oscillations might be important
Mike 21FM	not stable with S3	mesh generator not well suited for our application specificities	stability problem with high gradient; could require a specific meshing treatment	threshold system and oscillation can be lowered enough for our purpose
TELEMAC 2D	no option for rainfall scenarios (S1, S2)	mesh generator more adapted to inclusion constraint lines but still not well suited	stable with finite elements and finite volumes	finite element method uses threshold; finite volumes "well-balanced" method allows an efficient treatment

PART. 4. HIGH-RESOLUTION TOPOGRAPHIC DATA USE OVER LARGER URBAN AREAS

Spreading of Unmanned Aerial Vehicle (UVA) use (Remondino *et al*., 2011), goes in this direction of HR LiDAR or imagery based topographic datasets easily available for a specific study purpose. Stakeholders wish to assess accurately the potential of flood risk (due to intense runoff, river flood, coastal surge, etc.) and to evaluate the damages on equipment and infrastructures in order to increase resilience (Gourbesville, 2014). Consequently, hydraulic numerical modelling community increasingly uses DSM information gathered from airborne and UVA technologies for urban flooding modelling (Tsubaki and Fujita, 2010). The previous part of this chapter confirmed the feasibility of HR modelling of overland flow generated by local intense rainfall event over an industrial site.

Nevertheless, above-ground features are not equally represented in DSM generated based on LiDAR and photogrammetric data (see chapter 1). Moreover optimal use of high definition DSM in standard 2D numerical modelling tools might be challenging in terms of feasibility of data integration within modelling tools. Possibilities and challenges of these surface features inclusion in highly detailed runoff 2D models for runoff flood hazard assessment deserve a specific consideration and are therefore the topic of this part. In this part of the chapter, the problematic of high density topographic information inclusion in standard 2D modelling tools is tackled as well as the assessment of possibilities and impact of fine features inclusion. Dissimilar sets of DSM have been created based on two different sets of HR topographic data gathered from *(i)* a LiDAR and *(ii)* a photogrammetric campaign. A case study with typical characteristics of industrial site has been selected in Nice Low Var river valley (France) based on following criterions: *(i)* a spatial extent compatible with a large industrial platform or an urban district/suburb size (600,000 m^2), *(ii)* the presence of a high variety of above-ground structures creating a complex environment having typical characteristics of industrial site, and *(iii)* the availability of HR topographic dataset. An intense rainfall event is simulated over the selected site using a LiDAR and a 3D photo-interpreted HR topographic datasets. Lastly, a river flood event is simulated at HR (1 m) using the 3D photo-interpreted dataset a large scale (17.8 km^2) over the low Var valley in Nice.

Standard 2D numerical modelling tools used for our test were based on 2D SWEs resolution. This category of modelling tool has different numerical strategies to solve 2D SWEs and discretize the spatial information in different ways (see chapter 1, section 1.3). Interest was to assess possibilities and limits of strategies for spatial discretization used by modelling tools, exploring HR DSM use with structured and non-structured meshing approaches.

Section 4.1 presents a case of HR runoff modelling, using LiDAR and photo-interpreted datasets, over a selected site in Nice. The site and the runoff scenarios are first described, then specificities of the used HR topographic datasets are presented. Following section goes through the description of implemented strategies for HR DSM use with models comparison and outcomes are presented and analyzed to conclude this section.

Section 4.2 presents the use of HR photo-interpreted dataset for a river flood simulation over the lower part of Nice Var valley. The Site, the river flood scenario and the code are first presented, specific method for HR photo-interpreted data use is then explained and lastly, a feedback on HR topographic data use from this specific test case is given.

4.1 HR RUNOFF SIMULATION OVER AN URBAN AREA

4.1.1 Site configuration and runoff scenarios specificities

The selected site is the MIN (Marché d'Intêret National) platform located in Nice (France), which has a spatial extent of 603,920 m^2 (Figure 4.1). The site and its surroundings were covered by both a LiDAR and a photogrammetry topographic data gathering campaigns, respectively in 2005 and 2010-2011. The MIN platform and the above-ground features located on it have not changed in a significant way between the two topographic campaigns. Occurrences of above-ground features such as buildings, sidewalks, roundabouts, road gutters etc. are dense on the MIN platform. Moreover, the site presents the interest of including various categories of above-ground features which can range from few centimeters height and width, to larger structures with a metric to decametric size.

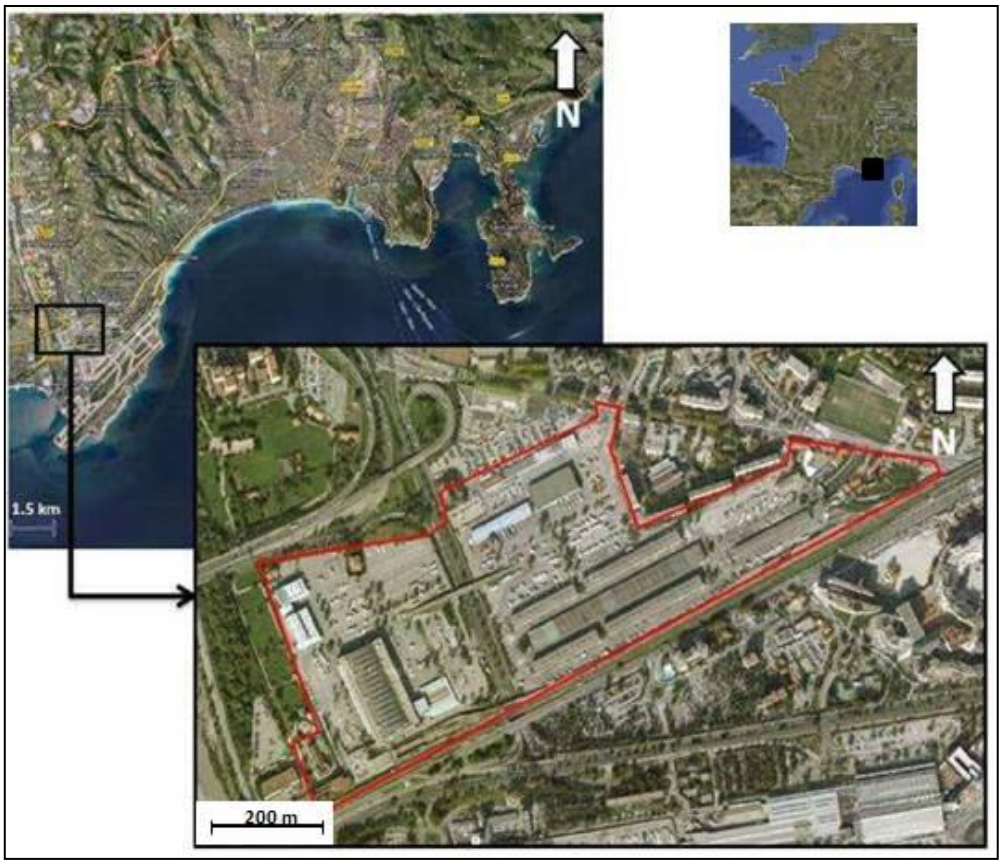

Figure 4.1. *Location and spatial extent of MIN platform case study (France).*

MIN platform is surrounded by elevated roads and railway. These structures were used as closed boundaries for the numerical model whereas two surrounding roads and one cross road have a lower elevation and represent runoff outlet.

Two runoff scenarios matching with the RFS recommendation for runoff hazard assessment from the ASN guide have been elaborated and tested following the same philosophy a introduced in previous section 3.1.1. These scenarios have in common the fact that they considered the sewer system as non-available and as the platform is fully urbanized, infiltration was consider null as it is an impervious area. Here, first scenario (S1) is a one hour long intense rainfall event with constant 100 $mm.h^{-1}$ intensity. Second scenario (S2) is an initial 0.1 m water high layer covering up the whole site. This second scenario is considered as interesting as it allows to address surface features effects on hydrodynamics though not physical. Both scenarios introduce the same quantity of water over the domain, but simulating phenomena with different behavior, they will not be directly compared here.

4.1.2 Presentation of HR topographic datasets

LiDAR dataset

The LiDAR dataset has been gathered for Nice Municipality Geographic Information Services (DIGNCA: Direction d'Information Géographique de la métropole Nice Côte d'Azur) in 2005 during a specific flight with an average flight altitude of 1300m. The produced airborne LiDAR mapping covers 350 km^2. Average density of laser point is 1 per 1.25 m^2. Thirty georeferenced markers located over the domain were used for the georeferencing of the dataset. Large width above-ground features such as buildings, roundabouts, and sidewalks are properly captured by the LiDAR technique whereas narrow features such as walls, fences, *etc.* are not. Bridges, elevated roads and tunnels are included in the LiDAR information. The vegetation has been removed from the raw LiDAR signal. Resulting LiDAR based DSM is a 2 x 2 m resolution grid with an average horizontal accuracy of 0.3 m and a vertical accuracy of 0.15 m. The Figure 4.2 illustrates a part of the LiDAR based DSM where buildings are not included.

Photo-interpreted dataset

A photogrammetric dataset has been gathered for the DIGNCA in 2010-2011. This dataset has been photo-interpreted and covers more than 400 km^2 (Figure 4.3). Principle of photo-interpreted classified dataset created from photogrammetry is explained in chapter 1 (section 1.1.3), and details for this process regarding this specific dataset can be found in Andres (2012).

The number of class of elements created as vector features is about 50. Over the MIN area, more than 79,000 3D objects introduced under vector form information (points, polylines and polygons). Classes include fine above-ground features as narrow as concrete walls and

fences (Figure 4.2 and 4.3). Combination of *(i)* a low altitude flight, *(ii)* a pixel resolution of 0.1m at the ground level, *(iii)* a high level of overlapping among aerial pictures (80%) and *(iv)* the use of an important number of markers for geo-referencing (about 200), lead to a high level of accuracy over the urban area of the city. The accuracy of the data over the MIN area is 0.15 - 0.2 m in both vertical and horizontal dimension. Errors in photo-interpretation is estimated to be around 5% after verifications with terrestrial topographic measurements performed by DIGNCA over 10% of the domain covered by the photogrammetric campaign.

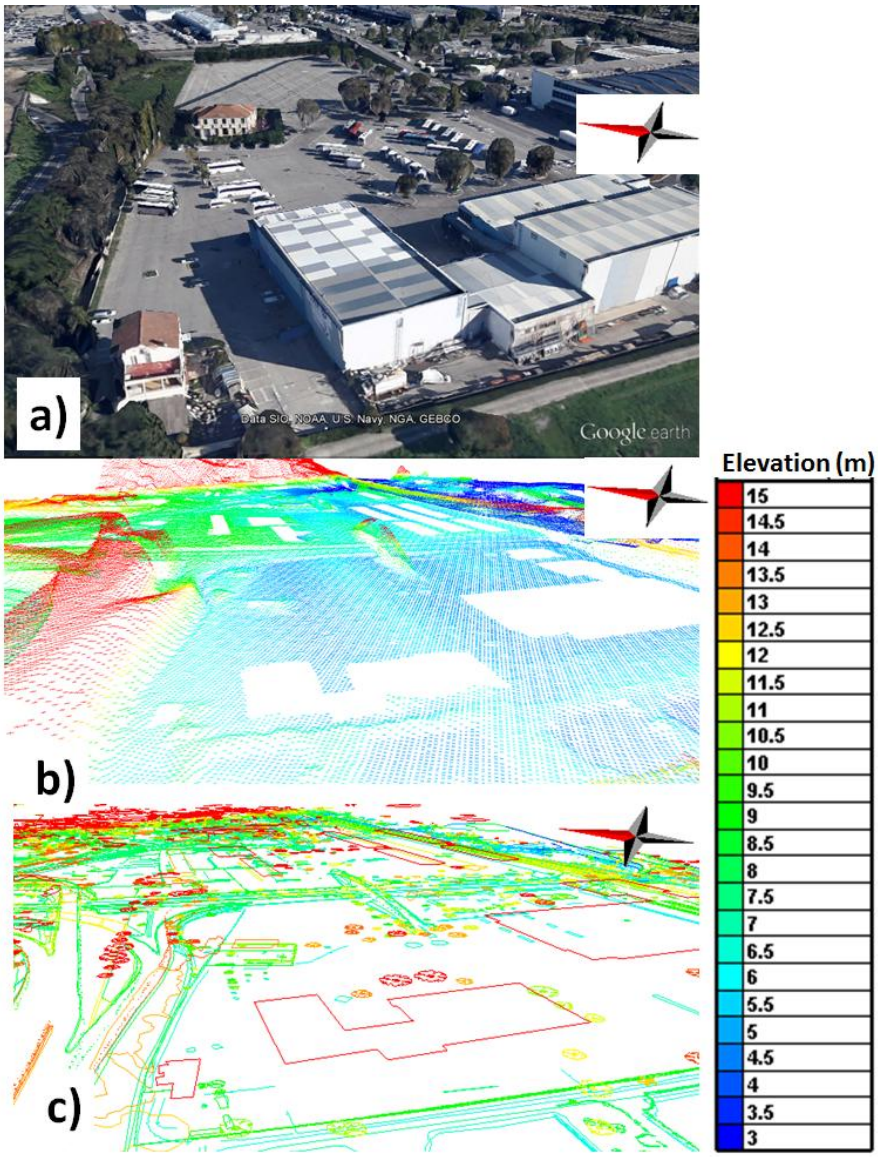

Figure 4.2. *Visualization of a part of MIN platform of LiDAR and photo-interpreted topographic data, with: a) GoogleEarth visualization; b) LiDAR dataset; c) Photo-interpreted dataset with all the classes of features represented.*

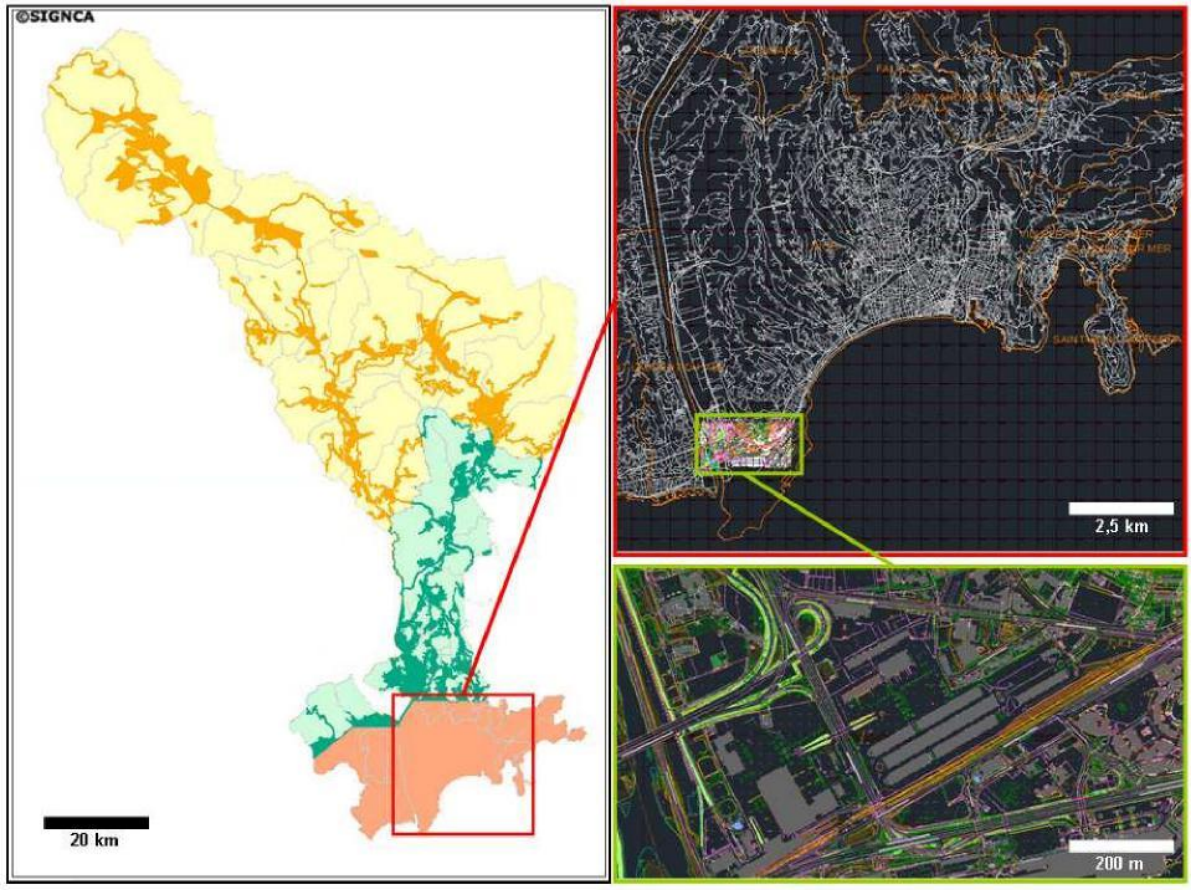

Figure 4.3. *Spatial extent and overview of the DIGNCA Photo-interpreted dataset with a focus on the MIN platform area.*

4.1.3 High-Resolution DSMs for overland flow modelling purpose

DSM and hydraulic modelling tools

Different sets of DSM have been created for our specific runoff application. As previously mentioned, LiDAR and photo-interpreted datasets both allow production of High-Resolution (HR) DSM, but they do not include the same information. On one hand, LiDAR based DSM will represent/include all above-ground features with a certain width, but will not represent properly in the DSM the narrow vertical structures such as walls which could influence runoff hydrodynamic. On the other hand, classified photo-interpreted data allow creation of DSM based on selection of classes. Not all the classes of features are relevant to create a DSM devoted to a hydraulic modelling purpose. Therefore, a class selection has to be done. Classes that are relevant for a given application are those that represent surface structures impacting runoff flow path. In our case, we have selected 12 classes which encompass all above-ground features having a vertical concrete footprint (*e.g.* building, walls, concrete

streets features such as road curbs, sidewalks, *etc.*). Selected features represent in total more than 2000 3D polygons and polylines over the MIN area.

Two types of DSMs were generated, using either the LiDAR data or combining the LiDAR data with the photo-interpreted dataset, following process detailed in table 4.1 The approach which combines the two types of datasets has the interest of including class selections of fine features and increasing density of the ground information, which is more dense in the LiDAR data (1 point every 2 m) than in the 3D classified data (1 point every 5 m). Use of photo-interpreted classified data alone to generate DSM has been done (see annex A).

- When using LiDAR data, a predominant aspect to consider for the elaboration of a DSM relevant for a runoff simulation application is at least to make sure that no structure included in the DSM would erroneously block the water flow (Abily *et al*., 2015b). Note that macrostructures, such as bridges and elevated roadways inclusion in DSM would block the runoff flow and might consequently result in flood estimation errors (Abdullah *et al*., 2012).
- For the DSM generation, based on classified data, the key point is the selection of classes that would be relevant to include in the DSM generation. For the DSM using the photo-interpreted data combined with the LiDAR data, two different resolutions of DSMs were created. This type of approach of HR DSM generation includes infra-metric features elevation information. The deviations with the reality rely here in the fact that during the step 2, the features finer than the grids resolutions are actually widened to the grids resolution size.

Table 4.1. Detail of processes for DSMs generation

	High-Resolution DSM generation process			DSM integration in the 2D SWEs sbased hydraulic codes
HR topographic dataset used	**Step 1**	**Step 2**	**Step 3**	**Step 4**
LiDAR dataset	Removal of overland flow blocking structures (*e.g.* bridges, elevated road, *etc.*)			Use of the created 2m per 2m resolution grid as a structured mesh
Photo-interpreted classified dataset combined with LiDAR dataset	a) Check of matching between coordinate systems of the datasets b) Selection of relevant class features from the classified dataset	a) Conversion of features classes (vectors) to raster at desired resolution (here 0.3m per 0.3m and 1m per 1m) b) Conversion of LiDAR data grid to a grid having the same resolution	Extrude classes grids over the LiDAR grids	a) Generated grids -here one having 0.3m per 0.3m resolution and one having a 1m per 1m resolution- can be used as structured grid and include classes elevation information b) If a non-structured grid is to be used, the classes selected (from step 1 b) are used as constraint lines.

Standard 2D SWEs based numerical modelling tools used in this study were Mike 21 (product of DHI Water & Environment) and TELEMAC-2D (product of EDF & TELEMAC-MASCARET consortium). These codes numerical methods (presented in chapter 1 concluding part) and summarized in Part 1 section 1.1 of current chapter) are well known by hydraulic community. Mike 21 and TELEMAC-2D codes have significant differences, but the interest of these modelling tools for our study purpose relies on the fact that they have different property in the numerical scheme spatial discretization: structured mesh for Mike 21, whereas TELEMAC-2D uses a non-structured mesh.

Consequently, using the two spatial discretization approaches would help to address possibilities and constraint related to meshing strategy effects on *(i)* HR data integration feasibility and *(ii)* consequences in flood estimation results. Beside spatial discretization, other parameters for the hydraulic simulations are not of a prime interest here, and have been set to match with classical urban modelling approach for aspects such as boundary, and energy losses parameters (Manning and eddy parameters). Moreover indicators of computation reliability (mass balance/CFL/artificial polarization) have been checked to make sure that no important numerical perturbations arise in simulations, as described in Abily (2013a).

DSMs and their integration in standard 2D SWEs based hydraulic codes

When comparing DSMs, main differences arise from the fact that those incorporating 3D classified data from photogrammetry include more above-ground features compared to DSM only based on LiDAR information. Therefore, finer structures are included in DSM as illustrated in figure 4.4. Beside fine above-ground structures inclusion in photogrammetry combined with LiDAR DSM, other differences can be observed in figure 4.4. B1 is a building which has been constructed between the two data gathering campaigns. B2 is a small building which was not captured by LiDAR information. Three containers around B2 illustrate errors of misclassification of photogrammetric data which can occur during photo-interpretation as they were classified as buildings. Errors in photo-interpretation can be of two types: *(i)* omission or adding of structures and *(ii)* misclassification.

When including the DSM as a regular calculation grid in Mike 21, photogrammetric data combined with LiDAR DSM represents 12.8 million (at 0.3 m resolution) and 1.1 million (at 1 m resolution) of computation points, whereas LiDAR DSM (at 2 m resolution) represents a 300,000 points grid.

- DSMs use as computational grid under this form does not lead to troubles with the regular mesh based modelling tool Mike 21. Non-structured mesh creation based on LiDAR DSM use generates a 400,000 elements mesh and does not lead to specific problems for mesh generation.
- For a non-structured mesh creation adequately matching with the photogrammetric combined with LiDAR DSM, a specific work is required. Indeed, the elevated number of constraint lines required for mesh refinement to properly represent small features. This might lead to over constraint issues with standard meshing tools (BlueKenue for TELEMAC-2D). Therefore, a highly important time investment for a proper mesh creation is required. Built non-structured mesh is here of 1.4 million elements (cells) with an average element area of 0.28 m^2, a maximal element area of 1.38 m^2 and a minimum element area below 1 cm^2.

Beside these non-structured mesh generation aspects, feasibility of High-Resolution DSMs use at MIN site scale is found to be operational for runoff simulation. Nevertheless, a good optimization in terms of model parameterization is required and use of indicators of computation reliability recommended (Abily *et al.*, 2013a).

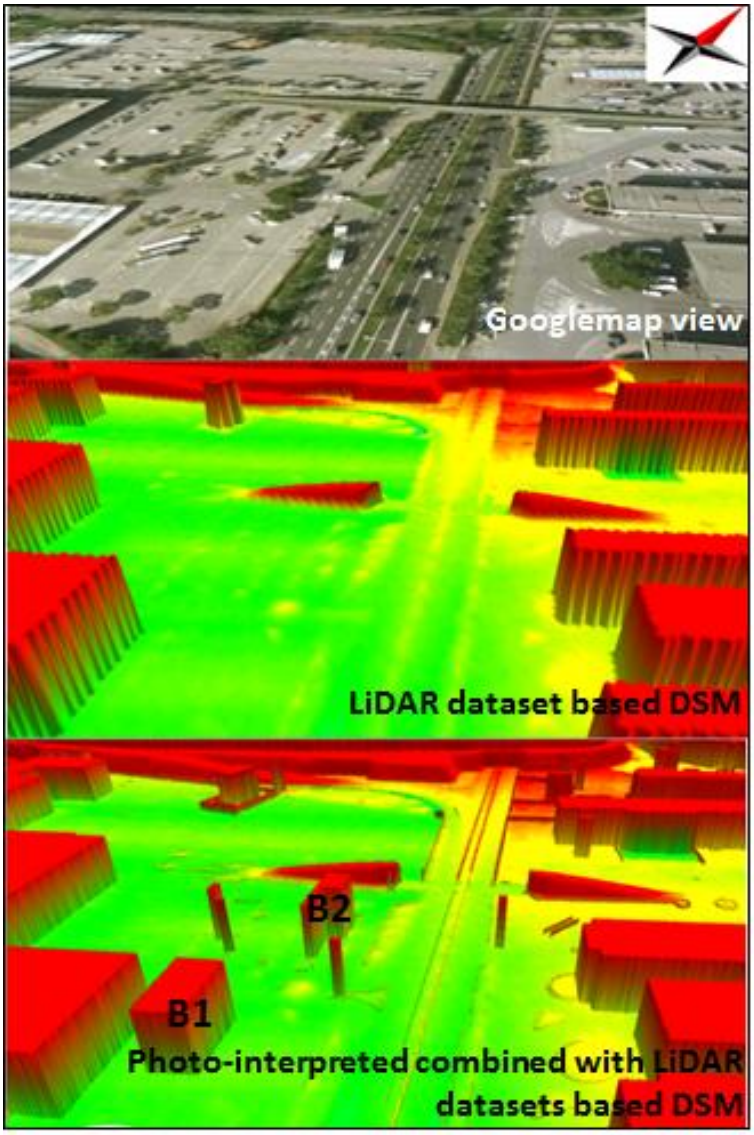

Figure 4.4. *3D visualization of DSMs used as computation grid in Mike 21.*

4.1.4 Impact of fine above-ground features inclusion in DSMs for runoff simulations

Differences in maximal water depth (h_{max}) calculation depending on type of employed HR DSMs are revealed to be important. Figure 4.5 illustrates this observation as non-inclusion of small scales above-ground structure leads to both under or over estimations of h_{max}. In our specific case, inclusion of concrete fine vertical structures generates differences in h_{max} estimations up to 0.5 m. In fact, as represented in figure 4.6, these structures play a major role in runoff flow drainage path and consequently on h_{max} evaluation. This observation is valid disregarding the resolution used for fine structures inclusion in DSM. When comparing results on h_{max} and water depth evolution calculated from the photo-interpreted combined with LiDAR DSMs either at 0.3 m and 1m resolution, h_{max} estimations are comparable.

If these results underline the importance of small scale above-ground features for runoff h_{max} estimations, limits due to errors in classification have to be enhanced. For instance errors such as misclassification of water non-blocking structures (fences) as walls are observed. Locally this leads to important runoff flow path and h_{max} misevaluations. When comparing results on simulated runoff h_{max} regarding spatial discretization strategy (structured or non-structured), results are comparable in a large extent, as illustrated by figure 4.7. This is observable as well and confirmed when comparing simulated water levels from structured and non-structured mesh based models at specific points of interests as illustrated by figure 4.8.

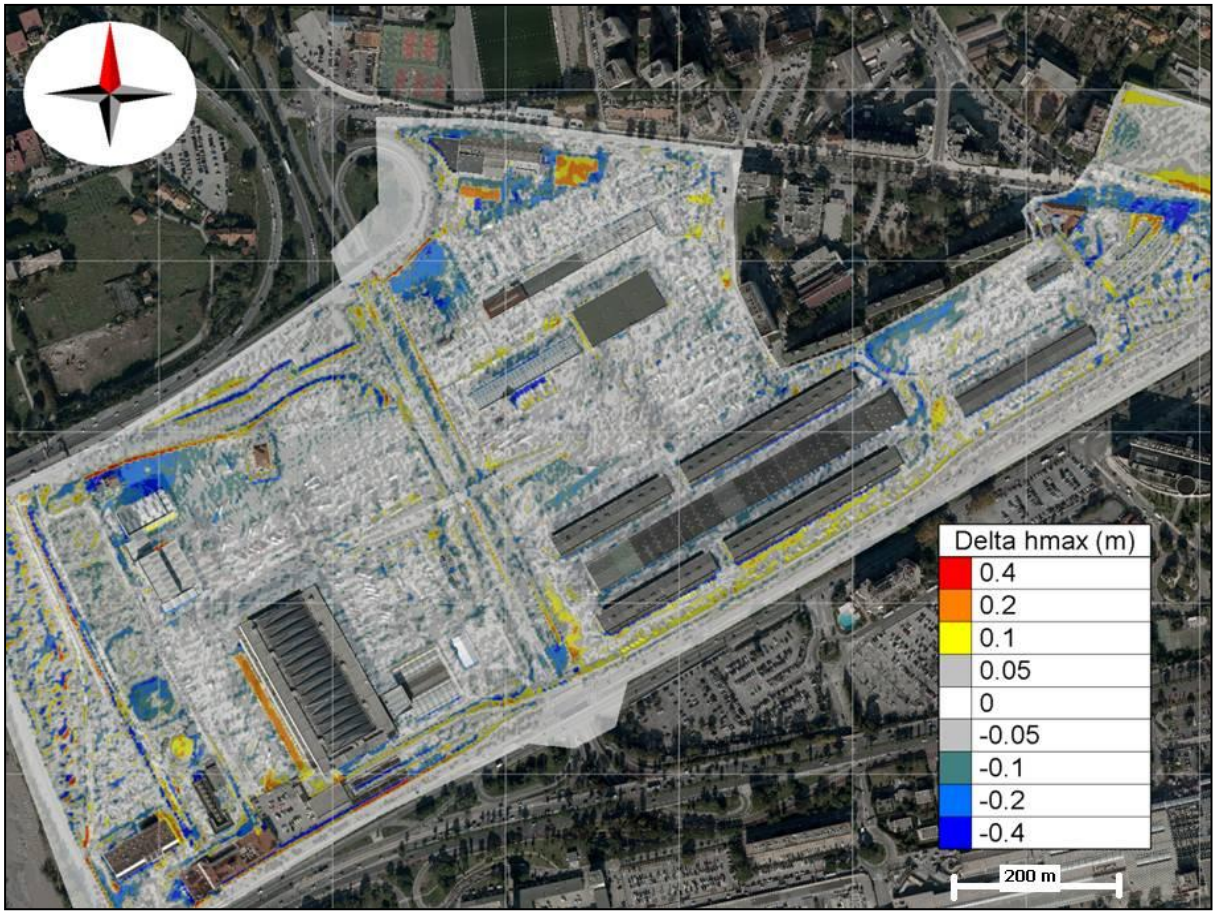

Figure 4.5. *Differences in maximal water depth (h_{max}) estimated with Mike 21 for S1 simulation based on Photo-interpreted combined with LiDAR DSMs and h_{max} estimated with Mike 21 for S1 simulation based on LiDAR DSM.*

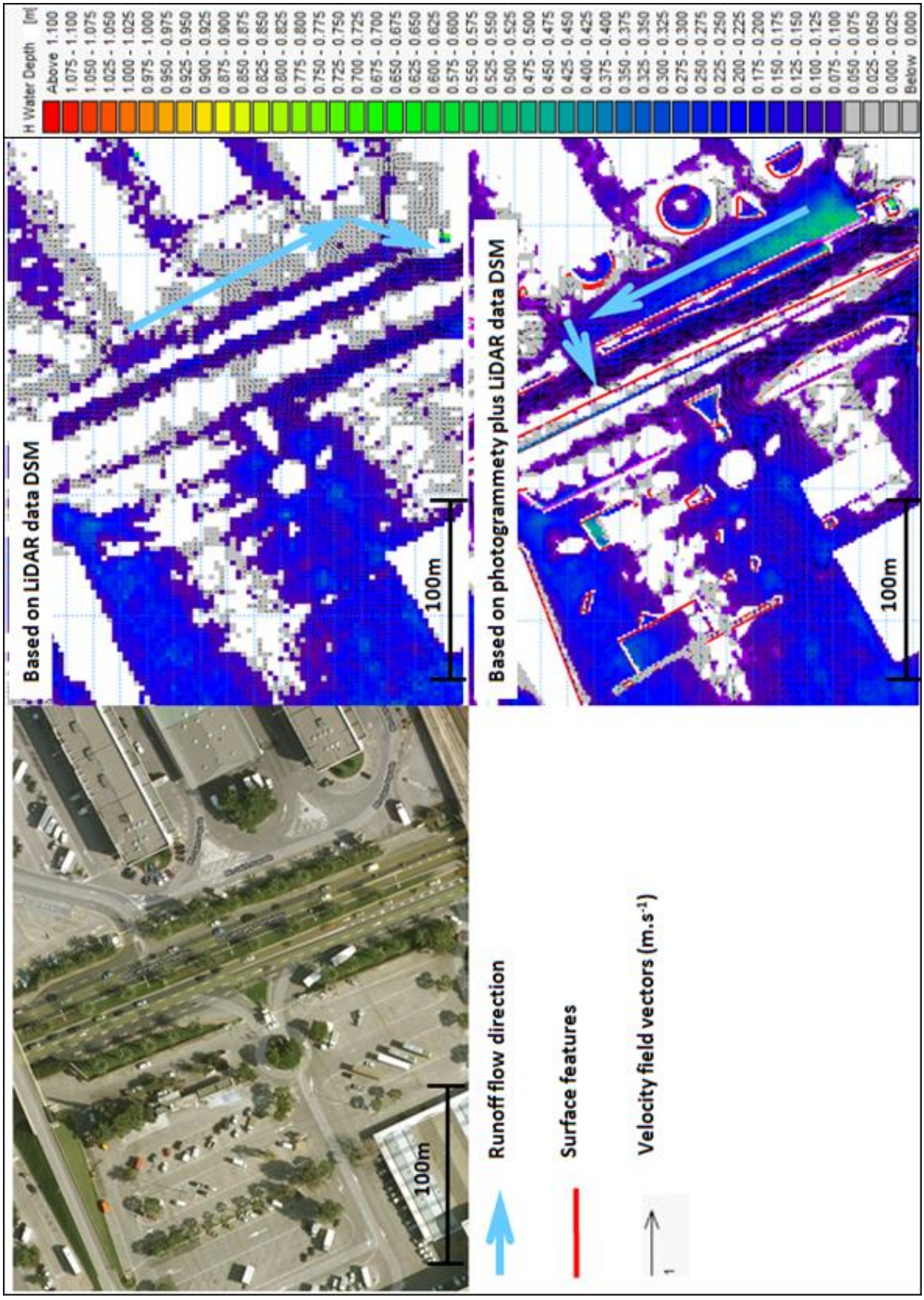

Figure 4.6. *Water depth estimated from S1 scenario at simulation t=1 hour, with Mike 21.*

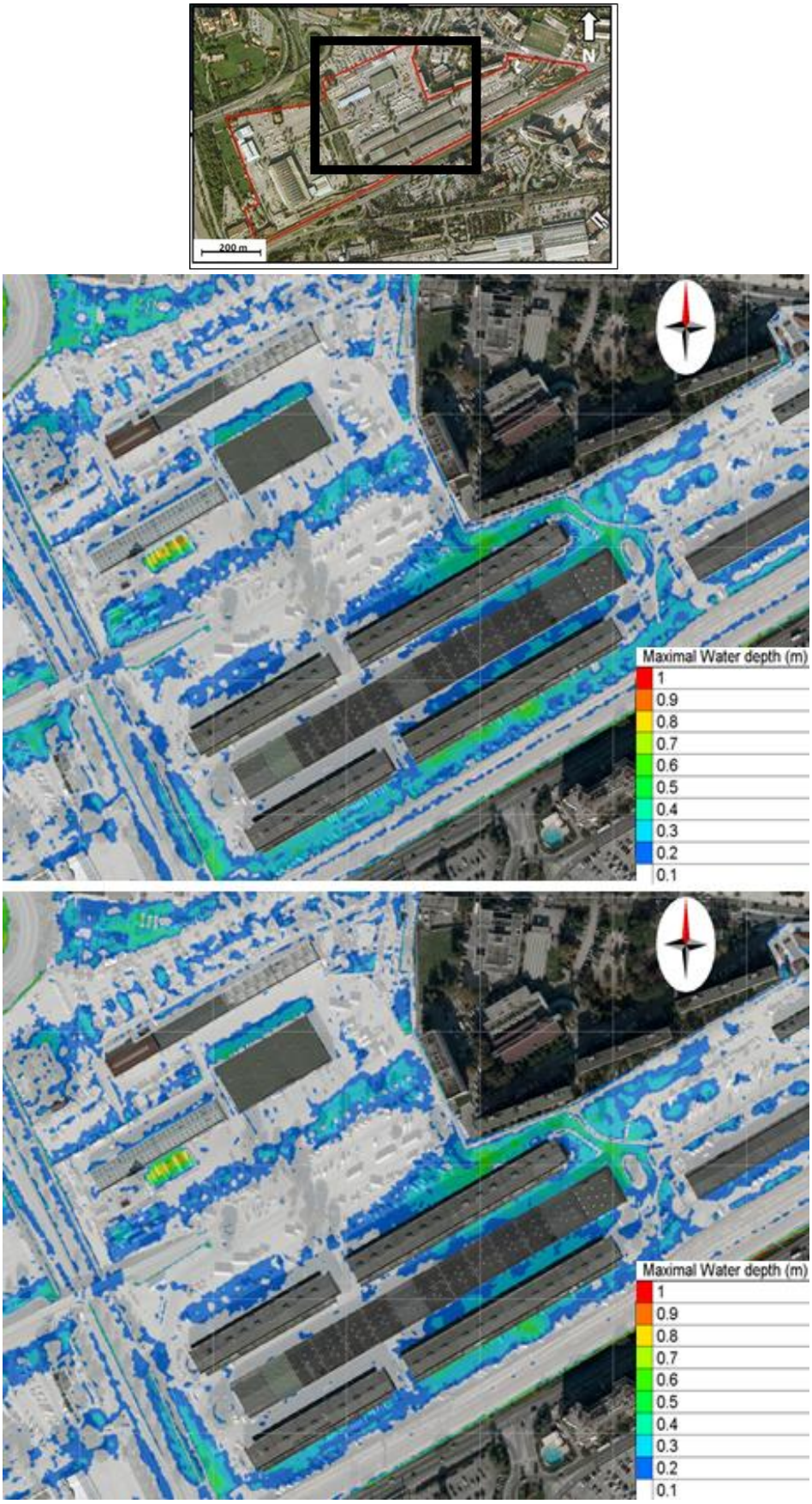

Figure 4.7. *H_{max} for S1 scenario using photo-interpreted combined with LiDAR DSM (resolution 0.3 m) with a structured (Mike 21, up) and a non-structured mesh (TELEMAC-2D, down).*

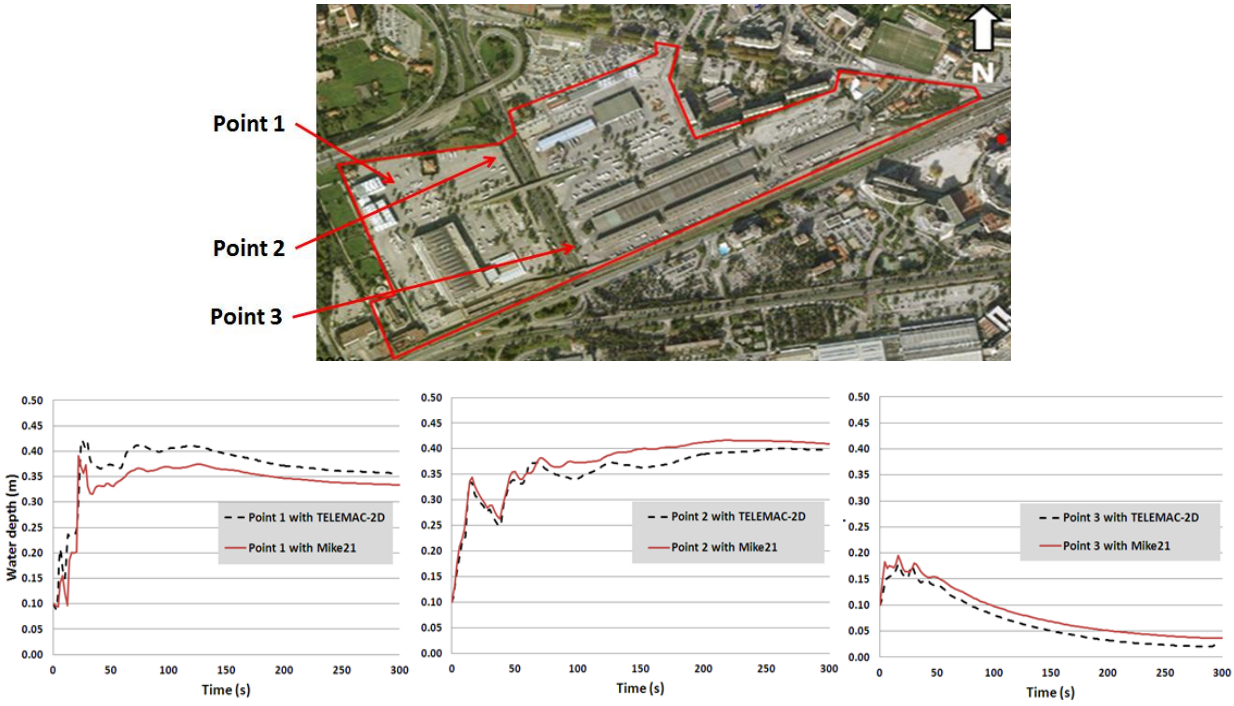

Figure 4.8. *Illustration of water levels evolution simulated at 3 locations for scenario S2, with non-structured mesh (TELEMAC-2D) and structured mesh (MIKE 21) approaches, based on DSM created Photo-interpreted data combined with LiDAR data (0.3 per 0.3 m resolution).*

4.1.5 Outcomes

Objectives of the analysis presented in this section focused on:

(i) feasibility assessment of HR topographic data use for runoff simulation over a complex environment such as an industrial and densely urbanized sites, using standard 2D SWEs based modelling tools;

(ii) evaluation of issues which might arise from HR topographic data use and integration for overland flow modelling.

Feasibility of High-Resolution topographic data use is confirmed for runoff scenario simulations at an industrial site scale with different categories of standard numerical modelling tools (Mike 21 and TELEMAC-2D) relying on different spatial discretization strategies. Results are highly influenced by the quality of HR DSMs. Therefore, when using HR topographic data for practical urban hydraulic application it is important to have deep insight on quality of row HR dataset and on quality of created DSM.

Possibilities of runoff influencing above-ground features inclusion in DSM is revealed to be unequal depending on HR topographic data gathering technology. In present case, the LiDAR data resolution (2 m per 2 m) is not fine enough to capture fine small scale above-ground features (*e.g.* concrete walls) which can highly influence runoff drainage path.

Inclusion of small scale above-ground structures information in DSMs was achieved using photo-interpreted data from photogrammetry technology combined with the LiDAR data. Added value of this approach for fine runoff influencing features inclusion in DSM is clearly observed disregarding resolution used for their inclusion (either 0.3 m or 1 m). fine above-ground features inclusion can lead locally up to a 0.5 m difference in maximal water depth estimations compared to simulation where they are not included.

Integration of HR DSM information within 2D SWEs based standard hydraulic modelling tools depends on spatial discretization strategy. Structured and non-structured meshes use gives comparable results. Yet, the workload for an optimal non-structured mesh creation is much more important as required refinement lines, in densely urbanized areas, will tend to over constraint meshing algorithm due to their elevated number and density (developed in Abily (2015b) - see Annex A).

Most of the topographic data used in practical engineering application for flood risk assessment have not been acquired specifically for hydrological application, but have been gathered for multipurpose applications. Consequently for LiDAR data, aspect such as removal of flow blocking macrostructures (bridges, elevated roads, *etc.*) has to be properly handled by modeller when creating DSM. At larger scale, this task can be particularly time consuming. With photogrammetry based classified data (photo-interpreted), choices of practitioner regarding which categories of above-ground features have to be included in DSM will highly impact results. Feedback to photo-interpretation operators such as differencing vertical structures classes or subclasses depending on their permeability nature (*e.g.* fences or concrete walls) is technically accessible and might improve the ease of data use for hydraulic orientated application. Unavoidable errors of classification in photo-interpretation might lead to important consequences on simulations and have to be carefully controlled. This might lead to restriction of 3D classified data use at larger scale (city scale) independently of computational cost concern, as it would imply a large workload of data control.

4.2 HR FLOOD RIVER EVENT SIMULATION OVER THE LOW VAR VALLEY

The use of HR photo-interpreted topographic dataset for a flood river event modelling is introduced in this section. A specific approach has been elaborated for a medium scale HR DSM creation (5,000 m per 3,500 m). Approach, is designed based on the use of HR 3D classified data included as a structured grid for computation. Following the outcome of studies that were based on the use HR topographic data for runoff modelling over industrial sites previously presented in this chapter, this test aims:

- to implement HR photo-interpreted dataset over a larger scale;
- to apply a method to create a HR DSM from selection among photo-interpreted dataset classes for DSM extrusion;
- to test the possibility of structured grid use for such a purpose using a HPC structure, as previous tests showed that non-structured grid based and structured grid based discretization, leads to comparable results when properly done and underlined the difficulty to generate non-structured mesh over densely constrained urban environment.

The selected area is the low part of the Var river valley. This area has experienced, in November 1994 a flood event (Guinot and Gourbesville, 2003). The area has been covered by a high accuracy photogrammetric data gathering campaign conducted by Nice Municipality (DIGNCA) in 2010-2011. Overland flow influencing structures such as concrete walls, road gutter, sidewalks, *etc.* are photo-interpreted. These structures are included in the dataset and their elevation properties will be part of the topographic information included in the HR DSM specifically created for the hydraulic modelling purpose.

4.2.1 Site, river flood event scenario and code

- ***Site and scenario***

The 5th and the 6th of November 1994, an important flood event occurred in the low part of the Var catchment. This historical flood event had severe economic consequences as well as created issues for the local civil society. The flood scenario for our test is based on estimated hydrograph of this event (Lavabre *et al.*, 1996; Guinot and Gourbesville, 2003). Through our test, we want to produce a HR map of maximal water depths reached in the low Var valley, producing a HR DSM and using it as a structured grid with FullSWOF_2D code. The code properties are described in the chapter 1 and summarized in next section. However, the objective here is not to reproduce the flood event. It should be noted that major changes occurred on the site since 1994: levees, dikes and urban structures have been intensively constructed in this area whereas topographic data has been gathered in 2010-2011.

To shorten the simulation length, we chose to simulate a 9-hours scenario. First, a constant discharge of 1,500 $m^3.s^{-1}$ is run for 3 hours to reach a steady state. This steady state is used as a hot-start. Then the overtopping part of the hydrograph is run, reaching the estimated peak discharge (3,700 $m^3.s^{-1}$) and then decreasing long enough to observe a receding of the overland flow water depth (Figure 4.9). The Manning's n coefficient is spatially uniform on overland flow areas with a value of 0.015. This value corresponds to energy losses over a concrete surfacing (Chow, 1959). No energy losses properties have been included in the hydraulic model to represent the bridges piers effects. Downstream boundary condition is an open sea level with a Neumann boundary condition.

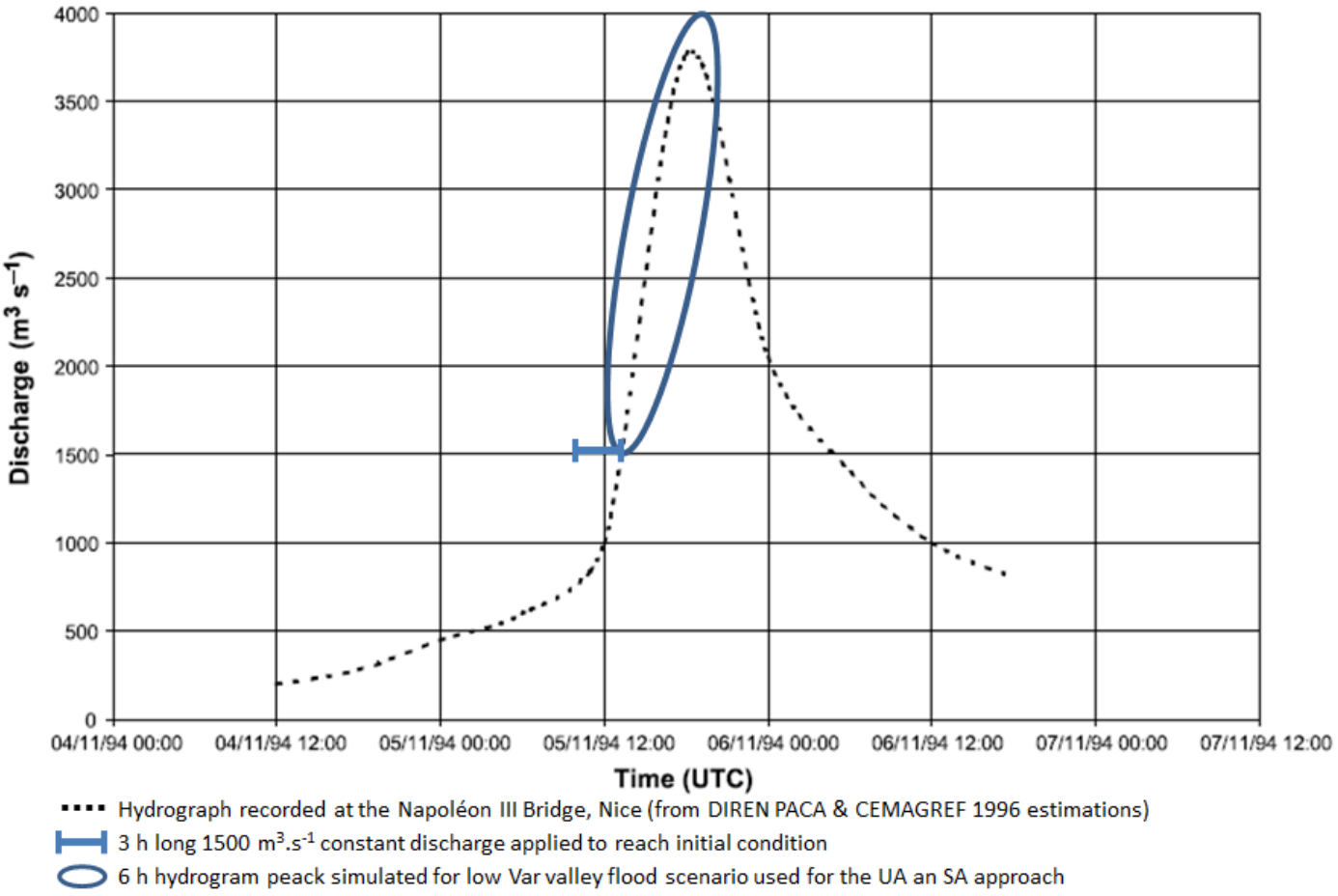

Figure 4.9. *Estimated 1994 flood event hydrograph at Napoleon bridge with schematization of simplification of the hydraulic scenario used for our HR simulation.*

- ***Code description***

FullSWOF_2D is used in this study. The code has been presented in chapter 1, section 2.3. As a reminder, this code approximate the solution of the SWEs relies on a well-balanced

finite volume method over a regular grid using numerical method based on hydrostatic reconstruction scheme (Delestre *et al*., 2012; 2014). FullSWOF's above mentioned properties are of good interest for urban overland flow modelling. Interest regarding specificities of HR topographic data use in our study relies in the use of structured mesh. Two parallel versions of the code have been developed allowing to run calculations under HPC structures (Cordier *et al*., 2013; Delestre *et al*., 2016). The MPI version of the code has been used. The HLL solver has been used in this study with a second order MUSCL reconstruction method as recommended in Delestre (2010).

4.2.2 Method for High-Resolution photo-interpreted data use for High-Resolution hydraulic modelling

Principle of Nice city photo-interpreted dataset is explained in Andres (2012) and in section 4.1.2. As a reminder, the mean accuracy of the photo-interpreted data over the low Var valley area is 0.15 - 0.2 m in both vertical and horizontal dimensions. The number of class of elements created as vector features is about 50. The high level of accuracy has allowed photo-interpret fine above-ground features as narrow as concrete walls and road gutters. Over the low Var river area selected for the study, total number of polyline features represents more than 1,100,000 objects introduced under vector form.

To create the HR DSM, the following approach has been carried out. First, a DTM using multiple ground level information sources: points, polygons and polylines is created and provided at a 0.5 m resolution by DIGNCA. Then, a selection procedure among classified data is performed. This selection is achieved by considering concrete elements that can influence overland flow drainage path only. It includes dikes, buildings, walls and "concrete" above-ground elements (such as sidewalks, road gutters, round abound, doors steps, *etc.*). 12 classes are selected among the 50 classes of the 3D photo-interpreted dataset (Figure 4.10). During this step, polylines giving information on elevated roads and bridges which might block overland flow paths are removed. The remaining total number of polylines is 52,600 after the two selection steps.

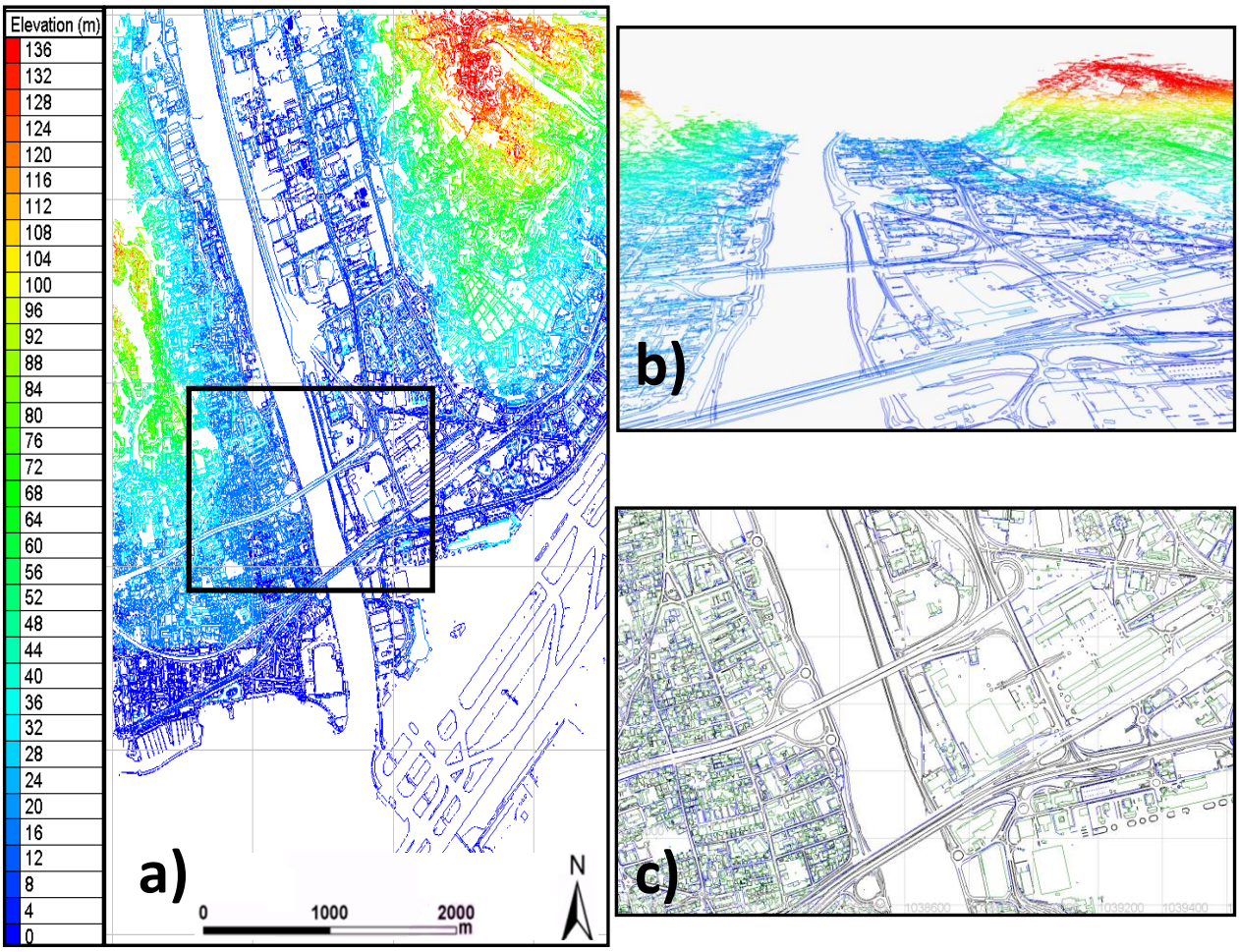

Figure 4.10. *Overview (a) and zoom (b and c) of the HR 3D dataset selected classes at step two of the HR DSM creation ,before bridges and flow blocking macro-structures removal.*

The final step of HR DSM elaboration consists in extruding elevation information of selected polylines on the DTM. To proceed, features represented by closed lines are converted to polygons (*e.g.* buildings, round abound, sidewalks). Polylines and polygons are then converted to raster at desired resolution (in our case 1 m resolution) for extrusion over the DTM. Eventually, HR DSM that has elevation information of selected 3D classified features is produced (figure 4.11). The HR DSM resolution is here 1 m. This choice of resolution will allow to integrate directly the HR DSM at desired regular mesh resolution in FullSWOF_2D. The previously described method has allowed inclusion of fine elements impacting flow behavior of infra-metric dimension, oversized to metric size, in the 1 m resolution regular mesh. At this resolution the number of mesh cells is above 17.8 million.

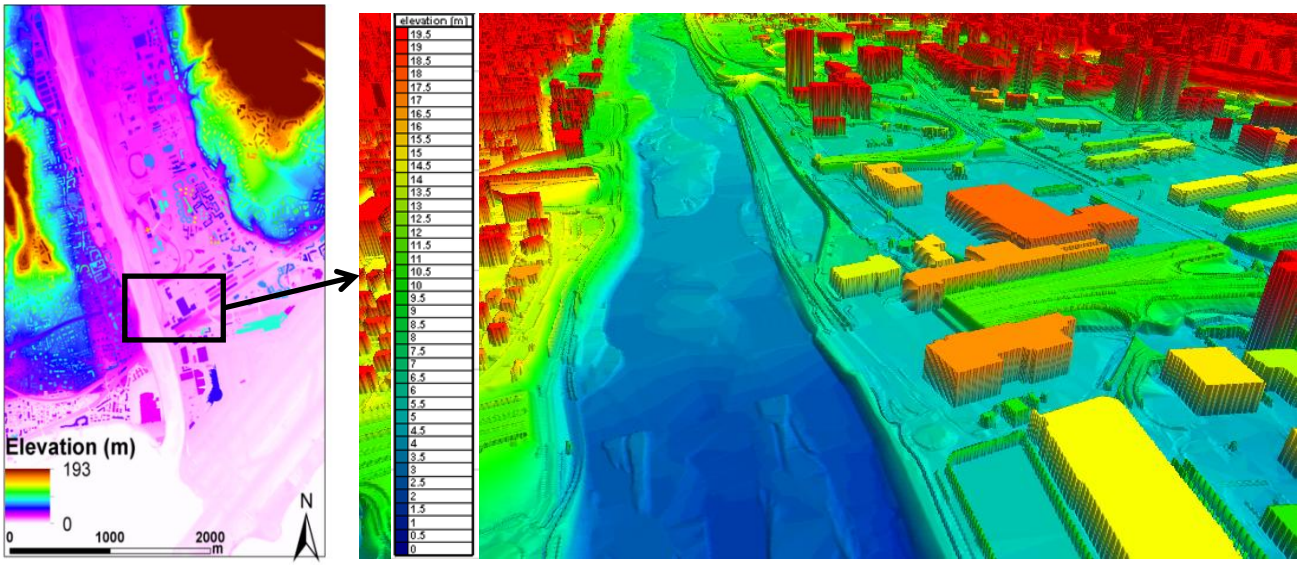

Figure 4.11. *HR DSM overview illustrating ground surface and above-ground elements elevation (with z axis scale multiplied by 2 for clarity sake of the 3D rendering visualization)*

4.2.3 Feedback from High-Resolution river flood modelling

An overview of the maximal water depths due to overland flow is given in figure 4.12. A proof of concept of HR photo-interpreted data integration in 2D SWEs based codes and use for river flood modelling over urban environment is given here. Advantages of such an approach rely: *(i)* in possibility to include detailed surface elements influencing overland flow, and *(ii)* in automatic process and modularity of classes' selection for HR DSM production.

Two limits, specific to HR DSM created for our case study, have to be emphasized. *(i)* The riverbed section itself was filled by 0.1 m to 0.2 m of water at the time of the photogrammetric campaign. Therefore the sections of the river are underestimated, not without standing uncertainties related to the fact that changes in riverbed occur during a flood event. *(ii)* Bridges piers, reducing river section are not included in the HR DSM for our workability test.

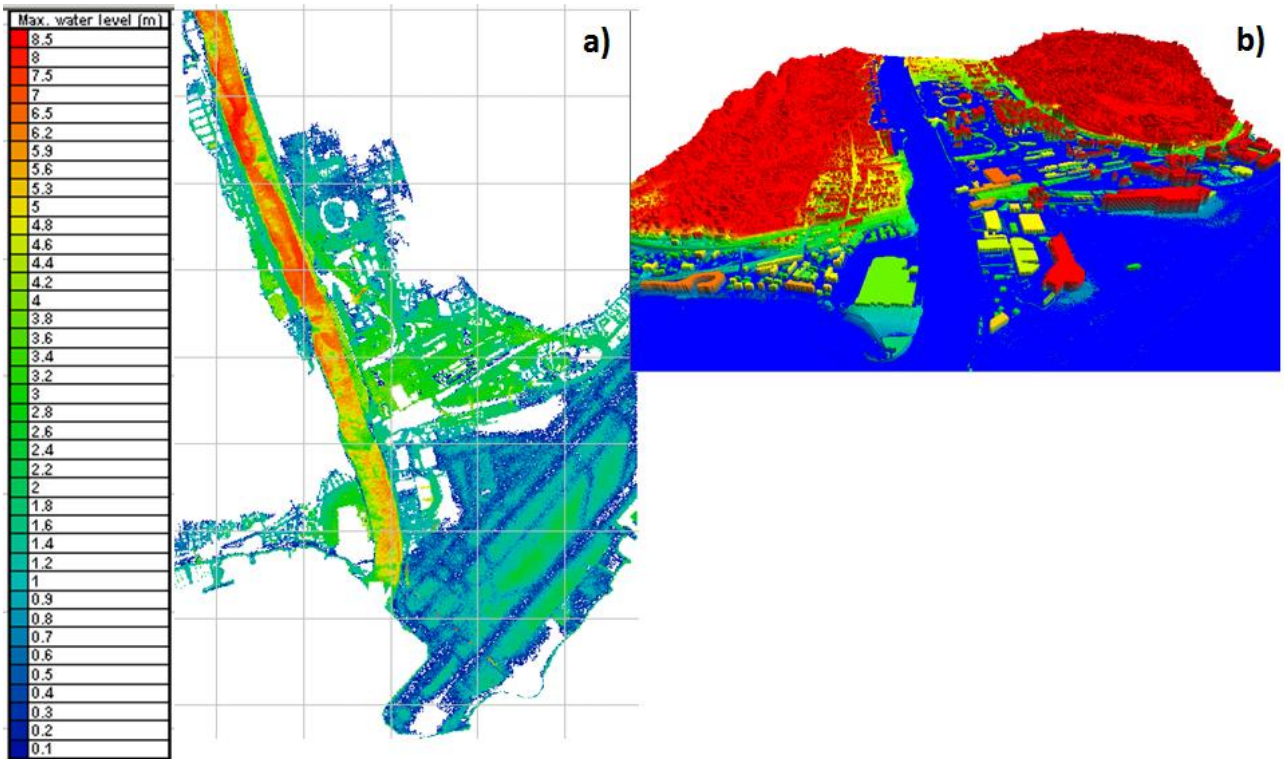

Figure 4.12. *Overland flow maximal water depths flood map calculated using HR DSM with FullSWOF_2D (a) and 3D global representation of flood extent (b).*

More generally speaking, when using such type of data for a HR flood river modelling purpose several categories of recommendations and limits deserved to be emphasized for practical engineering applications.

- The HR classified data are heavy and their manipulation for pre- and post-processing is computational resources demanding.
- Criteria used for photo-interpretation have to be checked, as they can highly influence HR DSM. Note that classification criteria for a given photo-interpreted dataset might not have been created specifically for water modelling purpose. For instance what will be classified as concrete wall, is not based on material recognition criteria but on structure width/elevation ratio. In that case permeable structures, such as fences, can be classified as walls. Another example in the photo-interpretation procedure can be criterion (for human operators or algorithm) to close a polyline. Such type of criterion often consists in a distance threshold between two points. This results in blocking the water flow in or out, in a given area if closed polyline artificially closes real overland flow path. Finally, a limitation appears regarding bridges piers where information is not given by aerial techniques.

- HR DSM use at this scale, with codes fully solving 2D SWEs, requires the use of intensive calculation resources. For this HR simulation, the computational time for simulation of the 9-hours hydrograph using FullSWOF_2D parallel version over 24 CPUs was more than 3 days.
- Lastly, even though HR DSM has a high level of accuracy, HR topographic dataset has different types of inherent errors. It includes white noise, biased, and local errors in measurement (see Fisher and Tate, 2006; Wechsler, 2007). Second type of errors is related to photo-interpretation. It can be omission, addition or misclassification of elements. These types of errors can lead to important changes in overland flow path in the hydraulic calculation.

CHAPTER II CONCLUSIONS

Objectives (T1) of this chapter were:

1) to tackle the problematic of High-Resolution (HR) topographic datasets inclusion in standard 2D modelling tools;
2) to assess possibilities and impacts of fine features inclusion in detailed flood modelling.

This chapter went through the use of three different case study, at different scales, with several standard codes using various numerical approaches and spatial discretization strategies. Two different HR topographic datasets were tested LiDAR and photo-interpreted.

The case study gave a proof of concept of HR topographic data use feasibility, *(i)* to produce a HR DSM for flood simulations in industrial/urban environments, and *(ii)* to integrate this HR DSM information in standard 2D SWEs based codes.

Tested categories of 2D SWEs based codes, show in a large extent similar results in water depth calculation under important optimization procedure. Major requirements are involved to get comparable results with a reasonable balance/ratio between mesh generation procedure - computational time - numerical parameters optimization (*e.g.* for wet/dry treatment. If results are found to be comparable between the different codes solving SWEs, advantage of finite volume well balanced scheme for steady state, equilibrium and wet/dry transition is enhanced, drawback being elevated computational cost compare to other numerical methods (e.g. Mike 21 ADI). Moreover to ensure that no important errors occur, controls have to be carefully done (*e.g.* on mass balance, velocities, *etc.*).

A methodology to design a HR DEM including fine elements influencing overland flow has been presented and tested for photo-interpreted datasets. The inclusion of detailed/thin features in DEM and in hydraulic models lead to considerable differences in local overland flow depth calculations compared to HR models that were not describing the urban or industrial environment with such level of detail. Moreover, added value of fine features inclusion in DEM is clearly observed disregarding resolution used for their inclusion (either 0.3 m or 1 m). Indeed, tests to include fine features (extruding theirs elevation information on DEM), through over sizing their horizontal extent to 1 m, lead to good results respect to their inclusion at finer resolution. On the other hand, fine above-ground features inclusion can lead locally up to a 0.5 m difference in maximal water depth estimations compared to simulation where they are not included.

The added value of HR models is put to the front to provide detailed information about flooding. The impact of fine features is important. A set of remarks and cautions were raised up in this chapter regarding an will be enhanced here regarding: *(i)* validity of the HR modelling approach; *(ii)* HR DSM generation for hydraulic modelling purpose; *(iii)* HR topography information integration in 2D SWEs based codes and *(iv)* computational resources requirement.

***(i)* Validity of the approach**

When using HR topographic datasets for HR flood modellings, high topographic gradient with respect to the water height occurs, especially when it comes to HR modelling of runoff scenarios. This makes the validity of the resolution of the momentum equation questionable in these specific cases. Reduction of the spatial discretization might reduce these effects (Delestre *et al*., 2012). However, due to fine features inclusions, these steep gradient occur anyway. Moreover, HR flood modelling requires from a numerical point of view an attentive control from practitioners. For instance, mass-balance check (especially if numerical scheme uses a threshold value for positivity preservation), spurious oscillation, velocity control, *etc*. This is due to the fact that such resource requiring simulations enhance the difficulties that might be encountered by numerical codes. As seen in chapter 1, numerical methods and solvers are not always suited for treatment of numerical difficulties related to wetting/drying and to flow regime changes.

Lastly, for the approach to be valid it requires a communication from practitioners to stakeholders is required (decision makers, non-specialists engineer using models results, *etc.*) concerning confidence and possible doubts about their results. For instance, it can be illustrated through basic communication on the approach validity, sensitivity analysis or uncertainty assessment possible (see chapter 3).

***(ii)* HR DSM generation for hydraulic modelling purpose and fine features inclusion**

The case study enhanced the possibility to create HR DEM (using LiDAR or photo-interpreted datasets) suited for free surface hydraulic modelling purpose. It mean that it is possible to treat the HR datasets in order to generate a HR DEM where the modeller can select above-ground elements that should be implemented (or not) in the DEM according to his judgment regarding impact of these features on overland flow.

When the extent of the domain increases, from a practical point of view, the data treatment/ease of use for DEM generation is not easy to handle on standard desktop computer resources. This is true for both LiDAR and photo-interpreted data. Advantage of photo-interpreted dataset is that it allows to manipulate classes of above-ground features

over an entire domain. For a LiDAR dataset, data pre-treatment is more time consuming as there is often no classification and above ground elements have to be added or removed one by one. In fact, in the photo-interpreted dataset, this manual treatment has been done previously during the photo-interpretation procedure (by operator from the geomatic community).

A method to design a HR DEM including fine elements influencing overland flow has been tested. For such a purpose, workability of HR 3D classified topographic data use is relevant up to a sub-city scale. Basic idea is simply to start from a DTM and to extrude elevation information of selected classes of feature at a 1 m resolution. Existing limits in this approach are put to the light. These limits mainly consist in *(i)* difficulty to handle this important amount of data, *(ii)* existence of unavoidable errors of classification in photo-interpretation, *(iii)* classification procedure which might not have been specifically designed following criteria for hydraulic purpose.

Thin features clearly impact flood models results. It is interesting to stress out one more time the fact that slightly over sizing fine features horizontal extent to 1m, lead results comparable using infra-metric resolution. This might allow better ease of HR DSM manipulation for HR DSM integration in 2D SWEs based codes and potentially computational time saving (see below).

***(iii)* HR topography information integration in 2D SWEs based**

Case study showed that in terms of overland flow maximal water depth estimation, structured and non-structured computational grid use for spatial discretization gave similar results. Nevertheless, in terms of mesh generation, and computational cost, several differences occur. Structured grid is interesting in terms of mesh generation as the HR DEM can easily be directly used as the computational grid. Nevertheless, it might lead to prohibitive number of computational points for a use over a desktop computer. Furthermore, not only there is a high computational cost but if heavy output data will be generated possibly involving resource requiring post-treatment for data handling and storage issues. Non-structured meshes are normally relevant in terms of optimizing number of computational points. Nevertheless, in such types of complex environment (urban/industrial) standard algorithms reach their limits as the number of constraint lines over the domain to refine the mesh around the features is important and therefore highly over-constrained the algorithm. Indeed, if the number of boundaries or the constraint vectors for refinement (*e.g.* polylines or polygons describing shapes of urban features) turns out to be important, the algorithms happen to fails and/or to be prohibitively time consuming. Time consuming manipulation from the modeller to generate a good refinement strategy is required. Moreover, if the algorithm is not preferment,

drastically small cells/element might be generated to describe fine features. Consequently, due to CFL restriction in most of 2D numerical schemes, the gain of a reduced number of computational points (compare to a fine structured mesh approach) might be annihilated due to the over small size of the cell that will lead to extra small temporal discretization

***(iv)* Computational requirement**

HR datasets manipulation is not easy but still feasible up to the scale of a densely urbanized district extent (such as the low Var valley). For larger scale, dedicated computing architecture are required to handle the HR data. Consequently it is possible, up to this scale to produce HR DEM for 2D HR flood modelling. Nevertheless, in terms of HR data integration in standard 2D SWEs based codes is not realistic to consider the use of standard non-structured mesh generation process.

Computation and simulation can be performed on desktop computers up a 1 km² domain. Obviously the speed of the computation will depend on code's numerical scheme performance and on number of computational points. Upper scales simulation requires HPC structures for simulations.

For the results handling, the same remake applies than for the HR datasets manipulation in the pre-treatment step. Furthermore, depending on types of output (*e.g.* structured grid of water level) and on format of output (*e.g.* ascii or binary files) robust hard storage capacity might be involved.

CHAPTER III - UNCERTAINTIES RELATED TO HIGH-RESOLUTION TOPOGRAPHIC DATA USE

Part of this chapter has been published as:

Abily, M., Bertrand, N., Delestre, O., Gourbesville, P., & Duluc, C.-M. (2016). *Spatial Global Sensitivity Analysis of High Resolution classified topographic data use in 2D urban flood modelling*. Environmental Modelling & Software (accepted).

Abily, M., Delestre, O., Gourbesville, P., Bertrand, N., Duluc, C. M., & Richet, Y. (2016). *Global Sensitivity Analysis with 2D Hydraulic Codes: Application on Uncertainties Related to High-Resolution Topographic Data.* In Advances in Hydroinformatics: Simhydro 2014, Springer Singapore, 301-315.

Abily, M., Delestre O., Bertrand, N., Richet, Y., Duluc, C.-M., & Gourbesville, P. (2015). *Global Sensitivity Analysis with 2D hydraulic codes: applied protocol and practical tool*. La houille Blanche, (5), 16-22.

Abily, M., Delestre, O., Amossé, L., Bertrand, N., Richet, Y., Duluc, C.-M., P. Gourbesville & Navaro, P. (2015*). Uncertainty related to high resolution topographic data use for flood event modelling over urban areas: toward a sensitivity analysis approach*. ESAIM: PROCEEDINGS AND SURVEYS, 48, 385-399.

In hydraulics, deterministic numerical modelling tools based on approximating solutions of the 2D Shallow Water Equations (SWE) system are commonly used for flood hazard assessment (Gourbesville, 2014). As described in chapter 1, this category of tools describes water free surface behavior (mainly elevation and discharge) according to an engineering conceptualization, in order to provide to decision makers information that often consists in a flood map of maximal water depths. As underlined in Cunge (2012), good practice in hydraulic numerical modelling is for modellers to know in detail the chain of concepts in the modelling process and to supply to decision makers possible doubts and deviation between what has been simulated and the reality. With regards to SWEs based models, sources of uncertainties come from *(i)* hypothesis in the mathematical description of the natural phenomena, *(ii)* numerical aspects when solving the model, *(iii)* lack of knowledge in input parameters and *(iv)* natural phenomena inherent randomness. Errors arising from *i*, *ii* and *iii* are considered as epistemic uncertainties as they can be reduced (*e.g.* by improvement of description, measurement). Errors of type *iv* are seen as stochastic errors where randomness is considered as a part of the natural process (*e.g.* in climatic based data) (Walker *et al*., 2003).

The quantification and understanding of uncertainties introduced by input parameters is a major concern in practical studies as interest for practitioners can be to identify the most influencing input. The aim can be to reduce the uncertainty related to the input parameter that introduces an important part of uncertainty (*e.g*. by improving measures of this parameter). Another illustration of interest in identifying most influent parameters is given in the field of protection of basic nuclear installation against flooding risk. Recommendation of the ASN guide (ASN, 2013) is to take uncertainty into consideration for each of the defined Reference Flood Situations (RFS). The general principle applied in the guide is to introduce conservative measures to cover uncertainties. For hydraulic flood propagation one good practice that is enhanced is to identify the most influencing parameter and then, to adopt unfavorable value of this influent parameter. Furthermore, the guide stresses out the fact that reliable uncertainty propagation model are lacking and consequently, that uncertainty related to each input parameter shall be examined.

The topography is one of the input parameters of 2D SWEs based overland flow models. The combination of the increasing availability of High-Resolution (HR) topographic data and of High Performance Computing (HPC) structures, leads to a growing production of HR flood models (Hunter *et al*., 2008; Erpicum *et al*., 2010; Fewtrell *et al*., 2011; Abily *et al*., 2014b; Meesuk *et al*., 2015). The added value and limits of such types of HR models has been raised in chapter 2. However, the level of accuracy of HR topographic data might be erroneously interpreted as the level of accuracy of the HR flood models by non-practitioners,

disregarding uncertainty inherent to this type of data use, not without standing the fact that other types of above mentioned errors occur in hydraulic modelling.

The specific study of uncertainty related to the use of HR topographic data for 2D flood modelling deserves to be assessed and is the topic of this chapter. Moreover, Uncertainty analysis (UA) in 2D is a challenging topic of study that has been seldom implemented in 2D free surface hydraulic modelling yet, mainly due to the curse of dimension (extensive computational cost). Therefore, developing practical tools and method for UA in HR 2D hydraulic modelling would be a good asset for researcher and practitioners.

Uncertainty analysis in deterministic modelling: general context

The study of uncertainty in modelling practice is a broad domain. Depending on one's objective and available information a wilde range of possible method can be considered (Uusitalo *et al*., 2014). Possible aims of an uncertainty study can be for instance to focus on model verification and understanding, on model simplifying and factor prioritization, *etc*. Possible methods for uncertainty assessment can be expert judgment, model sensitivity analysis, model emulation, data-base approaches *etc.* (Uusitalo *et al*., 2014). Refsgaard (2007) listed and presented 14 different categories of methods for uncertainty assessment in water management processing domain. Moreover, method can sometimes be a mixing of categories: an example for assessment of uncertainty arising from model calibration in the field of hydrology is a Bayesian approach relying on variance based method called Generalized Likelihood Uncertainty Evaluation (Beven and Binley, 1992) is often used by practitioners (Pappenbergen *et al*., 2006).

If the objective of the uncertainty study is to quantify and better understand uncertainty in models due to input parameters incomplete knowledge, statistical approaches are often performed. Actually, to quantify uncertainties related to input parameters, the idea is to include uncertainty aspects in the approach and to propagate it through the model realizations that explore the possible space of uncertainty. Then, the statistical analysis of the outcomes of the model provides tools for quantification and understanding. Quantification and understanding of uncertainty can be apprehended using Uncertainty Analysis (UA) and Sensitivity Analysis (SA).

- UA consists in the propagation of uncertainty sources through model, and then focuses on the quantification of uncertainties in model output allowing to check model's robustness (Saint-Geours, 2012).
- SA aims to study how uncertainty in a model output can be linked and allocated proportionally to the contribution of each input uncertainties.

Both UA and SA are essential to analyze complex systems (Helton *et al*., 2006, Saint-Geours *et al*., 2014), as study of uncertainties related to input parameters is of prime interest for applied practitioners willing to decrease uncertainties in their models results (Iooss, 2011).

UA and SA (detailed in this chapter, section 5.2.2) have started to be used (Saltelli *et al*., 2000, 2008) and broadly applied for a wilde range of water related environmental modelling problems as various as hydrological modelling for water quality (Zeng & Han, 2015), radionuclide migration in hydrogeology (Volkova *et al*., 2008), 1D river flood modelling (Pappenberger *et al*., 2008, Brozzi *et al*., 2015), flood hazard zoning (Fernàndez and Lutz, 2010) among many others. As introduced in Iooss (2015) who provides an educative synthesis of SA methods through an applicative framework related to 1D hydraulic modelling, SA objectives can include: *(i)* identification and prioritization of the most influent inputs, *(ii)* identify non-influent inputs in order to fix them to nominal values, *(iii)* maping of the output behavior in function of the inputs by focusing on a specific domain of inputs if necessary or *(iv)* calibrating model inputs using available information (*e.g.* real time output observations, constraints, *etc.*).

In the context of flood risk assessment, studying uncertainty of models results is a concern that is increasingly recognized (Pappenberger and Beaven, 2006) and that finds justification when it comes to urban areas and sensitive industrial sites flood risk assessment. In 1D and 2D flood modelling studies, approaches based on sampling based methods are becoming used in practical applications for UA for different purposes. For instance in 1D SWEs based modelling, Brozzi (2015) focused on distribution of water level distribution on two river reaches (Po and Garonne rivers). Their study focused on uncertainty related to input discharge and roughness coefficient. Monte-Carlo simulations using Probability Density Function (PDF) for characterization of discharge and roughness coefficient was used and the UA of the output distribution allowed to draw conclusions about output variation compare to introduced uncertainties. Their conclusion rose up non-linearity in uncertainty propagation and on PDF adjustments using output distribution skewness analysis. Alliaud (2013) and Nguyen (2015) used similar approach on a river reach but with a larger number of input parameters to disciminate those that have major impacts on output variability. Moreover, in Brozzi (2015) and Nguyen (2015) variance based SA were used to compute sensitivity index (described in section 5.2) allowing to compare relative weight of considered uncertain inputs to the output global uncertainty and therefore to rank their importance. These UA and SA approaches require important number of simulations. More parsimonious approaches in SA such as Local Sensitivity Analysis (LSA) were testes in 1D (Delenne *et al*., 2012) for numerous input parameters related to river flood and dam failure risk. LSA (described in section 5.2) advantage is that compare to Monte-Carlo approach only one simulation is

necessary as the uncertainties are introduced in the system of equations. The drawbacks of LSA are the assumed linearity of the system and the non-interaction between parameters (see section 5.2).

In 2D flood modelling a good illustration of UA possibility is given in Neal (2013). UA was conducted for a 2D flood river scenario to study the uncertainty of overland flow estimation and its interaction with the flood defenses and valley topography. It gave, through the use of map a structure to the inundation probabilities and risk. More recently, a SA (based on a screening method see 5.2) has been implemented in 2D urban flood modelling application (Willis, 2014) to quantify which inputs are most critical to model output. They notably enhance with their sensitivity analysis that the level of physical representation is a significant factors and that interactions strongly occurs. Both studies used a Monte-Carlo approach to propagate uncertainty underlining the computational coast such type of studies.

To date, UA and SA have not been performed yet to specifically study uncertainty in 2D urban flood simulations related to HR classified topographic data integration. Indeed, due to the curse of dimensionality, SA methods have seldom been applied to environmental models with both spatially distributed inputs and outputs (Saint-Geours *et al*., 2014). Such a problematic raises needs of specific tools, computational resource and methods application. Among SA methods that are still at an exploratory level in 2D hydraulic modelling, a Global Sensitivity Analysis (GSA) is implemented in this study. GSA approach is selected over LSA as 2D overland flow process simulation through SWEs system of partial differential equations, is viewed as being largely nonlinear, with discontinuous solution and interactions between parameters.

High-Resolution topographic data and associated errors

It has been enhanced in previous chapter (part 3 and 4) that topographic data is a major input for flood models, especially for complex environment such as urban and industrial areas, where a detailed topography helps for a better description of the physical properties of the modelled system (Djordjević *et al*., 2009; Abily *et al*., 2013a; Gourbesville, 2014). As a reminder, in the case of an urban or industrial environment, a topographic dataset is considered to be of HR when it allows to include in the topographic information the elevation of infra-metric elements (Le Bris *et al*., 2013). These infra-metric elements (such as sidewalks, road-curbs, walls, etc.) are features that influence flow path and overland flow free surface properties. At megacities scale, features classification carried out by photo-interpretation process, allows to have high accuracy and highly detailed topographic information (Mastin *et al*., 2009; Andres, 2010; Larfarge *et al*., 2010; Lafarge and Mallet, 2011). Photo-interpreted HR datasets allow creation of HR Digital Elevation Models (DEMs)

including classes of impervious above-ground features (Abily *et al*., 2013b, 2014b). Therefore generated HR DEMs can include above-ground features elevation information depending on modeller's selection among classes. Based on HR classified topographic datasets, produced HR DEMs can have a vertical and horizontal accuracy up to 0.1 m (Fewtrell *et al*., 2011).

Even though being of high accuracy, produced HR DEMs are assorted with the same types of errors as coarser DEMs. Errors are due to limitations in measurement techniques and to operational restrictions. These errors can be categorized as: *(i)* systematic, due to bias in measurement and processing; *(ii)* nuggets (or blunder), which are local abnormal values resulting from equipment or user failure, or to occurrence of abnormal phenomena in the gathering process (*e.g.* birds passing between the ground and the measurement device) or *(iii)* random variations, due to measurement/operation inherent limits (see Fisher and Tate, 2006; Wechsler, 2007). Moreover, the amount of data that composes a HR classified topographic dataset is massive. Consequently, to handle the HR dataset and to avoid prohibitive computational time, hydraulic modellers make choices to integrate this type of data in the hydraulic model, possibly decreasing HR DEM quality and introducing uncertainty (Tsubaki and Kawahara, 2013; Abily *et al*., 2015c, 2016a, 2016b). As recalled in the literature (Dottori *et al*., 2013; Tsubaki and Kawahara, 2013), in HR flood models, effects of uncertainties related to HR topographic data use on simulated flow is not yet quantitatively understood.

Objectives of the chapter

The research presented in this chapter aims to study uncertainty related to HR topographic data integration in 2D flood modelling approach. The objective is to perform an UA and a SA on two categories of uncertain parameters (measurement errors and uncertainties related to operator choices) relative to the use of HR classified topographic data in a 2D urban flood model. Specificity relies in the fact that spatial inputs and outputs are involved in our UA and GSA study. Among SA methods, a Global Sensitivity Analysis (GSA) is implemented to produce sensitivity maps based on Sobol index computation. Carrying out these objectives will demonstrate the feasibility, the added values and limitations of UA and SA implementation in 2D hydraulic modelling, in a context where spatial variability and interactions are likely to occur. Moreover, modeller knowledge about challenges and expectations related to HR classified data use in HR urban flood modelling will be enhanced.

To carry out our objective, the selected case study is the low Var river valley (Nice, France) where flooding events occurred in the last decades in the highly urbanized downstream part of the valley (Guinot and Gourbesville, 2003). The output of interest is the overland flow

water level ($Y_{(x)}$). The used HR DEMs are based on classified 3D dataset created from photo-interpretation procedure. A proof of concept of GSA application to 2D Hydraulic modelling voluntary choosing a resource requiring problem has been developed and the method applied over an innovative concern related to the use of HR topographic data.

Following this introduction, the next part of the chapter **(part 5)** introduces the test case context for SA methods uses, enhances description of used HR topographic dataset, and then gives overview UA and SA concepts. Lastly the implemented methodology for the spatial GSA and developed tools are described. The second part **(part 6)** of the chapter presents results of UA and GSA, first at points of interest, then at spatial levels. Eventually, outcomes and limits of our approach are then discussed **(part 7)**. Lastly concluding remarks are given.

In this chapter, scenarios are based on both HR Digital Terrain Models (DTMs) and HR Digital Surface Models (DSMs) use. This is the reason why all along this chapter we use the generic nomenclature Digital Elevation Models (DEMs).

PART. 5. METHODOLOGY FOR UNCERTAINTY ANALYSIS AND SPATIALIZED GLOBAL SENSITIVITY ANALYSIS

The case study (HR datasets, scenario, and 2SWE based code) used for this Uncertainty Analysis (UA) and spatial Global Sensitivity Analysis (GSA) is the same as the chapter 2 river flood case over the Low Var valley. The study area is a 17.8 km² domain that represents the last five downstream kilometers of the low Var valley, located in Nice, France (Figure 5.1). In the test basin, two major river flood events occurred in the last decades (5th and 6th of November 1994; 6th of November 2011). The characteristics of the river basin and of the 1994 flood event are described in Guinot and Gourbesville (2003). A HR topographic data gathering campaign fully covered the domain in 2010-2011 (Andres, 2012). Between 1994 and 2010-2011 (date of event used for simulation and the date of the HR topographic data gathering campaign), the study area has considerably changed. In fact, levees, dikes and urban structures have been implemented, changing physical properties of the river/urban flood plain system. The objective is not to reproduce the event, but simply to use the framework of this event as a case study to carry out the UA and the SA.

Section 5.1 recalls details about the HR photo-interpreted dataset and presents the case study. Section 5.2 presents in a fist part (5.2.1) details about UA and GSA methods and in a second part (5.2.2) part describes the specific method implemented to carry out the spatial GSA for our study. As mentioned in the introduction part of this chapter, a GSA approach using Sobol index is suitable to compute sensitivity maps (Marrel *et al*., 2011).Lastly, section 5.3 presents the coupling (warping) between the computational environment ant the 2D SWEs based finite volume code.

5.1 HR CLASSIFIED TOPOGRAPHIC DATA AND CASE STUDY

To recall general aspects about photo-interpreted dataset (see chapter 1, section 1.2), the design and the quality of a photo-interpreted dataset are highly dependent on photogrammetry dataset quality, on classes' definition and on method used for digitalization of vectors (Lu and Weng, 2007). For our application, the 3D classified data of the low Var river valley is used to generate specific DEM adapted to surface hydraulic modelling. This specific dataset has been presented in chapter 2, section 4.1.2. Main properties of this dataset are summarized to the reader here.

The photogrammetric campaign carried out over the low Var valley, at a low flight elevation, allowed a pixel resolution at the ground level of 0.1 m and had a high overlapping ratio (80%)

among aerial pictures. These characteristics allowed to produce a high quality photogrammetric dataset. Using the photogrammetric dataset, the photo-interpretation process has been carried out, to create a classified vector dataset through digitalization of classes of polylines, polygons and points. This photo-interpreted dataset has been designed with a total number of 50 different classes representing large and fine above-ground features (*e.g.* buildings, concrete walls, road-gutters, stairs, *etc.*). The total number of classified 3D polylines and polygones over the selected area is here above 1,200,000. For hydraulic modelling purpose, a selection of relevant classes over the 50 is considered in order to represent in the HR DEM the above-ground features impacting overland flow paths.

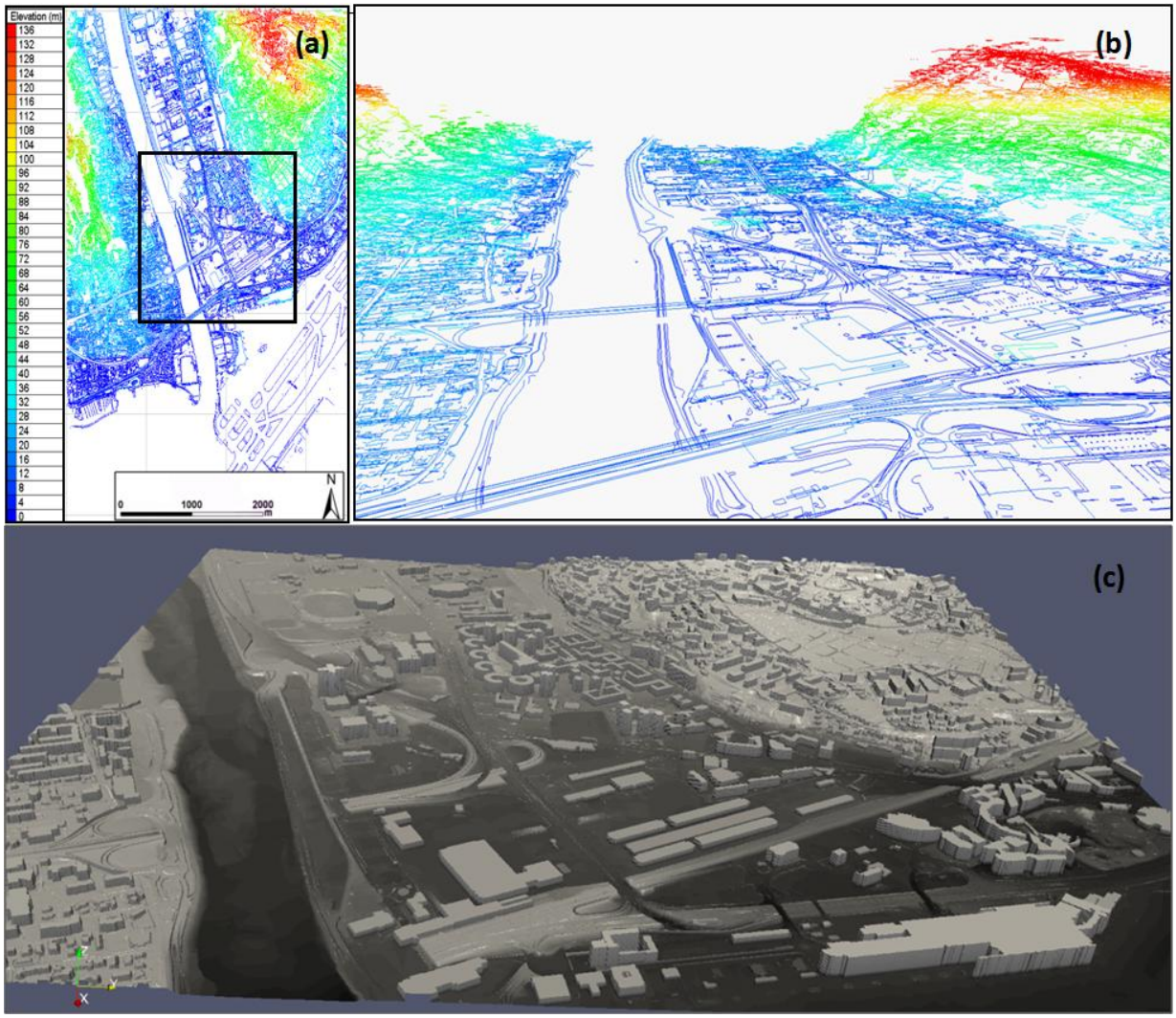

Figure 5.1. *Overview of the classes of photo-interpreted topographic data used over the study area (a, b) and HR DEM of a sub-part of interest of the domain (c).*

For our application, the 3D photo-interpreted data of the low Var river valley is used to generate HR DEM adapted to surface hydraulic modelling. Therefore, only 3D classes of above-ground features, which are considered as impacting flow direction, are selected for

DEM creation. It represents 12 classes, which includes buildings, concrete vertical structures above 2 m (walls) and low concrete features above paved roads (*e.g.* sidewalks, road gutter, *etc.*). These classes represent a total of 52,600 polylines over four areas (Figure 5.1). The 12 selected classes have been aggregated in 3 groups: buildings, "*concrete*" vertical structures (walls) and street concrete feature.

Classified data mean horizontal and vertical accuracy is 0.2 m. Errors in photo-interpretation which results from feature misinterpretation, addition or omission are estimated to represent 5% of the total number of elements. To control average level of accuracy and level of errors in photo-interpretation, the municipality has carried out a terrestrial control of data accuracy over 10% of the domain covered by the photogrammetric campaign.

For the GSA approach (described in next section), only the input DEM changes from one simulation to another and the hydraulic parameters of the model are set identically for the simulations. Hydraulic conditions of the case study implemented in the models can be summarized as follow: a constant discharge of 1,500 $m^3.s^{-1}$ is applied as input boundary condition to reach a steady flow state condition almost completely filling the Var river bed. This steady condition is the initial condition for the GSA and a 6 hours estimated hydrograph from the 1994 flood event is simulated (Guinot and Gourbesville, 2003) as described in figure 4.9. The Manning's friction coefficient (n) is spatially uniform on overland flow areas with a standard value of 0.015, which corresponds to a concrete surface. No energy losses properties have been included in the 2D hydraulic model to represent the bridges, piers or weirs. Downstream boundary condition is an open sea level (Neumann boundary condition) to let water flows out.

5.2 Concepts of UA, SA and implemented spatial GSA approach

In 1D and 2D flood modelling studies, approaches based on sampling based methods are becoming widely used in practical applications for UA. For SA, depending on applications and objectives, different categories of variance based approaches have been recently applied in flood modelling studies (mainly in 1D) such as Local Sensitivity Analysis (LSA) (Delenne *et al*., 2012) or more recently, a Global Sensitivity Analysis (GSA) based on a screening method has been implemented in 2D flood modelling application (Willis, 2014).

5.2.1 Uncertainty and Sensitivity Analysis

- **Uncertainty analysis**

As mentioned in this chapter introduction, UA consists in the propagation of uncertainty sources through model, and then focuses on the quantification of uncertainties in model

output allowing robustness to be checked (Saint-Geours, 2012). Methods based on performing multiple evaluations of the model with randomly selected inputs such as Monte-Carlo method are commonly used. The concept is that a distribution (often a Probability Density function, PDF) is assigned to the input factors. Through the random sampling, models runs produce a sample *N* of results. Then statistical analysis can be performed on *N*. To make sure that size of *N* is representative enough to perform statistical analysis, the convergence of the method is checked. Monte-Carlo approach random sampling has a rate of convergence which is equal to: $\frac{1}{\sqrt{N}}$. It means that an extensive number of runs are required to reach convergence (even though the criterion to determine if convergence is reached depends on expert opinion). Other sampling can be more parsimonious (requiring a smaller *N*) such Quasi Monte-Carlo or Latin Hypercube Sampling can be used to reduce computational burden of a Monte-Carlo random sampling strategies. Drawback might me a mistake in the non-appropriated exploration of the space of uncertainty which can lead to bias that and not easy to estimates.

- **Local Sensitivity Analysis**

LSA focuses on fixed point in the space of the input and aims to address model behavior near parameters nominal value to safely assume local linear dependences on the parameter. LSA can use either a differentiation or a continuous approach (Delenne *et al*., 2012). LSA based on differentiation approach performs simulations with slight differences in a given input parameter and computes the difference in the results variation, with respect to the parameter variation. LSA based on continuous approach differentiates directly the equations of the model, creating sensitivity equation (Delenne *et al*., 2012). The advantages of LSA approaches are that they are not resource demanding in terms of computational cost, drawback being that the space of input is locally explored assuming linear effects only. Linear effects means that given change in an input parameter introduce a proportional change in model output, in opposition to nonlinear effects. LSA approaches perform reasonably well with SWEs system even if nonlinear effects occur punctually (see Delenne *et al*., 2012). Nonetheless, important nonlinear effects in model output might arise when parameters are interacting and when solution becomes discontinuous. LSA consequently becomes not suited (Delenne *et al*. 2012) in such a context, which is likely to occur in case of 2D SWEs based simulation of overland flow.

- **Global Sensitivity Analysis (GSA)**

GSA approaches rely on sampling based methods for uncertainty propagation, aiming to fully map the space of possible model predictions from the various model uncertain input

parameters and then, allow to rank the significance of the input parameter uncertainty contribution to the model output variability (Baroni and Tarantola, 2014). GSA approaches are well suited to be applied with models having nonlinear behavior and when interaction among parameters occurs (Saint-Geours, 2012). These approaches going through an intensive sampling are computationally demanding, as they most often rely on Monte-Carlo (MC) approach, even though some more parsimonious sampling method such as Latin hypercube or pseudo-Monte Carlo are sometimes applied (see Helton *et al*., 2006 for a review). Most commonly, GSA approaches rely on:

- screening methods, such as Morris method (Morris, 1991);
- Sobol indices computation, that considers the output hyperspace (x) as a function ($Y_{(x)}$) and performs a functional decomposition (Iooss, 2011; Iooss and Lemaître, 2015) or a Fourier decomposition (FAST method) of the variance.

As fully detailed in Iooss and Lemaître (2015), screening techniques (*e.g.* Morris method) allow to classify uncertain input parameters in three categories: those that have negligible effect; those that have linear effect; and those that have nonlinear effects or effects in interaction with other input parameters (Herman *et al*., 2013). Sobol indices (or variance-based sensitivity indices) will explain the share of the total variance in the space of output due to each uncertain input parameter and/or input interaction.

GSA has started to be applied in 1D hydraulic modelling in practical applications for hierarchical ranking of uncertain input parameters (Pappenberger *et al*., 2008; Hall *et al*., 2005; Alliau *et al*., 2013; Jung and Merwade, 2014; Bozzi *et al*., 2015; Nguyen *et al*., 2015). As for 1D, applying a GSA to flooding issues in 2D modelling requires method awareness among the community, practical tools development and computational resources availability. Moreover an analysis on spatialization of input uncertain parameters and on output variable is specifically needed in 2D (Saint-Geours *et al*., 2011). Recently, GSA using a screening method has been implemented in 2D flood modelling application (Willis, 2014) tackling ranking of uncertain input parameters using points and zonal approaches. Computation of sensitivity maps such as maps of Sobol index is a promising outcome that has been achieved for other types of water related issues (Marrel *et al*., 2011.).

Falling within category of GSA approaches, screening methods allow in a computationally parsimonious way, to discriminate among numerous uncertain input parameters those that have little effect from those having linear, nonlinear or combined effects in output variance (Iooss and Lemaître, 2015). Screening methods principle consists in fixing an input parameters set and performing an initial run. Then, for one parameter at a time, a new value

of the parameter is randomly chosen and a new run is performed. Variation in the run output is checked. This operation is completed for all the parameters, n times with n equals to the total number of input parameters. Screening methods perform well to discriminate influencing parameters on output variability. Study applying screening methods have already been conducted in 1D flood modelling studies (Alliau *et al*.,2013; Nguyen *et al*., 2015) and recently in 2D flood modelling studies (Willis, 2014).

GSA approaches relying on Sobol index computation go one step further, allowing to quantify the contribution to the output variance of the main effect of each input parameters (Sobol, 1990; Saltelli *et al*., 1999; Saint-Geours, 2012). Sobol Index is based on functional decomposition of variance (ANOVA), considering Y the model output of interest as follow: Y= f(X); where f is the model function, X = (X1; …;Xi) are i independent input uncertain parameter with known distribution. Sobol indice (Si) of parameter Xi is defined as:

$$Si_{(Xi)} = \mathrm{Var}[\mathrm{E}(Y|X_i)]/\mathrm{Var}(Y), \qquad (13)$$

where E is the expectation operator. $Si_{(Xi)}$ being the variance of conditional expectation of Y for Xi over the total variance of Y, $Si_{(Xi)}$ value will range between [0; 1]. Si computations are computationally costly as it requires to explore the full space of inputs and therefore an intensive sampling is necessary (Iooss and Lemaître, 2015).

5.2.2 Implemented spatial GSA

The objective is to quantify impacts of uncertain input parameters and to discriminate their weight on the output uncertanty. Several approaches exist for spatial sensitivity analysis and are reviewed in Liliburne and Tarantola (2009). GSA approach using Sobol index is best suited for sensitivity maps production as we have here discrete spatial input parameters that are describes below. In this study, the implemented GSA follows standard steps used for such type of approach as summarized in Baroni and Tarantola (2014) or in Saint-Geours (2014).

The steps of the methodology are presented in the figure 5.2: specification of the problem notably by choosing uncertain parameters and output of interest (step A); assessing Probability Density Function (PDF) of uncertain parameters (step B); propagating uncertainty, using a random sampling approach in our case (step C); ranking the contribution of each input parameters regarding the output variance (step D). Complete details are provided in Annex B - Abily *et al*. (2015c).

First steps of the approach (A and B) are the most subjective ones. For the study purpose, steps A and B are treated as follow. Three input parameters related to uncertainties when willing to use HR 3D classified data in 2D Hydraulic models are *(i)* one parameter related to the topographic input error (called var. E) and *(ii)* two parameters related to modeller choices, when including HR data in 2D hydraulic code (called var. S and var. R) are considered in this GSA practical case. These three parameters are considered as independent.

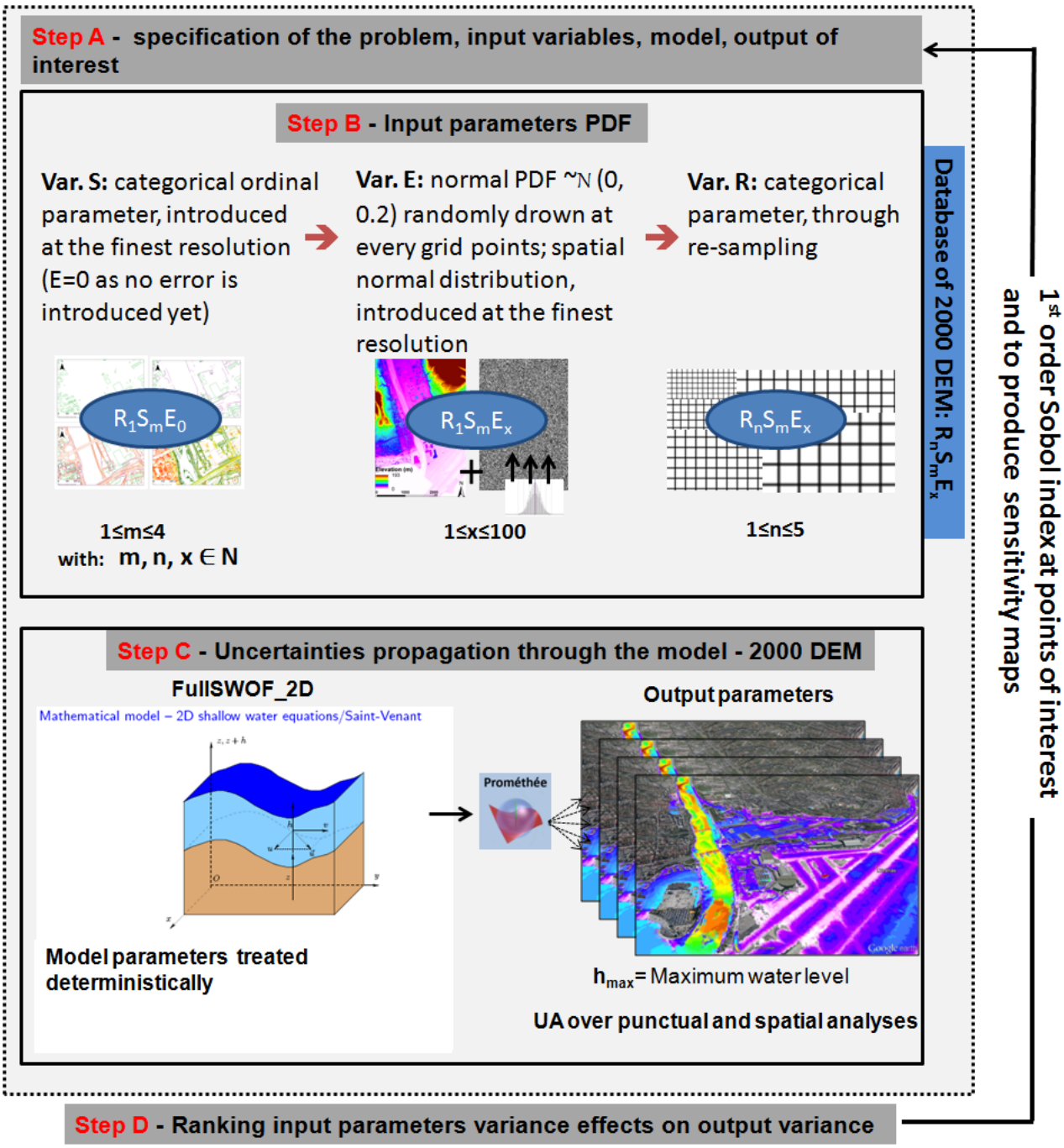

Figure 5.2. *Overview of the applied spatial GSA framework.*

- **Uncertainties related to measurement errors in HR topographic dataset are considered through var. E.**

  Var. E parameter is an error randomly introduced for every point of the highest resolution DEM (1 m) following a draw according to a normal distribution PDF, where the standard deviation is equal to the RMSE value (0.2 m): *N* (0, 0.2). As from one point to the next one, the normal PDF is drawn independently, it results in a spatialization that follows a uniform distribution. Hundred maps of var. E are generated and combined with the highest resolution (1 m) DEM to introduce uncertainty related to measurement errors through this parameter.

- **Uncertainties related to modeller choices when including HR data in hydraulic code, two variables are considered: var. S and var. R.**

  Var. S is a categorical ordinal parameter having values representing the level of above-ground features details impacting flow direction included in DSM. As illustrated in Figure 5.3, S1 is a DTM (Digital Terrain Model) only, S2 is S1 combined with buildings elevation inclusion, S3 is S2 completed with walls, and S4 is S3 plus fine concrete street structures (sidewalks, roar-curbs, *etc*.).

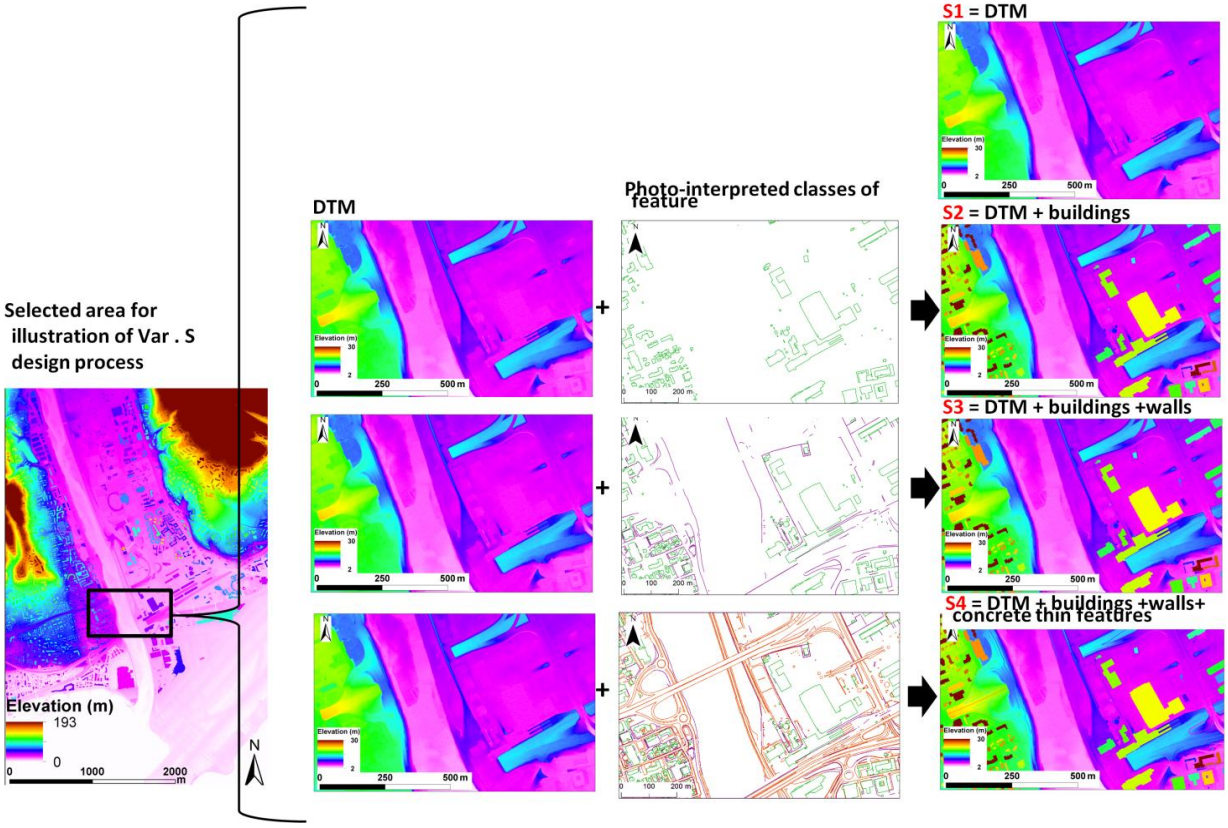

Figure 5.3. *Illustration of Process for var. S creation*

Var. R represents choices made by the modeller concerning the computational grid cells resolution in the model. In the hydraulic code used for this study (FullSWOF_2D described in next section), the grid cells are regular. This parameter var. R has five discrete values from 1 m to 5 m. At 1 m resolution, the number of computational points of the grid is above 17.5 million and at the 5 m resolution grid size is 700,000 computational points. The bounds of this parameter is justified as on one hand, a grid resolution lower than 1m would result in prohibitive computational time. On the other hand, resolutions coarser than 5 m do not sound to be a good choice for a modeller aiming to create a HR model, as up-scaling effects would make irrelevant the use of the HR topographic data that are used as input.

A total of 2,000 DEMs are generated and used in the implementation of the GSA. The DEMs generation process (step B, figure 5.2), explains as follow. Four DEMs at the finest resolution (var. R =1 m) are generated to implement all of the four var. S possible scenarios. Then each of these four DEMs is combined with the hundred var. E grids producing 400 DEMs. Eventually, the 400 DEMs combining all of the var. S and var. E possibilities combinations are resampled to resolution 2, 3, 4, 5 m creating a database of 2,000 DEMs where all the defined input parameters can possibly be combined.

The propagation of uncertainty (step C) is carried out using a Monte-Carlo approach to randomly sample in the produced results database. This non-parsimonious approach consisted in computing a maximum number of simulations among the 2,000 possible cases to generate a database of results. In total, 1,500 simulations out of the 2,000 possible were computed to feed the results database using the available 400,000 CPU hours on a Cluster (cluster described in next sub-section). Then, the MC approach randomly samples in the produced results database.

As mentioned 1,500 simulations out of the 2,000 possible were computed due to the computational cost. Therefore, for all of the 20 possible different var. R/ var. S combinations (five times four), at least 50 over the 100 possible var. E drawn were performed to make sure that the input space would be extensively explored in the result database. Actually, tests have been performed to make sure that the samples size (N) of var. E being equal to 50 would be enough to sufficiently explore var. E space of input. As illustrated by figure 5.4 (a), it appears that the distribution and the standard deviations of Y(x), which is the flood maximal elevation (h_{max}+ z), become stable with a N of var. E around 40 to 50. This gave qualitatively a first idea of what should be the minimum size of sample N of var. E to allow performing reliable statistical analysis with an acceptable level of convergence. To strengthen these findings, tests of convergence have been performed observing the evolution of mean h_{max}+z

value and the 95% confidence interval (CI) when N size increases. Figure 5.4 (b) shows this result for a given point of interest. The analysis shows the sample size is above 30, the mean and the CI become stable. It has to be noticed that similar results are obtained with the other selected points of interest, 30 to 40 realizations are sufficient to generate a representative sample of the uncertainties associated to the Var.E.

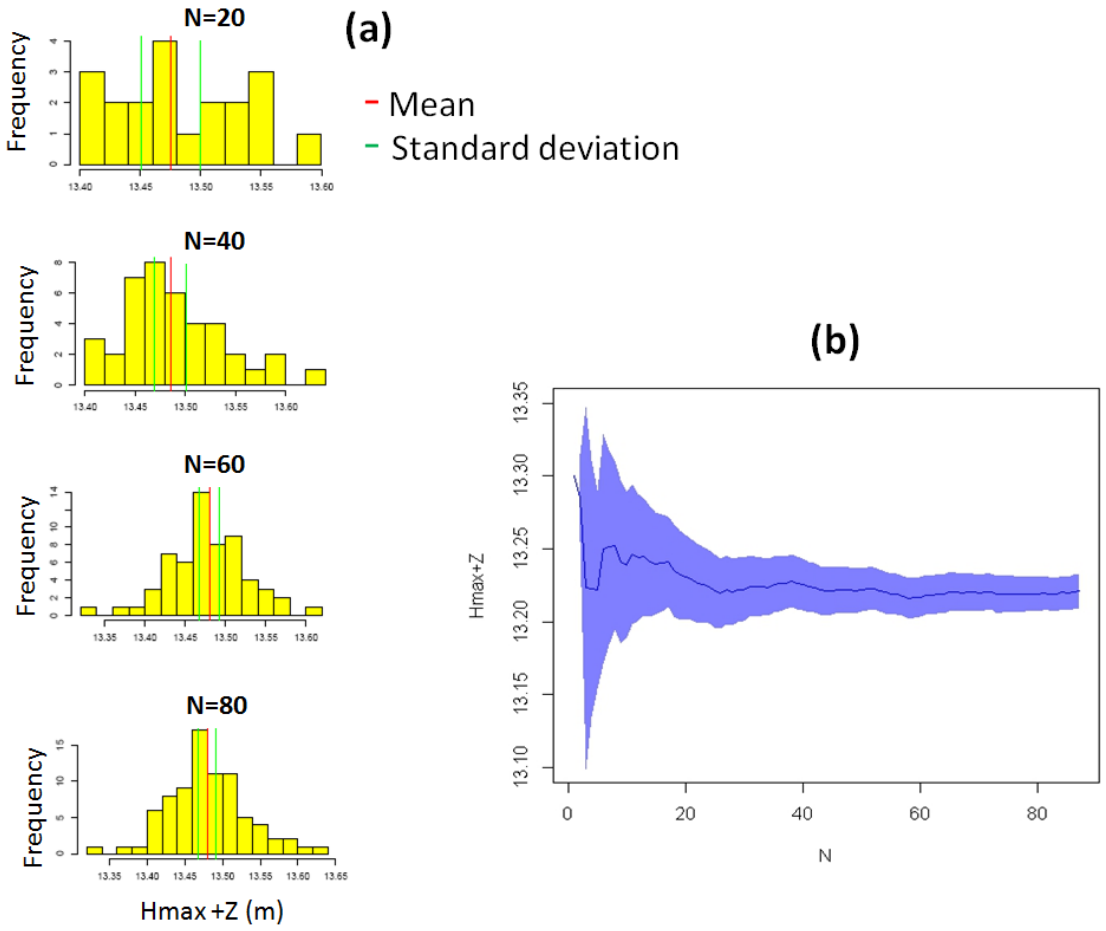

Figure 5.4. (a) *Illustration of output h_{max}+z distribution with fixed Var. S and Var. R when increasing sample of size of Var. E at a point of interest.;* ***(b)*** *convergence of mean and CI when increasing sample of size of Var. E with fixed Var. S and Var. R.*

As the exploration of the space of input is restricted to 1,500 simulations over 2,000 possible cases, an evaluation of the convergence is performed to assess if the convergence of the MC method is reached. Figure 5.5 illustrates the evolution of the convergence of the mean of the hyperspace of the output of interest $Y_{(x)}$ for three points (points located in Figure 6.1 and 6.2), increasing N through a random sampling in the result database. It is reminded that the output of interest is the simulated maximal overland flow water depth. An asymptotic convergence of the MC method is observed for the three points, respectively when the sample size (N) is larger to 900 simulations. Globally, over the 20 selected points (Annex C),

when N reaches a threshold value between 900-1000, the stabilization of the convergence is observed.

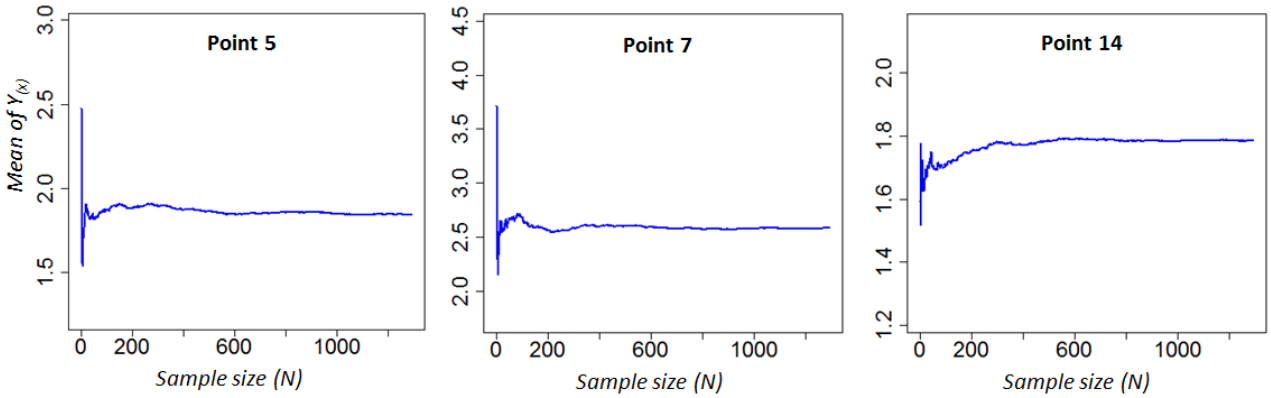

Figure 5.5. *Asymptotic convergence of random sampling at 3 points of interest (points 5, 7 and 14 located on Figures 6.1 and 6.2).*

Step D consists in the computation of Si using the output database. Sobol index of var. R, var. S and var. R, respectively $Si_{(R)}$ $Si_{(S)}$ and $Si_{(E)}$ are computed following eq. 13 at points of interest. Spatialization of GSA approach is based on discrete realization of spatially distributed input variables as described in Lilburne and Tarantola (2009), and discrete computation of output to produce sensitivity maps (as described in Marrel *et al*., 2011).

5.3 PARAMETRIC ENVIRONMENT AND 2D SWES BASED CODE

Prométhée (a parametric modelling environment), has been coupled with FullSWOF_2D (a 2D free surface modelling code) over a High Performance-Computing (HPC) structure (Abily *et al*., 2015c, 2015d, 2016b).

Prométhée is an environment for parametric computation that allows carrying out uncertainties propagation study, when coupled (or warped) to a code. This software is freely distributed by IRSN (http://promethee.irsn.org/doku.php). Prométhée allows the parameterization with any numerical code and is optimized for intensive computing. Moreover, statistical post-treatment, such as UA and SA can be performed using Prométhée as it integrates R statistical computing environment (Ross, 1998).

FullSWOF_2D is used in this study. The code has been presented in chapter 1, section 2.3. As a reminder, this code approximate the solution of the SWEs relies on a well-balanced finite volume method over a regular grid using numerical method based on hydrostatic reconstruction scheme (Delestre *et al*., 2012, 2014). FullSWOF's above mentioned properties are of good interest for urban overland flow modelling. Interest regarding

specificities of HR topographic data use in our study relies in the use of structured mesh (see conclusion of chapter 2). Two parallel versions of the code have been developed allowing to run calculations under HPC structures (Cordier *et al*., 2013). the MPI version of the code has been used. The HLL solver has been used in this study with a second order MUSCL reconstruction method as recommended in Delestre (2010).

The coupled code Prométhée-FullSWOF_2D is used to automatically launch parameterized computation through R interface under Linux OS. A graphic user interface is available under Windows OS, but in case of large number of simulation launching, the use of this OS has shown limitations as described in Nguyen (2015). A maximum of 30 calculations can be run simultaneously, with the use of 30 “*daemons*”. Daemons are small programs that will "*book*" a part of HPC resources and wait for a job from Prométhée-FullSWOF_2D to be submitted to them to start a parametric simulation.

On the HPC structure (Interactive Computation Centre of Nice Sophia Antipolis University), up to 1,152 CPU are available and up to 30 simulations can be launched simultaneously using Prométhée-FulSWOF_2D. A database of flood maps results has been produced using a total of 400,000 CPU hours. The required unitary computation time is two hours over 64 CPU, for simulations using the finest resolution grid size (1 m), which has 17.8 millions of computational points. At the coarsest resolution (5 m), the grids size is decreased to 712,000 computational points and using 64 CPUs, the computational time decreases to few minutes.

PART. 6. RESULTS OF UA AND GSA APPLIED TO HR TOPOGRAPHIC DATA USE WITH 2D FLOOD MODELS

This section presents the results of the UA and the GSA. A subarea is selected in the flooded area of the domain to carry out the spatial analysis. This subarea is 4.35 km², representing one quarter of the total spatial extent of the model.

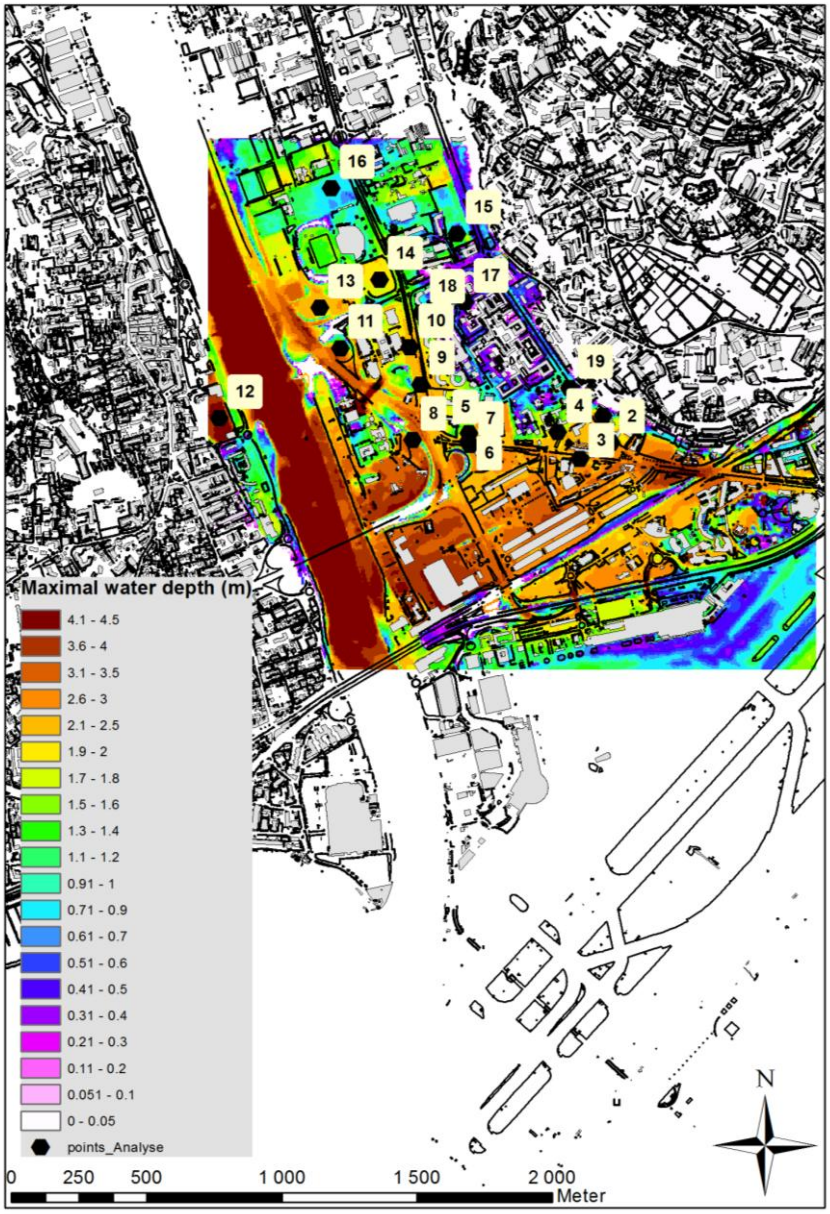

Figure 6.1. *Overview of location of the subarea and points of interest, where the UA and GSA are performed.*

20 points of interest are defined in the selected flooded area of the subarea (Figures 6.1 and 6.2). Points 1 to 10 are spread in and around the main streets. These streets are densely urbanized. Points 11 to 16 are located in less urbanized areas (stadium, parking, small

agricultural field, *etc*.). Moreover, from points 15 to 20, the points are located in areas which are at the edge of the flood extent, either in open area (points 15 and 16) or where above-ground features are densely present (points 17 to 20).

6.1 UA RESULTS

6.1.1 Analysis at points of interest

Mean and variance of computed maximal water depth ($Y_{(x)}$) at the different points of interest are presented in figure 6.2. Means and standard deviations of $Y_{(x)}$ values are computed using the full size database (N=1,500). Over the 20 points of interest, importance of the variability introduced by uncertain input parameter is significant (0.51 m in average). Moreover, variability in $Y_{(x)}$ variance can be important as the minimal variance is 0.28 m (point 17), and the maximal variance is 0.71 m (point 8). Further interpretation, such as the analysis of the trend in the magnitude of variance changes from one point to another, is not accessible for generalization using points observation only. Nevertheless, studying the distribution of $Y_{(x)}$ at points of interest gives another insight to carry out the uncertainty analysis.

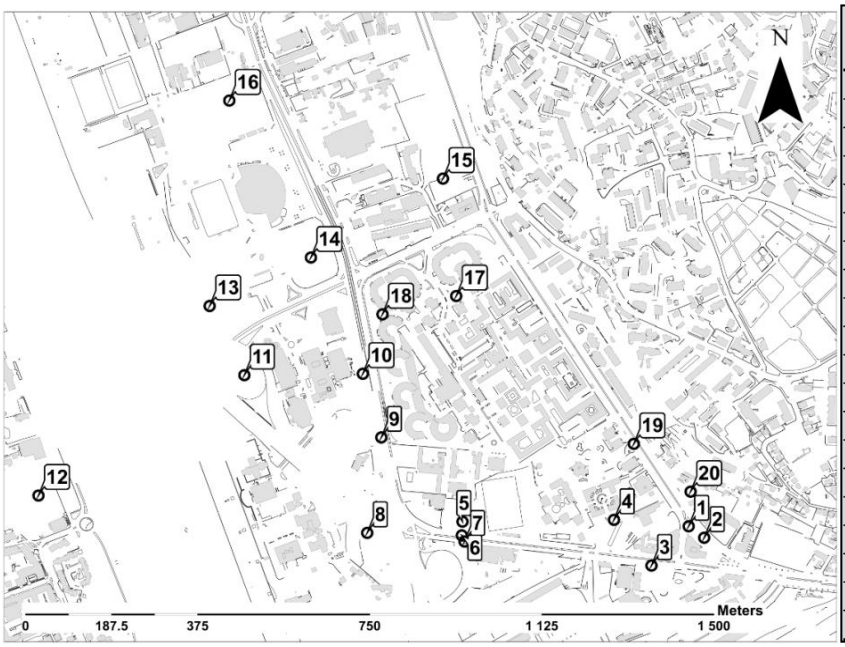

Point	mean of $Y_{(x)}$ (m)	Variance (m)
1	2,39	0,51
2	2,49	0,49
3	2,50	0,53
4	1,69	0,60
5	1,83	0,44
6	2,49	0,56
7	2,60	0,68
8	2,14	0,71
9	2,52	0,54
10	2,32	0,47
11	2,65	0,59
12	4,09	0,44
13	2,02	0,39
14	1,79	0,34
15	0,65	0,41
16	0,94	0,29
17	0,24	0,28
18	1,06	0,53
19	1,13	0,51
20	1,69	0,53

Figure 6.2. *Location of points of interest and associated mean and variance values.*

Figure 6.3 illustrates $Y_{(x)}$ distributions using the complete set of available model runs in the database for three points. $Y_{(x)}$ follows a normal distribution as observed for point 7 or distribution can be bi-modal as observed for point 14. The difference between the normal and bi-modal distribution of $Y_{(x)}$ is not always clearly observed (point 5). The distribution for the 20 points is enclosed in annex D. Most of the clearly observed bimodal distribution (ten out of

the twenty points) occurs for the points located in the central part of the highly urbanized area (points 1 to 10). This area is largely flooded and seven points have a clearly marked bimodal distribution. In largely flooded but relatively less urbanized areas, the trend is reversed as five out of six points have a normal distribution. Lastly for the points located at the edge of the flooded areas, two over four points have a bimodal distribution, whereas the two others have a normal one. Bimodal distributions lead to larger amplitude in $Y_{(x)}$ distribution. The bimodal distribution illustrates the non–linearity between the input and output. Explanations to link these observations with physical properties of phenomena and of uncertain input parameter properties are given, combining these observations with SA results, in the discussion section. Moreover, it is noticeable that points are sometimes not flooded at all, when $Y_{(x)}$ is equal to zero. Reasons for these zero values are that in seldom cases, var. E value gives at the point of interest a high ground elevation value (above $Y_{(x)}$ value) or that var. S produces critical threshold effects diverting flow direction.

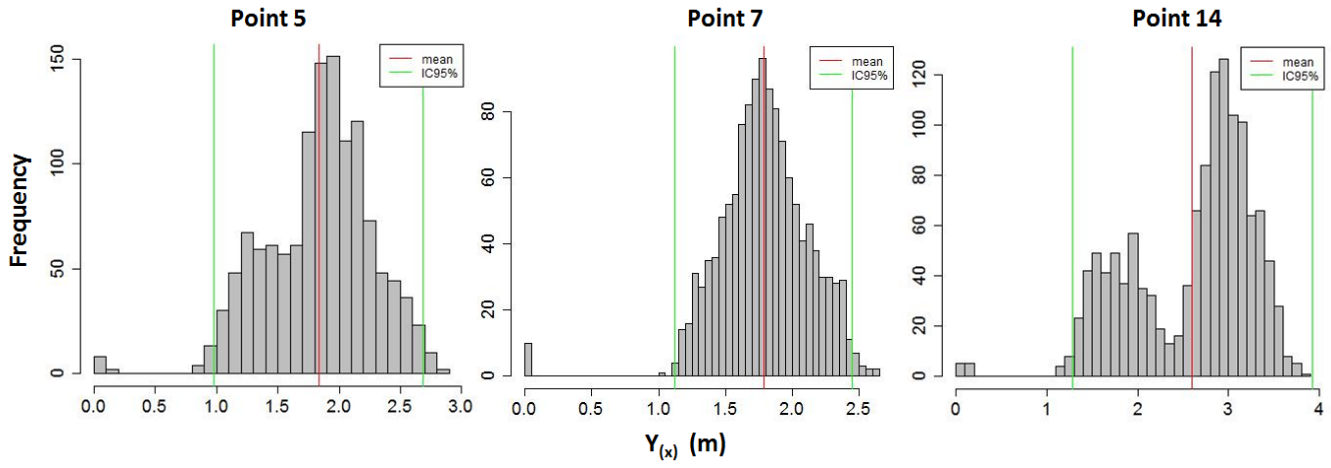

Figure 6.3. *Distribution of $Y_{(x)}$ (maximal water height) at three points of interest (points locations, on the figures 6.1 and 6.2).*

6.1.2 Spatial analysis

The comparison of maps of $Y_{(x)}$ mean and variance (Figure 6.4) puts to the light the fact that areas densely urbanized and having a high water depths and have a high variance in $Y_{(x)}$. This maps comparison also underlines the fact that areas having a high mean water depths in less densely urbanized areas and in areas close to the edge of flood spatial extent (having a smaller mean water depth) have a lower variance value of $Y_{(x)}$.

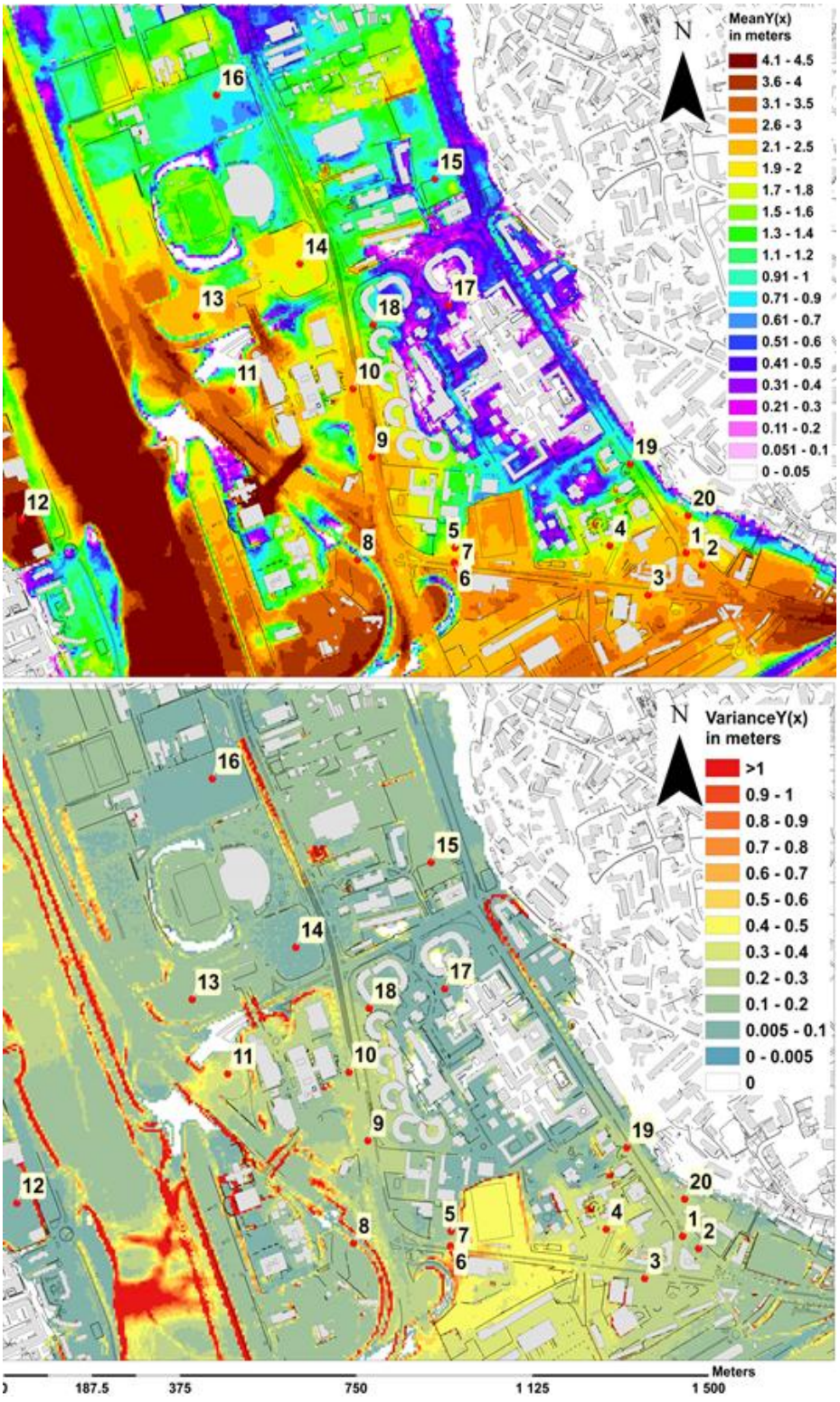

Figure 6.4. *Maps of mean and variance values of maximal water height $Y_{(x)}$.*

This confirms the local observations at points of interest. Moreover, a high variance of $Y_{(x)}$ is observed in the map for places that have steep slopes such as river bank, access roads, highway ramps or dikes. Intuition would lead to incriminate here resolution of discretization effects (var. R) as it will be confirmed by the SA (see next section and discussion part). Over

the river, variance is locally important. The spatial changes in variance in the river bed range from 0.1 m to 1 m. Amplitudes in variance in the river bed are most likely due to above-ground features additions when var. S changes (features such as walls, dikes levees, and roads elements in the main riverbed), that does change the width of the river bed itself. Consequently, these local important variance values are not surprising. Our study focuses on overland flow areas. Thus a GSA over riverbed itself would be out of the range of the spatial GSA defined for this study.

6.2 Spatial Global Sensitivity Analysis results

6.2.1 Analysis at points of interest

First order Sobol index (Si) of var. S ($Si_{(S)}$), var. R ($Si_{(R)}$) and var. E ($Si_{(E)}$) are computed for the 20 points of interest. Figure 6.5 (a) shows the evolution of computed Si increasing N through a random sampling in the results database for the same three points used in the figure 6.3. Evolution of Si computation for other points can be found in annex E. Stability of the computed Si values is observed when N is approximately 1,000, confirming that convergence of the random sampling is reached around this N value. It should be noticed that below a value of N= 500~600, the samples are too small to compute $Si_{(E)}$ (draws of var. E are too scarcely distributed in the matrix to allow computation of conditional expectation of var. E). A bootstrap is performed, to check confidence interval of the computed Si as it can be seen in figure 6.5 (b). For each point, independent samples of size N=1,000 are randomly drawn 10,000 times in the results data base to compute 10,000 times Si. Then, the Si 95% confidence interval is computed.

Over the 20 selected points, the average $Si_{(S)}$ value is 0.40, the average $Si_{(R)}$ value is 0.24 and the average $Si_{(E)}$ value is 0.06. $Si_{(S)}$ is ranked as the highest among the three Si for 13 out of the 20 points. For the seven other points, $Si_{(R)}$ is ranked as the highest Si. The results show that Var. E is never the variable which influences the most $Y_{(x)}$ variance and $Si_{(E)}$ is ranked as the second highest Si only for points 15 and 16. These points are located at the edge of the flood extent area where the Y(x) values are in average below 1 m.

For the 20 points, the difference between the highest ranked Si and the second one is often clear (around 0.35), but the difference between the Si ranked as 2^{nd} and 3^{rd} is often not important (around 0.1) and can be smaller than the 95% confidence interval calculated from the bootstrap.

The main outcome from the points GSA is that var. S and var. R, which are modeller choices when including HR topographic data in the model, are always the parameters contributing

the most to $Y_{(x)}$ variance. The analysis also highlights that var. E does not introduce much variance on $Y_{(x)}$. For the 20 points, Si ranking varies from one point to another one, enhancing the spatial variability of uncertain parameters influence on Y(x) variance and strengthening the interest of sensitivity maps production.

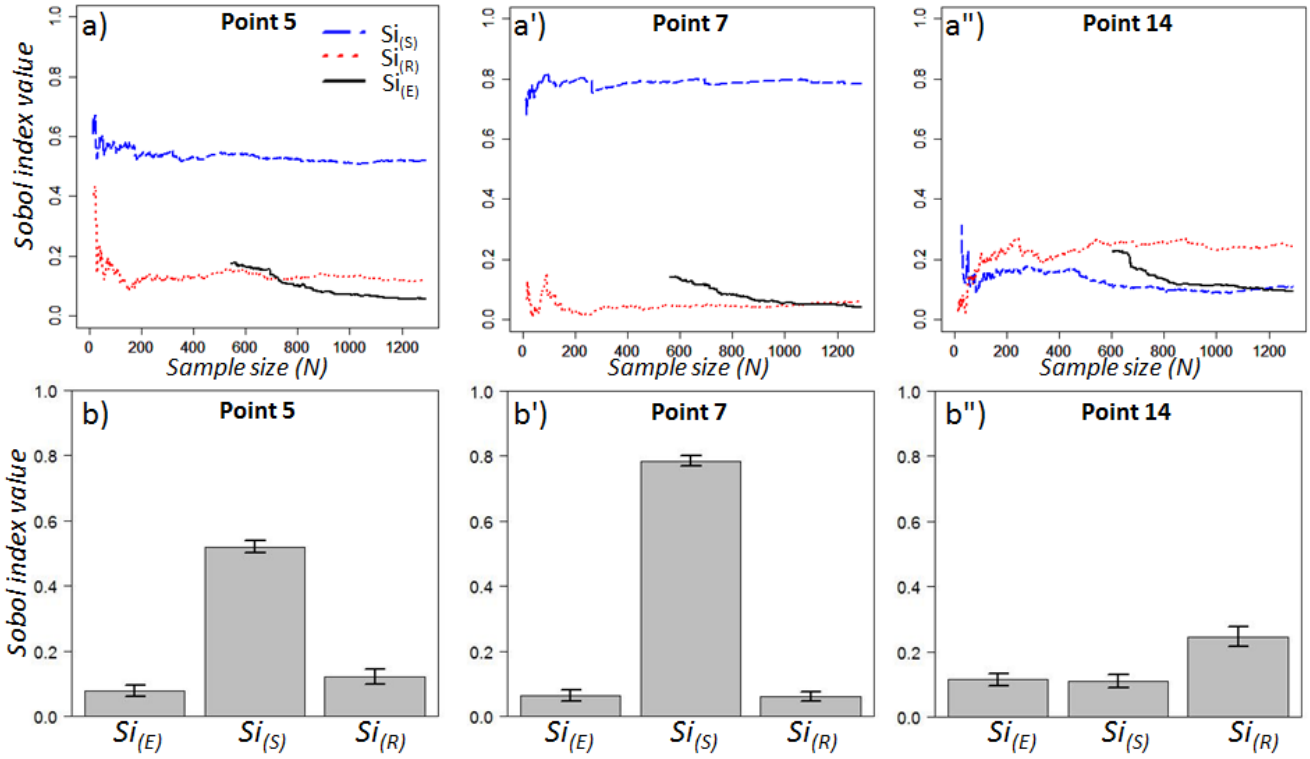

Figure 6.5. *Illustration for three points of interest of Sobol indices convergence (a, a', a") and of confidence interval computed using bootstrap method (b, b', b").*

6.2.2 Spatial analysis

Over the selected subarea, the Si are computed every 5 m to produce sensitivity maps. With this level of discretization, it represents a total of 120,000 points where Si are calculated. A test has been carried out at a finer resolution (1 m) over a 100 m per 100 m area for Si mapping. Results in Si maps at 1 m and 5 m are similar over this small area. Therefore, the Si maps are computed at a 5 m resolution, as the number of points to compute is then 25 times less important than for a 1 m resolution. The Si are computed at every points using N equal to the full size of available simulations in the results database (1,500).

A first analysis of the distribution of computed Si is illustrated in figure 6.6. (a). Non flooded areas are removed for this analysis as well as areas covered by buildings. In fact, inside the buildings which are represented as impervious blocks in the model, $Si_{(S)}$ is equal to one. Therefore, var. S explains the entire variance of $Y_{(x)}$ in building areas. Moreover, at the edges

of buildings, $Si_{(R)}$ is equal to one as well, due to buildings resolution effects. The number of points where Si have been calculated and that are plotted to produce Si maps in figure 6.6 (a) is around 60,000. The results show that:

- $Si_{(S)}$ is highly distributed around 0.1 and has two peaks in distribution around 0.6 and 0.75, the peak at 0.75 having a flatter shape;
- $Si_{(R)}$ is highly distributed around a value of 0.25. A second minor distribution peak around 0.60;
- $Si_{(E)}$ distribution is a single peak centered in $Si_{(E)}$ = 0.07, which is a value lower than both $Si_{(R)}$ and $Si_{(S)}$ peaks.

Analysis of these multi-modal distributions, confirms GSA results obtained at points of interest regarding the non-spatially homogeneous ranking of Si. The analysis of Si maps will help to understand the spatial distribution and the ranking of uncertain input parameters according to their influence over the output variance.

Figure 6.6 (c) presents the Sobol index maps. Analyzing in the first place the maximal Si spatial distribution, it appears that, $Si_{(R)}$ and $Si_{(S)}$ are always ranked with the highest value. $Si_{(R)}$ is ranked as the highest over 67% of the subarea whereas $Si_{(S)}$ is ranked as the highest over 32% of the subarea. Var. E is rarely the most impacting parameter. This confirms the GSA results at points of interest and the Si distribution analysis. In the second place, using the spatial repartition of Si values presented as sensitivity maps (Figure 6.6 (b)), the following remarks arise:

- $Si_{(s)}$ is ranked as the highest index in locations where $Y_{(x)}$ has a high variance. In the areas with a high $Y_{(x)}$ variance, $Si_{(s)}$ values range between 0.3 and 0.8. Areas with high $Si_{(s)}$ are characterized by a highly urbanized environment (where above-ground features strongly impact $Y_{(x)}$).
- $Si_{(S)}$ is ranked as the highest Si, where a given above-ground element strongly impact locally hydrodynamic and consequently $Y_{(x)}$.
- $Si_{(R)}$ happens to be the most impacting parameters in areas less densely urbanized.
- Moreover, high ranking of $Si_{(s)}$ also occurs when a given above-ground structure impacts upstream or downstream calculation of $Y_{(x)}$ whatever is the urban configuration/density of affected upstream or downstream areas.
- $Si_{(R)}$ is ranked as the highest Si when $Y_{(x)}$ is low (below 1 m), and when in the meantime, variance of $Y_{(x)}$ is low as well. It corresponds to areas close to the edge of the flood extent.

- $Si_{(R)}$ is ranked as the highest Si in areas which are less densely urbanized and where no above-ground features, at the given area, neither upstream nor downstream, have any important effects on $Y_{(x)}$.
- $Si_{(R)}$ is ranked as the highest Si in areas where the ground slope is steep. Indeed the level representation of a sloping area is highly affected locally by the degree of resolution of the discretization.
- $Si_{(E)}$ low and almost homogeneous over the subarea.

From this set of remarks and observations regarding the implemented spatial GSA, general remarks arise. First the spatial heterogeneity of impact of uncertain input parameters on the output variability is observed through points and spatial analysis. Second the most impacting uncertain parameters are var. S and var. R which depend on modeller choices. Furthermore the Sobol index maps are of great interest for detailed analysis. Lastly, these general observations have to be taken with care as important limits arises from our approach underlying hypothesis. Consequently results and their limits are discussed in more details in part 7.

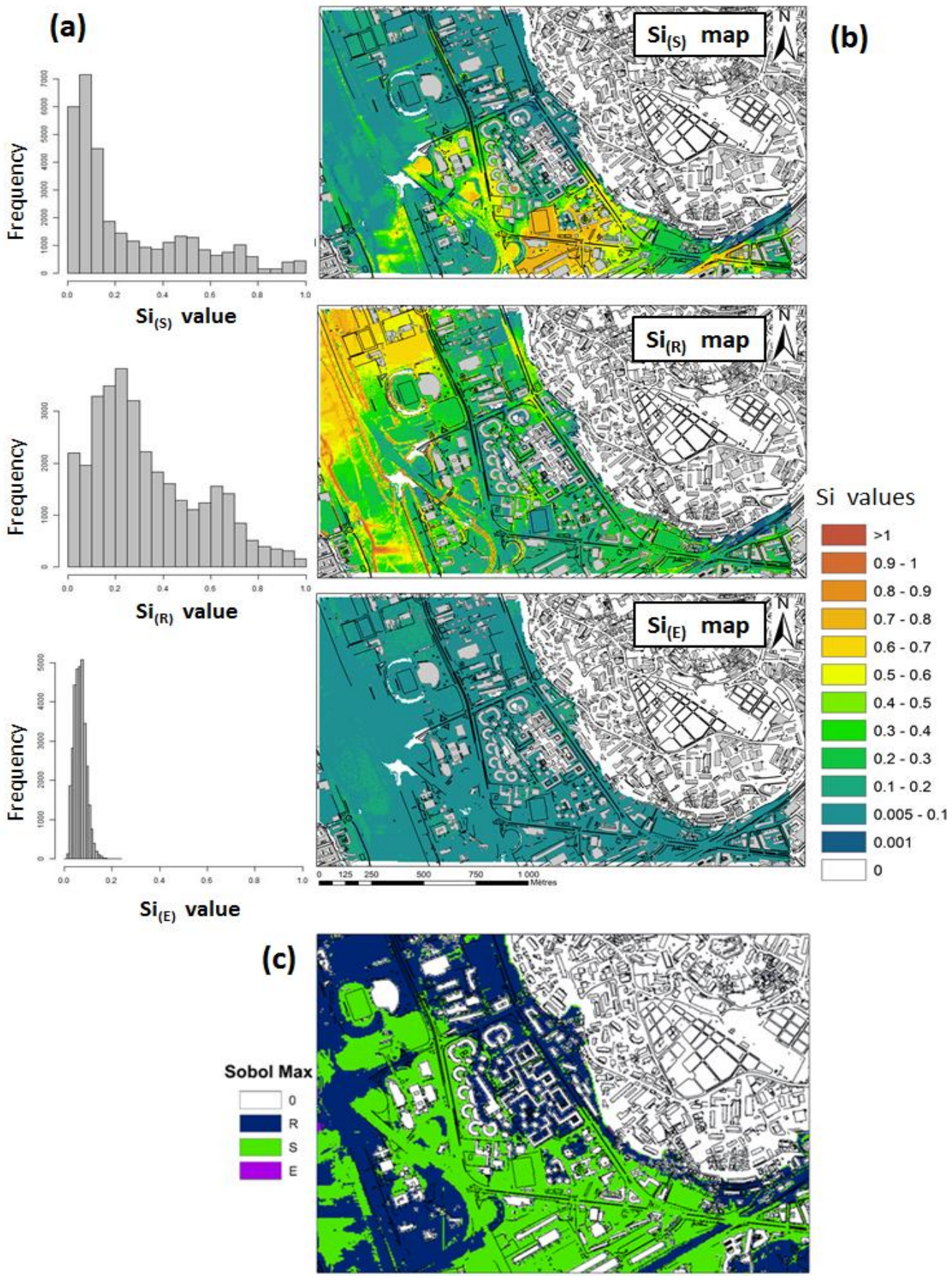

Figure 6.6. *Distribution of computed Si (a), details of Si maps (b) and map of highest ranked Si (c).*

PART. 7. DISCUSSION

The implemented approach is a proof of concept of applicability of spatially distributed GSA to 2D hydraulic problems. UA and spatial ranking of influent uncertain input parameters over the 2D HR flood modelling case study have been achieved. Nevertheless, being a first attempt, the approach can be improved. Outcomes, limits and perspectives are underlined in this section and compared with other research fields in geomatics, SA and hydraulic modelling.

7.1 OUTCOMES

A basic UA leads to the following conclusions on: output variability quantification, nonlinear behavior of the model and spatial heterogeneity. Within established framework for the UA, the considered uncertain parameters, related to the HR topographic data accuracy and to the inclusion in hydraulic models, influence the variability of $Y_{(x)}$ in a range that can be up to 0.71 m. This stresses out the point that even though hydraulic parameters were set-up as constant, the uncertainty related to HR topographic data use cannot be omitted and needs to be assessed and understood. These warnings were already raised up in Dottori *et al*., (2013) and Tsubaki and Kawahara (2013), and are strengthened in this study by $Y_{(x)}$ variance quantification. The quantification is not easily transposable in other contexts and it is not an easy process to give general trend for practical applications given the fact that *(i)* spatial heterogeneity of $Y_{(x)}$ variance is observed and *(ii)* specificities of different HR classified datasets can be highly variable. Nevertheless, this quantification of uncertainty goes in the direction of improvement of state of the art as common practice is still to quantify uncertainty using expert opinion only (see Krueger *et al*., 2012). Investigations on the UA can lead to deeper understanding of mechanisms leading to $Y_{(x)}$ variability. The analyses of the $Y_{(x)}$ distributions (either unimodal or multimodal) at points of interests illustrate the nonlinearity of uncertain parameters effects over the output. This nonlinearity in the output distributions is most likely due to var. S which represents the level of details of above-ground features incorporated in HR DEMs.

GSA at points of interest highlighted that depending on the location of considered points, maximal first order Si are different. This goes in the direction of a need of spatial representation of Si under the form of sensitivity maps for consistent analyses. This spatial distribution of Si showed the major influence of the modeller choices when using the HR topographic data in 2D hydraulic models (var. S and var. R) with respect to the influence of HR dataset accuracy (var. E). Hence as underlined in Marrel *et al*. (2011), if one wants to

reduce variability of $Y_{(x)}$ at a given point of interest, the use of sensitivity maps helps to determine the most influential input at this point. Moreover, sensitivity maps give possibility to link the spatial distribution of Si to the properties of the model, especially with the physical properties of represented urban sector topography. The fact that var. S is the most contributing parameter in densely urbanized areas is not surprising as it introduces a change in the representation in the model of physical properties of the urban environment. The var. R indirectly impacts quality of small scale elements representation well.

7.2 LIMITS OF THE IMPLEMENTED SPATIAL GSA APPROACH

GSA allowed to compute sensitivity maps, but simplifications and choices, especially regarding the way step A (setting up of the spatial GSA framework by choosing uncertain parameters and choosing a way to spatialize theme) and step B (assigning PDF to input parameters), lead to simplifications which are interesting to enhance.

For the uncertainties related to errors in HR topographic data (var. E), the followed Normal PDF having properties of the RMSE is randomly introduced, for every points of the highest resolution DEM (1 m). However, as from one point to the next one, the normal PDF is drawn independently; it results in an uniform spatial distribution. In practice an uniform repartition should increase entropy (maximize errors/uncertainties effects by giving all occurrences an equiprobability). In the present case, this consideration is not valid. Actually, the parameter used is a RMSE which is already averaged over the space. In fact as reminded in Weechsler (2007), the RMSE is calculated based on assumption of normality that is often violated. For instance, over open and flat areas (*e.g.* parking, roads), relative accuracy from one point to another should increase. In the case study, a comparison with ground topographic data measurement revealed that accuracy of HR DEM RMSE increases to 0.05 m. Hence, over flat areas where the var. E appears to be ranked as the second most contributing parameter to $Y_{(x)}$ variability, not without standing the fact that the Si confidence interval of ranked second and third parameters overlaps, it sounds reasonable to think that var. E is overestimated. Opposite effect is observable over sloping areas (*e.g.* dikes), where in our cases, after a regional control of the measurement quality, results show find that RMSE value is about 1 m. Therefore, especially over steep slope areas such as dikes where var. R has been found to be the most important parameter contributing to $Y_{(x)}$ variability, our Si ranking has to be taken with caution as var. E has probably been locally underestimated. For further work, it would be interesting to improve the approach, by using spatialized values of RMSE in function of topographic properties. This regionalization of characteristics of PDF might not be easy to be implemented by practitioners, as regional information of accuracy might not be available. In that case, basic assumption to attribute regionally different characteristics to PDF could be

relevant. For var. E, a component related to photo-interpretation errors should have been taken into consideration. Moreover, in order to improve our study, it would be relevant to include a new variable that would reflect errors in photo-interpretation. Basically, this should consist in a random error in classified data for 5% of the number of elements used for DEM generation. From a technically point of view, implementation of such process is not straight forward particularly, recalling that this study is a first proof of concept on the topic. Therefore, it has not been included in the SA. Nevertheless, errors in photo-interpretation, which are uncertainties inherent to the HR dataset would have locally a considerable impact on Y (x) variability and would require further research.

For modeller's choices, in terms of level of details in classified features to be integrated in the hydraulic models (var. S), it is reasonable to consider this parameter as a categorical ordinal parameter having a uniform PDF. Depending on availability of information of features influencing overland flow defined as classes and depending on model objective, modeller will select one of the available options in increasing complexity of DEM. The choice of a row HR DTM (without buildings, var. S1) is mostly responsible of the observed binomial distribution in the UA, leading to an under estimation of maximal water depth $Y_{(x)}$ compared to other cases. Nevertheless it appears as well that locally, at 1 m and 3 m resolutions, var. S4 leads to low $Y_{(x)}$ value as well due to local effects over flow paths.

For modeller's choices in terms of level of discretization (var. R), we constrained ourselves to resolution levels which are realistic with the use of such type of data considering that a resolution higher than 5 m is not compatible with the idea of producing HR models. Nonlinear effects of resolution are clear to the practitioners in the sense that the grid resolution will impact the level of details included in the model (Horritt and Bates, 2001; Mark *et al*., 2004; Djordjević *et al*., 2009).

CHAPTER III SUMMARY AND CONCLUSIONS

Implemented approach is a proof of concept of applicability of spatially distributed variance-based Global Sensitivity Analysis (GSA) to 2D flood modelling, allowing to quantify and to rank the defined uncertainties sources related to topography measurement errors and to operator choices when including High-Resolution (HR) classified dataset in hydraulic models. Interest focuses on *(i)* applying an Uncertainty Analysis (UA) and spatial GSA approaches in a 2D HR flood model having spatial inputs and outputs and *(ii)* producing sensitivity maps. Summary of outcomes and remarks are put to the front concerning these aspects.

Spatial GSA implementation

Using 400,000 CPU hours on the HPC architecture of the Centre de Calcul Interactif of Marseille and of Nice, a database of 1,500 simulations of a river flood event scenario over a densely urbanized area (described based on a HR classified topographic dataset) has been built. A random sampling on the produced result database has been performed to follow a Monte-Carlo approach. After convergence check, an UA and a variance based functional decomposition GSA have been performed over the output of interest. Output of interest being the maximal overland flow water depth ($Y_{(x)}$) reached at every point of the computational grids.

Feasibility of spatial GSA approach for HR 2D flood modelling has been achieved by this proof of concept case study.

Important requirements are involved when implementing UA and GSA as expertise and efforts are required *(i)* for method establishment (specification of the problem) and *(ii)* for characterization of input parameters, as complexity of this step increases to include spatial variability of the input parameters and can involve an important pretreatment phase (*e.g.* for DEMs generation). Eventually spatial information of HR topographic dataset accuracy might not be available. In that case, basic assumption attributing regionally different characteristics to PDF could be relevant. Not only this part of the process is subject to subjectivity, but it can be time consuming and his application in dedicated tools (such as Prométhée-FullSWOF_2D) might not be straight forward.

For practical application, restrictive computational resources requirement is raised for this specific case (in terms of CPU and in terms of hard drive storage) due to the use of big data combined with a Monte Carlo approach. More parsimonious strategies like Pseudo Monte Carlo sampling could be used or, depending on the objective other GSA method than use of

Sobol functional variance decomposition can be carried out: see Iooss and Lemaître (2015) for a review on optimization of GSA strategy in function of objectives and complexity of models.

Uncertainties related to HR classified topographic data use

The UA has allowed to quantify uncertain parameters impacts on output variability and to describe the spatial pattern of this variability. The spatial GSA has allowed the computation of Sobol indices (Si) maps over the area of interest, enhancing the relative weight of each uncertain parameter on the variability of calculated overland flow.

Within established framework, the considered uncertain parameters related to the HR topographic data accuracy and to the inclusion of HR topographic data in hydraulic models, influence the variability of $Y_{(x)}$, in a range that can be up to 1 m. This enhances the fact that the uncertainty related to HR topographic data use is considerable and deserves to be assessed and understood before qualifying a 2D flood model of being HR or of high accuracy. Moreover, UA reveals nonlinear effects and spatial heterogeneity of $Y_{(x)}$ variance. Nonlinearity in the output distributions is most likely due to var. S, which represents the level of details of above-ground features incorporated in DEMs.

The fact that var. S is the most contributing parameter in densely urbanized areas is not surprising. Indeed, in that case, a change in var. S highly influences the representation in the model of physical properties of the urban environment, therefore impacting model results. The Var. R indirectly impacts quality of small scale elements representation as well. Nevertheless var. E assumes a spatially uniform RMSE and does not take into consideration errors in photo-interpretation. Therefore, errors related to HR measurement are probably underestimated locally in this study.

GSA use to spatially rank uncertain parameters effects gives a valuable insight to modeller. Moreover, it can help to reduce variability in the output putting effort on improving knowledge about a given parameter or helps for optimization (*e.g.* to define relevant areas where spatial discretization is important before non-structured mesh use).

GENERAL CONCLUSION AND PROSPECTS

The motivation for this research work was related to the increasing availability o of High-Resolution (HR) topographical data combined with high performance computing resources that opens the door to HR hydraulic simulations for risk assessment. Moreover, there is a growing demand from decision makers to use HR topographic datasets in flood risk assessment studies. Indeed, the high level of accuracy of these HR datasets gives high expectations to both the numerical modelling community and the stakeholders the physical properties (topography) of the system can be better described and stakeholders ask for highly accurate description of flood risk. Nevertheless, issues arise from different aspects that are depicted in chapter 1 such as:

(1) validity of the approach compared to the original theoretical framework under which simplifying hypotheses were used to design the Shallow Water Equations (SWEs) system;
(2) feasibility, added values and limits of HR topographic data use with nowadays standard codes and meshing techniques.

If a better description of the topography in complex environment should be an important asset. However; regarding (1) one must not erroneously expect that results provide more than what the framework of the modelling exercise supplies or that the level of accuracy of the topographic dataset will define the level of accuracy of the models results. Moreover, (2) might make arise both added values and uncertainties related to modeller strategy for HR topographic data inclusion in models.

This thesis tackles these aspects through two targets designed as research objectives. The targets of this work were the following:

- the first target (T1) is to develop a method and to provide a list of good practices for HR urban flooding event modelling;
- the second target (T2) focuses on quantifying and ranking uncertainties related to HR topographic data use in 2D SWEs based models developing operational tools and method to carry out an uncertainty analysis.

Case study and tests presented and analyzed in chapters 2 and 3 gives opportunity to make a critical assessment of the reached findings, to draw general conclusions and furthermore to suggest perspectives for future researches. In this concluding part of the thesis, recommendations are summarized and given through two sections. The first section draws

the conclusions for the two targets and the second one focuses on global vision and prospects.

CONCLUSIONS AND RECOMMENDATIONS

The first chapter of the thesis presented HR topographic data gathering techniques considering their possibilities for a HR description of industrial and urban environment. Inclusion of fine overland flow influencing structures (walls, sidewalks, road gutters, *etc.*) in 2D HR flood models is challenging for an efficient spatial discretization and creates steep topographic gradient occurrences. Moreover, chapter 1 summarized the background of the theoretical framework of SWEs, in order to raise questions up regarding validity of the approach of 2D SWEs based modelling over complex environments. The presented research does not pretend to address fundamental aspects regarding the validity of the use of 2D SWEs in a framework different from the one for which they have been designed for (chapter 1). The aim was to test the validity of the approach from a practical point of view and to rise up limits of such an attempt. Three case study were selected (chapter 2) to test different contexts of HR flood modelling over industrial or urban sites. They were purposely highly challenging in terms of over passing the SWEs original framework. Moreover, the case study were voluntary highly challenging for standards numerical codes as they introduced: huge number of computational points, rainfall runoff over steep slope, wet/dry transition and flow regime changes occurrences. The chapter 3 consisted on a focus on uncertainties related to model inputs, and more specifically on uncertainties related to one type of inputs: HR topographic data use and inclusion in 2D SWEs based codes.

METHOD AND GOOD PRACTICES FOR HR TOPOGRAPHIC DATA USE (T1)

The feasibility, the performances and the relevance of HR flood modelling have been evaluated with a selection of different codes approximating the 2D SWEs, based on various spatial discretization strategies (structured and non-structured) and having different numerical approaches (finite differences, finite elements, finite volumes). A comparison has been conducted over computed maximal water depth and water deep evolution. The results confirmed the feasibility of these tools use for the studied specific purpose of HR modelling for three case study and various 2D SWE based codes. Nevertheless, optimal use of HR DEM in standard 2D numerical modelling tools appeared challenging in terms of feasibility of data integration within modelling tools. Table 8.1 summarizes main findings of the approach regarding: feasibility, HR topographic data integration, relevance and limits.

The feasibility was first tested on HR runoff modelling over a fictive industrial site for an intense local rainfall event simulation. The fictive site topography was finely described using a HR DEM that had a 0.1 m per 0.1 m horizontal resolution. Tested categories of 2D SWEs based codes, show in a large extent similar results in water depth calculation under important optimization procedure. Actually, major requirements were involved to get comparable results with a reasonable balance between mesh generation procedure, computational time and numerical parameters optimization (*e.g.* for wet/dry treatment). If results were found to be comparable between the different codes solving SWEs, advantage of tested finite volume well balanced scheme for steady state, equilibrium and wet/dry transition is enhanced; drawback being elevated computational cost compare to other numerical methods (*e.g.* Mike 21 ADI). Moreover, to ensure that no important errors occur, controls have to be effectuated (*e.g.* on mass balance, velocities, *etc.*). Tests of results reliability estimation using indicators of did not point out major critical aspects in calculation.

For HR topographic datasets integration, LiDAR and photo-interpreted HR datasets were tested. Their ease of use for building of HR DEM devoted to hydraulic purpose has been tested. The advantage of photo-interpreted data relies in the fact that classes of features can easily be handled for a HR DEM elaboration. Then, a method to design a HR DEM including fine elements influencing overland flow has been presented and tested for photo-interpreted datasets. This simple method was based on extrusion of selected classes of fine features elevation information on HR DTM. Tests have been carried out for intense rainfall and river flooding events, over a range of spatial extent up to a megacity urban district scale (lower Var valley). The inclusion of detailed/thin features in DEM and in hydraulic models lead to considerable differences in local overland flow calculations compared to HR models that do not describe the industrial or urban environments with such level of detail (*e.g.* we have tested a LiDAR dataset not fine enough to include fine features). For instance, fine above-ground features inclusion can lead locally up to a 0.5 m difference in maximal water depth estimations compared to simulations where they are not included in case of the tested local intense rainfall event. Moreover, added value of fine features inclusion in DEM Is clearly observed, even if resolution (either 0.3 or 1 m) is higher than fine features' typical size. Actually, tests to include fine features (extruding theirs elevation information on DEM), through an over sizing of their horizontal extent to 1 m, lead to good results with respect to their inclusion at a finer resolution.

Table 8.1. Summary of comments on feasibility, added values and limits of HR flood modelling over industrial and urban environments.

General comments	**+ Feasibility of HR flood modelling in urban environments with codes approximating 2D SWEs.** **+ Highly requiring in terms of preprocessing/optimization and controls/computational cost.** **+ Due to contrast between HR rendering and existing uncertainties, good practice to provide deviation and confidence in results is highly required.**	
Feasibility of HR modelling with 2D SWEs based codes	**Scale and scenario**	Feasibility of HR flood modelling is confirmed from industrial to megacity district scales, for river flood and intense rainfall events scenarios.
		Thin features are highly impacting overland flow properties particularly maximal water depth calculated for intense rainfall scenarios.
		In terms of HR dataset handling: quality control, computational cost and increases of the spatial extent (a whole city for instance) raises up difficulties.
	Codes and optimization	Theoretical limits regarding: high gradients occurrences, boundary/initial conditions and validity of energy losses coefficient are common to the category of SWE based codes.
		All the tested 2D SWEs based codes are able to provide similar results in water depth estimations under different efforts for optimization procedure.
		Efficient spatial discretization, wet/dry transitions and flow regime changes treatment are key numerical issues.
		Within codes, dissimilar numerical methods lead to different ease of treatment for numerical difficulties.
		Enhancement of controls requirement due to optimization.
HR topographic dataset integration	**HR DEM for hydraulic purpose**	LiDAR and photo-interpreted HR topographic datasets can equally represent fine above-ground structures. Differences occur in terms of ease of use for pretreatment depending on the nature of HR datasets.
		Detailed inclusion of elevation of fine above-ground structures information, even at a decreased horizontal resolution is relevant.
	Integration (spatial discretization)	Structured and non-structured meshing approach give similar results, but important differences arise in terms of ease of pretreatment: standard non-structured meshing algorithms failure is often observed due to over-constraint environment.
	Control	Requires survey to guaranty temporal validity of a HR dataset: fine above-ground structures quickly evolve in urban environment.
Relevance vs limits	**Objective**	Added value of the approach for detailed results, at least: to compare relatively flood risk at detailed scale and to understand hydrodynamic.
	Scale applicability and uncertainties	Quick temporal evolution of above-ground features at urban scale makes HR modelling hazardous without ground survey and update. At an industrial site scale, it appears reasonable to consider that site operator has a complete knowledge of these aspects.
		Other uncertainties exist and arise from conceptualization, numerical approach and input hydrologic parameters. They shall not be forgotten even if HR modelling results seems very accurate.
Efforts and requirements	**Preprocessing and post-processing**	Computational resource demanding for data handling. Operator time consuming for data control (each singularity with LiDAR and classification for photo-interpreted datasets). Computational resource demanding for result analysis.
	Computational effort	Important computational time which is nevertheless largely inferior to required operator time resources for computation optimization.

Results have pointed out differences, notably regarding ways and possibilities to integrate HR topographic dataset in 2D SWEs based codes. Photo-interpreted datasets provide interesting vectorial information that can be of great help to define mesh refinement zone in case of non-structured mesh generation. Nevertheless, due to meshing algorithm properties, the over constraints created by the density of vectors (in case of a HR urban environment) lead to errors and difficulties for non-structured mesh generation. For these reasons, the use of a structured mesh representing the HR DEM was find to be a more efficient compromise.

Relevance of this HR flood modelling approach was raised up as the integration of detailed features clearly impacts results of overland flow evaluation. When using HR DEMs for a HR flood modelling purpose, several categories of recommendations and limits deserved to be emphasized for practical engineering applications:

- HR photo-interpreted datasets are heavy and their manipulation for pre- and post-processes is computational resources demanding;
- Criteria used for photo-interpretation can highly influence design of the HR DEM and therefore have to be controlled by the modeller. Indeed, classification criteria for a given photo-interpreted dataset might not have been created specifically for water modelling purpose. For instance, what is classified as concrete walls is not based on material criteria, but on structure width/elevation ratio. This results in blocking the water flow if closed polylines artificially close real overland flow paths. Therefore, one key aspect is that the hydraulic modeller that will use the HR dataset should have a transparent vision on the dataset production procedure for the HR DEM generation. Finally, a limitation appears regarding bridges piers, where information is not given by aerial techniques;
- In case of a non-structured mesh, meshing algorithms are not able to generate in a parsimonious way mesh when over constrained. In the end, the computational time is not decreased;
- HR DEM use at these scales, with codes fully solving 2D SWEs, requires intensive calculation resources. Indeed, the reduced *dx* and *dy* to include topographic details in the model lead to a *dt* reduction due to methods inherent CFL restrictions. In case of a structured mesh use the number of points drastically increases, over areas where detailed representation is not necessary.

In terms of relevance, HR numerical modeling approach for detailed flood risk assessment can give a valuable insight to evaluate exposure to risk. Moreover the approach highlights comprehension of dynamical aspects of the phenomena and helps for management

regarding this category of risk exposure. For such a purpose the complementary use of different nature of scenarios is an interesting approach.

HR overland flow modelling approach appears to give a good asset if the focus is given on a site that has a relative small spatial extent such as an industrial site. Actually, regarding HR flood modelling, as detailed in our studies, fine features have important influence on overland flow properties. Consequently including them is an asset to have a better description of physical properties of the environment. Therefore, it allow a better detailed estimation of maximal water depth reached in case of a flooding event. However, our studies have shown that a small change in these overland flow influencing structures might lead to important difference in results (section 4.1 and chapter 2). Hence, if the site has an important spatial extent that evolves quickly with time and are not implemented in models, one might think that the validity of the detailed estimation of the flood risk is not relevant. Over an industrial site such as a nuclear basic installation, it is reasonable to consider that the evolution of this complex environment is controlled and can be surveyed regularly. Therefore, the applicability of the approach appears as an interesting asset for industrial sites to evaluate flood risk. At an urban scale size, control and survey of the above ground features might not be easily performed.

UNCERTAINTIES RELATED TO HR TOPOGRAPHIC DATA USE: METHOD AND TOOLS FOR UNCERTAINTY ANALYSIS IN HR 2D HYDRAULIC MODELLING (T2)

Uncertainties related to input data are one of the sources of uncertainty in a modelling approach. Even though HR DEM has a high level of accuracy, HR topographic datasets used for its elaboration have different types of inherent errors that can lead to important changes in overland flow path in the hydraulic calculation. Lastly modeller choices to integrate HR data in the hydraulic models yield to uncertainty as well. A focus was given on uncertainties related to model inputs and more specifically on uncertainties related to one type of inputs: HR topographic data use and inclusion in 2D SWEs based codes. The aim was:

(i) to be a proof of concept of spatial Global Sensitivity Analysis (GSA) applicability to 2D flood modelling studies using developed method and tools and implementing them on HPC structures;

(ii) to quantify uncertainties related to HR topographic data use, spatially discriminating relative weight of uncertainties related to HR dataset internal errors with respect to modeller choices for HR dataset integration in models.

The quantification and understanding of uncertainty can be apprehended using Uncertainty Analysis (UA) and GSA. It should be noted that concept of these methods has already been applied in different water issues modelling studies. Nevertheless, it has not been tested yet for 2D floods modelling that have spatially varying uncertain inputs and outputs. Briefly, UA consists in the propagation of uncertainty sources through model, and then focuses on the quantification of uncertainties in model output allowing robustness to be checked (Saint-Geours, 2012). GSA aims to study how uncertainty in a model output can be linked and allocated proportionally to the contribution of each input uncertainties. Our application on 2D HR flood models can be considered as a proof of concept and for sake of feasibility of implementation of the approach within the imparted time for the study, simplifying shortcuts have been taken in the problem definition step of the spatial GSA method and in the sampling strategy. The results are briefly summarized and impacts of simplifications are discussed in this part. Ways to overcome and improve the work are also described.

By applying a UA and a spatial GSA, the purpose was to specifically investigate on uncertainties related to HR topographic data use for hydraulic modeling. Two categories of uncertain parameters were considered in our approach: the first category is inherent to HR topographic data internal errors (measurement errors) and the second category is related to operator choices for this type of data inclusion in 2D hydraulic codes. Three uncertain parameters considered as independent have been studied: the measurement error (var. E), the level of details of above-ground element representation in DEM (buildings, sidewalks, *etc.*) (var. S), and the resolution of the spatial discretization (grid cell size for regular mesh) (var. R). Parameter var. E follows a normal probability density function, whereas parameters var. S and var. R are equally-probable discrete operator choices.

Combining these parameters, 2,000 HR DEM were produced and 1,500 HR simulations were run using a parametric environment (Prométhée) coupled with a code that approximates solutions of the 2D SWEs using a finite volume method on a structured mesh (FullSWOF_2D). Developed tool "*Prométhée-FullSWOF_2D*" was implemented on high-performance computing structures (HPC) to produce a results database of the simulations. This operational tool is transposable to majority of HPC structures requiring little adaptation.

In our case study, the output of interest is the maximal water surface of the set of simulations ($Y_{(x)}$) on the flooded areas. A random sampling on the produced results database has been performed through a Monte-Carlo approach.

The UA led to: output variability quantification, nonlinear behavior of the model observation and enhancement of the spatial heterogeneity of the output variance. Within established framework for the UA, the considered uncertain parameters related to the HR topographic

data accuracy and to the inclusion in hydraulic models, influence the variability of the overland flow) in a range that can be up to a 0.7 m² variance. This stresses out the point that even though other input hydraulic parameters were supposed to be fully known (set-up as constant) in the simulations, the uncertainty related to HR topographic data plays a major role in results quality and deserved to be assessed and understood.

The GSA led to Sensitivity indexes (Sobol indexes) computation. Sobol indexes (Si) have been calculated at given points of interest, enhancing the relative weight of each uncertain parameter on variability of calculated overland flow. Si maps production was achieved. The spatial distribution of Si illustrates the major influence of the modeller choices, when using the HR topographic data in 2D hydraulic models (var. S and var. R) with respect to the influence of HR dataset accuracy (var. E). Spatial variation of the Si ranking was clearly observable. Moreover, the study highlights the possibility to link the spatial distribution of the Si to the properties of the model, especially with the physical properties of represented urban sector topography.

If one aim is to reduce variability of $Y_{(x)}$ at a given point of interest, the use of sensitivity maps helps to determine the most influential input. Then, by reducing the uncertainty of this input it is possible to reduce the output variability. Outputs of UA and GSA implementation related to the specific concern of HR topographic dataset uses in 2D flood modelling enhanced the weight of modeller's choices. However, the work could be improved. More specifically to improve assessment of uncertainties related to HR topographic datasets integrations in model, it has to be mentioned that sources of uncertainty were identified in the photo-interpreted datasets, but not taken into account in the uncertainty and sensitivity analysis. Notably the fact that the provided dataset error (var. E) is already averaged over space (in reality this error is not spatially homogeneous) and photo-interpretation errors (misclassification, addition or omission) are not considered. Implementation of these two aspects would have made the approach more robust, and represents a way to improve our research. Nevertheless, the spatialization of the error (var. E) is not available as rarely provided to user. Intuitive hypothesis is that it would have decreased the Si of var. E in flat areas where Si of var. E is already really low and would have increased it in steep areas. Concerning implementation of random errors in photo-interpreted vector, it would have led to really important weight (which is already enhanced in our conclusion), and would have been technically more time requiring to implement. A focus on parameters spatial interaction would have been interesting as well.

HOLISTIC VIEW AND PROSPECTS

This research, related to HR topographic data use in 2D SWEs based flood modelling has been considered in the first place in the context of nuclear safety. The main objective was to consider one of the Reference Flood Situation of the ASN guide (see ASN, 2013) to test HR modelling for local intense rainfall events over sites conducting nuclear activities. This risk has to be assessed by the nuclear site operator. In this framework and in the context of democratization of HR topographic dataset, it sounds appropriate that the operator of a site has a HR knowledge of its site topography. Furthermore, operator should be able to control and survey the temporal evolution of above-ground features on the site environment.

In case of an urban environment, spatial extent is larger and above-ground elements features potentially influencing overland flow paths evolve quickly, permanently and seldom with control and survey updates. Consequently in case of an urban application, it appears that there is a gap between HR topographic dataset that a modeller will receive and the reality. Therefore, if small changes due to above-ground features have important impact on overland flow properties and cannot be implemented with their temporal evolution, it is irrelevant to provide "*detailed or accurate*" simulation results for a predictive flood risk assessment purpose. The Uncertainty Analysis (UA) and Sensitivity Analysis (SA) applied to our case study gave a good illustration of impacts of small features changes on model results variability. Beside the technical asset of UA and SA approaches, they offer valuable educative perspective for stakeholders regarding sensitivity versus accuracy of models results over urban environment.

The next section enhances global recommendations for HR modelling. The following one stresses out possibilities offered by spatial UA and GSA methods applied to 2D flood modelling. Lastly perspectives are given.

HIGH-RESOLUTION MODELLING

HR overland flow modelling is interesting to give detailed relative comparison of water height reached over a complex environment and to better understand hydrodynamic of a simulated flood event.

Tests highlighted disparities among modelling tools in terms of practical aspects. Indeed, HR topographic datasets integration can be properly done, but modelling tools cannot equally fulfill requirement for establishment of an adapted discretization. It requires control and

caution as mentioned in previous section and therefore the HR flood modelling approach requires times for its implementation (for pretreatment, computation, *etc.*).

As mentioned in the first paragraph of this general conclusion section and as noted inn figure 8.1, main drawbacks of the HR flood modelling are explained. fine features influencing overland flow can rapidly changes in megacities (depending on area, *e.g.* historical and downtown areas being less subject to temporal evolution). Therefore, the use of a non-updated datasets make results of HR modelling questionable. This is particularly true due to *(i)* time to post-treat aerial topographic campaign and *(ii)* time to produce HR model. Combination of these two points will lead to a couple of months to a year of delay between topographic campaign and presentation of results to decision makers. Therefore it can be hazardous to use a HR overland flow modelling as it can nourish an illusion of accuracy for non-specialists, whereas uncertainties related to HR topographic data use are not known, notwithstanding the fact that other numerous sources of uncertainties exist in the modelling process (see introduction of chapter 3). Lastly for the HR topographic data itself, it has to be kept in mind that when water velocities are important, the flow can move or destroy some of the features.

From an operational point of view, computational cost is not really a burden in case of a single or a couple of models run. Nevertheless, computational resources are needed for pre-processing/post-processing data manipulations if the spatial extent of the HR model is larger than a couple square kilometers. Moreover, the overall approach is highly time consuming requiring time for HR DEM building, data integration (meshing), computation, and post-computation results treatment.

Eventually, a standard HR deterministic modelling approach does not yield to assessment of the uncertainties of produced results. This uncertainty assessment will consequently rely on the modeller/expert opinion.

UNCERTAINTY AND SENSITIVITY ANALYSIS WITH 2D SWES BASED MODELS AND PROSPECTS

Quantification of uncertainty through UA goes in the direction of improvement of state of the art, compared to quantification of uncertainty based on expert opinion only. Investigations on the UA can lead to deeper understanding of mechanisms leading to $Y_{(x)}$ variability. GSA by ranking uncertain parameters allows practical approaches to better understand issues in the model and to improve the model. Indeed, even if GSA results can vary from one approach to another at least, it helps modeller to have a better understanding of its model results, and provides effective strategies for model improvement. Drawbacks are related to computational

cost and remaining subjectivity of the approach. In a global perspective, research is active to reduce the computational burden of UA and SA approaches. For instance, more parsimonious sampling strategies should be tested. For the subjectivity of the approach (*e.g.* in the characterization of uncertain inputs), outcomes of UA and GSA studies applied to flood modelling helps to give feedback and to improve practices.

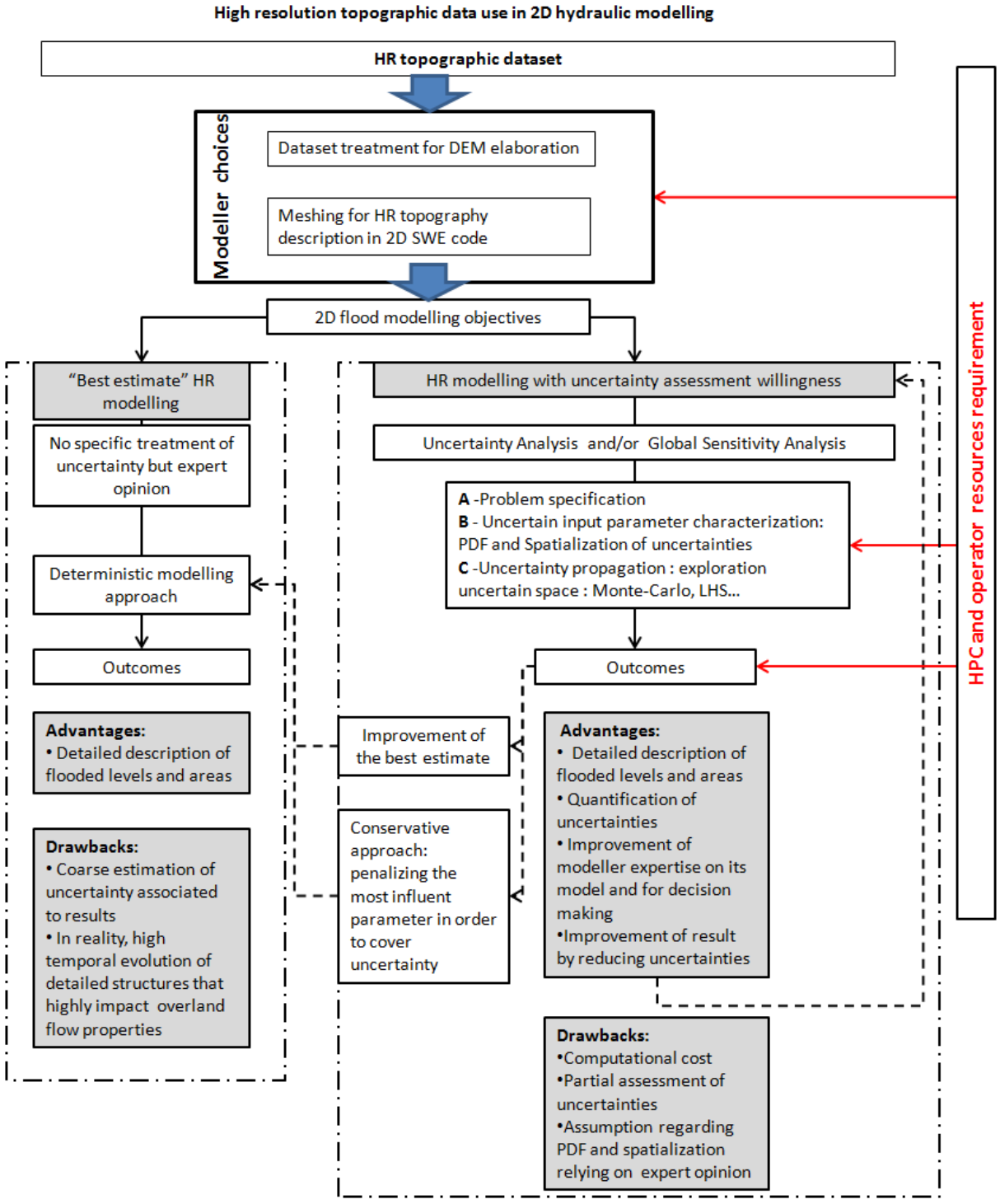

Figure 8.1. *Schematic overview of high-resolution topographic data use possibilities for flood modelling studies.*

It is interesting to mention that UA and GSA can feed the deterministic modelling approach (see figure 8.1) added value being for improvement of the model, for instance helping to find out ways to improve accuracy or means to improve the computational time by finding a better equilibrium in the balance (*e.g.* decreasing the discretization resolution in certain areas). Objective can be to improve the best estimate of an event modelling. Objective can be as defined in the ASN guide, to have a conservative approach by penalizing the identified most influent parameter to encompass uncertainty related to the specified uncertain problem.

Even though, as reminded in Pappenberger (2008) depending on the method, GSA might produce different results, added value of the UA and GSA approach is that quantification and ranking helps modeller to have a better knowledge of limits of what has been modelled. Drawbacks of the approach are (i) the subjectivity in the approach that relies on expert opinion for the problem specification and for input parameters uncertainty characterization; (ii) the resource requirement of the approach related to computational cost and to the relative complexity of the approach involving time for its practical implementation.

PERSPECTIVES FOR SPATIAL DISCRETIZATION AND COMMUNICATION ON HR FLOOD MODELLING RESULTS

As previously mentioned, commonly used algorithms for non-structured mesh generation encounter difficulties due to the over constrained environment. Nevertheless, non-structured meshing strategies (*e.g.* based on *z* gradient criteria for refinement) exist and could be interesting to test. Adaptive Mesh Refinement (AMR) can be an option to test as well. The uses of AMR generation that regenerates non-structured meshes are available, but seem challenging and prohibitive even though not tested here. The use of blocks of structured AMR would be promising and adapted to HR modelling of overland flow over urban environments. Moreover, the feedback from spatial UA and GSA can allow to define areas were a refined discretization, with respect to the topography effects, is crucial.

Last perspective that should be enhanced here, is the communication on HR flood models results. Nowadays, technologies such as urban reconstruction, visual analytics approaches or enhanced/immersive reality rendering will probably allow to map HR flood model results in a realistic and immersive way in upcoming years. These results will most likely be available through modern communication technologies, which is interesting for awareness on flood issues. Nevertheless this enhanced rendering is dangerous as it will strengthen the overconfidence from non-specialist and decision makers in models results; consequently such type of approach would be useful if used to disseminate scientific results about deviation and doubt about models results (*e.g.* mapping of uncertainties levels, warning about assumptions, *etc.*). Idea is that the Hydroinformatic community should take advantage

of these new visualization possibilities to educate and inform stakeholders on the limits of modelling practices. The danger being to providing a realistic rendering giving an over estimated illusion of accuracy of HR flood models results. Consequently, new way of communicating results and uncertainties to decision makers and stake holders has to be build up.

BIBLIOGRAPHY

Aackermann, P., Pedersen, P., Engsig-Karup, A., Clausen, T. and Grooss, J. (2013). Development of a GPU-Accelerated Mike 21 Solver for Water Wave Dynamics. In Keller, R., Kramer, D. and Weiss, J.-P., editors, Facing the Multicore-Challenge III, Springer Berlin Heidelberg, 7686, 129-130.

Abbott, M. B., Bathurst, J. C., Cunge, J. A., O'Connell, P. E., & Rasmussen, J. (1986). An introduction to the European Hydrological System—Systeme Hydrologique Europeen,"SHE", 1: History and philosophy of a physically-based, distributed modelling system. Journal of hydrology, 87(1), 45-59.

Abbott, M. B., Damsgaard, A., & Rodenhuis, G. S. (1973). System 21,"JUPITER" (A design system for two-dimensional nearly horizontal flows). Journal of Hydraulic Research, 11(1), 1-28.

Abbott, M. B. (1963). The solution of wave propagation problems using an iterative operator. La Houille Blanche, (5), 513-524.

Abily, M., Bertrand, N., Delestre, O., Gourbesville, P., & Duluc, C.-M. (2016a). Spatial Global Sensitivity Analysis of high resolution classified topographic data use in 2D urban flood modelling. Environmental Modelling & Software (accepted).

Abily, M., Delestre, O., Gourbesville, P., Bertrand, N., Duluc, C. M., & Richet, Y. (2016b). Global Sensitivity Analysis with 2D Hydraulic Codes: Application on Uncertainties Related to High-Resolution Topographic Data. In Advances in Hydroinformatics: Simhydro2014, Springer Singapore, 301-315.

Abily, M., Scarceriaux, C., & Duluc, C.-M. (2015b). Ruissellement de surface en milieu urbain: stratégies d'intégration de données topographiques haute résolution en modélisation hydraulique 2D. Techniques Sciences Méthodes, (5), 31-46.

Abily, M., Delestre, O., Amossé, L., Bertrand, N., Richet, Y., Duluc, C. M., P. Gourbesville & Navaro, P. (2015c). Uncertainty related to high resolution topographic data use for flood event modelling over urban areas: toward a sensitivity analysis approach. ESAIM: Proceedings and Surveys, 48, 385-399.

Abily, M., Delestre O., Bertrand, N., Richet, Y., Duluc, C.-M., & Gourbesville, P. (2015d). Global Sensitivity Analysis with 2D hydraulic codes: applied protocol and practical tool. La houille Blanche, (5), 16-22.

Abily, M., Duluc, C. M., & Gourbesville, P. (2014a). Use of Standard 2D Numerical Modeling Tools to Simulate Surface Runoff Over an Industrial Site: Feasibility and Comparative Performance Survey Over a Test Case. In Advances in Hydroinformatics, 19-33. Springer Singapore.

Abily, M., Delestre, O., Amosse, L., Bertrand, N., Laguerre, C., Duluc, C.-M & Gourbesville, P. (2014b). Use of 3D classified topographic data with FullSWOF for High Resolution simulations of

river flood event over a dense urban area. 3rd IAHR Europe Congress, Book of Proceedings, 2014, Porto, Portugal.

Abily, M., Duluc, C. M., Faes, J. B., & Gourbesville, P. (2013a). Performance assessment of modelling tools for high resolution runoff simulation over an industrial site. Journal of Hydroinformatics, 15(4), 1296-1311.

Abily, M., Gourbesville, Andres, L., & Duluc, C.-M. (2013b). Photogrammetric and LiDAR data for high resolution runoff modeling over industrial and urban sites. In Zhaoyin, W., Lee, J. H.-W., Jizhang, G., and Shuyou, C., editors, Proceedings of the 35th IAHR World Congress, September 8-13, 2013, Chengdu, China. Tsinghua University Press, Beijing.

Abdullah, A. F., Vojinovic, Z., Price, R. K., & Aziz, N. A. A. (2012). A methodology for processing raw LiDAR data to support urban flood modelling framework. Journal of Hydroinformatics, 14(1), 75-92.

Aktaruzzaman, M. & Schmidt, T. (2009) Detailed Digital Surface Model (DSM) Generation and Automatic Object Detection to Facilitate Modelling of Urban Flooding. ISPRS Workshop, Hannover.

Alliau, D., De Saint Seine, J., Lang, M., Sauquet, E. & Renard, B. (2013). Flood study of industrial site by extreme flood risk: uncertainties with hydrologic and hydraulic extreme values. Proceeding of congress SHF – Evènements extremes d'inondation 2013, 13-14 November 2013, Lyon, France.

Andres, L. (2012). L'apport de la donnée topographique pour la modélisation 3D fine et classifiée d'un territoire. Revue XYZ, 133(4), 24-30.

ASN (2013). Protection of Basic Nuclear Installations Against External Flooding - guide no.13 - version of 08/01/2013. Technical report, Autorité de Sûreté Nucléaire.

Audouin, Y., Moulinec, C., Barber, R. W., Sunderland, A. G., Gu, X.-J. and Emerson, D. R. (2011). Preparing TELEMAC-2D for extremely large simulations. Proceedings of the XVIIIth Telemac & Mascaret User Club 19–21 October 2011, EDF R&D, Chatou (France).

Audusse, E. & Bristeau, M.-O. (2005). A well-balanced positivity preserving "second-order" scheme for shallow water flows on unstructured meshes. Journal of Computational Physics, 206, 311-333.

Audusse, E., Bouchut, F., Bristeau, M.-O., Klein, R., & Perthame, B. (2004). A fast and stable wellbalanced scheme with hydrostatic reconstruction for shallow water flows. SIAM J. Sci. Comput., 25(6), 2050-2065.

Baroni, G., & Tarantola, S. (2014). A General Probabilistic Framework for uncertainty and global sensitivity analysis of deterministic models: A hydrological case study. Environmental Modelling & Software, 51, 26-34.

Baltsavias, E. P. (1999). A comparison between photogrammetry and laser scanning. ISPRS Journal of photogrammetry and Remote Sensing, 54(2), 83-94.

Bates, P. D., Marks, K. J., & Horritt, M. S. (2003). Optimal use of high-resolution topographic data in flood inundation models. Hydrological Processes,17 (3), 537-557.

Bates, P. D., Wilson, C. A. M. E., Hervouet, J. M., & Stewart, M. D. (1999). Two dimensional finite element modelling of floodplain flow. La Houille Blanche, (3-4), 82-88.

Bates, P. D., Anderson, M. G., Hervouet, J. M., & Hawkes, J. C. (1997). Investigating the Behaviour of Two ‐ Dimensional Finite Element Models of Compound Channel Flow. Earth Surface Processes and Landforms, 22(1), 3-17.

Bermudez, A., & Vazquez, M. E. (1994). Upwind methods for hyperbolic conservation laws with source terms. Computers & Fluids, 23(8), 1049-1071.

Beven, K. & Binley, A. (1992). The future of distributed models – Model calibration and uncertainty prediction. Hydrological Processes, 6, 279-298.

Bidmon, K., & Thomas E., (2005) Generation of Mesh Variants via Volumetrical Representation and Subsequent Mesh Optimisation. Proceedings, 14th International Meshing Roundtable, Springer-Verlag, pp.275-286, September 2005.

Bouchut, F. (2004). Nonlinear Stability of Finite Volume Methods for Hyperbolic Conservation Laws, and Well-Balanced Schemes for Sources. Frontiers in Mathematics. (4). Birkhäuser Basel.

Bozzi, S., Passoni, G., Bernardara, P., Goutal, N., & Arnaud, A. (2015). Roughness and Discharge Uncertainty in 1D Water Level Calculations. Environmental Modeling & Assessment, 1-11.

Bristeau, M.-O. and Coussin, B. (2001). Boundary conditions for the shallow water equations solved by kinetic schemes. Technical Report RR-4282, INRIA.

Brugeas, L. (1996). Utilisation de MPI en décomposition de domaine. CNRS-IDRIS, available from http://www.idris.fr/data/publication/mpi.ps, p. 27.

Ciliberti, S.A., Gomez, M., Macchione, F., Russo, B., & Villanueva, A. (2008) 2D analysis for local flooding assessment in a new square of Barcelona during storm events. 11th International Conference on Urban Drainage, Edinburg, Scotland, UK, pp. 9.

Chen, Y., Su, W., Li, J., & Sun, Z. (2009). Hierarchical object oriented classification using very high resolution imagery and LIDAR data over urban areas. Advances in Space Research, 43(7), 1101-1110.

Chow, V. T. (1959). Open-Channel Hydraulics. McGraw-Hill.

Cordier, S., Coullon, H., Delestre, O., Laguerre, C., Le, M.H., Pierre, D., & Sadaka, G. (2013). FullSWOF_Paral: Comparison of two parallelization strategies (MPI and SKELGIS) on a software designed for hydrology applications, ESAIM: Proc., 43, 59-79.

Coullon, H., Le, M.-H., & Limet, S. (2013). Parallelization of Shallow-water Equations with the Algorithmic Skeleton Library SkelGIS. International Conference of Computational Science. Barcelona Spain. Elsevier Procedia Computer Science, 18, 591-600.

Coullon, H. and Limet, S. (2013). Algorithmic skeleton library for scientific simulations: SkelGIS. International Conference on High Performance Computing & Simulation. Helsinki Finland. IEEE HPCS 2013: p. 429-436.

Cunge, J. (2012). What Do We Model, What Results Do We Get? Anatomy of Modeling Systems Foundations. In Gourbesville, P., Cunge, J., and Caignaert, G., editors, Advances in Hydroinformatics, Springer Hydrogeology, 5-18.

Cunge, J. (2003). Of data and models. Journal of Hydroinformatics, 5, 75-98.

Cunge J., Holly F. & Verwey A. (1980). Practical Aspects of Computational River Hydraulics. Pitman Publishing, London, T. Fisher Unwin.

Cunge, J. A. (1966) Comparison of physical and mathematical model test results on translation waves in the Oraison-Manosque power canal. La Houille Blanche No. 1, 55–70.

Cunge, J. A., & Wegner, M. (1964). Intégration numérique des équations d'écoulement de Barré de Saint-Venant par un schéma implicite de différences finies. La Houille Blanche, (1), 33-39.

Dawson, R.J., Speigh, L., Hall, J.W., Djordjevic, S. Savic, D., & Leandro. J. (2008) Attribution of flood risk in urban areas. Journal of Hydroinformatics, 10(4), 275-288.

Delenne, C., Cappelaere, B., & Guinot, V. (2012). Uncertainty analysis of river flooding and dam failure risks using local sensitivity computations. Reliability Engineering & System Safety, 107, 171-183.

Delestre, O., Abily, M., Cordier, F., Gourbesville, P., & Coullon, H. (2016). Comparison and Validation of Two Parallelization Approaches of FullSWOF_2D Software on a Real Case. In Advances in Hydroinformatics (395-407). Springer Singapore.

Delestre, O., Cordier, S., Darboux, F., Du, M., James, F., Laguerre, C., Lucas, C., & Planchon, O. (2014). FullSWOF: A Software for Overland Flow Simulation. In Gourbesville, P., Cunge, J., and Caignaert, G., editors, Advances in Hydroinformatics, Springer Hydrogeology, pages 221-231. Springer Singapore.

Delestre, O., Lucas, C., Ksinant, P. A., Darboux, F., Laguerre, C., Vo, T. N., James, F. & Cordier, S. (2013). SWASHES: a compilation of shallow water analytic solutions for hydraulic and environmental studies. International Journal for Numerical Methods in Fluids, 72(3), 269-300.

Delestre, O., Cordier, S., Darboux, F., & James, F. (2012). A limitation of the hydrostatic reconstruction technique for Shallow Water equations. Comptes Rendus Mathematique, 350(13), 677-681.

Delestre, O. (2010). Simulation du ruissellement d'eau de pluie sur des surfaces agricoles (Doctoral dissertation, Université d'Orléans).

de Saint Venant, A. J.-C. (1871). Théorie du mouvement non-permanent des eaux, avec application aux crues des rivières et à l'introduction des marées dans leur lit. Comptes Rendus de l'Académie des Sciences, 73:147–154.

DHI (2007a) MIKE 21 FLOW MODEL, Hydrodynamic module: Scientific Documentation. Danish Hydraulics Institute. p. 58.

DHI (2007b) MIKE 21 & MIKE 3 FLOW MODEL FM, Hydrodynamic and transport module: Scientific documentation, Danish Hydraulics Institute. p. 50.

DHI (2007c). MIKE SHE USER MANUAL: Reference guide. Danish Hydraulics Institute. V.2, p. 386.

DHI (2003) Hints and recommendation in application with significant flooding and drying. Danish Hydraulic Institute: p. 8.

Djordjević, S., Vojinović, Z., Dawson, R., & Savić, D. A. (2009). Flood modelling in urban areas, Chapter 10 in: Applied Uncertainty Analysis for Flood Risk Management, Ed. by K. Beven and J. Hall.

Dottori, F., Di Baldassarre, G., & Todini, E. (2013). Detailed data is welcome, but with a pinch of salt: Accuracy, precision, and uncertainty in flood inundation modeling. Water Resources Research, 49(9), 6079-6085.

Duluc, C. M., Bardet, L., Guimier, L., & Rebour, V. (2014). Un nouveau guide sur la protection des installations nucléaires contre l'inondation d'origine externe. La Houille Blanche, (5), 47-53.

Egels, Y. & Kasser, M. (2004). Digital Photogrammetry. Taylor & Francis.

Em Karniadakis, G., & Kirby II, R.M. (2003). Parallel Scientific Computing in C++ and MPI. Cambridge University Press.Ettrich, N. (2005) Generation of Surface Elevation Models for Urban Drainage Simulation. Bericht des Fraunhofer ITWM, 79, 1-29.

Erpicum, S., Dewals, B., Archambeau, P., Detrembleur, S., & Pirotton, M. (2010). Detailed inundation modelling using high resolution DEMs. Engineering Applications of Computational Fluid Mechanics, 4(2), 196-208.

Fernández, D. S., & M. A. Lutz. "Urban flood hazard zoning in Tucumán Province, Argentina, using GIS and multicriteria decision analysis." Engineering Geology 111.1 (2010): 90-98.

Feurer, D., Bailly, J. S., Puech, C., Le Coarer, Y., & Viau, A. A. (2008). Very-high-resolution mapping of river-immersed topography by remote sensing. Progress in Physical Geography, 32(4), 403-419.

Fewtrell, T. J., Duncan, A., Sampson, C. C., Neal, J. C., & Bates, P. D. (2011). Benchmarking urban flood models of varying complexity and scale using high resolution terrestrial LiDAR data. Physics and Chemistry of the Earth, Parts A/B/C, 36(7), 281-291.

Fisher, P. F., & Tate, N. J. (2006). Causes and consequences of error in digital elevation models. Progress in Physical Geography, 30(4), 467-489.

George, P. L., & Seveno, É. (1994). The advancing-front mesh generation method revisited. International Journal for Numerical Methods in Engineering, 37 (21), 3605-3619.

George, D. L. (2011), Adaptive finite volume methods with well-balanced Riemann solvers for modeling floods in rugged terrain: Application to the Malpasset dam-break flood (France, 1959). Int. J. Numer. Meth. Fluids, 66: 1000–1018.

Geuzaine, C. and Remacle, J.-F. (2009) Gmsh: a three-dimensional finite element mesh generator with built-in pre- and post-processing facilities. Int. Jo. for Numerical Methods in Engineering, Volume 79, Issue 11, 1309-1331.

Gomez, M., Macchione, F. & Russo, B. (2011) Methodologies to study the surface hydraulic behaviour of urban catchments during storm events. Water Sciences and Technologies. 63(11), 1-9.

Gopala, VR. & Wachem, BGM., (2008). Volume of fluid methods for immiscible-fluid and free-surface flows. Chem. Engineering Journal 141, 204-221.

Gourbesville, P. (2014). Hydroinformatics and Its Role in Flood Management. Hydrometeorological Hazards: Interfacing Science and Policy, 137-169.

Gourbesville, P. (2009) Data and hydroinformatics: new possibilities and challenges. Journal of Hydroinformatics, 11(3-4), 330-343.

Gourbesville, P., Pisot, N., Le Fur, H., Linberg, S. (2004) High resolution digital elevation models: A major interest for urban flooding management. 6th International Conference on Hydroinformatics, Singapore, 621-629.

Guinot, V. (2012). Wave propagation in fluids: models and numerical techniques. John Wiley & Sons.

Guinot, V. and Cappelaere, B. (2005). Méthodes Numériques Appliquées. Résolution numériques des équations différentielles de l'ingénieur, Polytech'Montpellier, Editor. 2005: Montpellier. p. 69

Guinot, V. and Gourbesville, P. (2003). Calibration of physically based models: back to basics ? Journal of Hydroinformatics, 5(4), 233-244.

Guinot, V. (2000). Linear advection modelling: the issue of divergent flows. Journal of Hydroinformatics, 2, 113-121.

Habib, A., Ghanma, M., Morgan, M. & Al-Ruzouq, R. 2005: Photogrammetric and LiDAR data registration using linear features. Photogrammetric Engineering and Remote Sensing 71(6), 699-707.

Hall, J. W., Tarantola, S., Bates, P. D., & Horritt, M. S. (2005). Distributed sensitivity analysis of flood inundation model calibration. Journal of Hydraulic Engineering, 131(2), 117-126.

Helton, J. C., Johnson, J. D., Sallaberry, C. J., & Storlie, C. B. (2006). Survey of sampling-based methods for uncertainty and sensitivity analysis. Reliability Engineering & System Safety, 91(10), 1175-1209.

Henrik R, (2002) Computational Fluid Dynamics of Dispersed Two-Phase Flows at High Phase Fractions. PhD thesis Imperial College, Department of Mechanical Engineering, p. 343.

Herman, J. D., Kollat, J. B., 1, Reed, P. M., & Wagener,T., (2013). Technical note: Method of Morris effectively reduces the computational demands of global sensitivity analysis for distributed watershed models Hydrol. Earth Syst. Sci. Discuss., 10, 4275–4299.

Hervouet, J.-M. (2007). Hydrodynamics of free surface flows. Wiley

Hervieu, A., & Soheilian, B. (2013). Road side detection and reconstruction using LIDAR sensor. In Intelligent Vehicles Symposium (IV),June 2013 IEEE (pp. 1247-1252). IEEE.

Hrvoje J., (1996) Error Analysis and Estimation for the Finite Volume Method with Applications to Fluid Flows. PhD thesis, Imperial College, Department of Mechanical Engineering, p.343.

Hunter, N. M., Bates, P. D., Neelz, S., Pender, G., Villanueva, I., Wright, N. G., Liang, D., Falconer, R.A., Lin, B., Waller, S., Crossley, A.J. & Mason, D. (2008). Benchmarking 2D hydraulic models for urban flood simulations. In Proceedings of the Institution of Civil Engineers: Water Management (Vol. 161, No. 1, pp. 13-30). Thomas Telford (ICE publishing).

Iooss, B. & Lemaître, P. (2015). A review on global sensitivity analysis methods. Uncertainty management in Simulation-Optimization of Complex Systems: Algorithms and Applications, Ed. By C. Meloni and G. Dellino Springer.

Iooss. (2011). Revue sur l'analyse de sensibilité globale de modèles numériques. Journal de la Société Française de Statistique, (152), 1-23.

Jung, Y., & Merwade, V. (2014). Estimation of uncertainty propagation in flood inundation mapping using a 1-D hydraulic model. Hydrological Processes 29 (4), 624–640.

Karypis, G. & Kumar, V. (1998). METIS: family of multilevel partitioning algorithm. Available from: http://glaros.dtc.umn.edu/gkhome/views/metis.

Krueger, T., Page, T., Hubacek, K., Smith, L., & Hiscock, K. (2012). The role of expert opinion in environmental modelling. Environmental Modelling & Software, 36, 4-18.

Küng, O., Strecha, C., Beyeler, A., Zufferey, J.-C., Floreano, D., Fua, P., & Gervaix, F.: The accuracy of automatic photogrammetric techniques on ultra-light UAV imagery, in: 15 UAV-g 2011 – Unmanned Aerial Vehicle in Geomatics, Zurich, Switzerland. Available from: http://infoscience.epfl.ch/record/168806 (last access: 30 April 2015), 2011.

Lafarge, F., Descombes, X., Zerubia, J., & Pierrot Deseilligny, M. (2010). Structural approach for building reconstruction from a single DSM. Trans. on Pattern Analysis and Machine Intelligence, 32(1), 135-147.

Lafarge, F. & Mallet, C. (2011). Building large urban environments from unstructured point data. In Computer Vision (ICCV), 2011 IEEE International Conference, 0, 1068-1075, Los Alamitos, CA, USA. IEEE Computer Society.

Lavabre, J., Mériaux, P., Nicoletis, E., & Cardelli, B. (1996). Catastrophic Var river flood of 5 November 1994. Convegno internazionale la prevenzione delle catastrofi idrogeologichi il contributo della ricerca scientifica, Alba, ITA, 375-380

Lax, P. D., & Richtmyer, R. D. (1956). Survey of the stability of linear finite difference equations. Communications on Pure and Applied Mathematics, 9(2), 267-293.

Lax, P. D., & Wendroff, B. (1960). Systems of conservation laws, Comm. Pure and Applied Maths, 13, 217-237.

Le Bris, A., Chehata, N., Briottet, X. & Paparoditis, N. (2013). Very high resolution land cover extraction in urban areas. in Proc. of the 8th EARSeL Imaging Spectrometry Workshop, April 2013.

Lemmens, M. 2007: Airborne LiDAR Sensors. GIM International 21(2).

Leitão, J. P., Moy de Vitry, M., Scheidegger, A., & Rieckermann, J. (2015) Assessing the quality of Digital Elevation Models obtained from mini-Unmanned Aerial Vehicles for overland flow modelling in urban areas, Hydrol. Earth Syst. Sci. Discuss., 12, 5629-5670, doi:10.5194/hessd-12-5629-2015, 2015.

Liang, D., Lin, B. & Falconer, R.A. (2006) A boundary-fitted numerical model for flood routing with shock-capturing capability. Journal of Hydrology, (332), 477-486.

Liliburne, L. & Tarantola, S. (2009). Sensitivity analysis of spatial models. International Journal of Geographical Information Science, 23(2):151–168

Linder, W. (2006). Digital Photogrammetry: A Practical Course. Springer Verlag.

Liu, X. (2008). Airborne LiDAR for DEM generation: some critical issues. Progress in Physical Geography, 32(1), 31-49.

Löhner, R., Applied Computational Fluid Dynamics techniques (2008) John Willey & Sons, Second edition, p. 433.

Löhner, R. (1997). Automatic unstructured grid generators. Finite Elements in Analysis and Design, 25(1), 111-134.

Lu, D. & Weng, Q. (2007). A survey of image classification methods and techniques for improving classification performance. International Journal of Remote Sensing, 28(5), 823-870.

Ma, Q., Abily, M., duong Vo, N., & Gourbesville, P. (2015). High Resolution Rainfall-Runoff simulation in urban area: Assessment of Telemac-2D and FullSWOF_2D. Proceedings of the 36th IAHR World Congress, The Hague, 2015

Madsen, P.A., Simonsen, H.J., Pan Cun-Hong (2005) Numerical simulation of tidal bores and hydraulic jumps. Coastal Engineering, 52, 409-433.

Mandlburger, G., Hauer, C., Höfle, B., Habersack, H., & Pfeifer, N. (2008). Optimisation of LiDAR derived terrain models for river flow modelling. Hydrology and Earth System Sciences (HESS), 5, 3605-3638.

Mark, O., Weesakul, S., Apirumanekul, C., Boonya-Aroonnet, S. & Djordjević, S. (2004) Potential and limitations of 1D modelling of urban flooding. Journal of Hydrology, 299 (3-4), 284-299.

Marrel, A., Iooss, B., Jullien, M., Laurent, B., & Volkova, E. (2011*). Global sensitivity analysis for models with spatially dependent outputs.* Environmetrics, 22(3), 383-397.

Mastin A., Kepner J. & Fisher J. (2009). Automatic registration of LIDAR and optical images of urban scenes. In 2009 IEEE Conference on Computer Vision and Pattern Recognition. Miami, FL, June 2009, IEEE, 2639–2646.

McCowan, A.D., Rasmussen, E.B. & P. Berg (2001) Improving the performance of a two-dimensional hydraulic model for floodplain applications, in Hydraulics in Civil Engineering. T.I.o. Engineers, Editor: Hobart, Australia. p. 11.

Meakin, R. L. (2000). Adaptive spatial partitioning and refinement for overset structured grids. Computer methods in applied mechanics and engineering,189(4), 1077-1117.

Meesuk, V., Vojinovic, Z., Mynett, A. E., & Abdullah, A. F. (2015). Urban flood modelling combining top-view LiDAR data with ground-view SfM observations. Advances in Water Resources, 75, 105-117.

Meng, X., Currit, N., & Zhao, K. (2010). Ground filtering algorithms for airborne LiDAR data: A review of critical issues. Remote Sensing, 2(3), 833-860.

Menter FR. (1993) Zonal two equation k-omega turbulence models for aerodynamic flows. AIAA Paper 93-2906.

Meselhe, E. A., and Jr, F. Holly. (1997). Invalidity of Preissmann scheme for transcritical flow. Journal of Hydraulic Engineering, 123(7), 652-655.

Morris, M. D. (1991). Factorial sampling plans for preliminary computational experiments. Technometrics, 33(2), 161-174.

Moulinec, C., Denis, C., Pham, C. T., Rougé, D., Hervouet, J. M., Razafindrakoto, E., Barber, R.W., Emerson, D.R., & Gu, X. J. (2011). TELEMAC: An efficient hydrodynamics suite for massively parallel architectures. Computers & Fluids,51(1), 30-34.

Moussa, R. & Bocquillon, C. (2000). Approximation zones of the Saint-Venant equations f flood routing with overbank flow. Hydrology and Earth System Sciences Discussions, Copernicus Publications, 4 (2), 251-260.

Musialski, P., Wonka, P., Aliaga, D. G., Wimmer, M., van Gool, L., & Purgathofer, W. (2013). A survey of urban reconstruction. Computer Graphics Forum, 32(6), 146-177. doi: 10.1111/cgf.12077

Nex, F., & Remondino, F. (2014). UAV for 3D mapping applications: a review. Applied Geomatics 6(1),1-15.

Nikuradse, J. (1933) Laws of flow in rough pipes. VDI Forschungsheft 361. In translation, NACA TM 1292, 1950.

Nguyen, T., Richet, Y, Balayn, P., Bardet, L. (2015). Propagation d'incertitudes dans les modèles hydrauliques 1D, La houille Blanche, (5), 55-62.

Novak, P., Guinot, V., Jeffrey, A., & Reeve, D. E. (2010). Hydraulic Modelling–An Introduction: Principles, Methods and Applications. CRC Press.

Ouarit, H. (2004). Réduction des systèmes à paramètres distribués. Application à la commande optimale robuste des canaux d'irrigation (Doctoral dissertation, Institut National Polytechnique de Grenoble-INPG).

Owen, SJ. & Saigal, S. (2000) H-Morph: an indirect approach to advancing front hex meshing. Int. J. Numer. Meth. Engng. 49, 289-312.

Owen, S. J. (1998, October). A Survey of Unstructured Mesh Generation Technology. In IMR (pp. 239-267).

Pappenberger, F.,& K. J. Beven (2006), Ignorance is bliss: Or seven reasons not to use uncertainty analysis, Water Resour. Res., 42, 1-8.

Pappenberger, F., Matgen, P., Beven, K. J., Henry, J. B., Pfister, L., & Fraipont, P. (2006). Influence of uncertain boundary conditions and model structure on flood inundation predictions. Advances in Water Resources,29(10), 1430-1449.

Pappenberger, F., Beven, K. J., Ratto, M., & Matgen, P. (2008). Multi-method global sensitivity analysis of flood inundation models. Advances in water resources, 31(1), 1-14.

Priestnall, G., Jaafar, J., & Duncan, A. (2000). Extracting urban features from LiDAR digital surface models. Computers, Environment and Urban Systems,24(2), 65-78.

Podhoranyi, M., & Fedorcak, D. (2015). Inaccuracy introduced by LiDAR-generated cross sections and its impact on 1D hydrodynamic simulations.Environmental Earth Sciences, 73(1), 1-11.

Refsgaard, J. C., van der Sluijs, J. P., Højberg, A. L., & Vanrolleghem, P. A. (2007). Uncertainty in the environmental modelling process–a framework and guidance. Environmental modelling & software, 22(11), 1543-1556.

Remondino, F., Barazzetti, L., Nex, F., Scaioni, M., & Sarazzi, D. (2011). UAV photogrammetry for mapping and 3D modeling - Current status and future perspectives. In Archives of Photogrammetry, Remote Sensing and Spatial Information Sciences, volume 38(1/C22). ISPRS Conference UAV-g, Zurich, Switzerland.

Saint-Geours, N., Bailly, J. S., Grelot, F., & Lavergne, C. (2014). Multi-scale spatial sensitivity analysis of a model for economic appraisal of flood risk management policies. Environmental Modelling & Software, 60, 153-166.

Saint-Geours, N. (2012). Sensitivity Analysis of Spatial Models: Application to Cost Benefit Analysis of Flood Risk Management Plans (Ph.D. thesis). University Montpellier 2

Saint-Geours, N., Lavergne, C., Bailly, J. S., & Grelot, F. (2011). Analyse de sensibilité globale d'un modèle spatialisé pour l'évaluation économique du risque d'inondation. Journal de la Société Française de Statistique, 152(1), 24.

Saltelli, A., Ratto, M., Andres, T., Campolongo, F., Cariboni, J., Gatelli, D., & Tarantola, S. (2008). Global sensitivity analysis: the primer. John Wiley & Sons.

Saltelli, A., Tarantola, S., & Campolongo, F. (2000). Sensitivity analysis as an ingredient of modeling. Statistical Science, 15 (4), 377-395.

Saltelli, A., Tarantola, S. & Chan, K. (1999). A quantitative model-independent method for global sensitivity analysis of model output. Technometrics, 41, pp. 39–56.

Sanders, B. F. (2007). Evaluation of on-line DEMs for flood inundation modeling. Advances in Water Resources 30 (8), 1831-1843.

Sanders, B. F., Schubert, J. E., & Gallegos, H. A. (2008). Integral formulation of shallow-water equations with anisotropic porosity for urban flood modeling. Journal of Hydrology, 362(1), 19-38.

Sart, C., Baume, J. P., Malaterre, P. O., & Guinot, V. (2010). Adaptation of Preissmann's scheme for transcritical open channel flows. Journal of Hydraulic Research, 48(4), 428-440.

Schubert, J.E., Sanders, B.F., Smith, M.J & Wright, N.G. (2008) Unstructured mesh generation and land cover-based resistance for hydrodynamic modelling of urban flooding. Advances in Water Resources 31, 1603–1621

Sørensen, O.R., Sørensen, L.S., & Carlson, J. (2010). Parallelization of the flexible mesh modeling systems with MPI. In International MIKE by DHI Conference 2010, Copenhagen, Denmark, 30.1–30.8.

Sobol', I. M. (1990). On sensitivity estimation for nonlinear mathematical models. Matematicheskoe modelirvanie, 2(1):112-118 (in Russian), MMCE, 1(4) (1993):407-414 (in English).

Tam, A., Ait-Ali-Yahia, D., Robichaud, M.P., Moore, M., Kozel, V., Habashi, W.G. (2000). Anisotropic mesh adaptation for 3D flows on structured and unstructured grids. Computer Methods in Applied Mechanics and Engineering, 189(4), 1205-1230.

Toro, E., Spruce, M., and Speares, W. (1994). Restoration of the contact surface in the HLL-Riemann solver. Shock Waves, 4:25–34.

Tsubaki, R., & Kawahara, Y. (2013). The uncertainty of local flow parameters during inundation flow over complex topographies with elevation errors. Journal of Hydrology, 486, 71-87.

Tsubaki, R. & Fujita, I. (2010). Unstructured grid generation using LiDAR data for urban flood inundation modelling. Hydrological Processes, 24, 1404-1420.

USACE-HEC (2000) Hydrologic modeling system HEC-HMS technical reference manual. US Army Corps of Engineers, Hydrologic Engineering Centre (HEC), Davis, USA

Uusitalo, L., Lehikoinen, A., Helle, I., & Myrberg, K. (2015). An overview of methods to evaluate uncertainty of deterministic models in decision support. Environmental Modelling & Software, 63, 24-31.

Versteeg, HK., Malalasekera, W. (2007) An Introduction to Computational Fluid Dynamics, The Finite Volume Method. Pearson, 2nd Edition.

Volkova, E., Iooss, B., & Van Dorpe, F. (2008). Global sensitivity analysis for a numerical model of radionuclide migration from the ``RRC Kurchatov Institute'' radwaste disposal site. Stochastic Environmental Research and Risk Assessment (22),17-31

Walker, W. E., Harremoës, P., Rotmans, J., van der Sluijs, J. P., van Asselt, M. B., Janssen, P., & Krayer von & Krauss, M. P. (2003). Defining uncertainty: a conceptual basis for uncertainty management in model-based decision support. Integrated assessment, 4(1), 5-17.

Weatherill, N. P. (1992). Delaunay triangulation in computational fluid dynamics. Computers & Mathematics with Applications, 24(5), 129-150.

Wechsler, S. P. (2007). Uncertainties associated with digital elevation models for hydrologic applications: a review. Hydrology and Earth System Sciences, 11(4), 1481-1500.

Weng, Q. (2012). Remote sensing of impervious surfaces in the urban areas: Requirements, methods, and trends. Remote Sensing of Environment, 117, 34-49.

Weitkamp, C. 2005: LiDAR: Introduction. In Fujii, T. & Fukuchi, T., editors, Laser Remote Sensing, Boca Raton, London, New York and Singapore: Taylor & Francis, 1-36.

Willis, T. D. (2014). Systematic analysis of uncertainty in flood inundation modelling. Doctoral dissertation, University of Leeds.

Zhou, G., Song, C., Simmers, J., & Cheng, P. (2004). Urban 3D GIS from LiDAR and digital aerial images. Computers & Geosciences, 30(4), 345-353.

LIST OF ABBREVIATIONS

ADI: Alternate Direction Implicit

AMR: Adaptive Mesh Reconstruction

ASN: French National Safety Authority (Autorité de Sureté Nucléaire)

BB: Building Block

BH: Building Hole

CPU: Central Processing Unit

CFL: Courant-Friedrich-Lewy

DEM: Digital Elevation Model

DHI: Danish Hydraulic Institute

DSM: Digital Surface Model

DTM: Digital Terrain Model

Fr: Froude Number

GSA: Global Sensitivity Analysis

h_{max}: Maximal water depth

HPC: High Performance Computing

IRSN: French Institute for Radioprotection and Nuclear Safety (Institut de Radioprotection et de Sûreté Nucléaire)

LiDAR: Light Detection and Ranging

LSA: Local Sensitivity Analysis

PDF: Probability Density Function

RFS: Reference Flood Situation

RMS: Root Mean Square Error

SA: Sensitivity Analysis

Si: Sobol Index

SWEs: Shallow Water equations

T_{lag}: Lag Time

TVB: Total Variation Bounding

U_{max}: flow maximal Velocity

UAV: Unmanned Aerial Vehicle

Var. E: Variable related to topographic data measurement error

Var. R: Variable related to modeller choicer regarding DSM resolution

Var. S: Variable related to modeller choicer regarding above-ground features included in DSM

VOF: Volume Of Fluid

TABLE OF FIGURES

TABLE OF TABLES

ANNEXES

Annex A: *Abily, M., Scarceriaux, C., & Duluc, C.-M. (2015). Ruissellement de surface en milieu urbain: stratégies d'intégration de données topographiques haute résolution en modélisation hydraulique 2D. Techniques Sciences Méthodes, (5), 31-46.*

Ruissellement de surface en milieu urbain : stratégies d'intégration de données topographiques haute résolution en modélisation hydraulique 2D

M. ABILY[1], C. SCARCERIAUX[2], C.-M. DULUC[3]

Mots-clés : modélisation hydraulique à surface libre, LiDAR, photogrammétrie, Mike 21, Mike Flood
Keywords: free surface hydraulic modelling, LiDAR, photogrammetry, Mike 21, Mike Flood

Introduction

Dans le cadre de la réalisation des plans de préventions des risques naturels prévisibles d'inondations (PPRI), de la mise en place des plans d'actions de prévention contre les inondations (PAPI) ou encore dans un contexte d'évaluation de sûreté d'installations industrielles [ASN, 2013], les outils de modélisation numérique bidimensionnelle (2D) sont couramment utilisés. La démarche « modélisation 2D » est une réponse à l'intégration du risque inondation dans les projets d'aménagements des collectivités. Des villes telles que Paris, Marseille ou Nice ont déjà intégré cette approche dans leur politique de gestion des risques d'inondation.

L'importance de la qualité des données topographiques utilisées en entrée des outils de modélisation numérique 2D dans les études d'hydrauliques a été soulignée dans de nombreux travaux [Mark *et al.*, 2004 ; SCHUBERT et al., 2008 ; GOURBESVILLE, 2009]. Les techniques et technologies aéroportées d'acquisition de données topographiques fines et denses, dites haute résolution (HR), telles que le LiDAR et la photogrammétrie, se sont démocratisées lors de la dernière décennie [ABDALLAH, 2005 ; VALLET, 2010]. Ces techniques, pouvant être embarquées sur des avions ou sur des drones [REMONDINO *et al.*, 2011], autorisent l'accès à une gamme de données fournissant une information topographique HR adaptable à différentes échelles et pour différentes problématiques. De nombreuses sociétés de service en géomatiques ont intégré à leur offre technique des produits de type « modèles numériques d'élévation » (MNE) sous la forme de « modèle numérique de terrain » (MNT) ou de « modèle numérique de surface » (MNS) constitués à partir de l'information topographique HR.

Les données topographiques HR sont de plus en plus utilisées dans des études et projets hydrauliques simulant des inondations d'origine fluviale ou côtière en milieu urbain [AKTARUZZAMAN et SCHMIDT, 2009 ; TSUBAKI et FUJITA, 2010]. La plus-value de l'emploi de ces données HR pour la modélisation de scénarios de ruissellement de surface est prometteuse [GOMEZ *et al.*, 2011 ; ABILY *et al.*, 2013]. Néanmoins, il convient de rappeler qu'une utilisation convenable des données topographique HR nécessite une connaissance approfondie sur les avantages et limites de ces données et sur leur mise en œuvre dans des outils de modélisation numérique. En effet, les outils commerciaux de modélisation numérique, classiquement utilisés en ingénierie, n'avaient pas vocation au moment de leur création à intégrer une donnée de cette nature, ni à être utilisés pour la modélisation de

[1] Institut de radioprotection et de sûreté nucléaire – PRP-DGE\SCAN\BEHRIG & Université de Nice Sophia Antipolis\URE 005 Innovative-CiTy – Polytech Nice Sophia – 930, route des Colles – 06903 Sophia Antipolis. Courriel : abily@polytech.unice.fr
[2] Safege, délégation Méditerranée Outre Mer, Space B – 208, route de Grenoble – 06200 Nice.
[3] Institut de radioprotection et de sûreté nucléaire – PRP-DGE\SCAN\BEHRIG – 31, avenue de la Division-Leclerc – 92260 Fontenay-aux-Roses.

phénomènes de ruissellement en milieux complexes. Ainsi, des pratiques, voire des méthodologies spécifiques doivent être définies et mises en œuvre pour l'intégration des données topographiques HR dans des études d'ingénierie basées sur l'utilisation d'outils de modélisation numérique 2D standard.

L'objectif de cet article est de faire ressortir des bonnes pratiques et méthodes à mettre en œuvre lorsque des données HR sont utilisées dans des modèles hydrauliques 2D en milieu urbain et industriel ainsi que des limites associées à l'emploi de cette donnée. Pour cela, deux études effectuées à Nice utilisant :

– deux jeux de données topographiques HR ;

– deux schémas de modélisation numériques différents ;

à deux échelles différentes sont ici présentées. Le § 1 présente le jeu de données topographiques HR utilisé. Le § 2 détaille la méthodologie employée pour intégrer la donnée topographique HR dans deux cas d'étude. Enfin, le § 3 met en relief les avantages et limites de ces approches d'intégration de la donnée topographique HR.

1. La donnée topographique haute résolution

1.1. Lidar

La technologie LiDAR (pour *light detection and ranging*), permet l'acquisition de données topographiques *via* l'utilisation de scanner laser aéroportés. Les impulsions émises par le scanner seront réfléchies par les objets se trouvant sur son chemin et reçues par le capteur embarqué, fournissant directement l'information de distance entre le capteur et les cibles atteintes [MUSIALSKI *et al.*, 2013]. Cette information fournit un nuage de points géoréférencé où le premier écho décrira la surface des objets (MNS) tandis que le dernier décrira la surface du sol (MNT). Un traitement du nuage de points est nécessaire et réalisable via l'emploi de logiciels spécialisés afin de générer MNT et MNS. La densité du nuage de points sera fonction de la méthodologie d'acquisition, des applications et de la nature du terrain. Lorsque la technologie LiDAR est aéroportée, cette densité varie de 1 point pour 10 m² à près de 5 points par m² [GERVAIX, 2010]. La précision altimétrique peut descendre jusqu'à 5 cm.

La donnée LiDAR de la métropole Nice Côte d'Azur (NCA)

Dans le cadre de la réalisation d'une orthophotographie numérique du territoire de NCA, une campagne d'acquisition de données LiDAR s'est déroulée en septembre 2005 sur 27 communes de la métropole de Nice Côte d'Azur. La précision annoncée par la société en charge des mesures est en moyenne de 15 cm en altimétrie et de 30 cm en planimétrie (calage du géoréférencement réalisé sur 30 points). Le LiDAR a été fourni à un pas de 2 m sur une emprise de 458 km².

La donnée LiDAR brute a été nettoyée de la végétation avant d'être fournie, cependant les ponts, les voiries surélevées et les tunnels sont intégrés à la donnée finale. Pour une utilisation de cette donnée en vue de modéliser un phénomène de ruissellement, un second traitement de la donnée sera indispensable pour écarter d'éventuelles erreurs et incohérences liées à des blocages des écoulements induits par ces éléments.

1.2. Photogrammétrie

La photogrammétrie est une technique de télédétection qui permet de mesurer les coordonnées en trois dimensions d'un espace et des objets qu'il comprend en utilisant des images 2D prises à partir de positions différentes. Le recouvrement entre photographies aériennes permet de restituer les propriétés tridimensionnelles de l'espace et des objets (principe de stéréoscopie). Une phase de calculs d'aérotriangulation, dans laquelle les informations sur les paramètres d'orientation des clichés et sur leurs points de liaison sont primordiales, est nécessaire pour une mesure correcte de l'altitude du terrain et de l'élévation des objets. La hauteur de vol, la multiplication du nombre de points de vues ainsi que des forts taux de recouvrement permettent de fiabiliser les restitutions automatiques [EGELS et KASSER, 2004 ; LINDER, 2006].

En photogrammétrie, la résolution spatiale correspond à la taille d'un pixel au sol. À une résolution spatiale donnée, un objet de taille égale à trois fois la taille du pixel peut être identifié, et un objet de taille égale à 20 fois la taille du pixel peut-être interprété [GERVAIX, 2010]. Sur la base de l'identification et de l'interprétation des objets, l'utilisation de logiciels spécialisés, et particulièrement d'outils de dessin

assisté par ordinateur (DAO) 3D, permet leur restitution sous forme vectorielle classifiée (points, polylignes, polygones). La mise en œuvre de ces procédés de restitution de la donnée sous forme vectorielle requiert des phases manuelles, contrôlées par l'utilisateur. Ainsi, la technologie photogrammétrique permet d'obtenir une donnée topographique fine en 3D et classifiée sur un territoire qui offre des perspectives d'exploitation variées et modulables en fonction des objectifs liés à l'utilisation de cette donnée [ANDRES, 2012].

La donnée photogrammétrique 3D classifiée de NCA

La campagne d'acquisition de données photogrammétriques s'est déroulée en 2010-2011 et couvre 400 km² de NCA (*Figure 1*). Les objets (éléments 3D) ont été interprétés en une cinquantaine de classes différentes sous forme de points, polylignes et polygones. Ces classes incluent les éléments fins du sur-sol tels que les murets, murs, trottoirs, etc. Les données obtenues sont précises en moyenne à 30 cm en planimétrie et à 25 cm en altimétrie. Néanmoins, sur la zone urbaine dense, l'ordre de grandeur de précision est plutôt de 15-20 cm en planimétrie et de 15 cm en altimétrie. En effet, lors du processus d'acquisition, ce secteur a fait l'objet d'un plan de vol de faible altitude, qui a fourni de nombreux clichés avec d'importants taux de recouvrement (supérieurs à 80 % en zone urbaine dense). Dans la mesure où le calage pour le géoréférencement des données de la campagne est très fiable (effectué sur environ 200 points balisés), l'incertitude sur la valeur absolue des données apparaît également de l'ordre de 15-20 cm en altimétrie et en planimétrie. La donnée est garantie à 95 % par le fournisseur. La direction de l'information géographique de NCA a effectué des contrôles *via* des levés topographiques terrestres sur 10 % du territoire couvert par la campagne de photogrammétrie afin de confirmer ce taux de garantie.

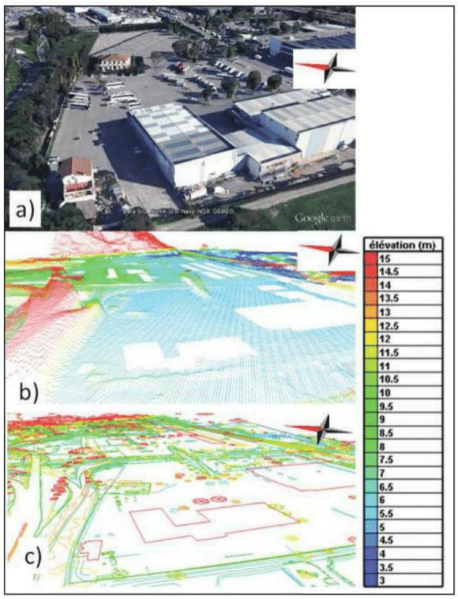

Figure 1. Vue d'une partie de la plateforme du marché d'intérêt national (MIN) de NCA : la zone du MIN avec Google Earth (a), et illustration de la donnée LiDAR (b) et de la donnée photogrammétriques 3D classifiée (c) sur cette zone

2. Cas pratique d'utilisation des données haute résolution pour des problématiques de ruissellement en milieu urbain

L'intérêt est ici uniquement porté sur les méthodes d'intégration de données topographiques HR dans des modèles numériques de ruissellement. Ainsi, les aspects liés au paramétrage des modèles (conditions aux limites, pertes de charges, pas de temps de calcul, nombre de Courant, etc.) ne sont pas détaillés dans cet article.

2.1. Présentation des outils de modélisation numérique

Les codes de calculs hydrauliques employés pour tester les possibilités d'utilisation de la donnée topographique HR pour créer des modèles de ruissellement de surface sont développés par le Danish Hydraulic Institute (DHI). Ces codes de calculs sont basés sur la résolution du système d'équations de Saint-Venant en deux dimensions [DHI, 2007a ; DHI, 2007b]. En dehors de l'aspect validité de l'approche liée à l'éloignement du domaine d'application par rapport à celui pour lequel l'outil a été créé (présence de forts gradients topographiques et validité de la prise en compte des pertes de charges), l'emploi de tels codes de calculs pour la modélisation de hauteurs d'eau faibles telles que celles que l'on peut rencontrer lors de phénomènes de ruissellements de surface est faisable. Néanmoins, les aspects liés à la présence

d'oscillations numériques et au traitement des découvrements/recouvrements (ici, fonctionnant avec un processus de valeurs seuils) doivent être contrôlés par l'utilisateur, mais ne sont pas bloquants pour une utilisation visant à simuler des scénarios de ruissellement [Abily et al., 2013].

• **MIKE 21** est basé sur la résolution du système d'équations de Barré-Saint-Venant en deux dimensions [DHI, 2007a]. Le code de calcul de MIKE 21 résout ce système d'équations en différences finies sur un maillage de calcul structuré cartésien. La méthode numérique utilisée est de type *alternate direction implicite* (ADI). Les méthodes ADI ne sont normalement pas capables de gérer les changements de régimes d'écoulements qui seront présents lors de phénomènes de ruissellements intenses. Cependant, la méthode implémentée dans MIKE 21 a subi des modifications (décentrement amont du terme convectif des équations de quantité de mouvement ajoutant localement une diffusion numérique) qui lui permettent de gérer ces changements de régimes d'écoulement en améliorant la stabilité du schéma au détriment, localement, de sa précision [McCOWAN *et al.*, 2001].

• **MIKE FLOOD** est un outil de simulation des processus hydrodynamiques basé sur le couplage dynamique de MIKE 21 FM pour la construction de la bathymétrie et de MIKE URBAN pour la modélisation 1D des réseaux souterrains.

• **M21FM** est également basé sur la résolution du système d'équations de Barré-Saint-Venant en deux dimensions [DHI, 2007b]. Le code de calcul résout ces équations en se basant sur un schéma numérique en volumes finis. Le maillage utilisé dans ce code est de type non structuré (flexible). Théoriquement, les méthodes de résolution numérique implantées dans MIKE 21 FM (Roe et TVD) permettent un traitement stable des changements de régimes d'écoulement.

• **MIKE URBAN** permet la modélisation des écoulements de réseaux enterrés ou à ciel ouvert à partir d'une résolution complète des équations de Barré-Saint-Venant en une dimension (modèle hydraulique) et de la modélisation des apports (modèle hydrologique) par de nombreuses méthodes de calcul (Caquot, réservoir linéaire, double réservoir linéaire, Horton, ...).

2.2. Utilisation des données LiDAR à l'échelle d'une ville

La métropole Nice Côte d'Azur a mandaté la société Safege pour réaliser une étude du risque pluvial urbain à travers une modélisation 2D permettant d'actualiser les cartes des aléas du risque de débordements sur la commune de Nice. En effet, la métropole souhaite disposer d'éléments caractéristiques du risque d'inondation sur la commune de Nice, pour pouvoir fournir les préconisations nécessaires en matière d'urbanisme afin de réduire la vulnérabilité des futurs aménagements.

<table>
<tr><th></th><th></th><th colspan="3">Processus de génération de MNS haute résolution</th><th>Intégration des MNS dans le code de calcul hydraulique</th></tr>
<tr><th>Approches</th><th>Donnée haute résolution utilisée</th><th>Étape 1</th><th>Étape 2</th><th>Étape 3</th><th>Étape 4</th></tr>
<tr><td>Approche 1 (A1)</td><td>Donnée LiDAR</td><td>Réduire la densité de points de la donnée LiDAR</td><td>Extrusion des volumes bâtis de la surface</td><td>Évictions des macrostructures bloquant les écoulements de surface</td><td rowspan="2">Utilisation de la grille en tant que maillage non structuré</td></tr>
<tr><td>Approche 2 (A1+)</td><td>Donnée LiDAR</td><td colspan="2">Analyse de la photographie aérienne, plans topographiques
Identification des éléments fins de sur-sol pouvant influencer les écoulements</td><td>Corrections manuelles du MNS aux endroits stratégiques</td></tr>
</table>

Tableau I. Processus utilisés pour la génération de modèles numériques de surface (MNS) spécifiques pour la modélisation de scénarios de ruissellement de surface à l'échelle d'une ville

2.2.1. Construction du modèle : mise en place d'une méthodologie spécifique

Le modèle a été créé avec Mike Flood. La méthodologie générale de construction d'une bathymétrie à des fins de modélisation hydraulique est largement répandue, mais l'originalité de cette méthode réside dans le fait qu'elle s'applique à l'échelle de la ville de Nice, soit 23,4 km².

Les approches testées pour générer des MNS (A1, A1+) adaptés pour la modélisation numérique du ruissellement à l'échelle d'une ville sont synthétisées dans le *tableau 1* et expliquées ci-avant.

La première étape de la méthodologie de construction est le nettoyage du fichier de points LiDAR. Compte tenu du nombre de points X, Y, Z fournis par la donnée LiDAR sur la zone d'étude (5,5 millions de points) et des capacités de traitement de la donnée des logiciels, des tests de sensibilité ont été réalisés en réduisant plus ou moins le nombre de points topographiques sur la zone modélisée. Les résultats de l'analyse de sensibilité étant concluants, la densité de la donnée LiDAR a été réduite par 4 (*figure 2*).

La seconde étape du processus d'élaboration du MNS nécessite l'extrusion des volumes bâtis de la surface et le regroupement des immeubles en pâtés de maisons. Cette étape apportera une stabilité au modèle, notamment lors de l'étape de génération du maillage (étape 3). En effet, les éléments structurant localement le maillage (les cours intérieures ou les entrées exiguës) surcontraignent l'algorithme de maillage (triangulation de type Delaunay) lorsque ceux-ci sont très rapprochés. Un maillage non structuré de mauvaise qualité rendrait le modèle instable. De fait, l'exclusion du domaine de calcul des cours intérieures, des entrées ou des ruelles exiguës crée un écart par rapport à la topographie réelle qui pourra influencer localement les résultats. Néanmoins, les faibles volumes et flux d'eau considérés dans ces zones apparaissent négligeables par rapport au volume total considéré dans l'étude. Compte tenu des objectifs de l'étude (définition des zones inondables de la ville de Nice), la précision potentiellement réduite en supprimant certains recoins ne dégrade que faiblement la qualité des résultats.

L'étape suivante (étape 3) consiste en un traitement manuel des données topographiques présentant des incohérences (A1). Certaines cotes altimétriques présentent des valeurs anormalement hautes et/ou basses. Il s'agit de ponts, auto-ponts ou tunnels pris en compte dans les levés LiDAR. Les points comportant des anomalies sont donc supprimés du fichier et les blancs sont remplacés par des données interpolées (interpolation linéaire).

En vue de modéliser un phénomène de ruissellement, un second traitement de la donnée a été indispensable pour écarter d'éventuelles erreurs et incohérences liées à des blocages des écoulements induits par des éléments fins du sur-sol non visibles dans la donnée LiDAR (A1+). Pour ce faire, un travail manuel de correction de cotes, d'ajout d'éléments fins de

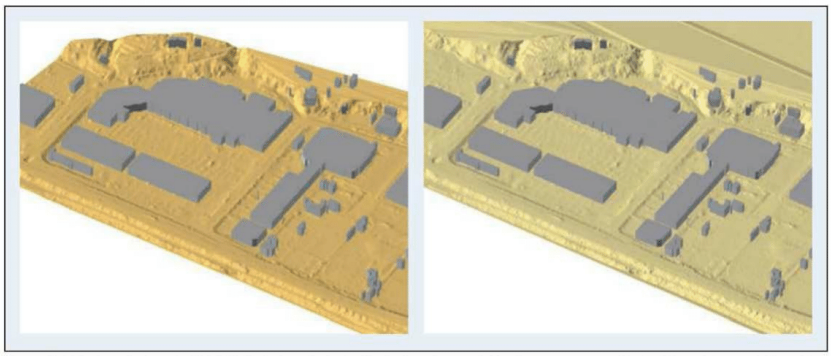

Figure 2. Extrait de la donnée LiDAR initiale (gauche) et allégée d'un facteur 4 (droite) sur une emprise de 0,5 km² (zone de Carrefour Lingostière, rive gauche du Var)

sur-sol a été réalisé à des endroits stratégiques en s'appuyant sur les informations fournies par la photographie aérienne ainsi que par des visites de terrains ou des levés topographiques.

La quatrième étape consiste en la définition du maillage. Le choix du maillage s'est porté sur la base d'un maillage non structuré (éléments triangulaires). Ce type de maillage est plus sensible aux instabilités mais permet de construire un maillage différencié dans un même domaine de calcul (*figure 3*). Un maillage fin est appliqué dans les zones à enjeux et les rues étroites (5 m² maximum). Les zones de moindre intérêt, les boulevards et les zones planes de grandes ampleurs sont constitués d'un maillage plus large (50 m² maximum). Afin de définir le maillage adapté à chaque espace, des tests de sensibilité ont été réalisés sous forme de trois sous-modèles. À chaque sous-modèle ont été appliquées plusieurs tailles de mailles : de 5 à 100 m² maximum. Ces modèles représentent les scénarios principaux de morphologies urbaines identifiés à Nice.

2.2.2. Résultats obtenus

La mise en application de la méthodologie détaillée ci-avant sur l'ensemble de la ville de Nice a permis d'obtenir des cartographies des hauteurs d'eau maximales calculées (h_{max}) telles que celles présentées en *figure 4* pour le secteur du centre-ville de Nice.

La fiabilité des résultats du modèle 2D a été validée par la comparaison des h_{max} calculées avec le témoignage des habitants de Nice pour la pluie du 24 septembre 2012 où d'importantes inondations ont pu

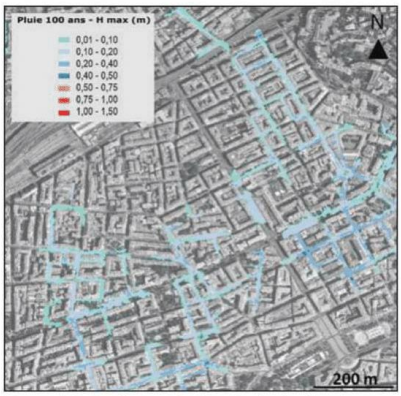

Figure 4. Hauteurs d'eau maximales calculées (h_{max}) sur le centre-ville de Nice – Pluie période de retour centennale (30 min – 4 h)

être observées. Les conclusions de l'étude, par comparaison à des faits avérés, montrent ainsi deux cas de figure bien distincts :

– les secteurs fréquemment inondés à cause de défaillances des réseaux (sous-dimensionnement) pour lesquels les simulations corroborent les observations effectuées. Sur ces secteurs, les inondations observées et les résultats du modèle sont similaires sur les mêmes emprises ;

– les secteurs inondés pour cause de défaut de drainage de surface (insuffisance du nombre de grilles avaloirs, défaut d'entretien de ces dernières…), secteurs pour lesquels les simulations ne corroborent pas les observations effectuées. Sur ces secteurs, des

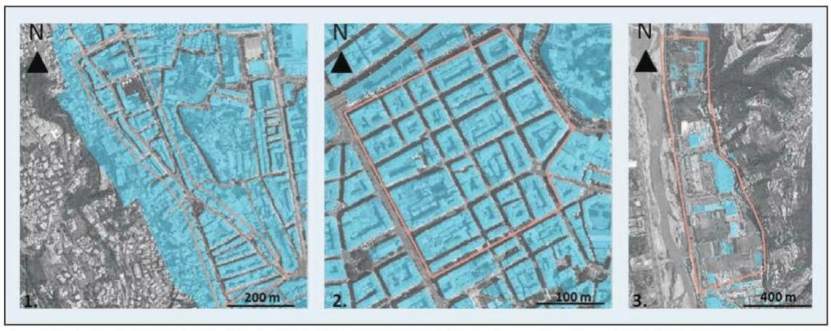

Figure 3. Extrait des sous-modèles : (1) grands boulevards, pente moyenne de 3 %, zone urbaine dense ; (2) rues du centre-ville, pente moyenne de 1 %, zone urbaine dense ; (3) grande étendue, topographie plane, zone urbaine peu dense

Types de voiries	Topographie	Densité urbaine	Taille maximum de la maille
Centre historique, ruelles, zones à forts enjeux (projets d'aménagement urbain)	Pente ≤ 3 %	Urbain dense	5 m² maximum
Centre-ville, géométrie des rues et des croisements régulière	Pente ≤ 1 %	Urbain dense	25 m² maximum
Centre-ville, grandes avenues parallèles	Pente ≥ 3 %	Urbain dense	40 m² maximum
Vaste plaine inondable	Pente ≤ 1 %	Urbain peu dense	50 m² maximum

Tableau II. Synthèse des conclusions de l'étude sur la génération d'un maillage non structuré efficace utilisant en entrée un modèle numérique de surface (MNS) HR acquis par technologie LiDAR

inondations sont observées sur le terrain alors que le modèle montre un réseau avec un reliquat débit pouvant être accepté (réseau non naturé), et donc pas de débordement sur la voirie.

À noter que seuls les ruissellements de surface générés par des débordements de réseaux sont simulés, et en aucun cas les écoulements en nappe liés au ruissellement urbain des zones minéralisées de surface.

La dégradation appliquée à la donnée topographique brute est fonction de la spécificité morphologique de la voirie (*tableau I*). Chaque cas est assez différent et demande une analyse spécifique pour obtenir un rendu pertinent. Les résultats présentés ci-après sont issus de nos cas tests de sensibilité. Il s'agit d'une tendance observée dans les modèles et non pas de valeurs prédéfinies. Ces valeurs permettent d'aboutir à une modélisation fine du phénomène de ruissellement en respectant un temps de calcul raisonnable, compte tenu de l'emprise modélisée dans le cas de Nice.

2.3. Utilisation de la donnée photogrammétrique 3D classifiée à l'échelle d'un site industriel

Afin de vérifier la faisabilité et l'intérêt d'intégrer l'information des éléments fins du sur-sol lors de la réalisation de simulations de scénarios de ruissellement de surface à l'échelle d'un site industriel, différents MNS ont été créés à partir des données topographiques HR. Les scénarios utilisés pour les tests ont été élaborés en se basant sur la situation de référence pour le risque inondation (SRI) « pluie locale » du guide inondation de l'ASN [ASN, 2013]. Cette SRI considère notamment les réseaux enterrés d'évacuation des eaux pluviales comme hors-service. L'approche pénalisante de non-prise en compte du réseau enterré dans la SRI est justifiée par la possibilité d'occurrence d'événements plus intenses que ceux définis et par la prise en compte du risque d'obstruction du réseau en cas d'événements extrêmes. Le code de calcul utilisé ici est MIKE 21.

2.3.1. Méthodologie de construction et d'intégration de MNS dédiés

Le secteur du marché d'intérêt national (MIN) de Nice (*figure 5*) a été choisi pour simuler des scénarios de ruissellements liés à une pluie d'intensité 100 mm/h pendant 1 heure. L'intensité de l'événement pluvieux considéré pour ce cas test correspond à une pluie horaire dont l'intensité correspond à la borne supé-

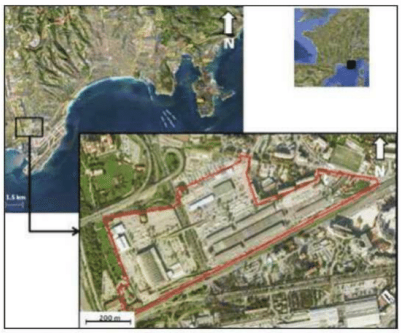

Figure 5. Localisation de la plateforme du marché d'intérêt national (MIN) de Nice

rieure de l'intervalle de confiance à 70 % de la pluie centennale (calcul Météo France sur le pluviographe de l'aéroport de Nice). L'intérêt de ce site de taille modeste (600000 m²), configuré en plateformes, repose sur la présence d'éléments du sur-sol nombreux et de natures diverses (murs, murets, caniveaux, ronds- points, etc.). Le site a été couvert par les deux campagnes d'acquisition de données topographiques (LiDAR et photogrammétriques). Entre les deux campagnes (2005 et 2011), le secteur du MIN a peu évolué. Par rapport à la donnée LiDAR, la donnée 3D classifiée issue de la photogrammétrie permet la représentation des éléments fins du sur-sol (murs, murets, éléments de voierie, etc.).

Plusieurs types d'approches basées sur l'emploi de données photogrammétrie 3D classifiées sont possibles pour générer un MNS. Les approches testées pour générer des MNS (A1, A2 et A3) adaptées pour la modélisation numérique du ruissellement sont synthétisées dans le *tableau III* et expliquées ci-après.

Les MNS ont été intégrés en tant que grilles de calculs (maillage structuré) dans MIKE 21.

Pour A1, un MNS basé sur l'emploi de la donnée LiDAR a été généré. Ce MNS intègre les éléments du sur-sol dont l'emprise a une largeur compatible avec la résolution de la technique d'acquisition LiDAR (Δx et Δy de 2 m) tels que les bâtiments, la chaussée, etc. Les macrostructures (telles que les routes élevées, ponts, etc.) pouvant bloquer les écoulements ont été enlevées manuellement du MNS.

A2, utilise la donnée photogrammétrique 3D classifiée. Au sein de cette donnée, le nombre de classe est élevé (50). Seule l'inclusion dans le MNS des classes représentant les éléments du sur-sol qui influencent les chemins d'écoulement en surface (tels que les trottoirs, caniveaux, murs, murets...) présente ici un intérêt. Certaines classes représentent des structures dont l'intégration n'est pas nécessaire pour générer un MNS pertinent pour le type d'application visé (ponts et routes élevées, végétation, éléments de

		Processus de génération de MNS haute résolution			**Intégration des MNS dans le code de calcul hydraulique**
Approches	**Donnée haute résolution utilisée**	**Étape 1**	**Étape 2**	**Étape 3**	**Étape 4**
Approche 1 (A1)	**Donnée LiDAR**	Évictions des macrostructures bloquant les écoulements de surface			Utilisation de la grille en tant que maillage structuré (résolution 2 m)
Approche 2 (A2)	**Donnée photogrammétrique 3D classifiée**	Sélection des classes d'entités pertinentes	Interpolation basée sur les classes d'entités sélectionnées	Conversion en grille	Ré-échantillonage des grilles générées en grilles de résolution équivalente au pas de discrétisation souhaitant être utilisé dans le maillage structuré (0,3 m ou 1 m)
Approche 3 (A3)	**Donnée LiDAR et donnée photogrammétrique 3D classifiée combinées**	(a) Conversion des systèmes de coordonnées si nécessaire (b) Sélection des classes d'entités pertinentes	(a) Conversion des classes d'entités sélectionnées en grille à la résolution désirée (b) Conversion des données LiDAR en grille de résolution identique	Extrusion des grilles de données classées sur la grille de données LiDAR	

Tableau III. Processus utilisés pour la génération de modèles numériques de surface (MNS) spécifiques pour la modélisation de scénarios de ruissellement de surface

toiture, etc.). Ainsi, l'un des aspects déterminants dans le processus de génération d'un MNS approprié pour une utilisation en modélisation hydraulique est la sélection de classes d'éléments du sur-sol ayant un impact potentiel sur les écoulements. Au total, 12 classes d'éléments ont été utilisées pour générer le MNS.

L'approche A3 consiste à combiner les deux jeux de données topographiques HR (donnée LiDAR et donnée photogrammétrique classifiée) afin de densifier les données du sol. En effet, la donnée photogrammétrique intègre avec haute précision les éléments fins du sur-sol, mais la densité de points représentant le terrain (un point tous les 5 m) est inférieure à celle de la donnée LiDAR (un point tous les 2 m).

2.3.2. Résultats obtenus

La comparaison des résultats sur les hauteurs d'eau maximales (h_{max}) et sur les directions d'écoulements calculées par les modèles reposant sur les différents MNS permet de quantifier et de qualifier l'impact de la prise en compte des éléments fins du sur-sol.

Les h_{max} calculées avec les MNS où les éléments fins du sur-sol sont représentés (A2 et A3) présentent des différences importantes par rapport aux h_{max} calculées à partir du modèle utilisant le MNS tiré de la donnée LiDAR seule (A1). Ces écarts dans les h_{max} estimées peuvent atteindre 0,5 m comme l'illustre la *figure 6* (droite) où la grille de résultats sur les h_{max} calculée avec A2 est soustraite à la grille de résultats calculée avec A1. Par ailleurs, les directions d'écoulement sont significativement modifiées (*figure 7*). Les h_{max} calculées avec les modèles utilisant le MNS A2 (basé sur la donnée photogrammétrique) et le MNS A3 (basé sur les données photogrammétriques

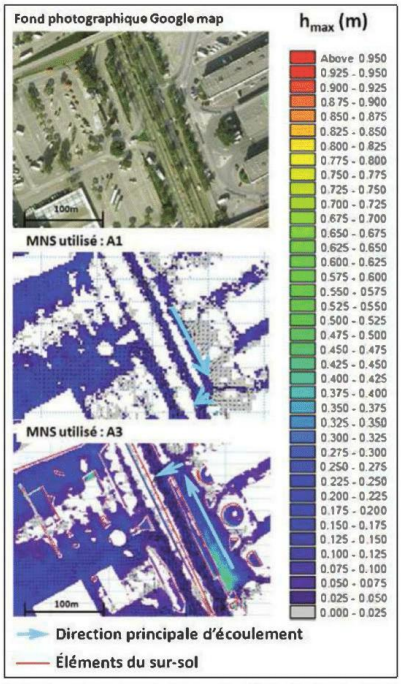

Figure 7. Focus sur un secteur du marché d'intérêt national (MIN) où l'inclusion des éléments fins du sur-sol entraîne des différences sur les hauteurs d'eau et dans les directions d'écoulements calculées

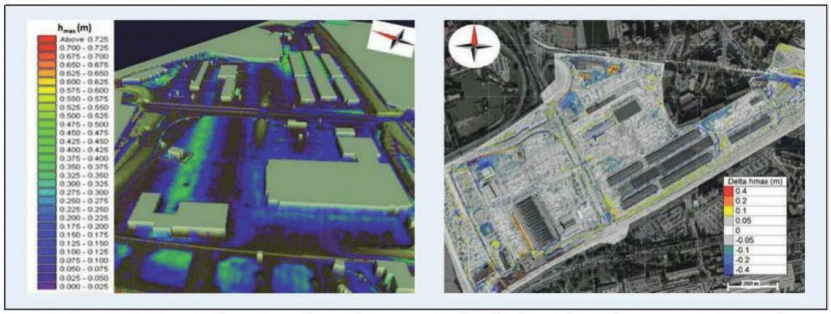

Figure 6. Illustration des h_{max} calculées sur le modèle numérique de surface (MNS) A2 (gauche) et différences entre les h_{max} estimées avec le MNS basé sur la donnée LiDAR seule (A1) et avec le MNS basé sur le couplage des deux jeux de données topographiques (A2) (droite)

et LiDAR combinées) sont similaires. La densification des points au sol n'apporte pas de plus-value dans notre cas.

Par ailleurs, à l'issue des tests avec les MNS de résolutions différentes, il apparaît que l'intégration de singularités telles que les éléments fins du sur-sol, même à résolution dégradée (1 m au lieu de 0,3 m), offrent des résultats très proches.

La plus value de l'intégration des éléments fins du sur-sol dans les MNS utilisés avec les modèles hydrauliques hautes définitions pour estimer les risques liés au ruissellement apparaît très clairement.

3. Retour d'expérience et conclusions sur l'utilisation des données haute résolution

La mise en œuvre d'approches consistant à intégrer des données topographiques HR dans des codes de calculs d'hydraulique 2D a été présentée sur des applications modélisant des scénarios de ruissellement. La faisabilité de ce type d'approche a été soulignée dans la section précédente ainsi que dans des travaux menés à échelle plus restreinte [ABILY *et al.*, 2013]. Les travaux menés montrent en premier lieu que, sur des milieux urbains denses, l'emploi de données haute résolution est un prérequis indispensable afin d'obtenir des résultats exploitables pour une meilleure appréhension du risque lié au ruissellement. En effet, l'emploi de données topographiques de résolution trop grossières ne peut permettre de décrire convenablement la topographie complexe de ce type d'environnement et, par conséquent, les d'écoulements qui s'y produisent.

Bien que les modèles hydraulique 2D créés produisent des résultats précis et à haute résolution, il convient de rappeler que, d'une manière générale, un modèle numérique reste une représentation de la réalité basée sur un modèle mathématique assorti d'un jeu d'hypothèses simplificatrices dans la description du phénomène d'écoulement. Le comportement des écoulements est calculé en négligeant certains aspects complexes ou en les appréhendant de façons simplifiées. Par ailleurs, les données d'entrées des modèles (hydrauliques et topographiques) comportent des incertitudes (liées aux erreurs de mesures et aux choix de modélisateurs), qui sont de fait introduites dans le modèle.

Cet article s'intéressant à l'emploi de données topographiques HR, les limites liées i) aux spécificités des jeux de données topographiques HR et ii) aux méthodes d'intégration de cette donnée dans les codes de calculs sont soulignées dans cette section. Les retours d'expériences sur ces deux points sont présentés ci-après.

3.1. Donnée et prétraitement

Dans le cas de la donnée LiDAR, les sources d'erreurs principales viennent du fait de la non-prise en compte d'éléments fins du sur-sol et de l'inclusion dans le MNS des éléments tels que les ponts et voies surélevées. Comme susmentionné, ces obstacles aux écoulements doivent être repérés et traités par le modélisateur. Le repérage et le traitement de ces éléments sont fastidieux à l'échelle d'une ville et nécessitent un temps ingénieur important.

Dans le cas de la donnée photogrammétrique, le fait que les éléments du sur-sol soient classifiés permet de sélectionner aisément les éléments jugés pertinents à inclure dans le MNS. Ainsi, il est possible de ne pas intégrer les éléments tels que les tabliers de ponts ou les voies surélevées dans le MNS. Dans le cas présenté (MIN de Nice) le pourcentage d'erreur dans la classification est évalué à 5 %. Compte tenu du nombre important d'éléments classifiés utilisés pour générer les MNS (plus de 2 000 sur le site du MIN), cette erreur (ajout, omission ou mauvaise classification) peut avoir un impact fort sur les écoulements modélisés et donc sur l'évaluation de h_{max}. Une vérification de la donnée est obligatoire afin de s'affranchir de ce type d'erreur lors de l'utilisation de données photogrammétriques 3D classifiées. Ce type de vérification est réalisable à l'échelle d'un site industriel ou à l'échelle de quelques kilomètres carrés [ABILY et *al.*, 2014a], mais sera en pratique difficile à mettre en œuvre à plus grande échelle.

3.2. Maillage et intégration de la donnée haute résolution

À l'échelle d'une ville, la quantité d'information topographique obtenue par des campagnes, LiDAR et photogrammétrique, est à l'heure actuelle prohibitive pour être utilisée directement avec les ressources informatiques et outils de modélisation standard en

ingénierie. Néanmoins, des tests de sensibilité conduits sur des secteurs à des échelles plus restreintes peuvent permettre de diminuer la densité d'information sans influencer de manière significative la qualité du MNS. Pour la donnée LiDAR cela s'est traduit par la dégradation de la densité de l'information. Pour la donnée photogrammétrique, les éléments fins du sur-sol (d'emprise inframétrique) sont inclus avec une taille légèrement amplifiée (à la taille unitaire du MNS) dans le maillage structuré, permettant de conserver les impacts de ces structures sur les chemins d'écoulement.

Afin d'intégrer le MNS haute résolution dans les codes de calculs d'hydraulique, il est nécessaire de s'assurer de la bonne adéquation du pas de discrétisation spatiale du calcul (maillage) avec le MNS HR utilisé. Un maillage non structuré performant est particulièrement délicat à créer lorsque le milieu est complexe et que la densité d'information est importante. À l'échelle d'une ville, la construction d'un maillage non structuré (discrétisation du maillage suivant les enjeux) permettant de trouver ainsi un compromis entre fiabilité de mesures, représentativité du phénomène et capacité de calcul, a été choisie volontairement. Néanmoins, générer un maillage non structuré en se basant sur la donnée topographique HR a nécessité un travail manuel de l'opérateur afin de vérifier la faisabilité d'utilisation de l'algorithme de maillage, ce qui nécessite un temps ingénieur considérable.

Enfin, l'emploi d'un maillage structuré en zone urbaine possède l'avantage de pouvoir permettre de créer directement un maillage à la résolution du MNS. Cette approche très directe permet un gain de temps ingénieur important. En revanche, il est évident que dans le cas d'un maillage structuré, l'optimisation du temps de calcul ne sera là encore pas maximale, car la taille de la grille de calcul (nombre de points de calculs) est ici maximale.

3.3. Perspectives d'amélioration

Si la donnée photogrammétrique 3D classifiée offre un fort potentiel pour créer des MNS HR optimisés pour des applications en modélisation hydraulique, la classification des éléments ne suit pas forcément des critères dédiés pour ce type d'application. En particulier, une classification discriminant la perméabilité des éléments classifiés du sur-sol (par exemple en distinguant entre structures type murs béton ou clôture grillagée) n'est pas usuellement prise en compte. De plus, le processus de traitement dans la classification de la donnée fait appel à des choix d'utilisateur qui peuvent avoir un impact important. À titre d'exemple, certaines lignes 3D sont fermées automatiquement lorsque l'écartement est inférieur à une valeur seuil. Cela peut conduire à une fermeture artificielle de voies de ruissellement. Dans l'optique d'une amélioration des MNS HR utilisés en modélisation hydraulique urbaine, ces aspects de classification et de processus de traitement lors de la classification de la donnée seraient, dans la mesure du possible, à prendre en compte dès la phase de photo-interprétation de la donnée photogrammétrique.

Lorsqu'une modélisation 2D d'hydraulique à surface libre est réalisée, les choix du modélisateur liés à l'intégration de la donnée topographique dans le code de calcul ont un impact significatif sur la qualité du modèle. Des travaux préliminaires d'analyse globale de sensibilités ont été effectués sur ces choix des modélisateurs [ABILY *et al.*, 2014b]. Il ressort de ce type d'étude que les choix du modélisateur pour la génération du MNS et pour la création du maillage sont responsables de l'introduction d'une incertitude dans la grandeur d'intérêt en sortie du model (ex. h_{max}) plus importante que l'incertitude introduite par l'erreur moyenne de la donnée topographique HR.

Remerciements

Le laboratoire I-City, la société Safege et l'Institut de radioprotection et de sûreté nucléaire remercient la métropole Nice Côte d'Azur pour les données qui ont été transmises à des fins de recherche. Les calculs I-CiTy Ces ont bénéficié d'un accès aux moyens de calcul et de visualisation du Centre de calcul interactif hébergé à l'université Nice Sophia Antipolis. Par ailleurs, les auteurs remercient particulièrement messieurs L. Andres, G. Tacet et F. Largeron de la direction d'information géographique de la métropole Nice Côte d'Azur pour leur soutien d'expertise sur le volet géomatique.

Bibliographie

ABDALLAH M. (2005) : *Sur les méthodes de discrétisation numérique de problèmes hyperboliques non linéaires appliquées aux équations de Barré de Saint-Venant pour la modélisation de l'hydraulique en réseau d'assainissement*. Thèse de doctorat, Strasbourg, 196 p.

ABILY M., DELESTRE O., AMOSSE L., BERTRAND N., LAGUERRE C., DULUC C.-M., GOURBESVILLE P. (2014a) : « Use of 3D classified topographic data with FullSWOF for High Resolution simulations of river flood event over a dense urban area », in : *Book of Proceedings*, 3rd IAHR Europe Congress, 2014, Porto, Portugal.

ABILY M., BERTRAND N., DELESTRE O., RICHET Y., DULUC C.-M., GOURBESVILLE P. (2014b) : « Global sensitivity analysis with 2D hydraulic codes: application on uncertainties related to high resolution topographic data use », in : SimHydro 2014: Modelling of rapid transitory flows, 11-13 June 2014, Sophia Antipolis, France.

ABILY M., DULUC C.M., FAES J.B., GOURBESVILLE P. (2013) : « Performance assessment of modeling tools for high resolution runoff simulation over an industrial site ». *Journal of Hydroinformatics ;* IWA publishing doi : 10.2166/hydro.2013.063 : p. 16.

AKTARUZZAMAN M., SCHMIDT T. (2009) : *Detaileddigital surface model (DSM) Generation and automatic object dection to facilitate modelling of urban flooding*. ISPRS Workshop, Hannover: p. 7.

ANDRES L. (2012) : « L'apport de la donnée topographique pour la modélisation 3D fine et classifiée d'un territoire ». *XYZ ;* 133 : 7.

ASN (2013) : *Protection des installations nucléaires de base contre les inondations externes*. Guide de l'ASN n° 13 : p. 44.

DHI (2007a) : *Mike 21 Flow Model, Hydrodynamic module: Scientific documentation*. Danish Hydraulics Institute: p. 58.

DHI (2007b) : Mike 21 & Mike 3 Flow Model FM, *Hydrodynamic and transport module: Scientific documentation*. Danish Hydraulics Institute: p. 50.

EGELS Y., KASSER M. (2004) : *Digital Photogrammetry*. Londres, Taylor & Francis.

GERVAIX F. (2010) : Éléments de photogrammétrie - *Cours de photo-interprétation* H.-V.E.c., Géoinformation, Ed. 2010, École polytechnique fédérale de Lausanne. Lausanne : p. 141.

GOMEZ M., MACCHIONE F., RUSSO B. (2011) : « Methodologies to study the surface hydraulic behaviour of urban catchments during storm events ». *Water Sciences and Technologies ;* 63(11) : 9.

GOURBESVILLE P. (2009) : « Data and hydroinformatics: new possibilities and challenges ». *Journal of Hydroinformatics ;* 11(3-4) : 12.

LINDER W. (2006) : *Digital photogrammetry: A practical course*. Springer Verlag.

MARK O., WEESAKUL S., APIRUMANEKUL C., BOONYAAROONNET S., DJORDJEVIC S. (2004) : « Potential and limitations of 1D modelling of urban flooding ». *Journal of Hydrology ;* 299 : 16.

McCOWAN A.D., RASMUSSEN E.B., BERG P. (2001) : « Improving performance of a two dimensional hydraulic model for floodplain application ». In: Conference on Hydraulics in Civil Engineering, Hobart, Tasmania, p. 11.

MUSIALSKI P., WONKA P., ALIAGA D.G., WIMMER M., VAN GOOL L., PURGATHOFER W. (2013) : « A survey of urban reconstruction ». *Computer Graphics Forum ;* 32(6) : 146-177.

REMONDINO F., BARAZZETTI L., NEX F., SCAIONI M., SARAZZI D. (2011) : « UVA photogrammetry for mapping and 3D modelling – Current status and future prespectives ». In : Conference on unmanned aerial vehicle in geomatics. International Archives of the Photogrammetry, Remote sensing and spatial information sciences: Zurich, Switzerland: p. 7.

SCHUBERT J.E., SANDERS B.F., SMIDTH M.J., WRIGHT N.G. (2008) : « Unstructured mesh generation and land cover-based resistance for hydrodynamic modelling of urban flooding ». *Advances in Water Resources ;* 31 : 1603-1621.

TSUBAKI R., FUJITA I. (2010) : « Unstructured grid generation using LiDAR data for urban flood innundation modelling ». *Hydrological Processes ;* 24: 17.

VALLET J. (2010) : « Relevé routier à très haute résolution par systeme LiDAR-Photogrammétrique héliporté ». Géomatique Suisse ; 9 : 4.

Résumé

M. ABILY, C. SCARCERIAUX, C.-M. DULUC

Ruissellement de surface en milieu urbain : stratégies d'intégration de données topographiques haute résolution en modélisation hydraulique 2D

Cet article présente deux études simulant numériquement des scénarios de ruissellement intense sur des zones urbanisées ou industrielles, en utilisant des jeux de données topographiques haute résolution (HR). Ces travaux de modélisation reposent sur des codes de calculs d'hydraulique à surface libre standard, basés sur la résolution bidimensionnelle du système d'équations de Saint-Venant. Les modèles ont été créés avec deux jeux de données topographiques HR différents : LiDAR et photo-interprétée ; à des échelles différentes et avec des stratégies de discrétisation spatiales différentes. L'article soulève les problématiques liées à l'intégration de ces « big data » dans les outils de calculs traditionnellement utilisés en ingénierie d'étude et présente des stratégies d'intégration optimisées de ces données dans les modèles hydrauliques. La faisabilité de la mise en œuvre de telles approches est confirmée. Par ailleurs, la plus- value de l'intégration de ces données topographiques HR est rappelée et les limites de sa faisabilité sont mises en avant. Un retour d'expérience issu de ces deux études permet de faire ressortir une série de remarques généralisables. Ainsi, les phases de prétraitement de la donnée topographique HR ne présentent pas les mêmes avantages et inconvénients selon que l'on travaille avec une donnée LiDAR ou photo-interprétée. Après analyse de sensibilité, la donnée LiDAR peut être dégradée pour une utilisation facilitée. La donnée photo-interprétée, quant à elle, permet d'intégrer les éléments fins du sur-sol (trottoirs, caniveaux, etc.). La problématique de prétraitement manuel non automatisable de la donnée LiDAR pour enlever les éléments bloquants les écoulements (ponts et voies surélevés, etc.) est rappelée. Sur une emprise d'étude restreinte à quelques km², l'emploi d'un maillage de type structuré, même s'il nécessite un temps de calcul plus important, apparaît pertinent pour modéliser les écoulements en tenant compte de données HR et permet un gain de temps ingénieur significatif lors de la génération du maillage.

Abstract

M. ABILY, C. SCARCERIAUX, C.-M. DULUC

Runoff hazard assessment in urban environment : strategies for high resolution topographic data use in 2D hydraulic modelling

This paper presents two studies modelling extreme runoff flood events over densely urbanized areas using High Resolution (HR) topographic data set with commercial codes. These standard codes solve 2D Shallow Water Equations (2D SWEs). Models of the presented studies are created using two different HR topographic dataset : LiDAR and Photo-interpreted data, at two different scales, with different spatial discretization strategies. This paper enhances the advantages and problems which arise from these "big data" integration within standard modelling tools. Strategies elaborated for HR topographic data optimal use with such type of codes are explained and put to the test. Feasibility of HR data use for flood hazard assessment is confirmed and feedback regarding added value and limits of this practice are given. It is put to the light here, that pretreatment step shows dissimilar advantages and limitations depending on the use of LiDAR or photo-interpreted dataset. After sensitivity analysis, LiDAR data can be resampled for a better ease of use. A reminder is given regarding non-automatisation problem of elevated flow blocking structures (bridges, elevated motorways...) with LiDAR data. Photo-interpreted data set allows to integrate tin above ground elements (road gutter, sidewalks, walls...) in the hydraulic model. Over few square kilometers areas, structured grid use seems to be more relevant, allowing to save engineer time for mesh generation even though computational time might not be optimal with this type of meshing approach.

Annex B: *Abily, M., Delestre, O., Amossé, L., Bertrand, N., Richet, Y., Duluc, C.-M., P. Gourbesville & Navaro, P. (2015). Uncertainty related to high resolution topographic data use for flood event modeling over urban areas: toward a sensitivity analysis approach. ESAIM: PROCEEDINGS AND SURVEYS, 48, 385-399.*

ESAIM: PROCEEDINGS AND SURVEYS, January 2015, Vol. 48, p. 385-399
N. Champagnat, T. Lelièvre, A. Nouy, Editors

UNCERTAINTY RELATED TO HIGH RESOLUTION TOPOGRAPHIC DATA USE FOR FLOOD EVENT MODELING OVER URBAN AREAS: TOWARD A SENSITIVITY ANALYSIS APPROACH

Morgan Abily[1], Olivier Delestre[2], Laura Amossé[3], Nathalie Bertrand[4], Yann Richet[5], Claire-Marie Duluc[6], Philippe Gourbesville[7] and Pierre Navaro[8]

Abstract. 2D Free-surface hydraulic modeling tools are commonly used to assess flood hazard for production of maximal water depth (h_{max}) maps, as support for flood risk assessment. High Resolution (HR) topographic data are big data getting commonly available and used by hydraulic modeling community. Topographical information and its strategy of inclusion in models, are inputs of great importance for overland flow h_{max} calculation. To strengthen the assessment of confidence level in these deterministic hydraulic models outputs, uncertainty analysis (UA) and global sensitivity analysis (SA) can provide useful information that is required by practitioners and decision makers. UA and SA approaches allow to identify effective strategies to reduce the uncertainty of a model output. In this paper, developed approach consists in parameterizing three factors which introduce uncertainty related to HR topographic data use with hydraulic models: the measurement error (var. E), the level of details of above ground element representation in DEM (buildings, sidewalks, *etc.*) (var. S), and the spatial discretization resolution (grid cell size of a regular mesh) (var. R). Parameter var. E follows a probability density function whereas parameter var. S and var. R are discrete operator choices. The coupling of an environment for parametric computation (Prométhée) and a code relying on 2D shallow water equation (FullSWOF_2D), Promethée-FullSWOF_2D (P-FS) tool has been set up. P-FS tool allows launching directly numerous set of computation using R software. 1200 simulations of a river flood event scenario were performed on the regular computational mesh, spatially discretizing a 17.5 km^2 urban area (Nice, France). The aim is to produce UA over points of interests and SA through Sobol index maps production.

Introduction

Over urban and industrialized areas, flood events might result in severe human, economic and environmental consequences. In mega-cities flood resilience context [Djordjević et al., 2011], as well as in a nuclear plant

[1] Institut de Radioprotection et de Sûreté Nucléaire & Lab. I-CiTy URE 005, EPU Nice Sophia, University of Nice, France, e-mail : abily@polytech.unice.fr, corresponding author
[2] Lab. J.A. Dieudonné UMR 7351 CNRS & EPU Nice Sophia, University of Nice, France, e-mail : delestre@math.unice.fr
[3] EPU Nice Sophia, University of Nice, France, e-mail : amoslau1@aquacloud.net
[4] Institut de Radioprotection et de Sûreté Nucléaire, France, e-mail : nathalie.bertrand@irsn.fr
[5] Institut de Radioprotection et de Sûreté Nucléaire, France, e-mail : claire-marie.duluc@irsn.fr
[6] Institut de Radioprotection et de Sûreté Nucléaire, France, e-mail : richet.yann@irsn.fr...
[7] Lab. I-CiTy URE 005, EPU Nice Sophia, University of Nice, France, e-mail : philippe.gourbesville@unice.fr
[8] IRMA, UMR 7501 CNRS, Unistra, France, e-mail : navaro@math.unistra.fr

Article published online by EDP Sciences and available at http://www.esaim-proc.org or http://dx.doi.org/10.1051/proc/201448018

hardened shell core safety context, accurate flood risk maps are required. These maps should provide fine information on maximal water depth (h_{max}) and maximal flow velocity (V_{max}) reached during a given flood event simulation. This high resolution information helps to make detailed estimations of flood impact on city functions (*e.g.* services: health, energy, communication, transport, *etc.*) [Batica et al., 2013] as well as to enhance nuclear safety by strengthening flood protection. These information estimated by deterministic models, will be inputs for flood mitigation strategies development.

For practical flood modeling applications over urban and industrial areas, standard deterministic free surface hydraulic modeling approaches most commonly rely either on (i) 2D Shallow Water Equations (SWEs) codes, (ii) simplified version of 2D SWE (*e.g.* diffusive wave approximation [Moussa and Bocquillon, 2000]) or (iii) multiple porosity shallow water approaches [Guinot, 2012]. These approaches are different in terms of mathematical description of flow behavior, computational cost and required dissimilar quantity and type of input data. In cities or at large suburb scales, these methods give overall similar results. Nevertheless, at smaller scales (street, compound or buildings scale) for a high resolution description of overland flow properties (h_{max} and V_{max}) reached during a flood event, codes based on 2D SWEs using fine description of the environment are required. Indeed, above ground surface features (buildings, walls, sidewalks, *etc.*) that influence overland flow path are densely present. These structures have a high level of diversity in urban and industrial areas and create a complex environment for overland flow. Category of numerical codes based on 2D SWEs use with high resolution topographic information provide a valuable approach which has been previously tested for runoff modeling scenario at industrial site scale [Abily et al., 2013a, Abily et al., 2013b].

In the context of fluvial flood events modeling over a large urban environment scale, 2D SWEs based modeling tools are intensively used in practical studies. Urban reconstruction relying on airborne topographic data gathering technologies such as imagery and Light Detection and Ranging (LiDAR) scans are intensively used by Geomatics communities [Musialski et al., 2013]. These technologies allow to produce Digital Elevation Models (DEM) with a high accuracy level [Lafarge et al., 2010, Lafarge and Mallet, 2011, Mastin et al., 2009]. Moreover, modern technologies, such as an Unmanned Aerial Vehicle (UVA) use, make high resolution LiDAR or imagery born data easily affordable in terms of time and financial cost [Remondino et al., 2011, Nex and Remondino, 2013]. Consequently, hydraulic numerical modeling community increasingly uses HR DEM information from airborne technologies to model urban flood [Tsubaki and Fujita, 2010]. Among HR topographic data, photogrammetry technology allows the production of 3D classified topographic data [Andres, 2012]. This type of data is useful for surface hydraulic modeling community as it provides classified information on complex environments. It gives the possibility to select useful informations for a DEM creation specifically adapted for flood modeling purposes [Abily et al., 2013b].

Even-though HR classified data is of high horizontal and vertical accuracy (in a range of a few centimeters), this data set is assorted of errors and uncertainties. Moreover, in order to optimize models creation and numerical computation, hydraulic modelers make choices regarding procedure for this type of dataset use. These sources of uncertainties might produce variability in hydraulic flood models output. Dealing with uncertainties in hydraulic models is a press-forward concern for both practitioners [Iooss, 2011] and new guidance [ASN, 2013]. Sources of uncertainties in hydraulic models come from a hypothesis in mathematical description of the natural phenomena, from input parameters of the model, from numerical aspects when solving the model. Input parameters are of prime interest for applied practitioners willing to decrease the uncertainties in their models results. Hydraulic models input parameters have hydrological, hydraulic, topographical and numerical nature. Identification, classification and impact quantification of sources of uncertainties, on a given model output, are a set of analysis steps which will enable to (i) analyze uncertainties behavior in a given modeling problem, (ii) elaborate methods for reducing uncertainties on a model output, and (iii) communicate on relevant uncertainties. Uncertainty Analysis (UA) and Sensitivity Analysis (SA) methods are useful tools as they allow robustness of model predictions to be checked and help to identify input parameters effects. UA consists in the propagation of uncertainty sources through the model, and then focuses on trying to quantify the resulting uncertainty on model output [Saint-Geours, 2012]. It allows robustness of model results to be checked. Various methods are then available to rank parameters regarding their impact on result variability (such as Sobol index).

This process goes one step beyond UA and constitutes a global sensitivity analysis (SA). SA stands in our study for global sensitivity analysis methods (omitting screening and local analysis methods) see [Jacques, 2011]. In practice, such type of approach is of a great interest, but is still at an exploratory level in applied studies relying on 2D SWE codes. Indeed, SA approach implementation is challenging, as it requires specific tools and deals with important computational capacity.

The purpose of the study presented in this paper is to provide both, (i) a tool and a protocol, to allow adaptable and ready-to use SA for 2D hydraulic modeling applications and (ii) to tackle impact of uncertainties related to HR topographic data use, over the variance of h_{max} calculated by 2D SWEs codes. Two categories of uncertain parameters are considered in our approach:

- first category is inherent to HR topographic data internal errors (measurement errors);
- second category is due to operator choices for this data inclusion in hydraulic codes.

The study is performed over the lower part of the Var river valley using an estimated hydrogram of the 1994 flood event. HR classified topographic data have been made available for the study area, which is 17.5 km^2, by Nice municipality. The HR topographic data are included in numerical models under the form of DEM which is directly used as a computational grid (structured mesh). Three uncertain parameters are studied: the measurement error (var. E), the level of detail of aboveground element representation in DEM (buildings, sidewalks, *etc.*) (var. S), and the spatial discretization resolution (grid cell size for regular mesh) (var. R). A process using a coupling of an environment for parametric computation (Promethée) and a code relying on 2D shallow water equations (FullSWOF_2D) is developed (P-FS tool) and implemented on a high performance computing structure (Marseille Mésocentre).

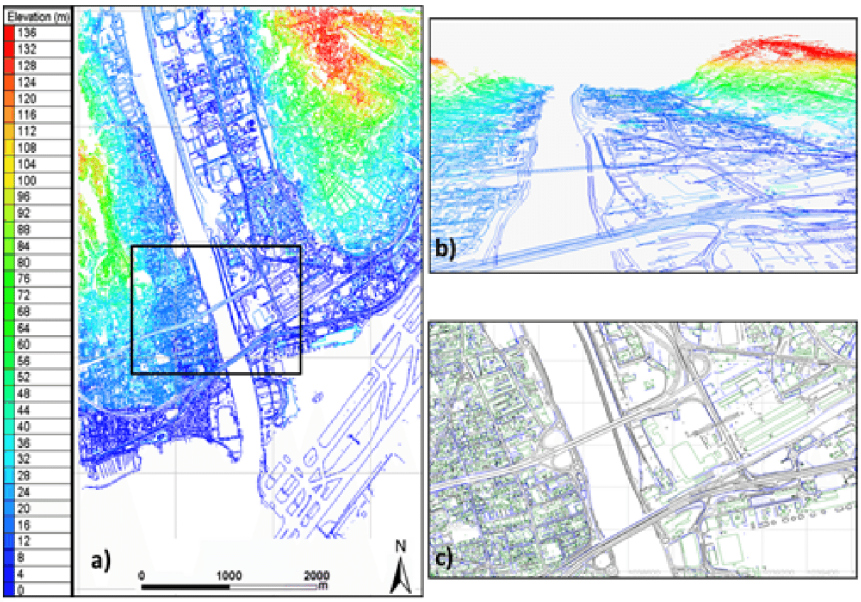

FIGURE 1. Overview (a) and zoom (b) of the HR 3D dataset selected classes with visualization (c) of buildings (green), walls (blue) and street concrete elements (black)

1. Material and methods

1.1. High resolution topographic data

1.1.1. *Photogrammetric 3D classified data : general aspects*

Aerial Photogrammetry technology allows to measure 3D coordinates of a space and its features using 2D pictures taken from different positions. The overlapping between pictures allows to calculate 3D properties of space and features based on stereoscopy principle. To measure accurately ground and features elevation, a step of aerotriangulation calculation is necessary, requiring information on picture properties regarding their position, orientation and bonding points. A low flight elevation, a high number of aerial pictures with different points of view and high levels of overlapping, allow to increase the accuracy and the reliability of the 3D coordinates measurement.

In photogrammetry, the spatial resolution is the size of a pixel at the ground level. For 3D classified data set creation a photo-interpretation step is necessary. Photo-interpretation allows creation of vectorial information based on photogrammetric dataset [Egels and Kasser, 2004, Linder, 2006]. A photo-interpreted dataset is composed of classes of points, polylines and polygons digitalized based on photogrammetric data. Important aspects in the photo-interpretation process are classes definition, vectorialisation methods and dataset quality used for photo-interpretation. These aspects will impact the design of the output classified dataset [Lu and Weng, 2007]. Class definition step has to be elaborated prior to the photo-interpretation step. The number, the nature and criteria for the definition of classes will depend on the objectives of the photo-interpretation campaign. Photo-interpretation techniques can be made (i) automatically by algorithm use, (ii) manually by a human operator on a Digital Photogrammetric Workstation (DPW) or (iii) by a combination of the two methods. The level of accuracy is higher when the photo-interpretation is done by a human operator on a DPW, but more resources are needed as the process becomes more time consuming [Lafarge et al., 2010]. Eventually, the 3D classification of features based on photo-interpretation allows to get 3D high resolution topographic data over territory which offer large and adaptable perspectives for its exploitation for different purposes [Andres, 2012].

Usually, when a photo-interpreted classified data set is provided to a user, the data is assorted with a global mean error value and with a percentage of photo-interpretation accuracy. The mean error value encompasses errors, due to material accuracy limits, to biased and to nuggets, which occurs within the photogrammetric data. The percentage of accuracy represents errors in photo-interpretation which can be feature misinterpretation, addition or omission.

1.1.2. *Low Var river Valley HR 3D classified data*

A HR photogrammetric 3D classified data gathering campaign has been held in 2010-2011 over Nice municipality, covering 400 km^2 [Andres, 2012]. The pixel resolution of aerial pictures is 0.1 m at the ground level. Features have been photo-interpreted under vectorial form in 50 different classes by human operators. These classes of elements include large above ground features such as building, roads, bridges, sidewalks, *etc.*. Thin above ground features, like concrete walls, road-gutters, stairs, *etc.*, are included as well in classes. An important number of georeferencing markers are used (about 200). Globally, over the whole spatial extend of the data gathering campaign, the mean accuracy of the classified data is 0.3 m and 0.25 m, respectively in horizontal and vertical dimension. Errors in photo-interpretation are estimated to represent 5% of the total number of elements. To control and ensure both, average level of accuracy and level of errors in photo-interpretation, the municipality has performed a terrestrial control of data accuracy over 10 % of the domain covered by the photogrammetric campaign. For the low Var river valley area, a low flight elevation combined with a high level of overlapping among aerial pictures (80 %), have conduced to a higher accuracy level. In the low Var river valley sector, classified data horizontal and vertical mean accuracy is 0.2 m. The total number of classified 3D polylines over this area is above 1,200,000. For our application, the 3D classified data of the low Var river valley is used to generate specific DEM adapted to surface hydraulic modeling. Therefore, only 3D classes of above ground feature, which are considered as impacting flow direction, are selected for DEM creation. It represents 12 classes, which includes buildings, concrete vertical structures above 2 m (walls) and low concrete features

above paved roads (*e.g.* sidewalks, road gutter, *etc.*). These classes represent a total of 52,600 polylines over our area (figure 1). The 12 selected classes have been aggregated in 3 groups: buildings, "concrete" vertical structures (walls) and street concrete feature.

1.2. **Physically based model – FullSWOF_2D**

The name FullSWOF stands for Full Shallow Water equations for Overland Flow [Delestre et al.,]. It is a set of open source C++ (ANSI) codes, freely available to the community (GPL- compatible license CeCILL-V2) from the website http://www.univ-orleans.fr/mapmo/soft/FullSWOF/. The structure of the code is made to facilitate the development of new evolutions. This software resolves the shallow water equations [Cunge et al., 1980] thanks to a well-balanced finite volume method based on the hydrostatic reconstruction (introduced in [Audusse et al., 2004,Bouchut, 2004]). This numerical method has good properties: water mass conservation, well-balancedness (at least preservation of a lake at rest equilibrium) and positivity water height preservation. Validations of FullSWOF_2D have already been performed on analytical solutions (SWASHES [Delestre et al., 2013]), on experimental data and on real events at small scales (agricultural parcels [Delestre et al., 2014]). The shallow water system in 2D (SW2D) writes:

$$\begin{cases} \partial_t h + \partial_x(hu) + \partial_y(hv) = 0, \\ \partial_t(hu) + \partial_x(hu^2 + gh^2/2) + \partial_y(huv) = gh(S_{0x} - S_{fx}), \\ \partial_t(hv) + \partial_x(huv) + \partial_y(hv^2 + gh^2/2) = gh(S_{0y} - S_{fy}), \end{cases} \quad . \tag{1}$$

The first partial derivative equation of system (1) is the mass conservation equation and the two other ones are the momentum equation where the 2D vector (u, v) is the fluid's horizontal average velocity across a vertical column of height $h(x, y, t)$ $[m]$ and $g = 9.81$ is the acceleration due to the gravity. The subscript x (respectively y) stands for the x-direction (resp. the y-direction): $-S_{0x} = \partial_x z(x, y)$ and $-S_{0y} = \partial_y z(x, y)$ are the ground slopes and S_{fx} and S_{fy} the friction terms.

In FullSWOF, we have chosen to solve the SW2D on a structured grid. So we have chosen a numerical method adapted to the shallow water system in 1D (SW1D) or the Saint-Venant system [de Saint Venant, 1871] and then it is generalized to 2D thanks to the method of lines. So in what follows, we describe the numerical method for the SW1D. The SW1D writes

$$\begin{cases} \partial_t h + \partial_x(hu) = 0 \\ \partial_t(hu) + \partial_x(hu^2 + gh^2/2) = gh(S_0 - S_f), \end{cases} \tag{2}$$

in what follows, we consider Manning's friction law

$$S_f = n^2 \frac{u|u|}{h^{4/3}} = n^2 \frac{q|q|}{h^{10/3}}, \tag{3}$$

with $q = hu$ the unit discharge $\left[\mathrm{m}^2/\mathrm{s}\right]$. The hydrostatic reconstruction is based on a general principle of reconstruction. We begin with a first order finite volume scheme for the form of SW1D (without source terms): choosing a positive and consistent numerical flux $\mathbf{F}(U_L, U_R)$ (*e.g.* Rusanov, HLL, kinetic, *etc.*), a finite volume scheme writes under the general form

$$\frac{U_i^* - U_i^n}{\Delta t} + \frac{\mathbf{F}(U_i, U_{i+1}) - \mathbf{F}(U_{i-1}, U_i)}{\Delta x} = \vec{0}, \tag{4}$$

where Δt is the time step and Δx the space step. The idea is to modify this scheme by applying the flux to reconstructed variables. Reconstruction can be used to get higher order schemes (MUSCL, ENO, *etc.*), in that case higher order in time is obtained through TVD-Runge-Kutta methods [Shu and Osher, 1988]. And the aim of the hydrostatic reconstruction is to be well-balanced. It is designed to preserve at least steady states at rest ($u = 0$). Since [Bermúdez and Vázquez, 1994], it is well known that the topography needs a special treatment

to preserve steady states without spurious oscillations. Schemes preserving at least lake at rest equilibrium are said to be well-balanced (a notion introduced in [Greenberg and LeRoux, 1996]). When it is directly applied to the initial scheme, it leads to an order one scheme, while coupling it with high order reconstruction increases the order and the accuracy of the scheme.

We describe now the implementation of this method for high order accuracy. The first step consists in performing a high order reconstruction (MUSCL, ENO, *etc.*). To properly treat the topography source term $\partial_x z$, this reconstruction is applied on u, h and $h+z$, for more details see [Audusse and Bristeau, 2005]. This gives us the reconstructed variables (U_-, z_-) and (U_+, z_+), on which the hydrostatic reconstruction is applied

$$\left\{\begin{array}{l} h_{i+1/2L} = \max(h_{i+1/2-} + z_{i+1/2-} - \max(z_{i+1/2-}, z_{i+1/2+}), 0), \\ U_{i+1/2L} = (h_{i+1/2L}, h_{i+1/2L} u_{i+1/2-}), \\ h_{i+1/2R} = \max(h_{i+1/2+} + z_{i+1/2+} - \max(z_{i+1/2-}, z_{i+1/2+}), 0), \\ U_{i+1/2R} = (h_{i+1/2R}, h_{i+1/2R} u_{i+1/2+}). \end{array}\right. \tag{5}$$

For a given space discretization, it may exhibit abnormal behaviors for some combinations of slope and water height [Delestre et al., 2012]. Particularly obvious for the order one scheme and on a coarse mesh, they disappear when refining the mesh, and are hardly noticeable at order two.

The finite volume scheme is modified as follows

$$\frac{U_i^* - U_i^n}{\Delta t} + \frac{F_{i+1/2L}^n - F_{i-1/2R}^n - Fc_i^n}{\Delta x} = \vec{0}, \tag{6}$$

where

$$F_{i+1/2L}^n = F_{i+1/2}^n + S_{i+1/2L}^n, \quad F_{i-1/2R}^n = F_{i-1/2}^n + S_{i-1/2R}^n \tag{7}$$

are left (resp. right) modifications of the numerical flux for the homogeneous system. In this formula, the flux is now applied to reconstructed variables $F_{i+1/2}^n = \mathbf{F}(U_{i+1/2L}^n, U_{i+1/2R}^n)$ and we take

$$S_{i+1/2L}^n = \begin{pmatrix} 0 \\ \frac{g}{2}(h_{i+1/2-}^2 - h_{i+1/2L}^2) \end{pmatrix}, \quad S_{i-1/2R}^n = \begin{pmatrix} 0 \\ \frac{g}{2}(h_{i-1/2+}^2 - h_{i-1/2R}^2) \end{pmatrix}. \tag{8}$$

Finally, for consistency and well-balancing, a centered source term is added

$$Fc_i = \begin{pmatrix} 0 \\ -g\dfrac{h_{i-1/2+} + h_{i+1/2-}}{2}(z_{i+1/2-} - z_{i-1/2+}) \end{pmatrix}. \tag{9}$$

The numerical strategy we choose consists in the HLL flux [Harten et al., 1983]

$$\mathbf{F}(U_L, U_R) = \left\{\begin{array}{ll} F(U_L) & \text{if } 0 \le c_1 \\ \dfrac{c_2 F(U_L) - c_1 F(U_R)}{c_2 - c_1} + \dfrac{c_1 c_2}{c_2 - c_1}(U_R - U_L) & \text{if } c_1 < 0 < c_2 \\ F(U_R) & \text{if } c_2 \le 0 \end{array}\right., \tag{10}$$

with two parameters $c_1 < c_2$ which are the approximations of the slowest and fastest wave speeds, respectively. We refer to [Batten et al., 1997] for further discussion on the wave speed estimates. The HLL flux is used with a modified MUSCL reconstruction [Bouchut, 2004]. It has shown to be the best compromise between accuracy, stability and CPU time cost (in [Delestre, 2010]). The MUSCL reconstruction [van Leer, 1979] of a scalar variable $s \in \mathbb{R}$ writes

$$s_{i-1/2+} = s_i - \Delta x.\frac{Ds_i}{2}, \quad s_{i+1/2-} = s_i + \Delta x.\frac{Ds_i}{2}, \tag{11}$$

with the minmod slope limiter

$$Ds_i = minmod\left(\frac{s_i - s_{i-1}}{\Delta x}, \frac{s_{i+1} - s_i}{\Delta x}\right), \quad minmod(x,y) = \begin{cases} \min(x,y) & \text{if } x,y \geq 0, \\ \max(x,y) & \text{if } x,y \leq 0, \\ 0 & \text{else.} \end{cases} \tag{12}$$

In order to keep the discharge conservation, the reconstruction of the velocity has to be modified as

$$u_{i-1/2+} = u_i - \frac{h_{i+1/2-}}{h_i}\frac{\Delta x}{2}Du_i \quad u_{i+1/2-} = u_i + \frac{h_{i-1/2+}}{h_i}\frac{\Delta x}{2}Du_i \tag{13}$$

If we take $Ds_i = 0$, we recover the first order scheme in space. The friction term is taken into account by a fractional step, with the following system

$$\partial_t U = \begin{pmatrix} 0 \\ -ghS_f \end{pmatrix}. \tag{14}$$

This system is solved thanks to a semi-implicit method (as in [Bristeau and Coussin, 2001])

$$\begin{cases} h^{n+1} = h^*, \\ \dfrac{q^{n+1} - q^*}{\Delta t} = -n^2 \dfrac{q^{n+1}|q^n|}{h^n (h^{n+1})^{4/3}}. \end{cases} \tag{15}$$

This method allows to preserve stability (under a classical CFL condition) and steady states at rest. Finally a TVD-Runge Kutta method is applied to get the second order in time. For the generalization to 2D, we use the HLLC flux introduced in [Toro et al., 1994], combined with the method of lines. Concerning boundary conditions, we have modified the code, in order to have the discharge only in the riverbed, it is based on Riemann invariants. Finally, as we aim at simulating with big data, we have used a parallel version of FullSWOF based on a domain decomposition and the MPI library developped in the framework of CEMRACS 2012 [Cordier, S. et al., 2013]. This version has been compared and validated with an other parallel version based on SkelGIS library [Cordier, S. et al., 2013, Coullon et al., 2013].

1.3. **The low Var valley modeling scenario**

The 5th of November 1994, a flood event occurred in the Var catchment, leading to serious flooding in the low Var river valley [Guinot and Gourbesville, 2003]. In this paper, hydraulic conditions of this historical event will serve as a framework for a test scenario. The objective here is not to reproduce the flood event. Indeed, the site has changed since 1994: levees, dikes and urban structures have been intensively constructed in this area. As our approach aims at studying uncertainties related to HR topographic data use in hydraulic models, all the hydraulic parameters of the models are set identically for the simulations. Only the input DEM will change from one simulation to another following strategy defined in the next section. The flood scenario for our tests is based on an estimated hydrogram on the 5th of November 1994 event [Guinot and Gourbesville, 2003]. This hydrogram is our upstream boundary condition of the low Var river valley. To shorten the simulation length, we chose to simulate a 9 hours scenario (figure 2). First, a constant discharge of 1,500 $m^3.s^{-1}$ is run for 3 hours to reach a steady state. This will serve as an initial condition for all the simulations. The overtopping part of the hydrogram is run, reaching the estimated peak discharge (3,700 $m^3.s^{-1}$) and then decreasing long enough to observe a diminution of the overland flow water depth. The Manning's n coefficient is spatially uniform on overland flow areas with a value of 0.015 which corresponds to a concrete surfacing [Chow, 1959]. No energy loss properties have been included in the hydraulic model to represent the bridges piers effects. Downstream boundary condition is an open sea level with a Neumann boundary condition.

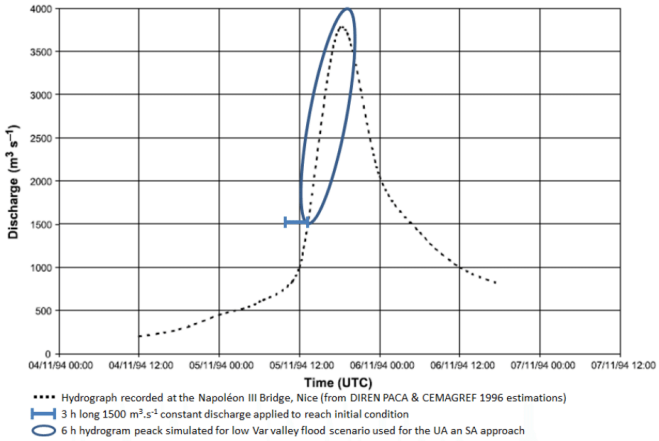

FIGURE 2. Estimated 1994 flood event hydrogram at the Napoléon bridge with schematization of simplification of the hydraulic scenario used for our UA orientated simulations.

1.4. **Material and method for the sensitivity analysis**

1.4.1. *Overview of the approach*

A schematization of our SA approach is presented in figure 3. As previously mentioned, this study focuses on two categories of parameters introducing uncertainty, in output of interest h_{max} calculation. These parameters are related to accuracy errors in HR classified data and to operator choices when building DEM and when integrating this DEM in hydraulic model. One parameter (var. E) encompasses uncertainty related to HR topographic data measurement errors. Two parameters (var. S and var. R), represent uncertainty introduced by operator, respectively when building a specific DEM (var. S) and when spatially discretizing topographic information within 2D hydraulic code (var. R). Var. E, S and R properties are detailed in the next section. A sample of 2,000 DEMs which are used directly as structured mesh in the hydraulic code FullSWOF_2D is created. This sample of DEMs combines all the possibilities of selected sets of the three input parameters var. S, R and E. Aim is to produce a database of variable output of interest (h_{max}) combining systematically parameters var. S, R and E. This experience plan might not be optimal, but will allow to proceed to Monte Carlo sampling within the output database, verifying convergence of the Monte Carlo run, through the use of bootstrap test as a post-treatment phase. To run the 2,000 hydraulic simulations, Prométhée software is coupled with FullSWOF_2D. Prométhée is an environment for parametric computation allowing to carry the uncertainties propagation study when coupled to a code. This software is an open source environment developed by IRSN (http://promethee.irsn.org/doku.php). Interest of Prométhée lies in the fact that it will allow to parameterize input of any numerical code and is optimized for intensive computing resources use. Moreover, statistical post-treatment can be performed using Prométhée as it integrates R statistical environment. The coupled code Prométhée / FullSWOF (P-FS) is used to automatically launch parametrized computation.

For UA and SA, the deterministic code FullSWOF_2D is considered as a blackbox model as described in [Marrel et al., 2012]:

$$\begin{array}{rl} f: & \mathbb{R}^p \to \mathbb{R} \\ & X \mapsto Y = f(X) \end{array} \quad ,$$

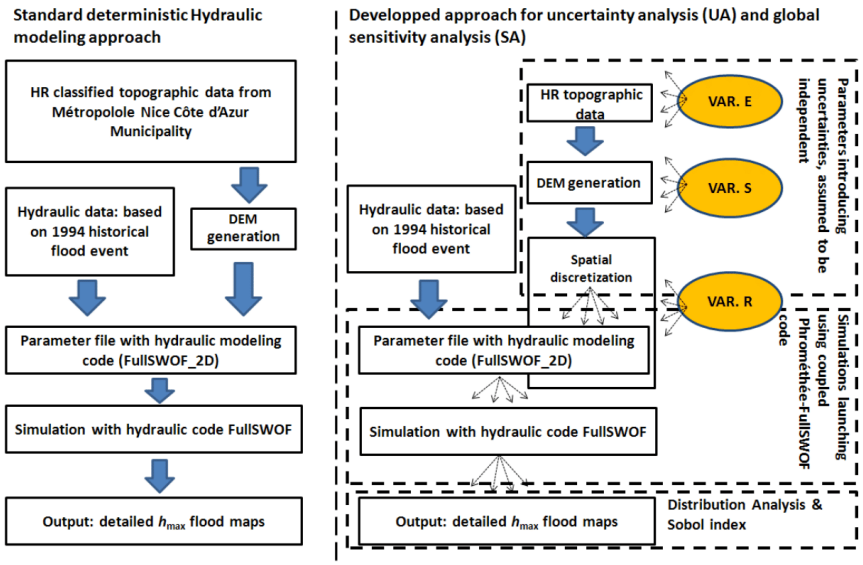

FIGURE 3. Schematisation of the experimental approach.

where f is the model function, $X = (X_1, ..., X_p)$ are p independent input random variables with known distribution and Y is the output random variable. The UA will be done over the selected points of interest (figure 4). It is a first approach for analysing impacts of the three parameters over h_{max}. Analysis is planned to be performed comparing the distribution at different points of h_{max} (minimum, maximum, mean, standard deviation and probability distribution shape). The principle of the SA method relies on estimation of the variance of the input variables (here S, E and R) contribution to output variance (here h_{max}). A unique functional analysis of variance (ANOVA) decomposition of any integrable function into a sum of elementary functions allows to define the sensitivity indices as explained in [Sobol', 1990, Marrel et al., 2012]. Sobol indices are defined as follow:

$$S_i = \frac{Var(\mathbb{E}(Y|X_i))}{Var(Y)}.$$

For our approach, we plan to calculate first order Sobol indices for each of the 40 points of interest and then at each grid cell of the area of interest (figure 4).

1.4.2. *Application of the approach*

Parameters var. S, E and R are independent parameters considered as described below.

- Var. S: modeler choices for DEM creation

  It represents modeler choices for DEM creation. Four discrete stages are considered: (i) S_1, is the DTM of the study case, (ii) S_2, the elevation information of buildings added to S_1, (iii) S_3, the elevation information on the walls added to S_2, and (iv) S_4, elevation information of concrete features in streets added to S_3. Var. S parameter is included in the SA as a categorical ordinal parameter. These discrete

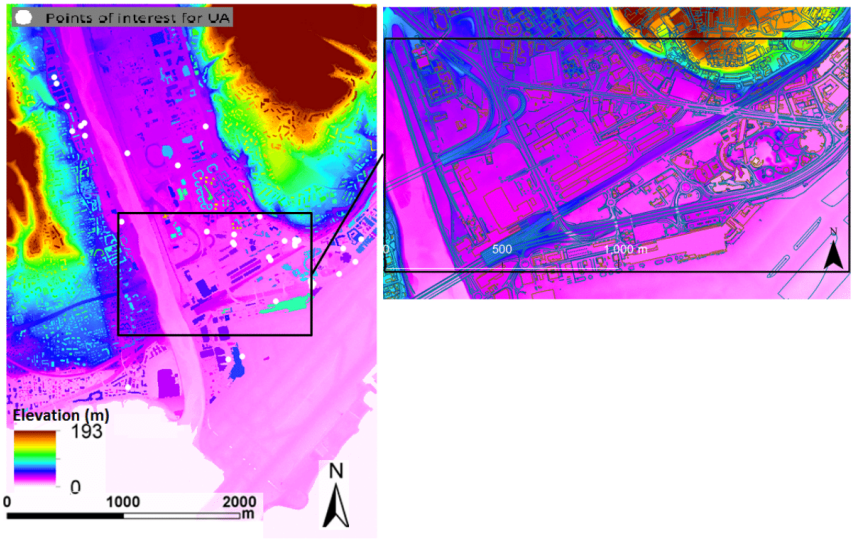

FIGURE 4. Location of points of interests for UA and focus on area of interest for Sobol index maps creation.

modeler choices are considered as having the same probability. Four DEM are generated at resolution 1 m, S_1 to S_4.

- Var. E: measurement errors of HR topographic dataset

  This parameter introduces in the DEM with the finest resolution (1 m) a random error in each cell of the DEM. For our study, only the altimetric errors are taken into account. Indeed, the planimetric dimension of the error is assumed to be relatively less significant for hydraulic study purpose compared to altimetric error. This altimetric measurement error follows a Gaussian probability density function $\mathcal{N}(0, 0.2)$, where the standard deviation is equal to the mean global error value (0.2 m). This error introduction is spatially homogeneous. This approach is a first approximation: mean error could be spatialised in different sub-areas having physical properties which would impact spatial patterns of error value. Moreover, errors in photo-interpretation (classification) are not considered here. One hundred grids of random errors are generated, E_1 to E_{100}.
- Var. R: modeler choices for mesh spatial resolution

  When included in 2D models, HR DEM information is spatially and temporally discretized. FullSWOF is based on structured mesh, therefore the DEM grid can be directly included as a computational grid without effort for mesh creation. Nevertheless, for practical application, optimization of computational time/accuracy ratio often goes through a mesh degradation process when a HR DEM is used. Var. R represents modeler choices when decreasing regular mesh resolution. Var. R parameter can take 5 discrete values: 1, 2, 3, 4 or 5 m. This range of possible discrete value for var. R has been selected on purpose to be compatible with modeler choices, when optimizing models, in regard with the range of different levels of details of above ground features (var. S). Indeed decreasing the finest resolution would lead to prohibitive computational time, whereas increasing the resolution above 5 m would make

the use high resolution topographic information pointless. Therefore in practical engineering flood modelling applications, depending on available computer resources, all combinations of var. R / var. S are consistent.

DEM is a generic term for Digital Terrain Model (DTM) and for Digital Surface Model (DSM). If the DEM represents the elevation of the bare ground, then it is qualified as a DTM. If the DEM include information of above ground features elevation, it is called a DSM. In urban-like environments, when a DEM includes detailed elevation information with an infra-metric resolution, the DEM is qualified as a High Resolution (HR).

The use of classified data allow to include elevation information about thin above ground features (narrower than 1m) which is under the vectorial form, in DEM (grid form) at a one meter resolution as explained in following section. To create the HR DEMs, the following approach has been carried out. An HR DTM using multiple ground level information sources (points, polygons and polylines) is created and provided at a 0.5 m resolution by DIGNCA. The HR DEM resolution is here degraded to 1 m resolution. At this resolution the number of mesh cells is above 17.8 million. Then, a selection procedure among classified data is performed. This selection is achieved by considering concrete elements which can influence overland flow drainage path only. It includes dikes, buildings, walls and "concrete" above ground elements (such as sidewalks, road gutters, roundabout, doors steps, *etc.*). 12 classes are selected among the 50 classes of the 3D photo-interpreted dataset (figure 1). During this step, polylines giving information on elevated roads and bridges, which might block overland flow paths, are removed. The remaining total number of polylines is 52,600. Selected above ground features are aggregated in 3 groups of features (buildings, walls and concrete street features). Extruding elevation information of selected polylines groups on the DTM (S_1), four 1 m resolution DEMs, S_1 to S_4, are produced. The previously described method has allowed inclusion of thin elements impacting flow behavior of infra-metric dimension, oversized to metric size, in the 1 m resolution regular mesh. Then, 100 grids of var. E are produced and added to var. S_1, S_2, S_3 and S_4 at resolution 1 m. Eventually, these 400 DEMs are used to create 2,000 DEMs having a resolution ranging from 1 to 5 m. DEMs are named $S_m R_n E_x$, with the parameters $m \in [\![1, 4]\!]$, $n \in [\![1, 5]\!]$ and $x \sim \mathcal{N}(0, 0.2)$ used in P-FS.

2. Results and perspectives

Modifications on FullSWOF_2D code allow to run described river flood event scenario. A proof of concept of 3D HR classified data use for river flood modeling is given here (figure 5). Advantages of such an approach rely on (i) possibility to include detailed surface elements influencing overland flow, and in automatization and modularity of class selection for HR DSM production and, (ii) taking advantage of FullSWOF_2D numerical properties of mass conservation, well-balancedness and positivity preservation, which are relevant for HR overland flow modeling in urban areas.

Performed version of P-FS couple allows to run simulations with a selected set of input parameters (var. E, S and R). Through R commands, it is possible to launch serial calculation. The coupled tool is operational on the HPC Mésocentre. P-FS would be transposable over any common HPC structures, requiring only slight changes in the coupling part of the codes. It is possible to run simultaneously up to 30 simulations.

For our simulations, calculations running times are important. Indeed, this computation time is CFL restriction dependent and therefore, is considerably affected by mesh resolution. Over a 12 cores node of the Mésocentre, the computation time is 2, 6, 12, 24, 40 hours respectively for 5, 4, 3, 2, 1 m resolution grids. Using about 200,000 CPU hours, it has been possible to run 1,200 simulations. The remaining 800 simulations are for R_2 and R_1 resolutions which are the most resource-demanding simulations. Due to the fact that these simulations are still missing, UA and consequently SA have not been fully achieved at this stage of the study.

Figure 6 illustrates perspectives for UA at a given point of interest. Output of interest h_{max} variability at this point is illustrated through maximal surface elevation use $h_{max} + z$. For a given resolution (here R_3), a sample of 200 results is used. It consists of 4 random sub-sets of 50 simulation results among $S_1 R_3 E_x$, $S_2 R_3 E_x$, $S_3 R_3 E_x$ and $S_4 R_3 E_x$. Perspectives for further analysis are following. Once all of the 2,000 simulations will be run, a Monte Carlo sampling will be done. Through a resampling method use (bootstrap, see [Cohen and

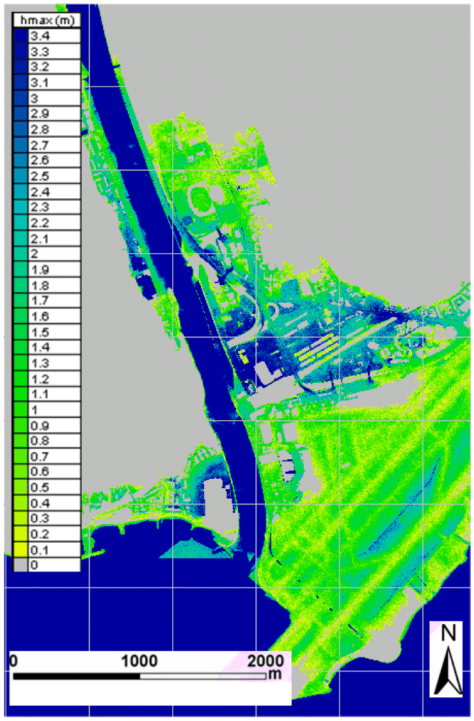

FIGURE 5. Illustration of h_{max} map obtained with HR topogrphic data use with P-FS for parameters R_3, S_4, $E_4$4.

Cohen, 2008]), the convergence of the uncertainty propagation will be checked. Then analysis part of UA and SA will be possible.

Limits and possible improvements of our approach can be put to the light. For the finest resolutions (R_1 and R_2), we might consider to increase the number of CPU used for computation. This will enable to reduce the running time of the simulations. The way measurement error (Var. E) has been taken into account is a first approximation. Indeed, it would be relevant to consider, in a more sophisticated approach, spatial zones where var. E would have different PDF properties to better reproduce existing error spatial variability. This would require to put efforts in the characterization of errors measurements spatial variability. Moreover, errors related to photo-interpretation misinterpretation are not taken into consideration yet.

ACKNOWLEDGMENTS

This project has been founded by I-CiTy and IRSN. Photogrammetric and photo-interpreted dataset used for this study have been kindly provided by DIGNCA for research purpose. Technical expertise on Métropole Nice Côte d'Azur dataset has been provided by G. Tacet. This work was granted access to the HPC resources

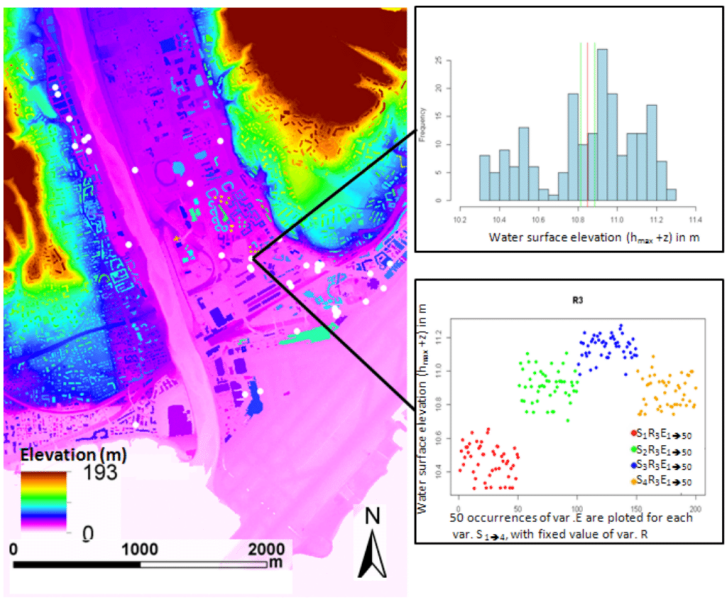

FIGURE 6. Illustration of UA possibilities at a point of interest using a sub-set of outputs.

of Aix-Marseille Université financed by the project equip@meso (ANR-10-EQPX-29-01) of the program "Investissements d'Avenir" sponsorised by the ANR. Technical support for codes adaptation on high performance computation centers has been provided by C. Laguerre, F. Lebas. and H. Coullon. Advices on uncertainty propagation have been kindly provided by B. Iooss, A. Marrel and CEMRACS organizers, in particular A. Nouy.

REFERENCES

[Abily et al., 2013a] Abily, M., Duluc, C. M., Faes, J. B., and Gourbesville, P. (2013a). Performance assessment of modelling tools for high resolution runoff simulation over an industrial site. *Journal of Hydroinformatics*, 15(4):1296–1311.

[Abily et al., 2013b] Abily, M., Gourbesville, Andres, L., and Duluc, C.-M. (2013b). Photogrammetric and LiDAR data for high resolution runoff modeling over industrial and urban sites. In Zhaoyin, W., Lee, J. H.-w., Jizhang, G., and Shuyou, C., editors, *Proceedings of the 35th IAHR World Congress, September 8-13, 2013, Chengdu, China*. Tsinghua University Press, Beijing.

[Andres, 2012] Andres, L. (2012). L'apport de la donnée topographique pour la modélisation 3d fine et classifiée d'un territoire. *Revue XYZ*, 133 - 4e trimestre:24–30.

[ASN, 2013] ASN (2013). Protection of Basic Nuclear Installations Against External Flooding - guide no.13 - version of 08/01/2013. Technical report, Autorité de Sûreté Nucléaire.

[Audusse et al., 2004] Audusse, E., Bouchut, F., Bristeau, M.-O., Klein, R., and Perthame, B. (2004). A fast and stable well-balanced scheme with hydrostatic reconstruction for shallow water flows. *SIAM J. Sci. Comput.*, 25(6):2050–2065.

[Audusse and Bristeau, 2005] Audusse, E. and Bristeau, M.-O. (2005). A well-balanced positivity preserving "second-order" scheme for shallow water flows on unstructured meshes. *Journal of Computational Physics*, 206:311–333.

[Batica et al., 2013] Batica, J., Gourbesville, P., and Hu, F.-Y. (2013). Methodology for flood resilience index. In Butler, D., Chen, A. S., Djordjevic, S., and Hammond, M. J., editors, *Proceedings of the International Conference on Flood Resilience: Experiences in Asia and Europe, held in Exeter, United Kingdom, 5-7 September 2013*, page 302. Centre for Water Systems, University of Exeter.

[Batten et al., 1997] Batten, P., Clarke, N., Lambert, C., and Causon, D. M. (1997). On the Choice of Wavespeeds for the HLLC Riemann Solver. *SIAM J. Sci. Comput.*, 18(6):1553–1570.

[Bermúdez and Vázquez, 1994] Bermúdez, A. and Vázquez, M. E. (1994). Upwind methods for hyperbolic conservation laws with source terms. *Computers & Fluids*, 23(8):1049 – 1071.

[Bouchut, 2004] Bouchut, F. (2004). *Nonlinear stability of finite volume methods for hyperbolic conservation laws, and well-balanced schemes for sources*, volume 2/2004. Birkhäuser Basel.

[Bristeau and Coussin, 2001] Bristeau, M.-O. and Coussin, B. (2001). Boundary conditions for the shallow water equations solved by kinetic schemes. Technical Report 4282, INRIA.

[Chow, 1959] Chow, V. T. (1959). *Open-Channel Hydraulics*. McGraw-Hill.

[Cohen and Cohen, 2008] Cohen, Y. and Cohen, J. (2008). *Statistics and Data with R: An Applied Approach Through Examples*. Wiley.

[Cordier, S. et al., 2013] Cordier, S., Coullon, H., Delestre, O., Laguerre, C., Le, M. H., Pierre, D., and Sadaka, G. (2013). Fullswof paral: Comparison of two parallelization strategies (mpi and skelgis) on a software designed for hydrology applications. *ESAIM: Proc.*, 43:59–79.

[Coullon et al., 2013] Coullon, H., Le, M.-H., and Limet, S. (2013). Parallelization of Shallow-water Equations with the Algorithmic Skeleton Library SkelGIS. *Procedia Computer Science*, 18(0):591–600. 2013 International Conference on Computational Science.

[Cunge et al., 1980] Cunge, J., Holly, F., and Verwey, A. (1980). *Practical Aspects of Computational River Hydraulics*. Pitman Publishing, London, T. Fisher Unwin.

[de Saint Venant, 1871] de Saint Venant, A. J.-C. (1871). Théorie du mouvement non-permanent des eaux, avec application aux crues des rivières et à l'introduction des marées dans leur lit. *Comptes Rendus de l'Académie des Sciences*, 73:147–154.

[Delestre, 2010] Delestre, O. (2010). *Simulation du ruissellement d'eau de pluie sur des surfaces agricoles/ rain water overland flow on agricultural fields simulation*. PhD thesis, Université d'Orléans (in French), available from TEL: tel.archives-ouvertes.fr/INSMI/tel-00531377/fr.

[Delestre et al., 2014] Delestre, O., Cordier, S., Darboux, F., Du, M., James, F., Laguerre, C., Lucas, C., and Planchon, O. (2014). FullSWOF: A Software for Overland Flow Simulation. In Gourbesville, P., Cunge, J., and Caignaert, G., editors, *Advances in Hydroinformatics*, Springer Hydrogeology, pages 221–231. Springer Singapore.

[Delestre et al., 2012] Delestre, O., Cordier, S., Darboux, F., and James, F. (2012). A limitation of the hydrostatic reconstruction technique for Shallow Water equations/Une limitation de la reconstruction hydrostatique pour la résolution du système de Saint-Venant. *C. R. Acad. Sci. Paris, Ser. I*, 350:677–681.

[Delestre et al.,] Delestre, O., Darboux, F., James, F., Lucas, C., Laguerre, C., and Cordier, S. FullSWOF: A free software for the simulation of shallow water flows. Submitted.

[Delestre et al., 2013] Delestre, O., Lucas, C., Ksinant, P.-A., Darboux, F., Laguerre, C., Vo, T.-N.-T., James, F., and Cordier, S. (2013). SWASHES: a compilation of shallow water analytic solutions for hydraulic and environmental studies. *International Journal for Numerical Methods in Fluids*, 72(3):269–300.

[Djordjević et al., 2011] Djordjević, S., Butler, D., Gourbesville, P., Mark, O., and Pasche, E. (2011). New policies to deal with climate change and other drivers impacting on resilience to flooding in urban areas: the CORFU approach. *Environmental Science & Policy*, 14(7):864–873. Adapting to Climate Change: Reducing Water-related Risks in Europe.

[Egels and Kasser, 2004] Egels, Y. and Kasser, M. (2004). *Digital Photogrammetry*. Taylor & Francis.

[Greenberg and LeRoux, 1996] Greenberg, J. M. and LeRoux, A.-Y. (1996). A well-balanced scheme for the numerical processing of source terms in hyperbolic equation. *SIAM Journal on Numerical Analysis*, 33:1–16.

[Guinot, 2012] Guinot, V. (2012). Multiple porosity shallow water models for macroscopic modelling of urban floods. *Advances in Water Resources*, 37(0):40–72.

[Guinot and Gourbesville, 2003] Guinot, V. and Gourbesville, P. (2003). Calibration of physically based models: back to basics? *Journal of Hydroinformatics*, 5(4):233–244.

[Harten et al., 1983] Harten, A., Lax, P. D., and van Leer, B. (1983). On upstream differencing and Godunov-type schemes for hyperbolic conservation laws. *SIAM Review*, 25(1):35–61.

[Iooss, 2011] Iooss, B. (2011). Revue sur l'analyse de sensibilité globale de modèles numériques. *Journal de la Société Française de Statistique*, 152(1):1–23.

[Jacques, 2011] Jacques, J. (2011). Pratique de l'analyse de sensibilité : comment évaluer l'impact des entrées aléatoires sur la sortie d'un modèle mathématique. http://math.univ-lille1.fr/ jacques.

[Lafarge et al., 2010] Lafarge, F., Descombes, X., Zerubia, J., and Pierrot Deseilligny, M. (2010). Structural approach for building reconstruction from a single DSM. *Trans. on Pattern Analysis and Machine Intelligence*, 32(1):135–147.

[Lafarge and Mallet, 2011] Lafarge, F. and Mallet, C. (2011). Building large urban environments from unstructured point data. In *Computer Vision (ICCV), 2011 IEEE International Conference on*, volume 0, pages 1068–1075, Los Alamitos, CA, USA. IEEE Computer Society.

[Linder, 2006] Linder, W. (2006). *Digital Photogrammetry: A Practical Course*. Springer Verlag.

[Lu and Weng, 2007] Lu, D. and Weng, Q. (2007). A survey of image classification methods and techniques for improving classification performance. *International Journal of Remote Sensing*, 28(5):823–870.

[Marrel et al., 2012] Marrel, A., Iooss, B., Veiga, S., and Ribatet, M. (2012). Global sensitivity analysis of stochastic computer models with joint metamodels. *Statistics and Computing*, 22(3):833–847.

[Mastin et al., 2009] Mastin, A., Kepner, J., and Fisher, J. I. (2009). Automatic Registration of LIDAR and Optical Images of Urban Scenes. In *Computer Vision and Pattern Recognition, 2009. CVPR 2009. IEEE Conference on*, pages 2639–2646.

[Moussa and Bocquillon, 2000] Moussa, R. and Bocquillon, C. (2000). Approximation zones of the saint-venant equations for flood routing with overbank flow. *Hydrology and Earth System Sciences*, 4(2):251–261.

[Musialski et al., 2013] Musialski, P., Wonka, P., Aliaga, D. G., Wimmer, M., van Gool, L., and Purgathofer, W. (2013). A survey of urban reconstruction. *Computer Graphics Forum*, 32(6):146–177.

[Nex and Remondino, 2013] Nex, F. and Remondino, F. (2013). UAV for 3d mapping applications: a review. *Applied Geomatics*, pages 1–15.

[Remondino et al., 2011] Remondino, F., Barazzetti, L., Nex, F., Scaioni, M., and Sarazzi, D. (2011). UAV photogrammetry for mapping and 3D modeling – Current status and future perspectives. In *Archives of Photogrammetry, Remote Sensing and Spatial Information Sciences*, volume 38(1/C22). ISPRS Conference UAV-g, Zurich, Switzerland.

[Saint-Geours, 2012] Saint-Geours, N. (2012). *Analyse de sensibilité de modèles spatialisés - Application à l'analyse coût-bénéfice de projets de prévention des inondations*. These, Université Montpellier II - Sciences et Techniques du Languedoc.

[Shu and Osher, 1988] Shu, C.-W. and Osher, S. (1988). Efficient implementation of essentially non-oscillatory shock-capturing schemes. *Journal of Computational Physics*, 77(2):439–471.

[Sobol', 1990] Sobol', I. M. (1990). On sensitivity estimation for nonlinear mathematical models. *Matematicheskoe modelirvanie*, 2(1):112–118 (in Russian), *MMCE*, 1(4) (1993) :407–414 (in English).

[Toro et al., 1994] Toro, E., Spruce, M., and Speares, W. (1994). Restoration of the contact surface in the HLL-Riemann solver. *Shock Waves*, 4:25–34.

[Tsubaki and Fujita, 2010] Tsubaki, R. and Fujita, I. (2010). Unstructured grid generation using LiDAR data for urban flood inundation modelling. *Hydrological Processes*, 24:1404–1420.

[van Leer, 1979] van Leer, B. (1979). Towards the ultimate conservative difference scheme. V. A second-order sequel to Godunov's method. *Journal of Computational Physics*, 32(1):101–136.

Annex C: *Convergence of the mean of computed overland flow water depth with increasing the sample size through random sampling within the computation results database for 20points of interest. (with coordinated in Lambert III).*

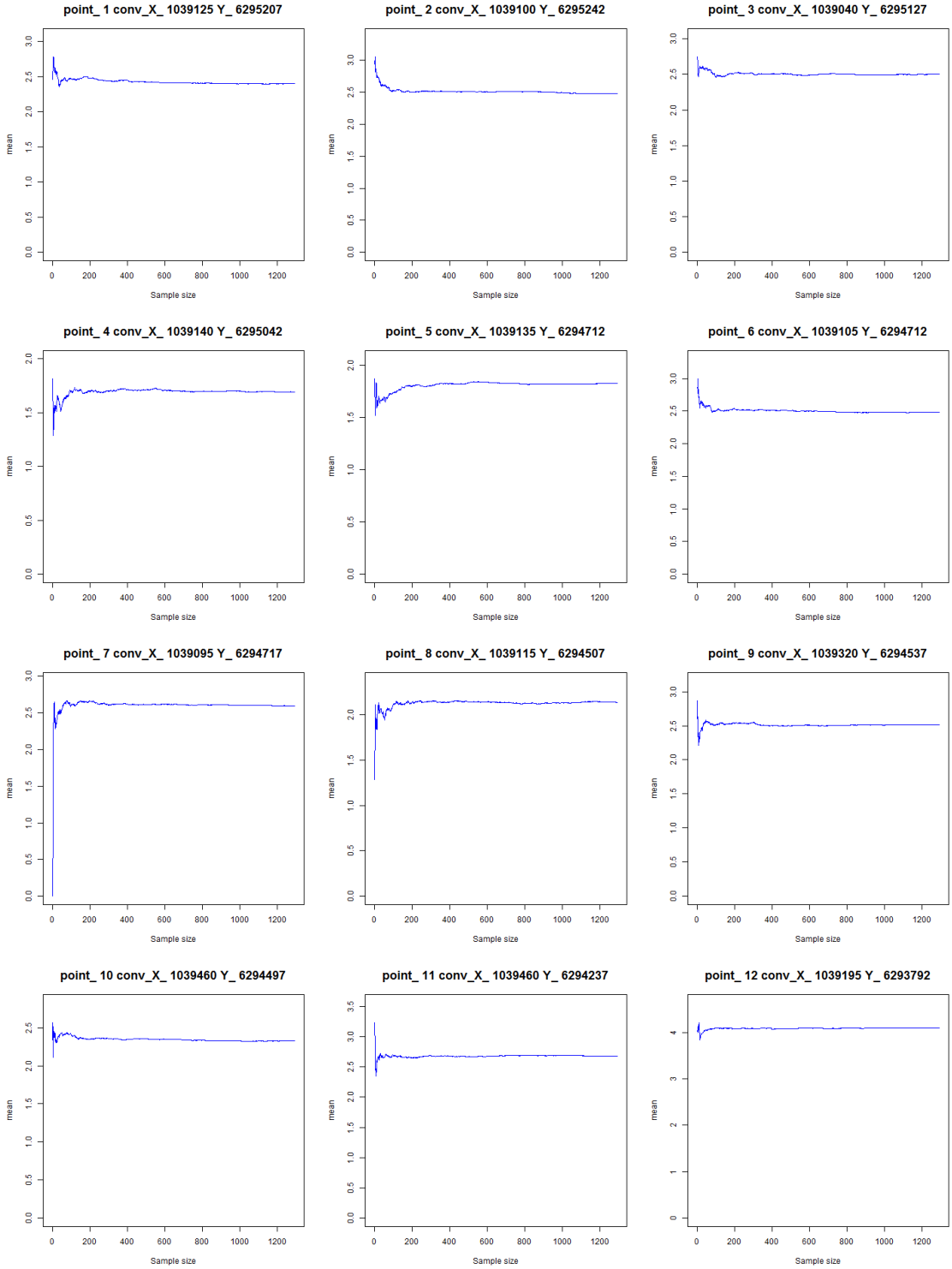

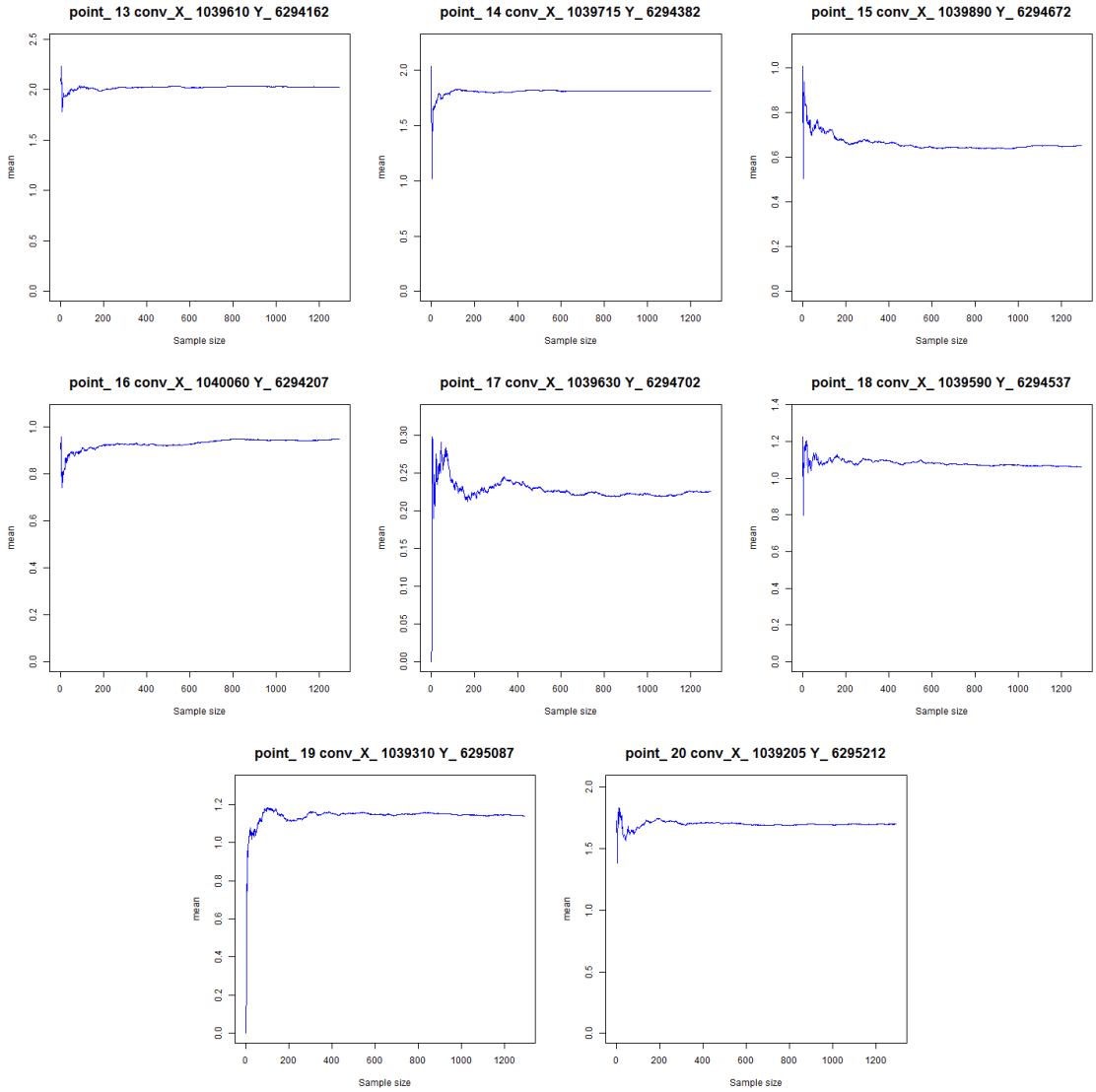
point_ 13 conv_X_ 1039610 Y_ 6294162
point_ 14 conv_X_ 1039715 Y_ 6294382
point_ 15 conv_X_ 1039890 Y_ 6294672
point_ 16 conv_X_ 1040060 Y_ 6294207
point_ 17 conv_X_ 1039630 Y_ 6294702
point_ 18 conv_X_ 1039590 Y_ 6294537
point_ 19 conv_X_ 1039310 Y_ 6295087
point_ 20 conv_X_ 1039205 Y_ 6295212
mean
Sample size

***Annex D**: Distribution of Y(x) at the 20 points of interest.*

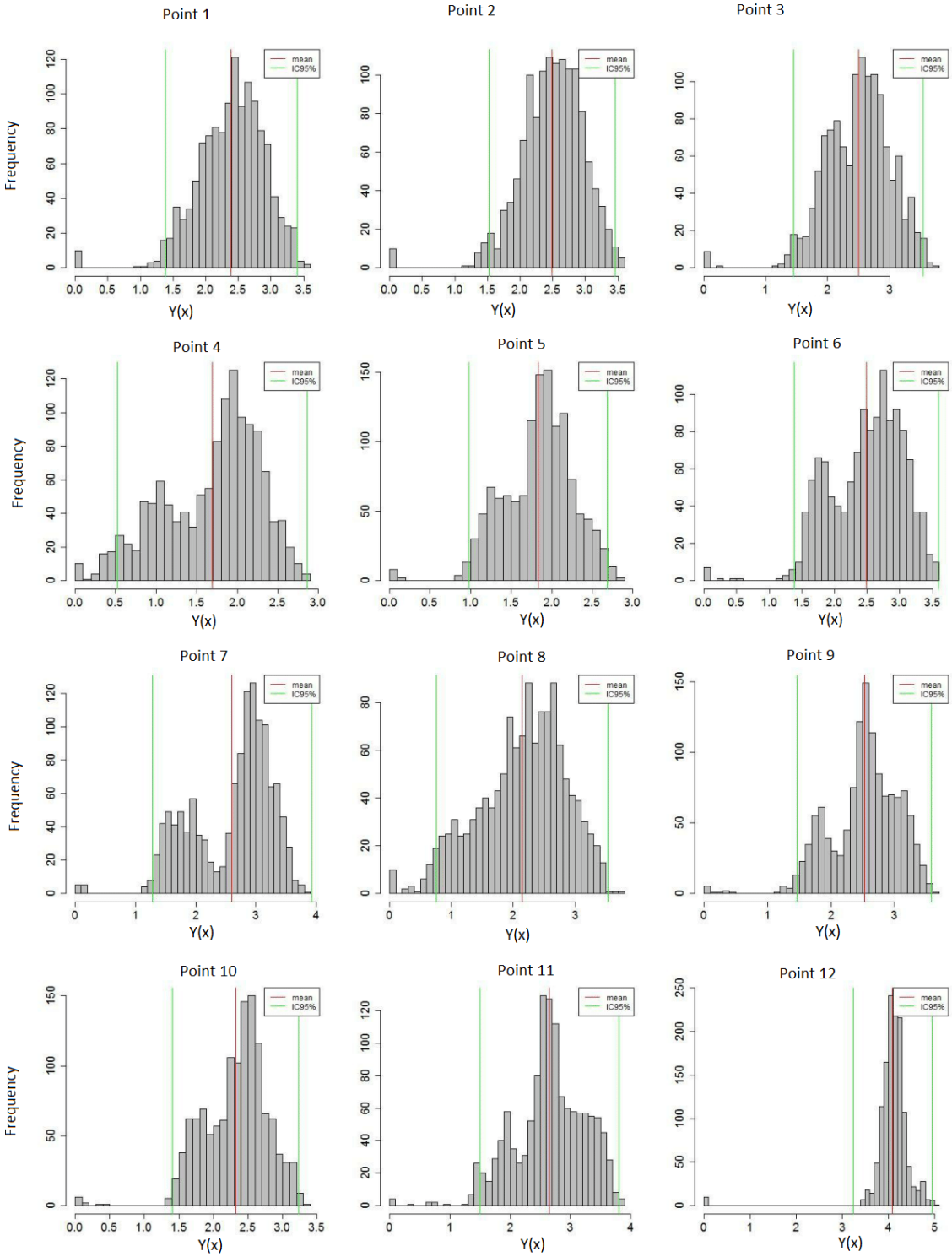

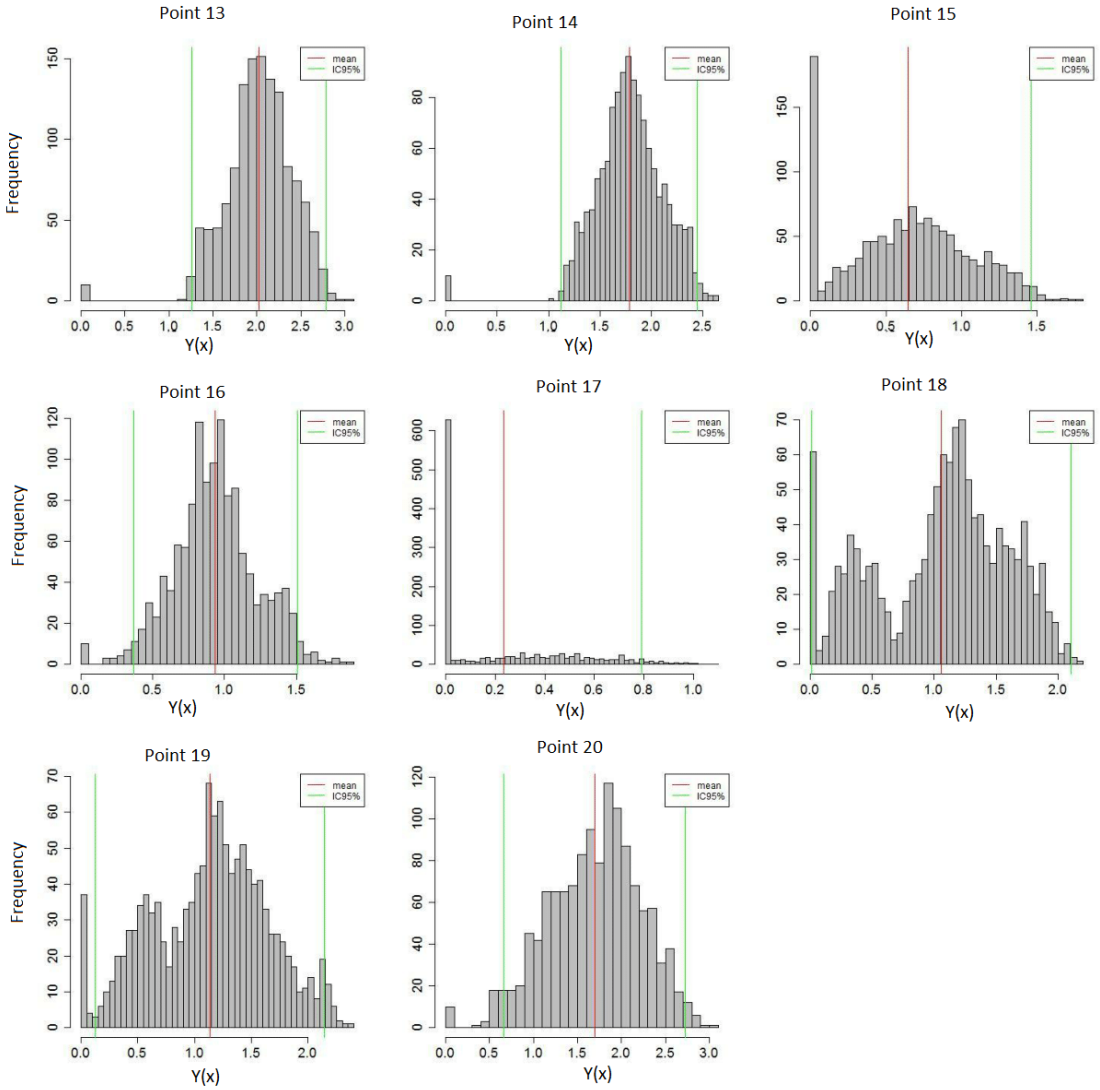
Point 13
Point 14
Point 15
Point 16
Point 17
Point 18
Point 19
Point 20
Frequency
Y(x)
mean
IC95%

***Annex E**: Sobol indices convergence at the 20 points of interest (points coordinate in Lambert III).*

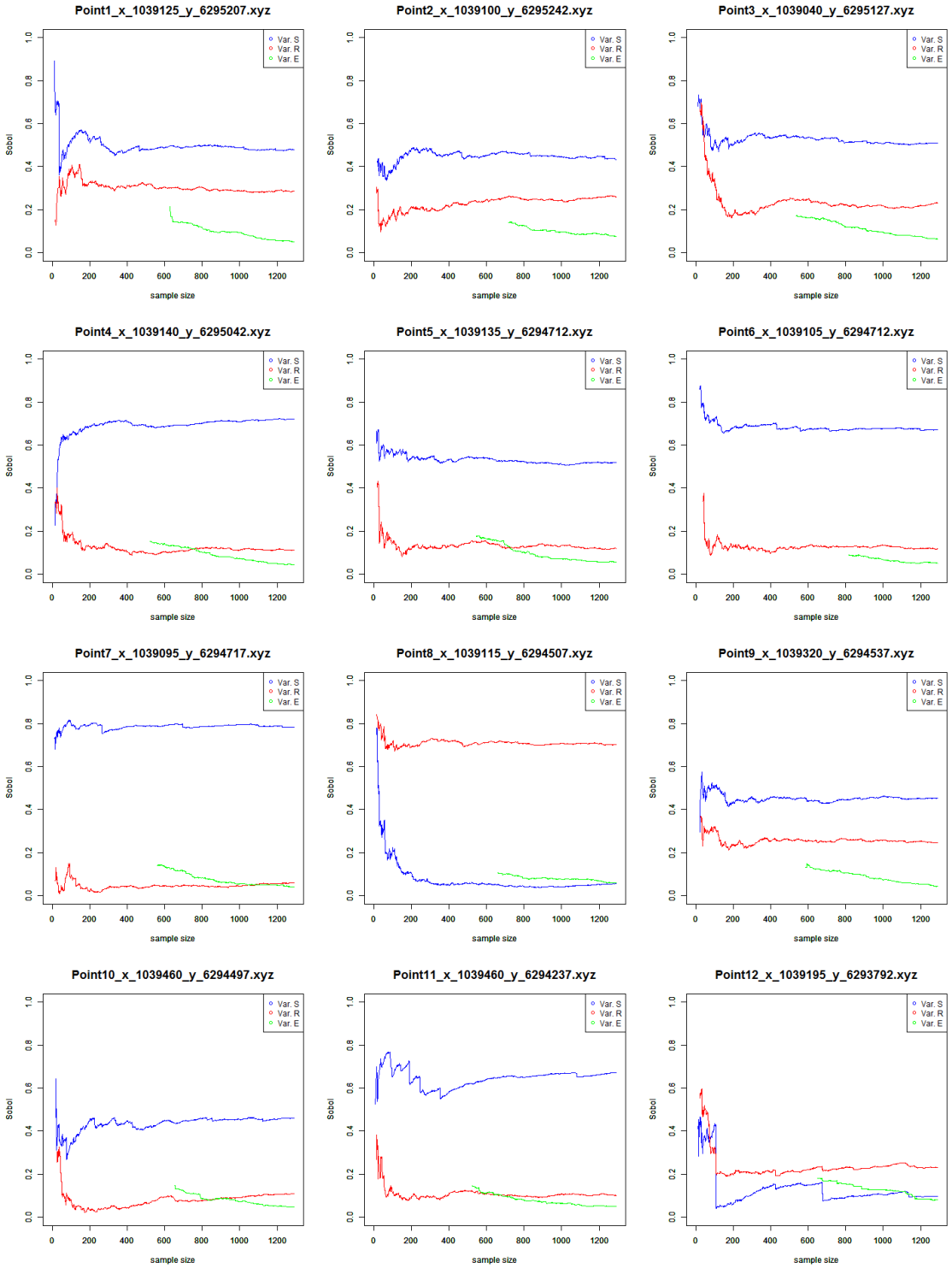

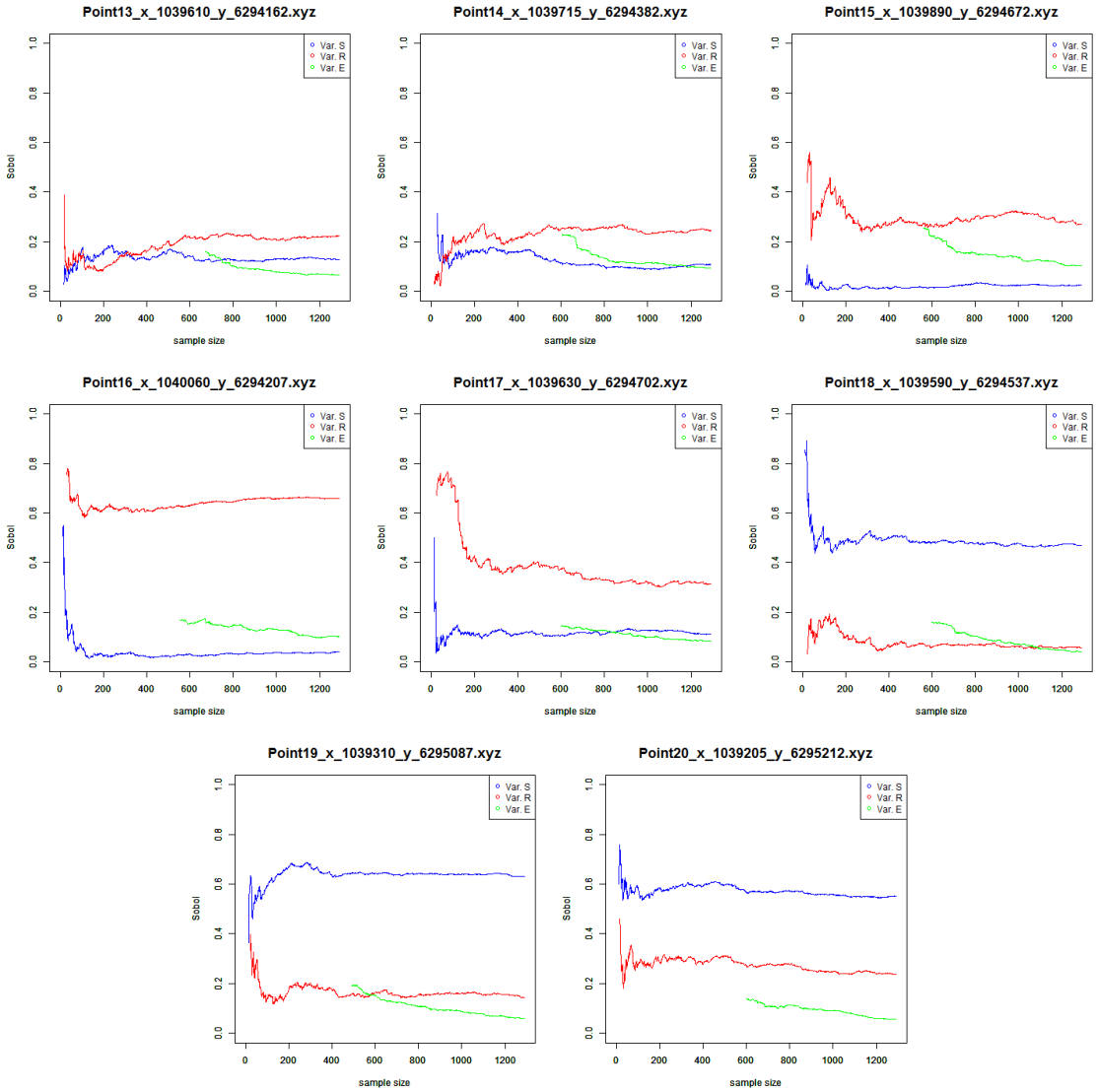
Point13_x_1039610_y_6294162.xyz
Point14_x_1039715_y_6294382.xyz
Point15_x_1039890_y_6294672.xyz
Point16_x_1040060_y_6294207.xyz
Point17_x_1039630_y_6294702.xyz
Point18_x_1039590_y_6294537.xyz
Point19_x_1039310_y_6295087.xyz
Point20_x_1039205_y_6295212.xyz
Var. S
Var. R
Var. E
Sobol
sample size